SEISMIC RESPONSE CONTROL OF LOW-RISE BUILDINGS USING FIBRE-REINFORCED ELASTOMERIC ISOLATOR

Thesis Submitted in Partial Fulfilment of the Requirements

for the Degree of

DOCTOR OF PHILOSOPHY

By

ANIMESH DAS

DEPARTMENT OF CIVIL ENGINEERING
INDIAN INSTITUTE OF TECHNOLOGY GUWAHATI
GUWAHATI-781039, INDIA

DECEMBER 2014

To the loving memory

of

my grandmother Late Sabitri Bala Das

CANDIDATE'S DECLARATION

I hereby declare that the work presented in the thesis entitled "**Seismic Response Control of Low-Rise Buildings using Fibre-Reinforced Elastomeric Isolator**" in fulfilment of the requirement for the award of the degree of Doctor of Philosophy is an authentic record of my own work carried out in Department of Civil Engineering of the Institute. The work has been carried out under guidance of Prof. A. Dutta and Prof. S.K. Deb.

The content presented in this thesis has not been submitted by me for the award of any other degree of this or any other Institute.

(ANIMESH DAS)

This is to clarify that the above statement made by the candidate is correct to the best of our knowledge.

Dr. Anjan Dutta
Professor
Department of Civil Engineering
Indian Institute of Technology Guwahati
Guwahati-781039
India

Dr. Sajal Kanti Deb
Professor
Department of Civil Engineering
Indian Institute of Technology Guwahati
Guwahati-781039
India

ACKNOWLEDGEMENT

This thesis is the outcome of analytical and experimental studies carried out in the department of civil engineering at Indian Institute of Technology (IIT) Guwahati, Assam, India. At the outset, I would like to express my sincere gratitude to the great human being, guide and philosopher Prof. Anjan Dutta and Prof. S. K. Deb for initiating an interesting and innovative research topic and for their unconditional support, valuable advices and continuous guidance.

The experimental studies conducted for this research work would not have been possible without the support of technical staff of the department of Civil Engineering, IIT Guwahati. I express my gratitude to Dr. Arun Chandra Borsaikia and Mr. Biswajit Debnath for their earnest effort during experimentation and data acquisition.

I would like to thank the members of my doctoral committee, Prof. Sudip Talukdar (Chairman), Prof. S. K. Dwivedi and Dr. Arunasis Chakraborty for their remarks and valuable suggestions during the entire course of my research. I would like to acknowledge the contribution of METCO Pvt. Ltd., Kolkata (India), for manufacturing FREI and FOSROC Chemicals Pvt. Ltd., Bangaluru (India) for providing carbon fibre wrap.

This thesis I am going to dedicate to my beloved grandmother Late Sabitri Bala Das. While I was doing my master in civil engineering, the thesis dedicated to her when she was alive. The primary education and values of life I have inherited from her. I have no words to show my affection to my parents, my in laws, my brothers and sisters, whom I have deprived without meeting them for a long time due to busy schedule work and research.

I have also deprived my beloved and devoted wife Bandana in many things, but she has been supporting me to carry forward the research work. I remember the days when she

was passing through the difficult days of her motherhood in absence of me. At the time of completion of writing this thesis my beloved sweet daughter, Anamika is only three months old and I am missing the opportunity to play with her.

I am very much grateful to my dear colleague and friends for their support in my official as well as personal life. Without their support this precious work would not have been completed. The list is never ending to include in this page. The last but not the least, I acknowledge the opportunity given by my organisation Bharat Heavy Electricals Limited, PEM, Noida to carry out this research work.

Animesh Das

TABLE OF CONTENTS

ABSTRACT

Modern base isolation technology has attracted attention of engineers and researchers for protection of building against damaging motions of earthquakes in last few decades. Both, the inter-story drift and floor acceleration can be reduced simultaneously by using base isolator. The use of multilayer elastomeric bearings which are made by vulcanization of rubber layers with thin steel reinforcement are flexible in horizontal direction to deflect the earthquake energy associated with strong ground motion. Though the force transmitted to the superstructure is reduced drastically by using these steel reinforced elastomeric bearing, but the use of these types bearings are limited to only important buildings. This is because of high cost and heavy weight associated with these bearings. The recent research in base isolation technology has evolved with the idea of reducing the weight and cost of isolator by using material like fibre reinforced polymer (FRP). The development of low cost bearing has made implementation of the seismic isolation technology to masonry building vulnerable to seismic ground motions, feasible. The weight reduction is possible because of availability of light weight fibre materials with an elastic stiffness of the same order of steel. In the present study, seismic performance of fibre reinforced elastomeric isolator (FREI) is considered.

The FREI can be used where top and bottom surfaces in contact with super and sub-structures may be either bonded or un-bonded. The un-bonded application has distinct advantages over bonded FREIs. However, the behaviour of un-bonded FREIs (U-FREI) are much complex and no classical solutions are available in literature for the evaluation of their mechanical properties. In view of this, preliminary design of bonded FREIs as obtained based on available closed form solutions are considered for U-FREIs as well. Further, some researchers have carried out experimental study on common shapes

(circular and square) of isolator and to some extent on long strip isolators. It is not however possible to carry out experimental study to determine the mechanical properties of isolator of all shapes and sizes before installation into structure.

Thus, in order to address cases where no available classical solutions are available as well as for investigation of different shapes, analysis of these bearings using general purpose finite element (FE) software (like ANSYS) is carried out. In the present study, square and circular isolators are considered for analysis. Horizontal cyclic displacement with varying amplitude is applied to the top of the isolator carrying a constant a vertical load. Force displacement hysteretic behaviour and damping properties of isolators are obtained from FE analysis. Performances of square and circular isolators under different horizontal loading directions are also analysed and comparisons of results are studied. Stress demands in elastomeric layer of the isolator for both types are studied. Bonded and un-bonded isolators of square and circular shape are analysed and results are compared. It is also observed that the lower tensile stresses are developed in the rubber and reinforcement in U-FREI as compared to bonded FREI, resulting in lower peeling stress demand on bond between layers in U-FREI.

In order to validate the numerical findings of FREIs, square un-bonded isolators are manufactured by vulcanisation of rubber and bi-directional fibre fabric. Cyclic vertical load is applied on the top of isolator to find out the vertical stiffness of the isolator. Horizontal stiffness and damping properties of isolator are determined by testing them under cyclic horizontal displacement applied along two different directions along with constant vertical load. Horizontal force displacement loops obtained from test are compared with the result obtained from FE analysis and good agreements are observed. The feasibility study of U-FREI as an alternative to steel reinforced elastomeric isolator (SREI) for seismic isolation of un-reinforced masonry buildings is studied. Shake table

testing of 1/5th scaled two storey masonry building supported on four square U-FREI is carried out to ascertain its effectiveness in controlling seismic response. Four different input earthquakes with different frequency contents are applied to the structure and dynamic responses are measured. To evaluate the performance of U-FREI, same building is placed directly on the shake table without isolator and fixed base (FB) condition is simulated by restraining the base of the building with the shake table. Dynamic response characteristic of base isolated (BI) un-reinforced masonry building subjected to different intensities of input earthquakes are compared with the response of the same building without base isolation system. Acceleration response amplification, peak response values of test model with and without base isolation system are compared for different intensities of table acceleration.

Shake table testing of base isolated model building is not always feasible due to high cost and time required for the preparation of model and test setup. Thus, as an alternative, numerical simulation of the model building is carried out using SAP 2000 Nonlinear, where FREIs are modelled using multi-linear pivot hysteretic plasticity model. Acceleration and displacements responses are evaluated at different floor levels and good agreement is observed with experimental findings. Results obtained from numerical analysis demonstrate that the expensive shake table testing can be avoided for ascertaining dynamic response characteristics of a base isolated building with fairly acceptable accuracy.

LIST OF FIGURES

LIST OF TABLES

Notations

Symbol		Meaning
A_b	=	Area of bearing
a	=	Width of bearing
b	=	Length of bearing
β	=	Damping ratio
C_b	=	Damping matrix of viscous isolation elements
C_{eq}	=	Equivalent damping of bearing
d_{max}	=	Maximum displacement in the bearing
d_{min}	=	Minimum displacement in the bearing
E_b	=	Bending modulus of the bearing
E_c	=	Compression modulus of the bearing
E_f	=	Young's modulus of fibre reinforcement
$(EA)_{eff}$	=	Effective compressive stiffness
$(EI)_{eff}$	=	Effective bending stiffness
$(EJ)_{eff}$	=	Effective warping stiffness
F	=	Horizontal force on elastomer
F_{max}	=	Maximum shear force in the bearing
F_{min}	=	Minimum shear force in the bearing
f_n	=	Natural frequency of base isolated structure
G	=	Shear modulus of elastomer
g	=	Acceleration due to gravity
h	=	Thickness of one elastomer layer
h_t	=	Total height of bearing including reinforcement

I	=	Moment of inertia of bearing
I_y	=	Moment of inertia of rectangular area about the Y-axis
K	=	Stiffness matrix of superstructure
K_b	=	Effective stiffness matrix of isolation system
k_b, k_c	=	Cross warping parameter
K_{eq}	=	Equivalent stiffness of bearing
K_h	=	Total horizontal stiffness of the isolation bearing
K^h_{eff}	=	Effectiveness horizontal stiffness of bearing
k_h	=	Horizontal stiffness of the individual bearing
k_v	=	Vertical stiffness of individual bearing
M_b	=	Mass matrix for base motion
m_t	=	Total mass of isolated structure
μ	=	Static coefficient of friction
N_b, N_c	=	Normal force related to warping
n_r	=	Number of elastomeric layer
ϑ	=	Poisson's ratio of elastomer
ϑ_f	=	Poisson's ratio of fibre reinforcement
P	=	Axial compression load
$\overline{P}$	=	Dimensionless compression force
P_{cr}	=	Buckling load of the bearing
P_n	=	Normal pressure
R	=	Radius of bearing
ρ	=	Ratio of the flexural rigidity to shear rigidity
S	=	Shape factor

s	=	Scale factor
S_{11}, S_{22}	=	Normal stress
t_e	=	Thickness of single layer of elastomer
t_f	=	Thickness of single layer of fibre reinforcement
t_r	=	Total thickness of single layer of elastomer
θ_b	=	Instantaneous direction of bearing displacement
W_d	=	Dissipated energy (hysteresis loop)
Δ_{max}	=	Average of positive and negative maximum displacement
ω	=	Angular frequency
$x_b(t)$	=	Displacement of base isolated structure
$x_{b1}(t)$	=	Displacement of spring and dashpot system
$\ddot{x}_t(t)$	=	Ground acceleration

भारतीय प्रौद्योगिकी संस्थान गुवाहाटी
Indian Institute of Technology Guwahati

Chapter 1

Introduction

1.1. General

In base isolation system, the isolation bearings are installed at the interface of sub-structure and super-structure to reduce transmission of earthquake motion to the super-structure. The development of multi-layered elastomeric bearings has facilitated its application in seismic base isolation. These bearings are made by vulcanization of sheets of rubber to thin steel reinforcing plates. These bearings are very stiff in the vertical direction so as to enable them to safely carry the vertical load of the building and very flexible in horizontal direction to allow the building to move laterally under strong ground excitations. The use of multi-layered elastomeric bearings in building for seismic base isolation is an extension of elastomeric bridge bearings. The base isolation concept is widely accepted across the world for protecting important structures as well as important sensitive instruments etc. from the damaging motion of earthquakes.

For earthquake resistant design of a building structure, the basic challenge faced by a structural engineer is how to minimize both inter-story drift and floor accelerations. Large inter-story drifts of flexible structure cause damage to non-structural components and to sensitive internal equipment housed in the building. Stiffening the structure can reduce inter-story drift but lead to amplification of the ground excitation. Due to amplification of ground excitation, floor level accelerations are also amplified causing damage to sensitive equipment. Floor accelerations can be minimized by making the structure more flexible, which leads to large inter-story drifts. To minimize both the floor acceleration and large inter-story drift simultaneously is to use base isolators at the interface of sub structure and super structure. These base isolators provide the flexibility

to the structural system, with the displacement concentrated at the isolator level. Various types of control system used to control the response of structure during earthquakes are briefly described below.

1.2. An Overview of Structural Control System

The ground acceleration due to earthquake transmits forces in a structure, which excites it dynamically. There are many types of control systems available to reduce the effect of seismic forces to superstructure. Control systems can be classified as (a) active control system, (b) passive control system, (c) semi-active control system and (d) hybrid control system. A schematic of structural control system classification is shown in Fig 1.1.

1.2.1. Passive Control System

Passive control systems are installed into the structural system permanently and generally these require no attention. For the functioning of these systems, no power supply is required and hence they are very effective at the time of earthquake. Few of the passive control systems are (a) base isolation, (b) visco-elastic dampers, (c) tuned-mass damper and (d) liquid-column and mass damper. Some of the passive control system, which are employed in civil structures, are shown in Fig. 1.2.

1.2.2. Active Controlled System

Active control systems are installed into the structural system after completion of the structure. In active control, earthquake input and response motion are measured by sensors and response of the building are controlled by adding a force using external

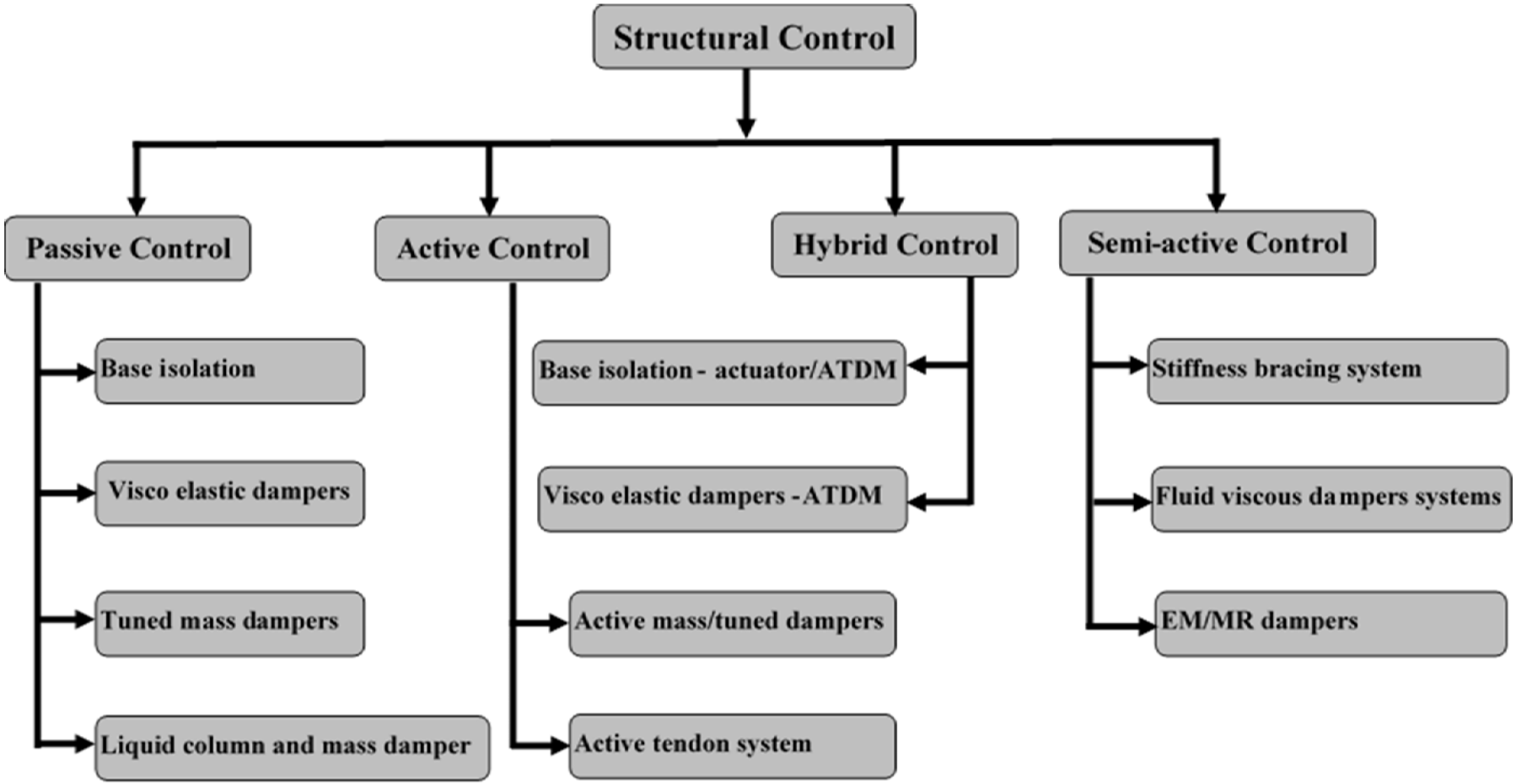

Fig. 1.1 Broad classification of structural control system

energy supply or changing the dynamic stiffness and damping characteristics of the structure. These require continuous power supply for functioning of the system. The active control systems which are generally used in structural control are (a) active mass/tuned dampers and (b) active tendon system.

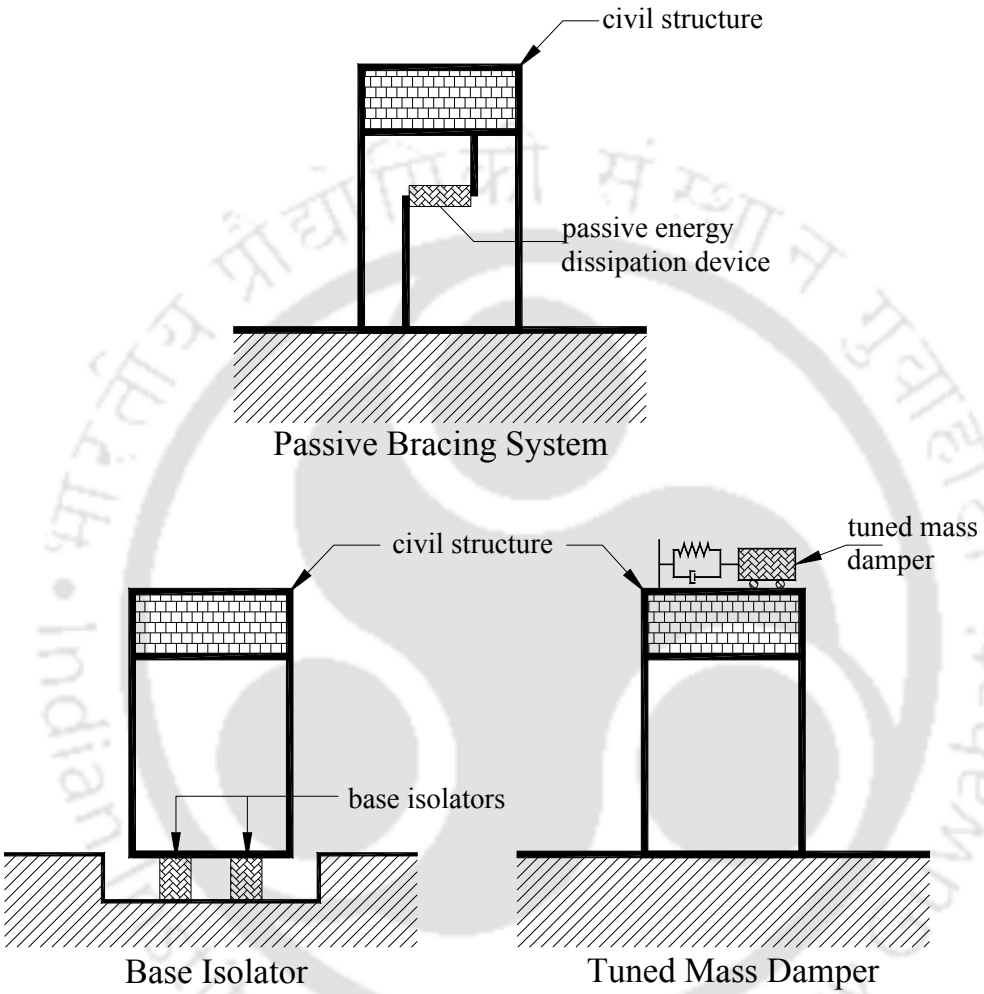

Fig. 1.2 Passive control systems in structure.
(*Datta T.K., 2003*)

1.2.3. Hybrid Control System

Hybrid control systems are combination of passive and active control system. The forces from the active system are employed to increase the efficiency of passive control systems. The energy and forces required to operate a hybrid system is far less than fully active control systems. Some of the hybrid control systems are (a) base isolation - actuator/ATDM (Active tuned mass damper) and (b) visco-elastic dampers - ATDM.

1.2.4. Semi Active Controlled System

Semi active control systems are active control systems, which require very less power to operate. These system do not directly add or remove energy to the structural system, but can control the parameter of structures such as spring stiffness or coefficient of viscous damping. Semi active system utilizes the motion of structure to develop the control forces. Performances of appropriately designed semi active system are better than passive control system. Some of the semi active control systems are (a) stiffness bracing system (b) fluid viscous dampers systems (c) Electromagnetic (EM) / Magneto-rheological (MR) dampers.

1.3. Base Isolation

The concept of base isolation is quite simple. The system decouples the building or any other structure mounted on those isolators from the horizontal components of the ground motion by interposing structural elements with low horizontal stiffness between the structure and the foundation. This gives the structure a fundamental frequency that is much lower than both its fixed base frequency and the predominant frequencies of the ground motion. The first dynamic mode of the isolated structure involves deformations only in the isolated system, the structure above acts as rigid body system. The base isolators reduce earthquake forces in the structure in two ways:

- By deflecting the seismic energy – The structure above base isolator behave as rigid body, hence reducing the lateral seismic forces attracted by the structure.
- By absorbing the seismic energy – Due to non-linear behaviour of the base isolator, energy is absorbed proportional to hysteretic stress-strain behaviour of the base isolator, hence increasing the damping of the structure.

1.3.1. Advantages of Base Isolation

Base isolation techniques have gained popularity in many parts of the world. It has distinct advantages both structurally as well as monetarily. For instance, in Japan, owners of base isolated apartment enjoy 30% discounts in insurance premium. Following are some of the basic advantages of base isolation.

(a) Reduces floor acceleration and inter-story drift.

(b) Less (or no) damage to structural members.

(c) Better protection of secondary structural systems.

(d) Prediction of response is more reliable.

(e) Economical due to uninterrupted functionality of building during earthquake.

Isolated building undergoes rigid body motion and isolators undergo large displacement or deformation and absorb the seismic energy through hysteresis. Typical deflected pattern of non-base isolated and base isolated building are shown in Fig. 1.3.

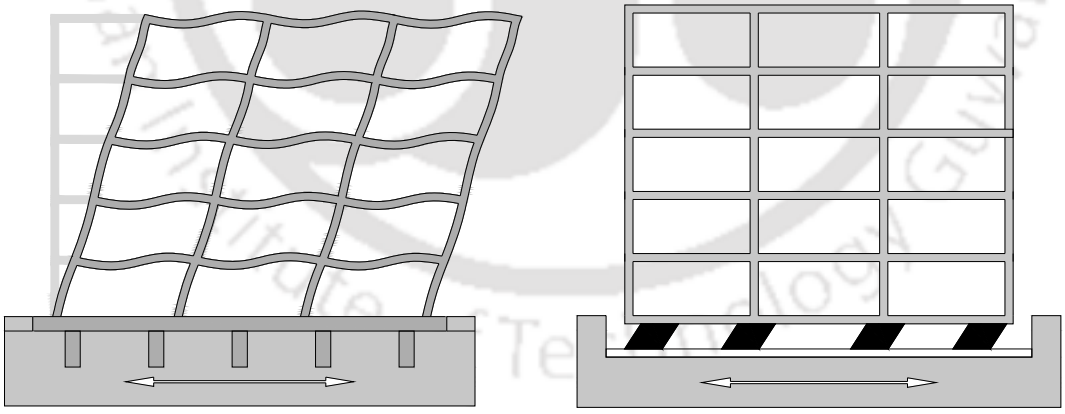

Fig. 1.3 Non base isolated and isolated building.

1.3.2. Leading Base Isolation System

The basic features of base isolated systems consist of the horizontal flexibility and energy absorption capacity. The horizontal flexibility of the bearing can increase the natural period of the isolated structure so as to avoid the frequency range in which

earthquake energy is dominant. However, due to the horizontal flexibility, the displacement of the isolated structure increases.

The energy absorption capacity and damping of the bearing counteract the excessive deformation of the structures. Owning to this characteristic of base isolated systems, they can attenuate the harmful horizontal acceleration transmitted to the super structure and reduce the member forces of the substructure. Various leading base isolated system, which have been used or are considered to have considerable potential for wide application, are briefly described.

(a) Pure-Friction (P-F) system

P-F system is classified as simplest system because it uses only stick-slip mechanism. When there is a sliding in the friction plates, the P-F system limits the maximum acceleration to be transmitted to the superstructure to a certain value, which is proportional to the friction coefficient. However, there may an excessive deflection or a residual deformation in the friction surface after the seismic event, because the P-F system has no recovering force. A schematic diagram of pure friction based isolator is shown in Fig. 1.4.

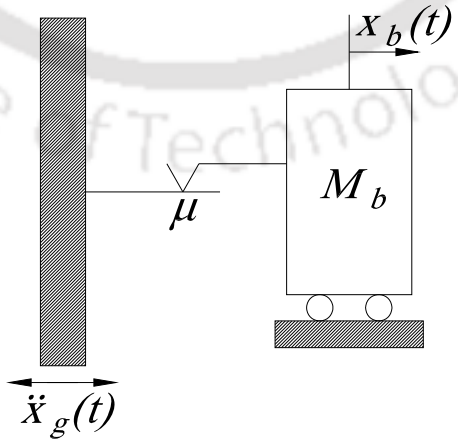

Fig. 1.4 Schematic diagram of P-F base isolator.
(*Lin et al., 1989*)

(b) Laminated Rubber Bearing (RB) system

The RB system is widely studied and used all over the world. It consists of alternating layers of rubber and steel with the rubber being vulcanized to the steel plates. The rubber layers provide horizontal flexibility, while the interleaved steel layers are responsible to provide adequate vertical stiffness. The dominant feature of the system is parallel action of spring and dashpot as shown in the following Fig. 1.5(a). Since damping capacity of RB system is relatively small, it mainly shifts natural period of the isolated structure to avoid detrimental earthquake energy.

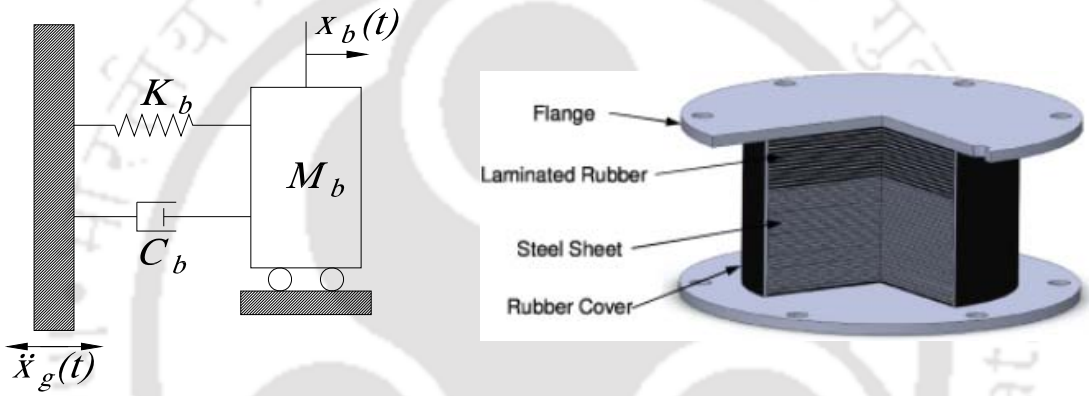

(a) Schematic of RB system. (*Lin et al., 1989*)

(b) View of RB (*Wang Y.P., 2002.*)

Fig. 1.5 Schematic and view of laminated rubber bearing.

Laminated rubber or elastomeric bearings can be classified into low-damping or high damping types. Schematic diagram of laminated rubber bearing is shown in Fig. 1.5(a) and view of laminated rubber bearing is shown in Fig. 1.5(b).

(c) Lead Rubber Bearing or New Zealand (NZ) system

The lead rubber bearing system or NZ system is also widely used like a RB unit. A central lead core improves performances of NZ system. It reduces relative deflection and provides an additional means of energy dissipation. Schematic diagram and pictorial view of NZ bearing system is shown in Fig. 1.6.

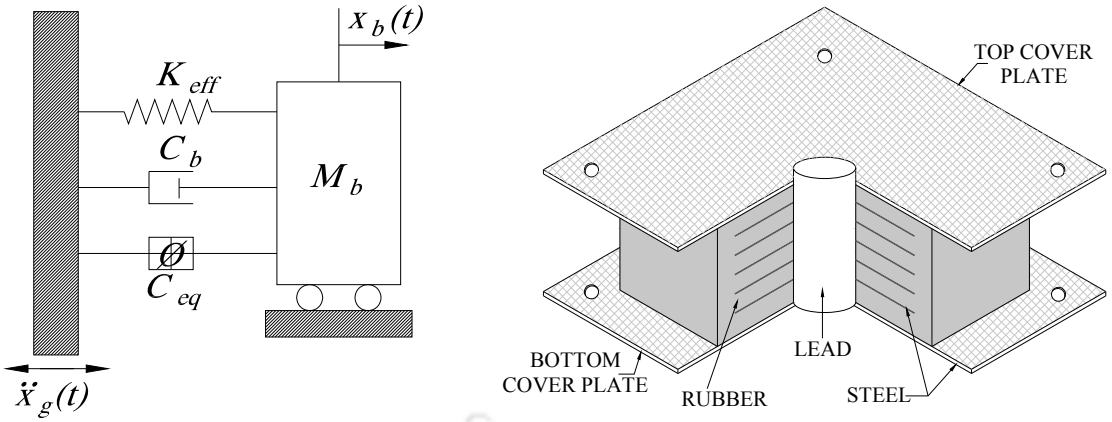

(a) Schematic diagram of NZ system base isolator (*Lin et al., 1989*)

(b) Pictorial view of NZ base isolation (*Buckle I. G., 1985*)

Fig. 1.6 Schematic diagram and pictorial view of NZ bearing.

(d) Resilient Friction Base Isolator (R-FBI) system

This isolator consists of concentric layers of plates with friction contact to each other and a central rubber core. The R-FBI system makes use of parallel action of resiliency of rubber and friction of teflon coated plates. This bearing does not slide below the frictional resistance similar to P-F system. However, the central rubber core provides an additional resistance to increase in deflection and a recovering force after sliding. Schematic diagram of R-FBI bearings system is shown in Fig. 1.7.

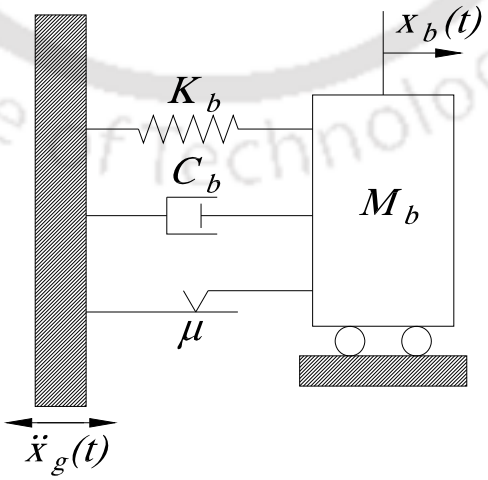

Fig. 1.7 Schematic diagram of R-FBI bearing system.
(*Lin et al., 1989*)

(e) Electricite de France (EDF) system

The EDF system consists of the laminated neoprene pad topped by a lead bronze plate which is in frictional contact with steel plates anchored to the structures. During a low intensity earthquake, it behaves as a rubber bearing unit and return to its original position after the seismic event. When the frictional resistance is exceeded, slip will occur and the EDF system may have a residual deformation in the friction surface during a high intensity earthquake. This system behaves as a combination of elastomeric bearing and friction plates in series is schematically shown in Fig. 1.8.

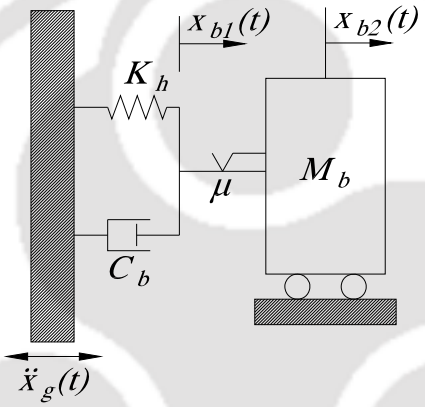

Fig. 1.8 Schematic diagram of EDF bearing system.
(*Lin et al., 1989*)

(f) Friction Pendulum Bearing system

The friction pendulum bearings are made up of a dense chrome over steel concave surface in contact with a articulated friction slider and free to slide during lateral displacement. Bearings can be designed to accommodate different magnitude of displacements simply by adjusting the curvature and the diameter of the bearing surface. Cross sectional view of a friction pendulum bearing is shown in Fig. 1.9.

(g) Spring Type Base Isolation Systems

The spring type vibration isolation system is popularly used in many applications and GERB Schwingungsisolierungen GmbH & Co., Germany is the leading manufacturer

of spring type base isolation system. The GERB system for seismic isolation was developed originally for the vibration isolation of power plant rotating equipment like turbine generator, fans, mills etc. GERB vibration control systems typically consist of spring elements and viscodampers. It uses large helical steel springs that are flexible both horizontally and vertically. The vertical frequency is around 3-5 times the horizontal frequency. The steel springs are completely without damping and the system is always used in conjunction with the viscodamper to provide damping to the system. Fig. 1.5(a) also represent the schematic of GERB base isolation system which consists of spring and viscodamper.

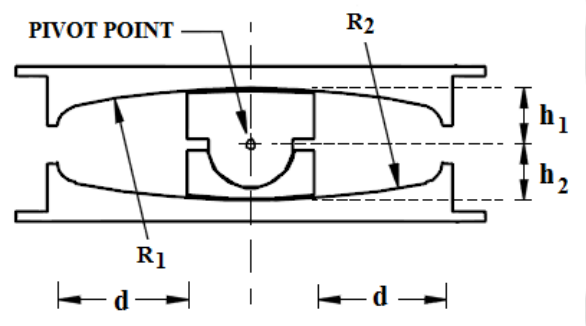

Fig. 1.9 Cross sectional view of FPB system
(*Zayas et al., 1989*)

1.4. Base Isolated Building in India

Base isolation technology is relatively new and its application has been very limited so far in countries like India. After the disastrous earthquake of Killari, Maharashtra in 1993, one school building and a shopping complex were built with rubber base isolator. Similarly, a four-storey Bhuj general hospital building in Gujrat was built on base isolators after the Bhuj (2001) earthquake.

Research activities have been undertaken in the country to develop the state of art capability to manufacture and construct base isolated building. Indian Institute of Technology (IIT) Guwahati is one of the pioneering institutes to start the research activities in this field and constructed a base isolated building (Funded by BRNS, Govt.

of India) in 2006 to study the performances of base isolated building. Fig. 1.10 shows a base isolated building in the campus of the institute, which is located in the most severe seismic zone (Zone V) as per IS 1893: Part 1: 2002.

Fig. 1.10 Base isolated building at IIT Guwahati

1.5. Problem Identification

A two storey un-reinforced masonry building is chosen for base isolation using FREI. This type of un-reinforced masonry building is considered since similar structures are built as low cost housing units in the north eastern part of India, which also happens to be in the highest seismic zone of the country. Building material for masonry constructions are easily available and are transported to the remotest hilly terrain of the region for construction.

In conventional fixed based structure, certain amount of seismic energy is transferred to the structure. This seismic energy must be dissipated in such a manner that it does not

cause high floor accelerations or inter-storey drifts in the structure and it is generally achieved through inelastic deformation of the structural framing members. Such a condition for fixed based structure may be achieved only by inserting damages in structural elements. However, in base isolated system, the isolators decouple the structure from foundation and deflect the seismic energy associated with ground motion and thereby reduce the floor accelerations as well as inter-storey drift of the structure.

In the present study, preliminary design of square and circular FREIs are carried out using the available formulation reported in previous literature. FE analyses of FREIs are carried out to find out mechanical properties of isolator and detailed stress/ strain profile at different layers of isolator. FE analysis is carried out by considering ends of isolators as bonded, un-bonded and also for different shapes as square and circular. In order to attain more confidence in the design and analysis, square isolators are manufactured and tested in the laboratory. Mechanical properties of square un-bonded isolator FREI is determined through experimental investigation and compared with FE analysis result. Shake table studies of a $1/5^{th}$ scaled two storey masonry building supported on four U-FREIs are carried out at the Structural Engineering Laboratory of Indian Institute of Technology, Guwahati. Analytical modelling of building and isolator is developed using SAP2000, Nonlinear. Responses are measured during shake table testing at various floor levels of the model building and compared with the SAP analytical model.

1.6. Objectives

The objective of this study is to develop and demonstrate the feasibility of fibre-reinforced elastomeric base isolators as a viable alternative to the conventional steel-reinforced isolators. The development of lightweight, low-cost isolator is crucial if this method of seismic protection is to be applied to a wide range of buildings, such as

residential buildings, school building and hospital buildings etc. in rural as well as urban earthquake-prone zones. Numerical approach may be adopted for the evaluation of seismic performances of isolators as well as base isolated buildings and the same may be validated through experimental investigations. Such validated numerical model may provide an effective tool for initial design of those isolators at relatively low cost. The major objectives of the present study are as follows:

I. To carry out numerical simulation of FREI for the evaluation of force displacement hysteretic behaviour for the evaluation of seismic performance.
II. To investigate vertical stability and stiffness along vertical as well as horizontal directions.
III. To develop lightweight, low cost FREI for seismic response control of low rise building in developing countries like India.
IV. To carry out experimental study on force displacement behaviour of FREI.
V. To carry out shake table testing of base isolated masonry model building supported on FREI.
VI. To develop numerical model for the base isolated building so that the expensive experimental investigation using shake table can be carried out only selectively.

1.7. Scope of Study

The scope of study in the present research comprises of both numerical and experimental investigation of FREI for seismic isolation of low-cost un-reinforced masonry building. The detailed scopes of studies are given as follows:

1.7.1. Experimental Study

I. To carry out experiments in laboratory for the evaluation of vertical stiffness of FREI.

II. To carry out experiments in laboratory to determine the force displacement relationship of FREI under cyclic horizontal displacement, mechanical and dynamic characteristics of isolator. The direction of loading to be changed to evaluate its influence on the performance parameters of FREIs.

III. To carryout shake table testing of base isolated un-reinforced masonry building supported on FREIs and subjected to four different earthquakes excitation of various intensities. The tests to be repeated to evaluate the effect of direction of loading.

1.7.2. Analytical Study

I. To carryout FE modelling and analysis of square and circular isolators using commercial software ANSYS. To evaluate force displacement hysteretic behaviour for the evaluation of mechanical characteristics and detailed stress and strain in different layers of elastomer.

II. To validate numerically evaluated mechanical characteristics of FREI with those obtained from laboratory tests.

III. To analyse un-reinforced masonry test building supported on un-bonded square FREI using commercial software SAP2000. The analysis to be performed by considering four different earthquakes excitation of varying intensities acting along X-axis and 45^0 to X-axis of FREI.

IV. To carry out comparative study of result obtained from shake table testing and numerical analysis.

1.8. Outline of the Thesis

In this thesis, detailed experimental investigation of square U-FREI and analytical studies of square as well as circular of FREI (both bonded and un-bonded) are conducted. Scaled un-reinforced masonry building is mounted on those U-FREIs and tested on shake table. The findings from shake table test are used to validate numerically simulated model. The scope and objective reported in this thesis are covered in eight chapters.

In Chapter 1, general description of isolated systems, summary of the scopes and objectives of the studies are presented.

Chapter 2 provides the brief review of the existing literature on elastomeric bearings developed in different parts of the world. Analytical and experimental behaviour of FREI as reported in different literature are presented in details. Study report on FE analysis aspect of rubber like material used in bearing is also reviewed. Literatures on testing of base isolated building are reviewed and presented in this chapter.

In Chapter 3, preliminary design of FREI is presented. Basic theory of FREI as reported in different literature is also presented in this chapter. Geometry of isolator, material properties of fibre reinforcement, elastomer and manufacturing process of square FREI is described briefly.

Chapter 4 describes the FE formulation of FREI using commercially available software ANSYS. Analysis of square isolators (both bonded and un-bonded) are carried out to determine stiffness and other dynamic parameter. The effect of variation in loading direction in the mechanical properties of FREI is studied. A circular isolator with same plan area and height as that of square isolator is also analysed and results are compared.

Chapter 5 describes the experimental investigation of square FREI. Tests are carried out to determine the vertical stiffness of isolator using cyclic vertical loading. Similarly,

tests are carried out for the evaluation of horizontal stiffness, where cyclic horizontal displacement is applied with a constant vertical load. Tests are repeated for applied horizontal load acting along different direction of isolators. Results of horizontal cyclic load test are compared with the result obtained from FE analysis of square isolator.

Chapter 6 describes the shake table testing of un-reinforced masonry building model supported on four square U-FREIs. This building is subjected to four different input earthquake excitations. Tests are conducted for different direction and intensities of input earthquake excitation. Various dynamic response parameters along the height of the base isolated masonry building are evaluated from the shake table. The same building is placed directly on the shake table without isolator and fixed base condition is simulated by restraining the base of the building with the shake table. Dynamic response characteristic of base isolated base isolated masonry building subjected to different intensities of input earthquakes are compared with the response of the fixed base building.

Chapter 7 describes the numerical simulation of base isolated building supported on un-bonded isolators using commercial software SAP2000. Nonlinear link elements are used simulate the isolator support of the building. Numerical analysis is carried out for different intensities of input earthquake excitation along different direction of the building model. The numerical analysis results are compared with those obtained from the shake table testing to ascertain the accuracy of the numerical model.

Chapter 8 presents the summary and conclusion of research work undertaken. Major finding during the work and scopes of future work have also been listed in this chapter.

भारतीय प्रौद्योगिकी संस्थान गुवाहाटी
Indian Institute of Technology Guwahati

Chapter 2

Review of Literature

2.1. Introduction

Base isolation technology has found world wide application generally in big, expensive buildings, which may be housing sensitive equipment, emergency operation centres and hospitals etc. Large, heavy and costly SREIs, which are made by vulcanization bonding of sheets of rubber to thin steel reinforcing plates are used in these applications. To extend this seismic base isolation technology to mitigate the seismic vulnerability of low cost housing, it is necessary to reduce the weight and cost of the isolator. The recent research in base isolation technology has evolved with the idea of reducing the weight and cost of isolator by using material like fibre reinforced polymer (FRP) in place of steel as reinforcement. The development of low cost bearing has made it a practical reality for the seismic isolation of low cost buildings, which are otherwise vulnerable to seismic ground motions. In this chapter, a brief review of seismic base isolators in general, FRP based isolators, FE modelling of isolators and shake table testing and application of isolator to building system are presented.

2.2. Base Isolation Bearing

Base isolation technology for seismic isolation of structures has been used from last few decades. Development of multi-layers elastomeric bearing has increased the popularity of this technology. SREI bearings are very stiff in the vertical direction and hence can safely carry vertical load of the building; but these bearings are very flexible horizontally, thereby enabling the building to move laterally under strong ground

motion. These bearings are costly and heavy due to the interleaved steel shim plates. The weight and cost of SREI is can be reduced by introducing fibre as reinforcing elements. Study on FREI has started at the end of 20th century. While large amount of literatures are available on the study of SREI, very few studies are reported on FREI till date. A brief review on the origin and development of elastomeric bearings in general are presented below.

Roeder and Stanton [1983] gave brief description of the state of art of knowledge of elastomeric bearing available throughout the world. This paper helps structural engineer to understand the material and large strain behaviour of elastomeric bearing. It summarized the material behaviour of elastomers, theoretical and experimental research on bearings. Various modes of failure of elastomeric bearings were also presented. Design methods of four major specifications like AASHTO, German procedure, British specification and International railway specification were compared by the researchers.

Kelly [1986] summarised the bibliography of all literature on theoretical aspect of seismic isolation as published from 1900 to 1984. The Foothill Communities and Justice Centre was the first base isolated building in United States. In the early years, it was tried to achieve base isolation by using sliding concept to decouple the structure from the ground. The first use of unreinforced rubber block as earthquake protection was in an elementary school in Skopje, Yugoslavia. The base isolated building underwent rigid body motion during the first mode of vibration with all the deformation mainly at the isolator level. For higher mode, seismic load was treated as an equivalent lateral load which was proportional to the rigid body mode. This is the property of a linear vibrating system with all higher modes being mutually orthogonal to each other. So, energy associated with higher frequency of earthquake ground motion cannot be transmitted to the structures. Thus working principle of base isolation system is to

deflect energy rather than to absorb energy.

A comparative study of laminated rubber bearing with and without lead plug and some frictional base isolation systems were carried out by Lin *et al.* [1989]. The performances and limitation of various types of isolators were discussed in details. A computer program was developed for integrating the equation of motions for various base isolated systems. A new design of friction base isolator named as sliding resilient-friction system was developed by combining the desirable features of Electricite de France and resilient-friction base isolator system. The peak acceleration transmitted to the superstructure was limited to μg for pure friction system, the sliding resilient-friction and the Electricite de France system, while sufficiently flexible rubber bearing isolator could even reduce the acceleration transmitted to superstructure.

Giuliani [1991] described the practical problems associated with the design of a group of base isolated buildings. Design aspects of some of first seismically base isolated structures in Italy were summarised. A net saving of 7% was achieved for base isolated structures as compared to conventional structures besides the increase in factor safety of the buildings. Sub structures were specially designed with provisions of man holes for periodic maintenance of bearing. Large relative displacement between building and surrounding soils were expected. To account these issues necessary provisions were made for water tightness of basement, entrances to the buildings, connections between adjacent buildings and duct connections. Steel reinforced rubber bearings isolators were used in the buildings.

Arya [1994] reviewed the various concepts of seismic response control approaches. Some examples of energy dissipation devices employed in seismic response control using steel plasticity, viscous fluid or lead were presented. An alternative methodology was developed to mitigate the horizontal response of low cost masonry building without

using any seismic control devices. The basic concept was to allow the superstructure to slide above plinth level by providing oily surface between superstructure bottom and plinth top. Experimental result reported a two-third reduction in acceleration responses under input earthquakes Koyna 1967 and El Centro 1940 earthquakes.

Park *et al.* [2002] carried out a comparative study on the performances of various base isolated systems such as pure friction, laminated rubber bearing, lead rubber bearing, resilient-friction base isolator and Electricite de France systems. They carried out sensitivity analysis for variation in natural period of the base isolated bridge and friction coefficient of the bearings, which were determined by reciprocal relationship between peak deck displacement and the peak overturning moments of the bridge. From the study, it was recommended to use first natural period of deck shorter than 4.0sec to avoid excessive deck displacement. It was also observed that the peck displacement increased with the increase in first natural period of isolated deck and as the friction coefficient of the device was decreased. Contrary to this, peak overturning moment was observed to increase with the increase in first natural period and as the friction coefficient was increased. With the selected design parameters, peak responses of bridge with friction type bearings were less sensitive to substantial variations in the frequency range and earthquake excitation as compared to rubber bearings.

Kelly [2009] presented the origin and development of base isolation system in various parts of the world. Two basic types of isolation system and their working principle using elastomeric bearings and sliding systems and their working principle were described. Pacific earthquake engineering research centre of the University of California at Berkeley was the pioneer centre to start the research on natural rubber bearing building isolators. Large numbers of theoretical and experimental studies were conducted. A review of the base isolated structures using rubber isolators in different

countries like Unites States, Japan were present in this paper. Stability, rollover behaviour and failure issues of isolators were addressed. Manufacture of bearing with high vertical load carrying capacity and size up to 1.5m in diameter were reported.

Detailed review and comparison among different base isolation systems were presented by various researchers. The review of origin, development of base isolation in different parts of world and their working principles were presented in literatures. This will thus help in enhancing the understanding of the state of the art of the system and applicability of different base isolation systems to protect structure against earthquake motion.

2.3. Experimental and Analytical Study of Elastomeric Isolators

Analytical and experimental study of both steel and fibre reinforced elastomeric bearings were studied by various researchers to determine the mechanical properties and stability of bearings. Laboratory testing of scaled and prototype bearings were also reported in literatures. Reviews of some of these literatures relevant to present study are summarised below.

Derham *et al.* [1985] developed rubber bearings for protecting buildings and their contents from earthquakes damage without requiring additional mechanical devices to enhance damping or to avoid problems of wind movement. Laboratory investigations indicated that the structure when isolated would experience a reduction in peak acceleration of around tenfold as compared to the peak acceleration experienced by similar structure with conventional foundation. These study include the field investigations, verification testing for displacement demand and cost comparison of building with and without base isolation.

Koh and Kelly [1989] studied the visco-elastic stability of high-damping rubber bearing. Axial load influence the stability and dynamic behaviour of elastomeric due to large horizontal displacement during earthquakes. An alternate analytical solution method was used to solve the Heringx's column theory to find the horizontal stiffness of elastomeric bearing carrying axial load. Horizontal cyclic loading tests of elastomeric bearings carrying constant axial load was carried out. Two bearings with and without lead plug was tested. The correlation between developed analytical model results and experimental results were explained.

Aiken *et al.* [1989] presented a report on the mechanics of low shape factor (LSF) elastomeric isolator used for seismic base isolation. LSF bearings are used to serve the purpose of seismic isolation in both vertical and horizontal directions. This report covered the basic design, manufacturing and testing of bearings including analytical verification. Extensive non-destructive testings were carried out with different loading conditions to evaluate the behaviour of bearing. These tests were performed on elastomeric bearing with bolted and doweled end connections. Various mechanical properties such as shear stiffness, vertical stiffness and damping of LSF bearings were determined from the test and results were compared. Performances of different bearings under different loading conditions were evaluated and comparisons of results were presented. It was concluded that vertical behaviour of different types of bearings were not influenced much by different types of end connections.

Stanton *et al.* [1990] studied the stability of steel laminated elastomeric bearings. They extended existing theories used to analyse the conventional buckling to evaluate the influence of axial shortening in the buckling stability of elastomeric bearings. Two different bearings were selected for testing and correlation results with theoretical results. Buckling load, bending stiffness and compressive stiffness test result were

compared with the basic theory and discrete layered model theory was developed. Generally, bridge design codes restrict the height to width ratio to prevent buckling instability of laminated bearings. Due to this restriction, bearings are very stiff in horizontal direction and results in costlier superstructure. The researchers provided a mathematical formulation derived from existing theory to predict the buckling load of SREIs. This formulation allowed to design more slender stable bearing under the specification of bridge design codes.

Chalhoub and Kelly [1991] developed the governing equation for hydrostatic pressure in the elastomer including bulk compressibility. The solution of equations of pressure under pure compression and pure moments were provided for long rectangular strip elastomeric isolator. Effect of shape factor on pressure distribution of isolator was derived. Compression modulus was overestimated for large shape factor bearing if the material was assumed incompressible. They recommended the use of bulk compressibility effect in the design of bonded rubber isolator and bulk compressibility could be ignored for very low shape factored bearings.

Nagarajaiah *et al.* [1991] developed an analytical model and solution algorithm for nonlinear dynamic analysis of three dimensional base isolated structures supported on elastomeric or sliding isolation bearings. Three dimensional analysis was carried out for the base isolated system considering nonlinear behaviour of isolator and elastic behaviour of superstructure. The solution algorithm developed especially for analysis of base isolated structures with elastomeric and sliding isolation systems to overcome the deficiency of existing programs, which were not capable of modelling sliding isolation systems accurately. Stick-slip behaviour of sliding bearing was represented by using hysteretic model. Shake table analysis results of previous experiments were compared with the result from the program developed by the researchers. Various dynamic

responses of a six-storey reinforced concrete structure obtained using the developed algorithms were also verified with the results of ETABS and DRAIN-2D.

Aiken *et al.* [1992] created an extensive data base for design of elastomeric bearings and refinements of analytical models. Three types of elastomeric bearings were tested under different loading conditions. Different types of rubber material such as a mixture of filled natural rubber and synthetic rubber, low modulus, filled natural rubber and unfilled natural were used to manufacture these bearings. Mechanical properties of isolators were determined by conducting tests under series of cyclic lateral displacements with varying axial loads, lateral displacement amplitudes and loadings frequency. Monotonic shear failure test and monotonic tension failure test of bearing bolted to their endplates were conducted. It was observed that the variations of axial load and rate of loading had very little effect on the bearing stiffness and damping properties of isolator for moderate level of shear strain.

Tsai and Lee [1998] derived a closed form solution for the compression stiffness of circular, strip and square shapes elastomeric layer bonded between rigid plates. The approximate pressure solution proposed by earlier researcher is only valid for high shape factor elastomeric layer with Poisson's ration of material between 0.49 and 0.50. Exact equilibrium equation and solution were presented by satisfying the boundary conditions, without using any approximation for normal stress component. The compressive stiffness calculated from proposed equations was compared with the FE result for validation for all values of Poisson's ratios.

Imbimbo and Kelly [1998] presented an analytical method to capture the behaviour of strain induced crystallization of elastomer at large range of shear strain. This strain induced crystallization at large shear strain enhanced horizontal stiffness of elastomeric bearing bolted to their endplates as compared to bearing doweled to their endplates.

They extended the linear elastic theories presented by Koh and Kelly (1986) to determine the buckling load carrying capacity of elastomeric bearing by replacing shear modulus by shear modulus-shear strain relationship. The analytical model adequately represented the stiffening behaviour of elastomeric bearing and result showed a good agreement with experimental result.

Naeim and Kelly [1999] wrote a book on the design of seismic isolation bearing and its theory in details. They compiled all the existing theories and equations available on this subject for complete design and analysis of elastomeric bearing used in seismic base isolation. Theoretical basis of seismic isolation, code provisions, mechanical characteristics including buckling and stability phenomena of elastomeric isolator were presented. Design examples and computer aided analysis by using different software such as N-PAD, 3D-BASIS, ETABS AND SAP-2000 were also included.

Tsai and Kelly [2001] carried out theoretical analysis of single layered elastomer bonded to flexible reinforcement to study the influence of reinforcement on the mechanical properties of FREI. Analyses were carried out for infinite long strip isolators, rectangular isolators and circular isolators subjected to compression loading and pure bending. Flexibility of reinforcement was included in the Pressure solution approach developed by Kelly to evaluate the stiffness of FREI. It was shown that shape factor and flexibility of reinforcement affect the compression and bending stiffness of FREI, evaluated from pressure solution. They observed that stiffness of circular reinforced isolator varied with the Poisson's ratio of reinforcement and this influence became insignificant as the reinforcement become more rigid. Approximate boundary conditions were applied for the solution of stiffness of rectangular isolator and the solution became independent of Poisson's ratio.

Koh and Lim [2001] presented the analytical formulation of compression stiffness of

bonded rectangular layer of elastomer. Using two kinematic assumptions and applying the principle of variable transformation, governing equations for compression stiffness of bonded rectangular elastomeric were derived and solved. The limitation of incompressibility of material which led to overestimate the bulking load and resonant frequency was also overcome by the theory. The square and strip layer of elastomer were special cases of their theory and compression modulus calculated by this theory was identical with the results of previous research. Parametric studies carried out by them showed that compression modulus decreased with the elongation for a given value of shape factor and Poisson's ratio.

Kelly and Takhirov [2001] carried out theoretical and experimental analyses for the evaluation of mechanical characteristics of multi-layer elastomeric isolation bearings, where the reinforcing elements, normally steel plates were replaced by fibre reinforcement. Compression stiffness of isolator with flexible reinforcement was derived. Four 305 mm diameter isolators were tested in shear in pairs under a vertical load equivalent to a pressure of 6.90Mpa. They were tested in cyclic shear, with three fully reversed cycles at three maximum strain levels of 50%, 100% and 150%. The test result showed that it was possible to use un-bonded isolators for seismic isolation of structures. Although a considerable amount of edge uplift occurs, the force-displacement curve always had positive stiffness, indicating that the bearing was still stable at 150% shear deformation even though it appears to be undergoing roll over deformation.

Mechanical behaviours in a laminated rubber bearing with different layer thickness or different layer diameters were analysed by Chang [2002]. From Haringx's theory, a closed form element stiffness matrix of a single rubber layers were derived. By using the obtained stiffness matrix, an analysis model for laminated rubber bearing was

successfully constructed. The model was discrete, in contrast to Haringx's continuous model, so it allowed internal forces and displacements to be computed at individual layers. Examples were presented to study the mechanical behaviour of laminated rubber bearings with different parameters. From these examples, it was shown that the developed method was most useful when studying the mechanical behaviours in a laminated bearing with different layer thicknesses.

Tsai and Kelly [2002] presented a theoretical approach for analysing the compressive stiffness and bending stiffness of fibre-reinforced rectangular isolators. The influence of fibre flexibility on the stiffness of isolators was studied. In addition to theoretical stiffness solution which was expressed in series form, simplified stiffness formulae based on the solutions of an infinitely long strip pad were also presented.

Tsai and Kelly [2002] presented a theoretical approach to analyse the bending stiffness of fibre-reinforced circular isolators. The elastomer was assumed to be incompressible and pressure dominant. The stiffness formula was derived. The influences of fibre flexibility on the mechanical properties of fibre-reinforced circular isolator subjected to pure bending moment were studied. Mechanical properties such as the pressure in elastomer, the stress in reinforcement and the bonding shear stress between elastomer and reinforcement affected by the bending moment were presented.

Moon *et al.* [2002] designed and manufactured some specimens of fibre reinforced multilayer elastomeric isolator using different kinds of fibres such as carbon, glass, nylon and polyester. They carried out experiments to determine their mechanical characteristic and to evaluate the performance of those specimens. They also compared the mechanical characteristic of the carbon fibre reinforced isolator with a similar steel reinforced isolator. Experiments showed that performance of the carbon fibre reinforced isolator was even superior to that of the steel reinforced isolator in view of vertical

stiffness and effective damping. They concluded that fibre reinforced isolators could replace steel reinforced isolator. Carbon and glass fibres were used to compare the vertical stiffness. The effects of carbon reinforcement and glass fibre reinforcement on vertical stiffness were examined. The result showed that vertical stiffness of carbon fibre reinforcement was higher than that of glass fibre reinforcement. Vertical stiffness of carbon fibre reinforced elastomeric bearing was three times higher than the vertical stiffness of the steel reinforced elastomeric bearing. Further, it was also observed that bulging of carbon fibre reinforced elastomeric bearing was lesser than the bulging of steel reinforced elastomeric bearing. This is because of more number of fibre layers in carbon fibre reinforced bearing than that of steel reinforcement layers in steel reinforced bearing.

Experiments and analytical study of strip isolator were carried out by Kelly and Takhirov [2002]. Conventionally, base isolation systems were designed to be isotropic and base isolators were always considered to be symmetric. So, the isolators being manufactured currently were either circular or square in shape. However, using long strips of rectangular isolators had many advantages over conventional isolators, especially in case of buildings where walls provide lateral resistance. Generally at base level of base isolated buildings, wall beams are provided between isolators to carry the load of walls. This base level wall beams can be avoided by using long strip isolators on continuous wall footing of the building. The test result showed that the concept of a strip isolator reinforced with carbon fibre was viable. The isolator could be made in long rectangular strip and cut to the required width for use as a strip below wall of the building. Manufacturing cost of large size rectangular strip isolator will be less as compared to the manufacturing of individual circular or rectangular isolator.

Tsai [2003] carried out flexure analysis and developed governing equations for

horizontal displacements function of circular elastomeric layer bonded between rigid plates subjected to pure bending. The horizontal displacement functions were solved by satisfying the stress boundary condition of the bonded elastomeric layer. Horizontal displacement in the middle plane of the layer and effective bending modulus calculated from the theoretical solutions were shown to be very close to the FE analysis result. The bonding shear stress in radial direction as obtained from theoretical solution was very close to FE analysis result except at the edges of circular layer. The bonding shear stress in tangential direction obtained from theoretical solution and FE analysis result showed large variation apparently due to numerical error in FE analysis.

Kelly [2003] derived the tension buckling load for elastomeric bearings. The tension buckling load would not be achievable in practice in most bearings since it would generally be much larger than the load that would induce cavitation in the elastomer. This could occur when extreme seismic loading on an isolated building would induce global overturning. Isolator at the periphery of the building could be in a state of combined tension and shear.

The effect of hole and lead plug on the FREI were studied by Kang, *et al.* [2003]. Experiments were carried out to evaluate and compare the performances of fibre reinforcement with steel reinforcement. The hole and lead plug effect on effective stiffness and effective damping of carbon FREI were also studied. From the experiments, the performance of the FREI was observed to be superior to that of the SREI in respect of horizontal stiffness and vertical stiffness of the isolator. It was shown that hole and lead plug did not make much difference with FREI without hole and lead plug.

Tsai [2004] derived a closed-form solution for the evaluation of compression stiffness for laminated elastomeric bearing of infinite-strip shape considering flexibility of

reinforcement sheet. Three types of the elastic layers bonded to flexible reinforcements were studied. The first type simulated the interior elastic layers of the bearings with shear-free ends. The second type simulated the exterior elastic layers of the free-end bearings. The third type simulated the elastic layers in the bearings where ends were bonded to rigid plates. In bearing with rigid reinforcements, each bonded elastic layer had the same compression stiffness because of rigid reinforcement. However, this might not be applicable to the bearings with flexible reinforcement, where the compression stiffness of bonded elastic layers varies with the deformation of flexible reinforcements. Moreover, the boundary condition at the ends of the fibre reinforced bearings could also affect the compression stiffness. When performing the compression analysis of the bearing subjected to vertical loading only, two types of boundary conditions could be imposed at the ends of the bearings, which were referred to as 'free end' and 'rigid end'. 'Free end' means the end of the bearing did not have any horizontal constraint so that it was free from any shear force. 'Rigid end' means the end of the bearing was bonded to rigid plate so that it did not have any horizontal deformation. The author showed that the theoretical solutions to the compression stiffness of the bearings were really close to the result obtained by the FE method.

Moon *et al.* [2004] provided the results of theoretical and experimental study of FREIs. Several samples of strip isolator were designed, manufactured and tested to prove its effectiveness in base isolation of building subjected to earthquake motion. The experiments on several specimens of isolators were carried out to determine the vertical stiffness and horizontal stiffness under a constant vertical load. Horizontal stiffness of strip fibre reinforced isolator in 0^0 and 45^0 direction were found to be superior to conventional rigid reinforced isolator. Further, the study suggested that the time period of building could be adjusted by staking strip isolator one above another.

Tsai [2005] developed closed form solution having faster convergence by extending the pressure solution approach to solve the compression stiffness of rectangular elastomeric layer bonded between rigid plates. The assumption of incompressibility of rubber material generally overestimates the compression stiffness and tilting stiffness of rubber layer bonded between rigid plates. The results of the closed form solution developed by using approximate shear boundary conditions were in good agreement with the results of FE solution and previous research result of square and strip rubber layers. The aspect ratio significantly affected the compression modulus when Poisson's ratio was closed to 0.5. The effect of relaxing the exact shear boundary condition was negligible on the compressive stiffness of rectangular layers but this relaxation would cause some error in calculation of horizontal displacement and bonding stress near the edges of rectangular layers.

The assumption of Haringx theory that plane section remains plane after the deformation of elastomeric bearing limits the study of influence of flexibility of reinforcement layer on buckling of isolators. Tsai and Kelly [2005] developed a theory that extends the Haringx theory by allowing the cross section to deform into a non-planner surface. The effect of warping and shear on the stiffness and buckling load of a beam carrying axial compression load and shear force at one end was derived. The numerical solution of buckling load of homogeneous rectangular and circular beam showed that buckling load increased with the increasing ratio of flexural rigidity to shear rigidity and cross section warping had also effect on buckling load.

Analysis was carried out by Tsai and Kelly [2005] for the evaluation of buckling load of multilayer elastomeric isolators considering the effect of flexibility of reinforcement layer. The analysis treated the isolator as short elastic column in which shear deformation and warping of the cross-section were included. A cubic equation for the

buckling load of the isolator was derived. The buckling load of the isolator was a function of the ratio of elastic modulus between the elastomeric layer and the reinforcement, the shape factor of the elastomeric layer, the width-thickness ratio of the reinforcement and the width-height ratio of the isolator. The buckling load decreased with reduction in reinforcement thickness.

Tsai [2006] derived closed form solution for the compression stiffness of circular bearing consisting of elastomeric layers interleaved with flexible reinforcement. The closed form solution was proposed incorporating the effect of bulk compressibility of reinforcement layer and boundary condition at the ends of bearing. Two types of boundary conditions were considered while performing the compression analysis with only vertical load. In the first type, ends of the bearing were not restraint against lateral displacement and it was free from any shear force. In the second type, ends of the bearing were bonded to the rigid plates so that its ends were restraint against lateral displacement. The theoretical and FE results showed that the end boundary conditions and flexibility of reinforcement affected the compression stiffness of elastomeric bearing.

Fibre reinforcement in elastomeric isolator provides in-plane rigidity when it is stretched, but loses rigidity when it is compressed. Tsai [2008] developed the solution to include this 'tension-only' nonlinearity in the deformation analysis of FREI. He developed the procedure to include this type of behaviour in deformation analysis of fibre reinforced elastomeric bearings. To validate the developed procedure, FE analysis of isolator was carried out and it showed a good agreement with FE result. The result showed that thickness reduction of elastomeric layers and tilting angle was proportional to the variation of compression force and bending moment. The lateral force variation effected the vertical buckling load carrying capacity of elastomeric bearing with

'tension-only' reinforcement and it was smaller than the buckling load of bearing with linear reinforcement.

Pinarbasi and Mengi [2008] formulated equation for the analysis of elastic layers bonded to flexible reinforcement under uniform compression, pure bending and pure warping. The limitations of previous methods considering some assumptions on stress and/or displacement, geometrical and material properties were eliminated by this formulation by representing the displacement and stress distribution in the elastic layer in terms linear combination of a complete set of shape functions. The governing equations were derived in general form and used to solve the infinite-strip elastomeric isolator bonded to flexible reinforcement. It was found that shape factor, Poisson's ratio and reinforcement stiffness have significant effect on layer stiffness, displacement, stress distribution and location of maximum stress in the elastic layer.

Nezhad *et al.* [2008] studied the lateral response characteristics of square FREI in an un-bonded application. Isolators were manufactured by using unfilled soft neoprene compound as elastomer and bidirectional carbon fibre fabric as the reinforcement. They conducted lateral cyclic testing on $1/4^{th}$ scaled carbon FREI bearings. The bearings were employed in an un-bonded application as they were not attached to the upper and lower platens of the test machine. As the fibre reinforcement had no appreciable flexural rigidity, the un-bonded application resulted in a stable rollover deformation in the bearings when they were laterally deformed. They found that effective lateral stiffness and damping increased with an increase in the rate of lateral displacements.

Nezhad *et al.* [2008] provided a brief literature review on the experimental investigation carried out on FREI. They manufactured FREI using soft compound of natural gum rubber as elastomer and bi directional carbon fibre fabric as the reinforcement. Bearings were fabricated without using mould. Vertical compression test, rate sensitivity test and

cyclic lateral load test of bearings were conducted to evaluate the performance of FREI. Influence and first and second shape factors were reported in the study.

Ashkezari *et al.* [2008] designed, manufactured and tested FREI. Dynamic and mechanical characteristics were studied by performing vertical and cyclic horizontal tests. To manufacture the fibre reinforced isolator, initially the woven fibres were completely impregnated by adhesive. The raw rubber compounds which were filled with carbon black, was also formed as sheets of desired thickness. The fibre layer and raw rubber sheets were then cut to desired dimensions and set in the mould. For comparison of mechanical properties of FREI, a similar type of steel reinforced isolator was also tested and test result showed that behaviour of the manufactured FREI was similar to that of steel reinforced isolator. Therefore, the FREI was named as 'steel like FREI'. It was observed from the test that the effective shear modulus decreased, when the horizontal test was repeated at different shear strains. In contrary to this, damping values of isolator increased for the above sequence of test.

Nezhad *et al.* [2009] carried out parametric studies of un-bonded FREI to investigate their vertical and lateral behaviour. They evaluated the influence of amplitudes histories on lateral displacement and variations in vertical loads on isolators. Two types of sinusoidal lateral displacement time histories were considered for the study. The first type was ascending lateral displacement pattern and second type is descending lateral displacement pattern. Significant stiffening behaviour was observed at the ends of hysteresis for the test with ascending types of lateral displacement. However, this response was not observed for the test with descending types of lateral displacement. Generally for 0^0 and 90^0 orientations, bearing exhibit higher effective stiffness and lower damping ratio as compared to 45^0 orientation. Damping ratios of tested bearings were higher than that of elastomer layers and it was postulated that additional damping

was attributed by the relative volume of fibre to elastomer. Vertical cyclic loading test result showed that effective stiffness and damping ratio increased with the increased vertical pressure. From the test result with different loading cycle and variation of pressure, it was concluded that the full scale FREI can be used to mitigate the seismic response of structures located in moderate to high seismic regions.

Nezhad *et al.* [2009] presented two simplified analytical models to predict the seismic response of low rise building isolated using U-FREI. Both of these model were constructed from the load-displacement hysteresis loops of bearing testing results. In the first model, the parametric constants were evaluated from the lateral load-displacement hysteresis loops of cyclic shear test by using least square methods. In the second model, bilinear idealization of load displacement hysteresis loop was considered for prediction of response. Simplified equation with some parameters were derived for prediction of response of building supported FREI. These parameters were evaluated from the load-displacement hysteresis loops of the bearings. Iterative procedure was used for the evaluation of solution of equation to determine the responses of the building. Accuracy of both the models in predicting the responses of isolated structures were dependent on the input earthquake and discrepancy up to 24% and 23% were observed between the models in predicting the drift and base shear respectively.

Michael *et al.* [2011] investigated the stability of U-FREI bearing through experimental investigation employing two experimental procedures. In the first test, the stability of bearings was investigated by applying cyclic lateral excitation and monotonically increasing axial load. Bearing were tested under larger axial load and increased lateral displacement until hysteresis instability was observed. During the second test, the bearings were loaded to design axial pressure and unidirectional lateral displacement of 275% and 300% of rubber thickness were applied to the bearings. From the test result

and curve fitting method, the critical buckling loads of isolators were estimated. The transverse stiffness decreased with the increase in axial load and critical buckling load was the axial load where transverse stiffness was zero. Critical buckling decreased with the increase in excitation amplitude. Effective stiffness of FREI bearing decreased with the increase in axial load and difference in effective stiffness between first cycle and second cycle of lateral displacement were more prominent with higher axial load. Effective damping of the bearing increased with the increase in axial load on the bearings. The tested bearings maintained a positive lateral stiffness during the rollout test with lateral displacement up to 300% rubber thickness.

Van Engelen *et al.* [2012] simulated the load displacement behaviour of U-FREI using a bilinear model calibrated using experiments data. They conducted study of two strip FREI, with and without holes in the loaded surface area to modify the vertical and horizontal properties of isolators. It was observed that the bilinear model matched the experimental hysteresis loops at low and moderate displacement amplitudes. The seismic response of isolator with holes had lower values as compared to the isolator without holes. Hence, it was observed that with proper design modification of isolator by introducing holes, the seismic repose of a base isolated structure could be minimized.

Sanchez *et al.* [2013] carried out comprehensive experimental studies of bonded SREI to determine their stability. Tests were carried out using three different methods. In first method, the axial load was monotonically increased until the horizontal load resistance of the bearing become zero or negative under a predefined horizontal displacement. Method 2 was a quasi-static experimental procedure, where monotonically increasing horizontal displacement was applied to the bearing under a constant vertical load until the bearing reached its stability limit. In third method, the stability of bearing was

investigated under extreme ground motion generated by earthquake simulator. The study showed that quasi-static test method provided a direct estimate of critical load carrying capacity of bearing without requiring further analytical estimation. Dynamic stability test indicated that the bearing was able to recover and re-centre its original position beyond the stability limit. Dynamic stability limits were concentrated at large displacement with low axial load due to limitation of testing. This study concluded that instability of bearing was rear for ratio less than 0.2 of critical load in deformed configuration obtained by reduced area method to the critical load obtained at the un-deformed configuration.

Russo *et al.* [2013] proposed a simplified analytical model to calculate the horizontal stiffness of U-FREI by modifying the formula used to calculate horizontal stiffness of steel reinforced isolator. Experimental result of vertical and horizontal stiffness of different specimen of isolator made with low and high damping neoprene reinforced with bidirectional and quadri-directional fabric were presented. Effect of aging on stiffness and damping were also summarized. It was concluded that the process of aging leads to an increase in average horizontal stiffness and reduction in damping ratio. Isolator with quadri-directional fibre reinforcement exhibited higher horizontal stiffness than isolator with bidirectional fabric. The proposed formula for calculating the horizontal stiffness was based on the simplified geometrical configuration of the displaced isolator. Shear modulus was considered as constant and this value was assumed to be independent of shear strain applied in the elastomer.

Russo and Pauletta [2013] carried out investigation for the evaluation of influence on friction behaviour of different parameter such as compressive stress, shear strain, concrete roughness, aging etc. of U-FREI. Isolator with shape factor between 20.53 and 25.7, the lateral stiffness increased with the increase in compressive stiffness.

Elastomeric compound influenced the sliding behaviour of U-FREI. Isolator made with non-seismic compound like poly-chloroprene required almost 50% more compressive stress to limit the sliding as compared to the isolator made with natural rubber. Lower limit of minimum compressive stress of aged isolator should be assumed 50% than un-aged isolator to avoid sliding instability. Higher loading rate increased the stiffness and maximum force of isolator as compared to lower loading rate and quasi-static test results provided conservative strength values with respect to those actually occurring. The limiting value of compressive stress recommended to avoid sliding instability was based on the particular geometry and shape factor of isolator, which might not hold good for isolators with different geometry, shape factor and aspect ratio.

Nezhad [2014] presented two simplified analytical model to evaluate horizontal stiffness of U-FREI. These two models were derived based on the geometry. The net contact area and free area of the bearing under horizontal displacement was used to derive the horizontal stiffness of bearing. Results of analytical solution for horizontal stiffness showed a close agreement with FEA results with maximum error up to 13%. These formulae can be used for preliminary design of FREI. However 3D effects were neglected and influence of vertical load and stress-softening of elastomer were not addressed in the developed simplified model. Limitation of these models were identified by the author.

Naghshineh *et al.* [2014] carried out experimental studies to compare the fundamental properties of fibre meshed reinforced elastomeric with the conventional SREI. Influences of lead in both types of isolators were also investigated. Steel-reinforced bearing have higher horizontal stiffness as compared to fibre mesh reinforced bearing. However, damping values are comparable for the bearing without lead core. Presence of lead plug increased the horizontal stiffness of fibre mesh reinforced bearing up to 52%

and conventional bearing up to 89% at 100% strain level of the tested bearings. Experimental results of vertical stiffness were compared with the theoretical results from existing literature and observed that for low shape factor bearing, the experimental results were comparable with the theoretical result. However, for high shape factor bearing, the effect of material incompressibility played a vital role. Presence of lead plug reduced the difference of vertical stiffness between the fibre mesh reinforced isolator and conventional isolators.

Verumu *et al.* [2014] presented a nonlinear analytical model capable of modelling the dynamic response of bearings more accurately at all displacement ranges, especially beyond the stability limit. The results obtained from this analytical model was verified with experimental data from an earlier experimental study. It was observed from the results of dynamic experiments that the bearings have a far larger capability to sustain horizontal loads at displacements exceeding their stability limit than predicted by earlier models and more importantly the bearings re-centred themselves after these large displacement excursions.

In this sub-section, the stability of rubber bearing and analytical model for determining the mechanical properties of elastomeric bearing with rigid reinforcement are reviewed. Initially, theory of rigid reinforcement bearing is extended by Kelly, incorporating the influence of flexibility of reinforcement to analyse FREI bearings. Pressure solution approach is used to find out the compression stiffness of single layer of elastomer bonded to flexible reinforcement. Due to complex behaviour of rubber, bonded to flexible reinforcement, solution for horizontal stiffness is not reported in any literature. Recently, approximate solution for horizontal stiffness is reported in literature by considering approximate deformed cross section of displaced isolator. However, in all calculation, initial shear modulus is considered to determine the horizontal stiffness and

buckling load capacity of isolators. Influence of shear modulus of elastomer at large shear strain is not accounted in the solutions. In all the literature, a preliminary geometry of the isolator is assumed and bearing is manufactured for testing. Experimental investigations are carried out to determine the mechanical properties of isolators. The basis of assumption of preliminary geometry is not reported anywhere.

2.4. FE Analysis of Elastomeric Bearing

FEs modelling and analysis of rubber material is a challenge using modern commercially available software. Brief review of relevant previous research on material modelling and analysis of elastomeric bearing reinforced with steel and fibres are summarized below.

Jankovich *et al.* [1981] developed a FE method for nonlinear analysis of rubber part and results are compared with closed from solution of Mooney material. They proposed penalty type FE formulation for highly incompressible materials. The experiments and analytical results were observed to be in very good agreement for local elongation up to 110%.

Lim and Herrmann [1987] presented an equivalent homogeneous, orthotropic model analysis procedure and FE analysis of elastomeric bearing of arbitrary shape subjected to arbitrary loadings. The accuracy of three dimensional model result was partially verified by showing that it produced similar result to the earlier two dimensional theory.

Sussman and Bathe [1987] provided a displacement-pressure (u/p) based FE methods for compressible and nearly incompressible solids having material and geometrical nonlinearities to overcome the difficulties of displacement based analysis. In this formulation the pressure computed from the displacement field was explicitly replaced by a separately interpolated pressure using a general procedure. Material model

description such as isotropic linear elasticity, anisotropic linear elasticity, von Mises elasto-plasticity, Mooney-Rivilin nonlinear elasticity and Ogden nonlinear elasticity were implemented in the formulation. Some examples were solved using the u/p formulation, including the contact analysis of rubber material to demonstrate the robustness of the process.

Chang [1988] investigated three commercially available software ABAQUS, B-RUBBER, and MARC for FE analysis of rubber material. Basic mechanics, element technology, numerical solution schemes, contact elements and slip/friction features adopted in the three codes were compared by the investigator. After comparison of analysis capability, ABAQUS was used for modelling the load displacement behaviour of a rubber seal used in automobile industry.

Herrmann *et al.* [1989] conducted parametric study using FE for wide range of elastomeric bearing. Computer codes were developed for the FE analysis for plain strain (2D) conditions and for general 3D conditions. Results were presented in non-dimensional form in order to extend the use of these results to a wide range of bearing designs. Various parametric study result presented for different shape factors included the effect of elastomeric parameter on compressive response, effect of reinforcement stiffness on compression response, effect of bulking on compressive response, effect of eccentrically loading on compressive stiffness, effect of shear response on compressed bearings, beading effect on compressed bearings and combination of bending, shear on compression. Modified shape factor definition was provided for different 3D elastomeric bearings.

Kulak and Wang [1991] presented the methodology for performing 3D FE analysis of individual rubber bearings and for simulating the response of 3D systems of isolated reactor structures including the surrounding soil under earthquake excitation. The

NEPTUNE computer program was used to perform the 3D analysis of bearing. An eight node hexahedral element was used to model the elastomer with Mooney-Rivilin material. A four node quadrilateral plate element was used to model the interleaved steel plates. To model the global response of isolator and isolated structure with surrounding soil, a preliminary computer program was developed. Two sample problems of strip and cylindrical bearings were analysed using the code. Response and performances of structures with and without elastomeric bearings were compared.

The continuum formulation of finite strain visco-elasticity and its numerical simulation with FE method were studied by Holzapfel [1996]. For sufficiently slow processes, the material responded in rubbery elastic manner which was modelled with an Ogden type material model. Ogden model, with only three pairs of coefficients known from empirical rubber elasticity, excellently replicated the finite extensibility domain of polymer chains and represented the best-known approximation to real behaviour.

Lee and Oh [1999] carried out FE of analysis of laminated rubber bearings to determine the buckling load carrying capacity of bearing with an aim to formulate numerical technique for critical load analysis. Buckling load under the combined action of compression and shear was calculated using Southwell method from load-displacement curve for each shear displacement. The 2D FE analysis to study the buckling behaviour of bearing was performed using computer program LUSAS, which has the capability to address geometrical and material nonlinearities including compressible and nearly incompressible material behaviour. It was observed that critical load obtained by FE method became smaller than the theoretical analysis when shape factors were larger than 5. From the study it was concluded that a significant reserve of vertical capacity of bearing exist even after the shear displacement reaches 40% of the width of bearings.

Jerrams *et al.* [2001] carried out the testing of rubber material to determine the material

properties required for FEs analysis. The uni-axial compressive test data were subjected to regression analysis to determine parameter of neo- Hookean and Ogden physical model properties for describing rubber material in FE program. Physical properties of rubber material were influenced by the technique used for manufacturing. Cross linked density influence the force in elastomer, since high cross linking material were less prone to swelling. Force displacement behaviour of elastomeric bearing subjected to combined axial and shear loading were compared by using FE analysis, test and theoretical analysis. The force-displacement relationship as obtained from FE analysis using Ogden material model differed slightly with the test result. However, the Neo-Hookean model under-predicted the force by around 22.5% at 2mm displacement.

Matsuda [2004] evaluated mechanical properties of natural rubber material (NR) which had very small damping and the high damping rubber material (HR) which had large material damping. He formulated a displacement/pressure mixed FE method for hyper-elastic material like rubber by considering compressibility, visco-elastic and damage model. The strain energy function for NR material was derived, which gave stress response of rubber material. For high HR, strain energy function was defined by using the material modulus and strain energy function of natural rubber material. Visco-elastic and softening properties were observed in the result of the analysis of high damping rubber bearing.

Amin *et al.* [2006] proposed an improved hyper elastic model for compression and shear regime to represent the rate independent instantaneous and equilibrium responses and implemented in general purpose FE program. Numerical study on a rubber block subjected to compression and combination of compression and shear was carried out to verify the FE analysis code.

Mordini and Strauss [2008] carried out numerical investigation and parametric study of

high damping rubber bearings strengthened with glass fibre to find out its mechanical behaviour under both static and dynamic loads. Parametric study was performed numerically by using commercial FE code ABAQUS and modelling technique was also described. The hyper elastic behaviour of rubber material was defined by Ogden model. For static analysis, vertical load was applied in several steps and horizontal displacement was applied keeping the vertical load constant. In dynamic analysis, the mass was applied to the top surface and acceleration time history was applied to the bottom surface. Computational time for analysing full scale 3D model of base isolated structures including nonlinear behaviour of bearing is very high and expensive. Therefore, an alternative solution methodology was proposed in the study to include the bearings in full scale 3D model analysis. Comparison of vertical and shear displacement for analytical and numerical solution showed close agreement but in contrast, horizontal stiffness provided different result as the shear displacement increases. FE analysis of liquid storage tank was performed for both isolated and fixed based condition. All the analyses showed substantial reduction in dynamic responses using bearings and validity of design was also established.

Hyper-elastic behaviours of rubber-like materials were mostly model by Mooney-Rivlin and Ogden model. In both of these material model, at least uni-axial and bi-axial stretching test results were required to fit the material model. Sasso *et al.* [2008] carried out uni-axial and equi-biaxial test coupled with optical devices to measure the real time values of stress and elongation level of specimen. Test data were used to calibrate the constitutive model and FE analysis results were compared with the test result. They concluded that the use of second order Mooney-Rivlin model and Ogden model in FE analysis produced the most accurate result among the various models available.

The lateral responses of both bonded and U-FREI under monotonic loading were

investigated using FE based analysis by Nezhad *et al.* [2011]. Plain strain FE analyses of strip FREI with bonded and un-bonded conditions were carried out. Different states of stress within the isolator were also evaluated. It was shown that tension in the stable U-FREI was limited to outer rubber layer at the regions where the bearing had rolled of support. Further, tensile stress in the U-FREI was shown to be much lesser as compared to bonded FREI. Vertical load on the isolator was carried by the central compression core in case of both types of isolator. Un-bonded isolator exhibited stable roll over deformation on application of horizontal load. Due to high geometrical nonlinearity in lateral direction, horizontal stiffness varied with isolator lateral deformation. No closed form analytical solutions were available for ascertaining the horizontal stiffness of this type of complex U-FREI. Further, closed form solution of even bonded FREI served for the preliminary design. They observed that the dependency of rubber material properties on the amplitude of the shear strain, rate and history of the lateral displacement on the lateral response of isolator were not addressed in the closed form solution. Hence, FE solution flowed by experimental load testing of FREI should be carried out before eventual installation in any structure.

Kelly and Calabrese [2012] presented the study report of the mechanical behaviour of un-bonded fibre reinforced elastomeric bearing. The roll over deformation of bearing eliminated the tensile stresses in the bearing and thereby reducing the stringent bonding requirement of fibre and elastomer. They presented a comparison between the approximate linear elastic theory and the FE analysis result of strip, circular and square isolators. For FE analysis 2D models under plain strain assumption for strip bearings and 3D models for circular and square bearings were considered. The contact between isolator and support was modelled by Coulomb friction in MSC.Marc 2005 software. The FE result of the vertical load analysis of strip isolator for different shape factor

showed a good agreement with the pressure solution. The stress at peak horizontal force and with constant vertical load was twice the stress due to compressive load. Shape factor had only effects on the distribution of stresses in the bearings, but the magnitude of stress was same. FE analyses of circular and square bearings were carried out only for compressive load and comparisons of results with pressure solution were shown.

Dezfuli and Alam [2013] presented a multi-criteria optimization process for FREIs used in bridges. A numerical material was developed for high damping rubber using FE simulation to capture its highly nonlinear behaviour. The mechanical properties of high damping rubber bearing were modelled in FE software, ANSYS. The result showed that the effective horizontal stiffness, vertical stiffness and viscous damping are highly dependent on the shear modulus of the elastomer, number of rubber layers and thickness of FRP composite. Seismic behaviour of bridge structure supported on FREI were studied through dynamic time history analysis.

Osgooei *et al.* [2014] carried out 3D parametric numerical FE analysis on sixteen circular FREI bearings. All the bearing were of same overall dimensions, while the thickness of elastomer layers and the axial stiffness of reinforcement were the parameters that were varied. FE analysis results were compared with the predicted values obtained using the pressure solution and the pressure approach methods. FE analysis showed a good agreement with the result obtained from analytical solution. It was concluded that the end boundary conditions affect the vertical response of FREI.

Osgooei *et al.* [2014] carried out three-dimensional FE analysis to investigate the lateral response of square FREIs having different aspect ratios and loaded in different horizontal directions. The FE analysis results were validated using experimental test results. The result showed that effective horizontal stiffness of the bearing increased as the loading direction changes from 0^0 to 45^0. Further, as the aspect ratio was decreased,

the sensitivity of the lateral response to the loading directions also increased.

Spizzuoco *et al.* [2014] carried out the experimental study on the un-bonded square carbon recycled rubber-fibre reinforced bearings to investigate their lateral and vertical behaviour under seismic loading. The seismic performance of the bearings were investigated by means of both experimental tests and FE analysis. The effective lateral stiffness of the bearings decreased significantly with the increasing amplitude of lateral displacement. Similarly the equivalent viscous damping ratios of the bearing significantly increased with increasing lateral displacement. All bearings exhibited a rollover type of deformation when subjected to significantly large lateral loads due to the un-bonded boundary condition of the specimen.

In last few decades, FE modelling of rubber material was done using computer codes developed by researchers for particular industrial and research projects. However, use of commercial software for analysis of rubber parts was limited to automobile industry only. Limited use of FE method for analysis of elastomeric bearing was mainly concentrated on rigid reinforced bonded bearings. This limited application of FE analysis mainly attributed to material modelling of rubber and efficient computer code for modelling the hyper-elastic material behaviour of rubber. Previous studies suggested that Ogden material model gave suitable results of force-displacement behaviours of rubber like material. Some recent studies involving both 2-D and 3-D analysis of FREI were carried out to determine the mechanical properties and stresses at different level of elastomer and fibre by few researchers. The FE analysis for rubber material, though quite involve is observed to be pretty useful in assessing the distribution of stresses across layers of FREI and would thus help in more accurate estimate of design requirement.

2.5. Testing of Base Isolated building

Testing of base isolated building supported on different types of isolators were carried out by many researchers. Brief reviews of some of the literatures are presented in this section.

The early concept of base isolation was demonstrated by using of sand as a sliding medium against earthquake motion. Lee [1985] presented a sand slide slit base isolation technique to reduce the dynamic response of structure subjected to ground acceleration. A welded steel channel basement was fixed to the shake table. On this steel basement, a layer of terrazzo plates were laid facing the smooth surface upwards. A layer of selected sand was laid over the terrazzo plates and then covered with another layer of terrazzo plates with smooth faces towards sand. The test building was constructed over the terrazzo plates. Accelerometers were fixed at different location of the building to record the response of input El Centro earthquake to the shake table. The building constructed on the method of sand slide slit method was tested on a shake table. The same building was later tested with fixed based condition and damages in the building were observed. The test result showed that slide slit isolation method could reduce the seismic response of the masonry building.

Paulson *et al.* [1991] presented the result of experimental studies of two identical masonry buildings, one supported on base isolator and other with fixed base. Earthquake simulator tests were conducted on these buildings with a series of input base motions. Lateral response, drift and damage pattern of both the structures were compared and details data of the response of two structures were correlated including table acceleration, natural frequencies, stiffness, force distribution etc. The isolation systems comprised of natural rubber interleaved with seven steel shim plates. The acceleration of isolated structure was measured as 41% of fixed based structure. There

was no crack observed in isolated structure while large amount of cracking and yielding of reinforcement were observed in fixed based structure. The force and displacement histories of base isolated structure measured from experiments could be matched with the computed waveform considering the isolated structure as linear single degree freedom oscillator.

Deb [1993] carried out both analytical and experimental studies of laminated rubber bearing for seismic isolation of structures. Effectiveness of bearings were assessed by shake table test. A simple computer algorithm was developed to compute the seismic response of medium rise isolated building subjected to both unidirectional and bidirectional motions. From the shear test of bearing, it was concluded that shear modulus and shear stiffness decreased with the increase in shear strain level (up to 55% maximum strain) and increasing vertical load. Damping of bearing increased with the increase in vertical load on the bearing. Shake table studies confirmed that the peak acceleration at the roof level was reduced by 50% of the peak table accelerations.

Kikuchi and Aiken [1997] proposed an analytical model for accurately predicting the seismic response of elastomeric bearings. The analytical model was developed by modifying the Ramberg-Osgod model to take into account of high nonlinearities and stiffening behaviour of hysteretic loops of bearings. To verify the results of mathematical model, shake table tests were performed on four types of seismic isolation bearing that included two types of high damped rubber bearings, one type of lead rubber bearings and one type of silicon rubber bearings. The experimental and analytical results showed good agreement between peak values of responses, hysteresis behaviour, response accelerations and floor spectra.

Nagarajaiah and Xiaohong [2000] evaluated the seismic performances of base isolated USC hospital building during 1994 Northridge earthquake using a nonlinear analytical

model. The accuracy of model was verified using system identification and data recorded during the earthquake. Comparisons of responses of base isolated building were presented with a probable response if the building were of fixed base. For the purpose of verification of linear identification technique, a linear 3D model of base isolated structure was modelled with a rigid floor slab assumption. The comparison of absolute acceleration and relative displacements responses computed from nonlinear analytical model and data recoded during earthquake ground excitation in EW and NS direction were found satisfactory. The spectra of the recorded response and computed nonlinear analytical model matched well. However, response spectra of linear model were not matching with the recorded responses. The computed fixed based responses of the analytical models were few times higher than the base isolated building responses recoded and computed from nonlinear analytical model. The effectiveness of base system were captured by the authors and concluded that period lengthening and dominant fundamental model responses were the main reasons for the effectiveness of base isolation system. High damping in the fundamental mode provided additional reduction in the displacement of the structure. Further, base shear, acceleration and story drifts were decreased due to base isolation.

Wu and Samali [2002] developed a five-storey benchmark steel frame building model to study seismic response of isolated model using mild steel laminated rubber bearings. The benchmark model possessed the flexibility to test various building configuration due to its innovative connection design accommodating varying floor height, plan dimensions, masses on the building and base support types. The natural frequency and damping ratios of fixed based and base isolated structures were determined experimentally by impulse-hammer test and shake table test, which were validated by numerical analysis. From the numerical analysis result and shake table test, it was

confirmed that efficiency of isolator to attenuate the floor acceleration and inter storey drift against different earthquakes highly dependent on the types and nature of input earthquakes.

Lakshmanan *et al.* [2008] presented the result of experimental and analytical studies of a 1/3rd scaled reinforced concrete soft first storey structure supported on natural rubber based steel reinforced bonded bearings. The acceleration and displacement at various floor level were recorded from the test. The floor forces, shear, drift of structures and hysteresis loop of bearings were calculated from the recorded accelerations and displacements. Four different synthetic input earthquakes with different frequency contents were applied to the shake table for the tests. Acceleration and displacement response of base isolated structure were compared with the fixed base structure and substantial reductions in responses values were observed. The rigid body motion of the superstructure was observed for base isolated structure. Analytical validations of experimental results were done through the computer program developed for the purpose of linear elastic analysis of base isolated structures and it showed very good agreement for acceleration as well as displacement responses. They also suggested for further studies on rocking modes of base isolated structure based on importance of frequency content of earthquakes.

Nezhad *et al.* [2009] conducted a shake table study on a two storey structure having well defined elastic response characteristics supported on U-FREI. Detailed dynamic response result of shake table study of base isolated steel structure and corresponding fixed based structures were compared when subjected to three different input earthquakes. The initial fundamental frequency and equivalent viscous damping of the structures were determine by performing free vibration tests on the structures using Fourier amplitudes spectra of measured roof accelerations. Dynamic response

parameter measured at each floor level were used to calculate the inertia forces, base shear, base moment and inter storey drift of the structures. Lateral load displacement hysteresis of the stable U-FREI for maximum level of different input earthquakes were obtained from the shake table test. The maximum recorded accelerations at roof level were 24-32% lesser in base isolated structure as compared to fixed based structure. Similarly the base shear, base moment and total drift of the base isolated structure were 30-45%, 23-33% and 28-42% lesser respectively in base isolated structure as compared to fixed based structure. There was no damage to the bearings after the completion of entire test program. From the testing it was concluded that the U-FREI has significant potential of reducing the seismic response of structures in high seismic regions.

Nath *et al.* [2013] carried out the performance study of base isolated reinforced concrete prototype building located at Indian Institute of Technology, Guwahati, India. Two identical buildings, one on conventional fixed base foundation and other supported on SREIs were considered for study. These building were instrumented to record the seismic response data during earthquake excitations. Substantial reduction in peak floor accelerations were observed as compared to the building with conventional foundations. The acquired acceleration response data from these buildings were used to identify system parameters of both the buildings.

Field investigation and performance studies of base isolated building located in different part of the world were carried out by researchers. The study results show the effectiveness of base isolator in reducing the seismic response by many folds. Shake table testing of structural steel framed building and reinforced concrete frame building supported on base isolators were carried by few investigators. Investigation of earthquake response of structure supported on U-FREIs were however limited. Further, field investigation study of seismic response of structure supported on U-FREI is not

yet reported in any literature. One of the primary aims of development of U-FREI is not fulfilled without the application of this technology in low cost un-reinforced masonry building. The masonry buildings are inherently vulnerable under seismic excitations. Thus, in this study, shake table testing of un-reinforced masonry building supported on U-FREIs are targeted to be carried out to determine the seismic responses subjected to earthquake motion of different characteristics.

2.6. Concluding Remarks

The feasibility of FREI as a viable alternative to the conventional SREI is reviewed in previous sections. The distinct advantages of FREI bearings over SREI bearing were published in different literature. Very limited numbers of studies were carried out in FE modelling and analysis of the FREI till date. Some experiments have been conducted in the past to assess the effectiveness of FREIs. Validating these results by numerical modelling would further assert the suitability of these bearings and also allow analysis of bearings when it is not possible to do so experimentally. The development of lightweight, low-cost isolator is crucial if this method of seismic protection is to be applied to a wide range of buildings, such as residential buildings, school building and hospital buildings etc. in rural and urban earthquake-prone zones.

भारतीय प्रौद्योगिकी संस्थान गुवाहाटी
Indian Institute of Technology Guwahati

Chapter 3

Preliminary Design and Material Characterization of FREI

3.1. Introduction

Base isolation technology using elastomeric bearing is mostly applied to expensive building housing sensitive equipment and important building. Generally SREIs are used, which are large, heavy and expensive. To use elastomeric bearing for base isolation of low cost building as seismic demand mitigation strategy, the weight and cost of isolators are to be reduced.

The weight of SREIs are due to the interleaved steel plates used as reinforcement to provide desired vertical stiffness of the isolator by constraining the lateral bulging of elastomer layers when subjected to compressive load. Currently, the SREIs are manufactured by vulcanization of elastomer and steel plates. Before vulcanization of isolator assembly, surface preparation of steel plates are necessary for proper bonding of steel plates with elastomer. Steel plates are cut into proper sizes, sand-blasted, acid-cleaned and then coated with bonding compound. The layers of elastomer and steel plates are placed into the mould and heated under pressure for several hours to complete the manufacturing process. However, if the steel plates are replaced with the fibre reinforcement, the weight and cost of the bearing will reduce. Fibre material has modulus of elasticity, which is comparable to that of steel. This material can be used as reinforcing layer in elastomeric bearing to prevent lateral bulging under compressive load. Fibre can be cut into desired shape easily and no special surface preparation is required as in case of steel reinforcing plates. The weights of fibres are negligible as

compared to steel shim plates used in SREI. It is also possible that the current process of vulcanization for several hours under pressure in a mould can be replaced by microwave heating in an autoclave. Thus, both weight and production cost of isolator can be reduced by using of fibre reinforcement.

FREI can be manufactured in long strip and individual isolator may be cut into desired shape by using advanced jet cutting tool. Strip isolator can also be used at the base of masonry building, where load bearings walls are used to transfer the load of super structure to the foundation. This is a distinct advantage of FREI over SREI.

FREI can be classified into bonded and un-bonded bearings based on the end fixity conditions of isolator. In case of bonded isolator, thick end plates are used at the top and bottom surface of isolator. While the top plate is fixed to the bottom of superstructure, the bottom plate is fixed to the top of substructure. In case of un-bonded isolators, there is no thick end plates, the isolator is simply placed between the superstructure and substructures. There is no bonding or fixity of top and bottom surfaces of isolator. Horizontal load at the isolator surface is transferred through friction only. The behaviour and load transfer mechanism of un-bonded isolator is however quite complex and different from bonded isolator. Thus, closed form solutions which are available to evaluate the horizontal stiffness of bonded isolators are not directly applicable for un-bonded isolators.

A properly designed base isolator provides appropriate flexibility and energy dissipation capacity to structures placed on these isolators. The seismic demand of structure is reduced by using base isolators and safety against seismic excitation is enhanced. To get an idea of preliminary size of U-FREI, the closed form formulae applicable to other types of isolators are used. Material properties of elastomer and FRP considered during design and manufacturing are based on available experimental data.

FE analyses of both bonded and U-FREIs are carried out to evaluate their performances utilizing the mechanical properties of constituent materials considered during preliminary design. Finally, square FREIs are manufactured for testing its effectiveness in un-bonded application.

3.2. Design of Isolators

Mechanical properties of bonded FREI such as vertical stiffness, horizontal stiffness and damping properties can be evaluated from the closed form solution as available in the existing literature. Analytical solution of U-FREI undergoing rollover deformation due to applied horizontal displacement is rather complex and the equations used for bonded isolators are no longer applicable. However, in the absence of any closed form solution for un-bounded FREI, the preliminary design of bonded FREI for a desired level of isolation is used as the basis for both bonded as well as U-FREI. Analysis and design of isolators are carried out for a model building of 48 kN supported on four number of isolator, such that each isolator carries a vertical load of 12kN. In order to study the performances of different shapes of FREIs, square and circular isolators having same cross section area and height are considered. In the subsequent chapters, FE analysis of square and circular isolator with bonded and un-bonded end conditions are carried out. FE analysis result provides a good estimation of stress, strain and mechanical properties of isolator to proceed further for manufacturing. Though the FE analysis of square and circular isolators are carried out, only square isolator is manufactured and experimentally investigated. Shake table testing of an un-reinforced masonry building mounted on those manufactured FREI is performed using four input earthquake excitations of different frequency content.

The isolator is designed for the horizontal stiffness to achieve the desired horizontal

frequency, vertical stiffness so that no undesirable vertical or rocking mode may occur. A base isolated building is generally designed for a natural frequency of 0.5 Hz for deflecting energy associated with higher modes of vibration, while keeping the base displacement within acceptable limit.

Thus, for a fundamental frequency of 0.5 Hz of the prototype structure, the corresponding model ($1/5^{th}$ scale) frequency will be $\sqrt{\text{Scale factor}}$ x 0.5 = 1.118 Hz. The design of isolators for the$1/5^{th}$ scaled model structure is carried out for a target frequency of 1.118 Hz. Geometrical properties of square and circular isolators as adopted for achieving the target frequency of model building are listed in Table 3.1 and material properties considered for design of isolators are shown in Table 3.2. A typical cross section of isolator is shown in Fig. 3.1.

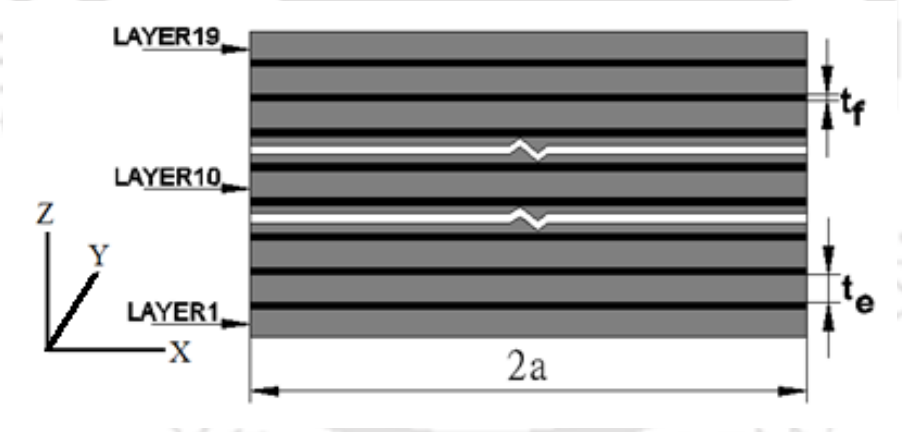

Fig. 3.1 Cross section of isolator

Table 3.1 Geometrical properties of isolators

Description		Square	Circular
Width (2a) or diameter (2R) of isolator	=	100 mm	112 mm
Thickness of fibre layer (t_f)	=	0.55 mm	0.55 mm
Number of fibre layer	=	18	18
Thickness of single rubber layer (t_e)	=	5 mm	5 mm
Number of rubber layer	=	19	19
Total height of isolator (h)	=	104.9 mm	104.9 mm

Table 3.2 Material properties of isolator

Hardness IRHD	=	60
Shear modulus of elastomer (G)	=	0.7 MPa
Elongation at break	>	400%
Young's modulus of carbon fibre reinforcement (E_f)	=	4400 MPa
Poisson's ratio of carbon fibre reinforcement (υ_f)	=	0.20

3.2.1. Bonded Fibre Reinforced Elastomeric Isolator

The analytical solution available for calculation of stiffness of SREI is not directly applicable to FREI due to the fact that the steel plates have different mechanical properties as compared to fibre reinforcement. In SREI, the steel plates are assumed to be inextensible and rigid in flexure, while the fibre reinforcements in FREIs are highly flexible in bending and show some extensional flexibility. The compressive stiffness of FREI is determined by the effective compressive modulus. Pressure solution approaches for determining the compressive and bending modulus of bonded FREI of infinite long, rectangular and circular shapes are presented by Tsai and Kelly [2001].

The Haringx theory, which is used to analyse the stability of multi-layer elastomeric bearing is based on the assumption that the bearing is a beam and plane sections, normal to un-deformed axis before deformation are assumed to remain plane, but not necessarily normal after deformation. This assumption is no longer valid to explain the influence of flexibility of fibres of the reinforced layers of FREI. Tsai and Kelly [2005] developed a theory that extends the Haringx theory by allowing the cross-section to deform into non planner surface and warping effect due to flexibility of reinforcement is also taken into account. In this theory the lower end of the beam is assumed to be fixed against displacement, rotation and warping and the upper end is considered to be constrained against rotation and warping, but allowed to move laterally and in axial direction. They derived the equation for horizontal stiffness and buckling load of a

beam including shear and warping effect, when the beam is subjected to axial compression load and lateral shear force at one end, while the other end is fixed. Elastic compression modulus and bending modulus of bonded FREI can be evaluated from the "pressure solution" developed by Tsai and Kelly [2001] and Kelly and Calabrese [2012].

3.2.1.1. Bonded Square FREI

Horizontal and vertical stiffness solution of bonded FREI developed by Tsai and Kelly [2005] are presented briefly in this section. These formulae are used to calculate stiffness of isolator and to determine the preliminary geometry.

Determination of Horizontal Stiffness

A beam is shown in Fig. 3.2 with lower end fixed against displacement, rotation and warping and upper end is allowed to move laterally and axially, but restrained against rotation and warping. The upper end of the beam is subjected to axial compression P and a lateral force F. Eq. 3.1 shows the horizontal stiffness of this beam derived by Tsai and Kelly [2005].

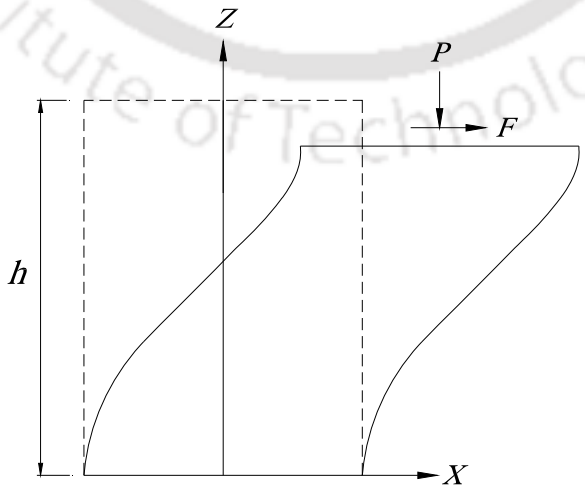

Fig. 3.2 Beam subjected to axial compression and lateral shear at one end

$$K_h = \left(\frac{GA}{h}\right) \frac{\overline{P}}{\frac{2\overline{P}(1+\overline{P})+\beta_2}{\overline{P}(\beta_1+\beta_2)}\sqrt{2\rho\beta_1}\,tan\sqrt{\frac{\beta_1}{8\rho}} + \frac{2\overline{P}(1+\overline{P})-\beta_1}{\overline{P}(\beta_1+\beta_2)}\sqrt{2\rho\beta_2}\,tanh\sqrt{\frac{\beta_2}{8\rho}} - 1} \quad (3.1)$$

which is the solution for $(1+\overline{P})k_c - k_b \geq 0$.

when $(1+\overline{P})k_c - k_b < 0$, then $\beta_2 < 0$.

The above equation can be expressed in terms of real numbers as

$$K_h = \left(\frac{GA}{h}\right) \frac{\overline{P}}{\frac{2\overline{P}(1+\overline{P})+\beta_2}{\overline{P}(\beta_1+\beta_2)}\sqrt{2\rho\beta_1}\,tan\sqrt{\frac{\beta_1}{8\rho}} - \frac{2\overline{P}(1+\overline{P})-\beta_1}{\overline{P}(\beta_1+\beta_2)}\sqrt{2\rho|\beta_2|}\,tanh\sqrt{\frac{|\beta_2|}{8\rho}} - 1} \quad (3.2)$$

where A is the plan cross section area of the isolator, $\bar{P} = P/GA$ is the dimension less compression force and, $\rho = (EI)_{eff}/GAt_r^2$ is the ratio of the flexure rigidity to shear rigidity.

k_b and k_c are two parameters corresponding to cross-section warping

$$k_b = \frac{EI}{EJ}\left(\frac{GB+N_B}{GA}\right)^2 \quad (3.3)$$

$$k_c = \frac{EI}{EJ}\left(\frac{GC+N_C}{GA}\right)^2 \quad (3.4)$$

In which N_B and N_C are two normal forces related to cross-section warping, defined as

$$N_B = -\int_A \sigma_{zz}\,\Omega_X dA \quad (3.5)$$

$$N_C = -\int_A \sigma_{zz}\Omega_X^2 dA \quad (3.6)$$

where G is being shear modulus, EA is the axial stiffness, EI is the bending stiffness, EJ is warping stiffness, B and C are cross section properties of warping defined as

$$B = \int_A \Omega_X\,dA \text{ and } C = \int_A \Omega_X^2\,dA \quad (3.7)$$

If the beam is homogeneous and has symmetric cross-section, the Eqs. (3.3) and (3.4)

becomes as

$$k_b = \frac{1}{J}\left(\frac{B}{A}\right)^2 (1+\bar{P})^2 \tag{3.8}$$

$$k_c = \frac{1}{J}\left(\frac{C}{A}\right)^2 (1+\bar{P}) \tag{3.9}$$

For rectangular isolator having sides *2a* and *2b* along the two perpendicular axes as shown in Fig. 3.3, the warping parameter that satisfy the condition $\int_A^{\cdot} X\Omega\, dA = 0$ is

$$\Omega(X) = \left(\frac{X}{a}\right)^3 - \frac{3}{5}\left(\frac{X}{a}\right) \tag{3.10}$$

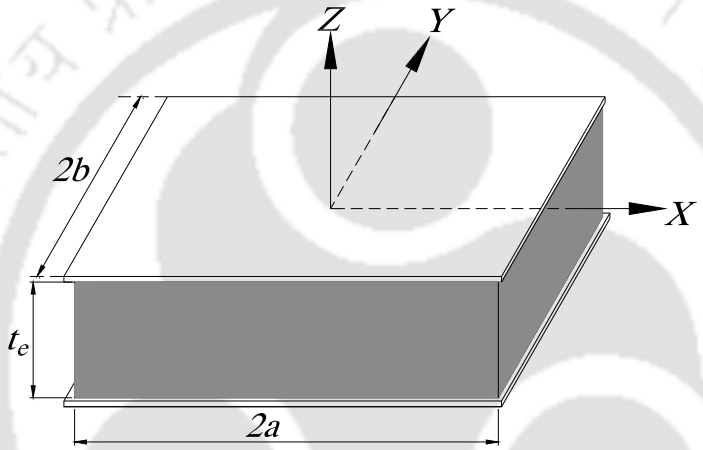

Fig. 3.3 Axes system for a rectangular pad showing dimensions

Substituting this and in Eqs. (3.7) and cross section property of warping shape $J = \int_A^{\cdot} \Omega^2 dA$ and other cross sectional properties the warping parameter of Eqs. (3.8) and (3.9) become

$$k_b = \frac{7}{3}(1+\bar{P})^2 \text{ and } k_c = 14(1+\bar{P}) \tag{3.11}$$

which satisfy the condition $(1+\overline{P})k_c - k_b \geq 0$ and parameter β_1 and β_2 in Eqs. 3.1 and Eqs. 3.2 become

$$\beta_1 = \frac{10}{3}(1+\overline{P})\left[\left(\overline{P}-\frac{7}{2}\right) + \sqrt{\left(\overline{P}-\frac{7}{2}\right)^2 + \frac{21}{5}\overline{P}}\right] \tag{3.12}$$

$$\beta_2 = \frac{10}{3}(1+\overline{P})\left[-\left(\overline{P}-\frac{7}{2}\right) + \sqrt{\left(\overline{P}-\frac{7}{2}\right)^2 + \frac{21}{5}\overline{P}}\right] \tag{3.13}$$

Effective bending stiffness $(EI)_{eff}$ of rectangular isolator FREI is defined by Kelly and Calabrese [2012] as

$$(EI)_{eff} = E_b I_y, \text{ where } I_y = \frac{4}{3}a^3 b \tag{3.14}$$

and

$$E_b = \frac{72GS^2}{\pi^2(\alpha a)^2}\left(1+\frac{a}{b}\right)^2 \sum_{n=1}^{\infty}\left\{\frac{1}{n^2}\left(\frac{tanh\bar{\gamma}_n b}{\bar{\gamma}_n b} - \frac{tanh\bar{\beta}_n b}{\bar{\beta}_n b}\right) + \frac{1}{(n-0.5)^2}\left[\frac{1}{\bar{\gamma}_n a \tanh \bar{\gamma}_n a} - \frac{1}{(\bar{\gamma}_n a)^2} - \frac{1}{\bar{\beta}_n a \tanh \bar{\beta}_n a} - \frac{1}{(\bar{\beta}_n a)^2}\right]\right\} \tag{3.15}$$

By considering a=b, the effective bending stiffness $(EI)_{eff}$ of square isolator can be calculated from above equation.

where $\bar{\gamma}_n = n\frac{\pi}{a}$, $\bar{\beta}_n = \sqrt{\bar{\gamma}_n^2 + \alpha^2}$ and $\alpha = \sqrt{\frac{12G\left(1-\vartheta_f^2\right)}{E_f t_f t_e}}$ (3.16)

Using the geometrical properties shown in Table 3.1 and material properties shown in Table 3.2, the value of horizontal stiffness K_h of the adopted square isolator is 61.42 N/mm as evaluated from Eqn. (3.1).

For a simple single degree-of-freedom, natural frequency (f_n) of the base isolated model structure is given by

$$f_n = \frac{1}{2\pi}\sqrt{\frac{K_H}{m_t}} \tag{3.17}$$

where, m_t is the total mass of the model structure and K_H is the total horizontal stiffness of bearings. Substituting the values of f_n and m_t in the Eqn. (3.17), gives $K_H = 240.87$ kN/m.

Therefore, Horizontal stiffness of single bearing

$$K_h = \frac{K_H}{\text{Number of bearings}} = 60.217 \text{ kN/m}$$

For conventional SREI, the most important mechanical property, the horizontal stiffness is given by simple shear formula (Eqn. 3.18).

$$K_h = \frac{GA}{t_r} \tag{3.18}$$

where, t_r is height of rubber in the bearing and A is area of the bearing. The equation assumes that lateral deformation of the bearings is due to shear. Substituting the values of K_h, G and A in Eqn. (3.18), gives t_r=95 mm. To achieve high vertical stiffness of the bearings, 19 layers of elastomer, each of 5 mm thick, is selected. The elastomer layers are separated by 0.55 mm thick fibre reinforcement.

Determination of Vertical Stiffness

The vertical stiffness of an elastomeric isolator can be calculated from the relation given by Kelly and Calabrese [2012] as shown in Eqn. (3.19).

$$K_v = \frac{E_C A}{t_r} \tag{3.19}$$

where, E_C is the bearing compression modulus.

The compression modulus E_C of square isolator is given by Eqn. (3.20) as

$$E_c = \frac{96GS^2}{\pi^2(\alpha a)^2} \sum_{n=1}^{\infty} \frac{2}{(n-1/2)^2} \left(\frac{tanh\gamma_n a}{\gamma_n a} - \frac{tanh\beta_n a}{\beta_n a} \right) \tag{3.20}$$

Where $\gamma_n = (n - 0.5)\frac{\pi}{a}$

$\beta_n = \sqrt{\gamma_n^2 + \alpha^2}$

S = shape factor, which is the ratio of one loaded area of a single layer of elastomer to its unloaded faces.

= 5

The above expression is used to determine the compression modulus of square isolator.

Substituting values of $G, S, \gamma_n, \beta_n, and\ a$ in Eqn. (3.20), E_c= 101212.6 kN/m^2. From Eqn. (3.19), compressive stiffness $K_v = 10653.96$ kN/m is obtained. Therefore, ratio of the compressive stiffness to shear stiffness is equal 173. This ratio is of importance in the design of bearings as the vertical stiffness has to be many times greater than the horizontal stiffness to minimize the rocking and other unwanted modes of vibration.

Determination of Buckling Load of Isolator

For calculation of buckling load of SREI, numbers of theories were proposed by different investigators. These theories are used to get an approximate value of buckling load of FREI in the present study. Some of these theories are briefly discussed below.

The modified linearized theory of an elastic column taking shear deformation into accounts is applied to rubbers in past research. By considering shear deformation and flexural stiffness, the buckling load of elastomeric bearing is expressed by Koh [1989] as:

$$P_{cr} = \frac{P_S}{2}\left[\left(1 + \frac{4P_E}{P_S}\right)^{1/2} - 1\right] \tag{3.21}$$

where, $P_S = GA_S, P_E = \frac{\pi^2 (EI)_{eff}}{l^2}$ and $(EI)_{eff} = \frac{1}{3} E_C I$, l=combined height of the elastomer layers and the steel shims, I= moment of inertia of cross sectional area and A_S =shear area.

Elastomeric bearings are generally quite squat, with height of the bearings comparable to its lateral dimensions. This leads to an approximation for critical load P_C given by following equation.

$$P_C = \sqrt{P_S\, P_E} \tag{3.22}$$

Koh and Kelly [2003] defined the effective shear and flexural rigidity as:

$$(GA_S)_{eff} = GA\frac{l}{l_r} \tag{3.23}$$

where, l_r = the total thickness of all elastomer layers. The scaling factor l/l_r is to account for the presence of steel plates, which are assumed to be rigid as compared to the elastomer to treat the bearing as if it is made of homogeneous material. The effective *EI* of the bearing is defined as,

$$(EI)_{eff} = EIg(S^2, \vartheta)\frac{l}{l_r} \tag{3.24}$$

where, $g(S^2, \vartheta)$ is a dimensionless function, ϑ is Poisson's ratio. For incompressible rubber ($\vartheta = 0.5$) the dimensionless term becomes as

$$g(S^2, 0.5) = 96S^2 \sum_{n_r=1}^{\infty} \frac{1}{n_r^4 \pi^4}\left(1 - \frac{\tanh n_r\pi}{n_r\pi}\right) \approx 0.7425\, S^2 \tag{3.25}$$

for a square shaped elastomeric bearing, thus

$$(EI)_{eff} \approx 2.23\, S^2 r^2 (GA_S)_{eff} \tag{3.26}$$

where *r* is the radius of gyration, n_r is the number of rubber layers.

Buckling load formula of isolation bearing derived by Kelly [2003] considering bottom of bearing restrained against rotation as well as translation and top loaded end as restraint against rotation only is as given below.

$$P_C = \frac{\sqrt{2}\,\pi GAS\, r}{t_r} \tag{3.27}$$

Buckling load of the model elastomeric bearings estimated from these formulae proposed by different investigators are listed in Table 3.3.

Table 3.3 Predicted Buckling Load of Square Bearing.

l No.	Investigator	Buckling Load (kN)
1	Gent	43.99
2	Koh and Kelly	42.77
3	Kelly	40.50

As the maximum load on a bearing is 12.0 kN, therefore, the elastomeric isolation

bearings have high factor of safety against the buckling. Further, high vertical stiffness can withstand heavy vertical load and prevent rocking mode of vibration during high intensity of earthquake [Wu and Samali, 2002].

3.2.1.2. Bonded Circular FREI

Similar to bonded square isolator, the horizontal and vertical stiffness solution of bonded circular FREI developed by Tsai and Kelly [2005] are presented briefly in this section. These formulae are used to calculate stiffness of isolator and determine the preliminary geometry.

Determination of Horizontal Stiffness

For circular cross section of radius a as shown in Fig. 3.4, the warping parameter that satisfy the condition $\int_A^{\cdot} X\Omega\, dA = 0$ is

$$\Omega(X) = \left(\frac{X}{a}\right)^3 - \frac{1}{2}\left(\frac{X}{a}\right) \tag{3.28}$$

Substituting this in Eqs. (3.7) and cross section property of warping shape $J = \int_A^{\cdot} \Omega^2 dA$ and other cross sectional properties the warping parameter of Eqs. (3.8) and (3.9) become

$$k_b = (1+\bar{P})^2 \text{ and } k_c = 10(1+\bar{P}) \tag{3.29}$$

which satisfy the condition $(1+\overline{P})k_c - k_b \geq 0$ and parameter β_1 and β_2 in Eqn. (3.1) and (3.2) become

$$\beta_1 = 2(1+\overline{P})\left[\left(\overline{P} - \frac{9}{2}\right) + \sqrt{\left(\overline{P} - \frac{9}{2}\right)^2 + 9\overline{P}}\right] \tag{3.30}$$

$$\beta_2 = 2(1+\overline{P})\left[-\left(\overline{P} - \frac{9}{2}\right) + \sqrt{\left(\overline{P} - \frac{9}{2}\right)^2 + 9\overline{P}}\right] \tag{3.31}$$

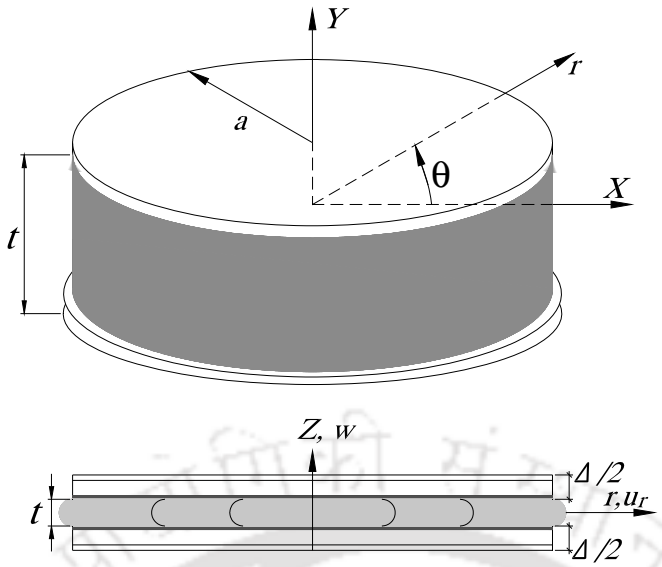

Fig. 3.4 Coordinate system for a circular pad of radius *a*

Effective bending stiffness of $(EI)_{eff}$ of circular isolator FREI is defined by Kelly and Calabrese [2012] as

$$(EI)_{eff} = 6\pi GS^2\,(1+\vartheta)\,\frac{a^2}{\alpha^2}\left[\frac{\alpha a\, I_1(\alpha a) - 4I_2(\alpha a)}{\alpha a I_1(\alpha a) - 2(1-\vartheta)I_2(\alpha a)}\right] \tag{3.32}$$

where, the Bessel functions

$$I_1(\alpha a) \approx \frac{\alpha a}{2} + \frac{(\alpha a)^3}{16} \tag{3.33}$$

$$I_2(\alpha a) \approx \frac{(\alpha a)^2}{8} + \frac{(\alpha a)^4}{96} \tag{3.34}$$

Substituting the values of geometrical properties from Table 1 and material properties from Table 2 in Eq. (3.1), the horizontal stiffness K_h of circular isolator is calculated as 57.16 N/mm.

Substituting the values of f_n and m_t in Eq. (3.17), gives $K_H = 240.87$ kN/m. The Eqn. (3.1) is independent of shape of isolator and hence the horizontal stiffness as obtained from this formula is same for both square and circular isolator.

Therefore, Horizontal stiffness of single bearing K_h

$$K_h = \frac{K_H}{\text{Number of bearings}} = 60.217 \text{ kN/m}$$

Substituting the values of K_h, G and A in Eqn. (3.18), gives t_r=95 mm. To achieve desired stiffness of the bearings, 19 layers of elastomer, each of 5 mm thick, is selected. The elastomer layers are separated by 0.55 mm thick fibre reinforcement. Cross section area, number and thickness of elastomer layers of square and circular isolator are considered same to compare the performances of both the isolators.

Determination of Vertical Stiffness

The vertical stiffness of circular isolator is also determine by using Eqn. (3.19) and compression modulus E_C of circular FREI is given by Tsai and Kelly [2001] as

$$E_c = 24GS^2 \frac{(1+\vartheta_f)}{(\alpha a)^2}\left[\frac{\alpha a I_0(\alpha a) - 2I_1(\alpha a)}{\alpha a I_0(\alpha a) - (1-\vartheta_f)I_1(\alpha a)}\right] \tag{3.35}$$

where the Bessel functions are

$$I_0(\alpha a) \approx 1 + \frac{(\alpha a)^2}{4} \tag{3.36}$$

$$I_1(\alpha a) \approx \frac{\alpha a}{2} + \frac{(\alpha a)^3}{16} \tag{3.37}$$

S = shape factor is 5.6,

Substituting values of $G, S, \vartheta_f, \alpha, I_0, I_1 and\ a$ in Eqn. (3.35), the compression modulus is obtained as 112889.26 kN/m^2. From Eqn. (3.19), compressive stiffness $K_v =$ 11707.25 kN/m is obtained. Therefore, ratio of the compressive stiffness to shear stiffness is equal 202.

Buckling load of the model bearing estimated from different formulae as proposed by different investigators are listed in Table 3.4.

Table 3.4 Predicted Buckling Load of Circular Bearing.

l No.	Investigator	Buckling Load (kN)
1	Gent	38.65
2	Koh and Kelly	45.77
3	Kelly	43.35

As the maximum load on a bearing is 12.0 kN, the elastomeric isolation bearings have high factor of safety against buckling as may be evident from the values of buckling load in Table 3.4.

3.2.2. Un-bonded Fibre Reinforced Elastomeric Isolator

Un-bonded isolator exhibits stable roll over deformation on application of horizontal load. Due to high geometrical nonlinearity in lateral direction, horizontal stiffness varies with isolator lateral deformation. No closed form analytical solutions are available for ascertaining the horizontal stiffness of this type of complex U-FREI. Further, the closed form solution of even bonded FREI discussed earlier serves only as preliminary design. Influence of rubber material properties on the amplitude of shear strain, rate and history of the lateral displacement on lateral response of isolator is not captured in closed form solution derived by earlier researcher. So, experimental evaluation of isolator is to be carried out before their installation in any structure.

3.3. Characterization of Material of Isolator

Square FREIs have been manufactured by M/s METCO Ltd, Kolkata, India using the geometry and material shown in previous section. These isolators are tested at IIT, Guwahati for the evaluation of their vertical stiffness, horizontal stiffness and damping. Subsequently, shake table testing of un-reinforced masonry building supported on these FREIs are also carried out to evaluate the performance of FREIs in seismic isolation. A brief characteristics of materials used for manufacturing of FREIs are described in the next few sections. The important mechanical properties of elastomer testing are summarized in Table 3.5.

3.3.1. Testing of Elastomer

FREI consist of mainly two components, viz (a) Neoprene or synthetic rubber and (b) Carbon fibre composite system. The Neoprene is the synthetic chloroprene rubber, suitably compounded to attain mechanical properties for manufacturing of the square isolator. Self-life or durability of Neoprene (synthetic chloroprene rubber) is very long compared to other types of rubber.

3.3.1.1. Hardness Test

Hardness test is conducted as per Indian Standard IS: 3400 (Part II). The hardness test is based on measurement of the indentation of rigid ball into the rubber specimen under specific conditions. The measured indentation is converted into International Rubber Hardness Degrees (IRHD) from table and graphs given in the code. The scale being so chosen that zero represents a material having an elastic modulus 0 and 100 represents a material of infinite elastic modulus. The elastomer as used in the manufacturing of bearings in the present study has IRHD of 60.

3.3.1.2. Tensile Stress-Strain Properties

This test is conducted as per IS: 3400 (Part I). In this test, dumb-bell shape specimen is stretched by movable grip of tensile testing machine at a constant rate. Readings of load and elongation are taken during the stretching of the test piece when it breaks. Tensile strength is calculated by dividing the load at break by initial area of cross section of the test piece. The elongation at break is calculated by subtracting initial distance between reference lines on the dumb-bell test piece from the distance between the same lines at break point and expressing the result as percentage of initial distance. Tensile strength and elongation at break are found to be 17 MPa and 400% respectively.

3.3.1.3. Compression Set at Constant Strain

This test is conducted as per IS: 3400 (Part X). A test piece in the shape of a cylindrical disk is subjected to a constant strain under compression in compression device for a given time (24 Hrs) and it is allowed to recover for a given time. The difference between original thickness and the thickness after recovery is expressed as percentage of initially compression. Compression set is found to be 35%.

Table 3.5 Mechanical properties of Elastomer.

Mechanical Properties	Unit	Test method, I.S. specification reference		Value of the characteristic specified
Hardness	IRHD	IS : 3400 (Part II)		60
Minimum tensile strength	MPa	IS : 3400 (Part I)		17
Minimum elongation at break	%	IS : 3400 (Part I)		400
Maximum compression set	%	IS : 3400 (Part X)		
		Duration	Temperature	
		(h)	(ºC)	
C.R.		(+0 to 24-2)	100 ± 1	35
Accelerated ageing		IS : 3400 (Part IV)		
		Duration	Temperature	
		(h)	(ºC)	
C.R.		72	100 ± 1	

3.3.1.4. Accelerated Ageing Test

Accelerated ageing tests or exposure to heat tests are designed to estimate the relative resistance of rubber vulcanizates to deterioration with the passage of time. For this purpose, rubber is subjected to controlled deteriorating influences for definite periods, after which appropriate properties are measured and compared with the corresponding properties of the un-aged rubber. The purpose of the test is to assess the deterioration of rubber either during prolonged periods at normal or at high temperature in air or during use at elevated temperatures and at the elevated oxygen pressure. This test is conducted as per IS: 3400 (Part IV). Testing result obtained from this test is tabulated in Table 3.5.

3.3.2. Testing of CFRP

The material used for manufacturing of isolators are supplied by Fosroc Chemicals (India) Pvt. Ltd. Woven sheets of CFRP are used in this study. The important properties of the CFRP are furnished in Table 3.6.

Table 3.6 Physical properties of FRP

Physical Properties	Unit	Value of the Characteristic value
Fibre orientation	-	Unidirectional.
Weight of the fibre	g/m^2	200
Density of fibre	g/cc	1.80
Ultimate elongation (%)	-	1.5

Further, the most essential properties of CFRP used in FE analysis are tensile strength and modulus of elasticity obtained from testing result previous researcher. The stress-strain plot for CFRP coupon is shown in Fig. 3.5. The slope of this graph is reported as the value of modulus of elasticity of CFRP. The ultimate tensile strength for CFRP is found to be 630 N/mm^2 and the modulus of Elasticity of CFRP is found as 4.40×10^4 N/mm^2.

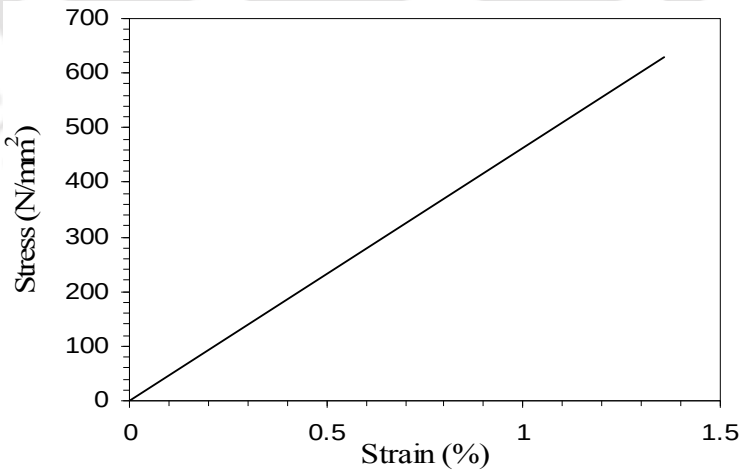

Fig. 3.5 Stress-strain plot for CFRP coupon

(*Choudhury A.M.,* 2010)

The manufacturing of FREI is done by placing a pair of woven sheets of CFRP with stacking sequence of $0^0/90^0$ on Neoprene (un-vulcanized) sheets. This is repeated for

the designed number of layers. The combination of CFRP and Neoprene sheets is vulcanized inside a proper mould under appropriate pressure and temperature. After certain time interval, the assembly is kept under natural cooling.

3.4. Concluding Remarks

In this chapter, the preliminary design of square and circular FREIs are carried out based on the available closed-form solution and mechanical properties of different constituent materials. Buckling loads of isolators are also calculated using different closed form solution proposed by previous investigators. The adopted size of isolator based on preliminary design is further analysed using FE method in the next chapter, where detailed studies on strain and stress in elastomer as well as fibre reinforcement layers are carried out.

Chapter 4

FE Simulation of Isolator

4.1. Introduction

Experimental studies carried out in the past show that the vertical and horizontal stiffness of FREIs are comparable to the stiffness of SREI. Further, the experimental studies on FREI were carried out generally on circular and square shapes of isolator and to some extent on long strip isolators. It is not practically feasible to experimentally determine mechanical properties of isolator for all shapes and sizes. Thus, analysis of FREI bearings using FE method can address more general scenario.

It is however observed that very limited studies of FREIs are conducted so far using FE analysis. Nezhad et al. [2011] carried out 2D FE analyses of bonded and un-bonded strip FREI. Stress demands in both types of isolators are studied and it is observed that the lower stress demands prevail on rubber and fibre interface for U-FREI. Kelly and Calabrese [2012] carried out 3D FE analysis of isolator of different geometry and shape factor and compared the evaluated stiffness of isolator, stresses in fibre reinforcement with those obtained from pressure solution method.

In this chapter, the details of FE modelling and analysis technique of FREIs are studied. Lateral stiffness, damping and stresses in elastomeric layers of U-FREI and bonded FREI of square and circular shapes are evaluated. Performances of square and circular isolators for different lateral loading directions are also analysed and comparisons of results are presented. In the next chapter, comparison of FE analysis results and experimental results are presented. This comparison would further encourage the base isolator designer to rely on the FE analysis result when it is not possible to do so experimentally.

4.2. Finite Element Modelling

FE analyses of bonded and U-FREI of square and circular shapes are carried out to determine the mechanical properties of those isolators. The isolators are analysed under the action of constant vertical load and cyclic horizontal load acting along different directions of isolator. The size of square isolator, number and thickness of rubber layers is taken from the preliminary analysis presented in previous chapter. A circular isolator having same cross sectional area and number of elastomeric layers as that of square isolator is considered for FE analysis to compare the performance of both square and circular isolator. The FE analysis facilitates evaluation of the detailed stresses in isolator, which is useful for arriving at more efficient design of isolator. The geometries of square and circular isolators are described in Chapter 3.

In the present study, the isolator is modelled using ANSYS 14.0, multi-physics finite-element software. FE modelling of FREI is a challenging task as it involves large strain, incompressibility of the material and nonlinear solution convergence. Incompressible material behaviour may lead to some difficulties in numerical simulation, such as volumetric locking, inaccuracy of solution, checkerboard pattern of stress distributions or occasionally, divergence. Lagrange multiplier based mixed u-P element is used to overcome incompressible material problems. These elements are designed to model material behaviour with high incompressibility such as fully or nearly incompressible hyper-elastic materials and nearly incompressible elasto-plastic materials (high Poisson ratio or undergoing large plastic strain). Lagrange multipliers extend the internal virtual work so that the volume constraint equation is included explicitly. This introduces hydrostatic pressure (or volume change rate for nearly incompressible hyper-elastic materials) as a new independent variable.

The isolators have been modelled and analysed for bonded and un-bonded cases. As the

conventional isolators are bonded, the comparison of bonded and un-bonded isolators would provide information about the advantages, which fibre reinforced un-bonded isolators are likely to possess.

4.2.1. Element Type for Finite Element Model

In FE analysis using any general purpose code, the major task is to choose the correct types of elements for representation of realistic behaviour of the physical model. The main components of FREIs are elastomeric and multi-layered fibre reinforcement layers. Bonded isolators are modelled with rigid end plates connected to top and bottom rubber surfaces as the super structure and sub structure are directly connected to the isolator. However, in case of U-FREI, the top and bottom plates loose contact on application of lateral displacement. To address the issues of large strain, contact conditions and near incompressible behaviour of isolator, suitable elements are chosen for modelling of isolator.

4.2.1.1. Element type of fibre reinforcement layer

In the FE model of FREI, the fibre reinforcement is modelled using SOLID46, which is an 8-node layered structural solid designed to model layered thick shells or solids. Fibre-reinforcements are provided in the form of bidirectional ($0^0/90^0$) layers interleaved and bonded between rubber layers. The element has three degrees of freedom at each node: translations in the nodal x, y, and z directions. Arrangement of fibre layers ($0^0/90^0$) as used for the reinforcement of isolators is shown in Fig. 4.1.

4.2.1.2. Element type of elastomeric layer

The elastomer used is neoprene rubber, which exhibits non-linear behaviour.

SOLID185, which is an 8-node structural solid element, is used to model the elastomer. It is defined by eight nodes having three degrees of freedom at each node: translations in the nodal x, y, and z directions. This element has the capabilities to model the plasticity, hyper-elasticity, stress stiffening, creep, large deflection and large strain behaviour of material. It also has mixed formulation capability for simulating deformations of nearly incompressible elasto-plastic materials, and fully incompressible hyper-elastic materials.

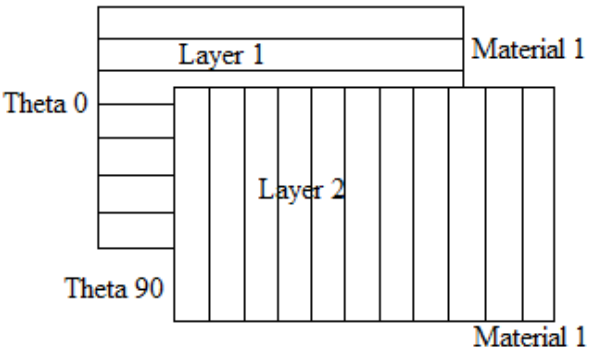

Fig. 4.1 Layer stacking of the fibre-reinforcement in isolator

4.2.1.3. Contact and Target Elements

In the numerical simulation, two rigid horizontal plates are considered at the top and bottom of the isolator to represent the super structure and sub structure. Vertical and horizontal loads are applied at the top plate, which is allowed to move both in the vertical and horizontal directions, while all degrees of freedom of bottom plate are constrained. Initially top and bottom surfaces of un-bonded isolator are in contact with the top and bottom plates. On increasing the displacement, the top and bottom surfaces of isolator leave contact with the top and bottom plates. In order to model this contact problem, paired elements are used in ANSYS i.e. one surface is defined as contact element and other as target element between the isolator and support plates. Contact element CONTA173 is used to define the exterior rubber surfaces and target element

TARGE170 for interior surface of top and bottom rigid plates. The contact element supports the Coulomb friction model to transfer the shear forces at the interface of contact and target surface. Once the equivalent frictional stress exceeds the limiting frictional stress, the contact and target surfaces will slide relative to each other. The maximum friction coefficient parameter is used to prevent the sliding of contact and target surfaces.

The FE model of bonded FREI is same as the model of U-FREI with contact and target elements being removed. The rigid end plates used to represent the super structure and sub structure are directly connected to the top and bottom rubber surfaces of isolator respectively.

The model is meshed with hexagonal volume sweep. The volume sweep fills existing unmeshed volume with elements by sweeping the mesh from an adjacent area through the volume. If the area is not already meshed, volume sweep meshes the area and then extrudes it. In case of nonlinear and large displacement FE analysis, size of mesh plays an important role for solution convergence and duration of solution. Generally a refined mesh gives more accurate solution in FE analysis. However, very fine mesh size of nonlinear analysis model required large storing space as well as more time to complete the analysis. To overcome this problem, a relatively coarser mesh size is chosen for initial analysis of isolator. Finally an acceptable refined mesh size is considered for the detailed analysis by studying the solution convergence with mesh refinement. Influence of mesh size on the analysis result of FREI is described briefly in subsequent section.

4.2.2. Material Model

Material properties of fibre reinforcement as shown in Table 3.2 are used in FE model. Elastomer is modelled with hyper-elastic and visco-elastic parameters. Hyper-elasticity

refers to materials which can experience large elastic strain that is recoverable. Rubber-like and many other polymer materials fall in this category. The constitutive behaviours of hyper-elastic materials are usually derived from the strain energy potentials. Further, hyper-elastic materials generally have very small compressibility. This is often referred to as incompressibility. Hyper-elastic materials have a stiffness that varies with the stress level.

Ogden 3-terms model has been adopted to model the hyper-elastic behaviour of the rubber and the visco-elastic behaviour is modelled by Prony Viscoelastic Shear Response parameters. The material parameters of elastomer used in the analysis is taken from the paper by Holzapfel [1996] and reproduced below.

Ogden (3-terms) $\mu_1 = 1.89 \text{ X } 10^6$; $\mu_2 = 3600$; $\mu_3 = -30000$ and $\alpha_1 = 1.3$; $\alpha_2 = 5$; $\alpha_3 = -2$

Prony Shear Response $a1 = 0.3333$; $t1 = 0.4$; $a2 = 0.3333$; $t2 = 0.2$

4.2.3. Loading History for Vertical Load

A varying vertical load as shown in Fig. 4.2 is applied on the top surface of isolators, while carrying out analysis under vertical load.

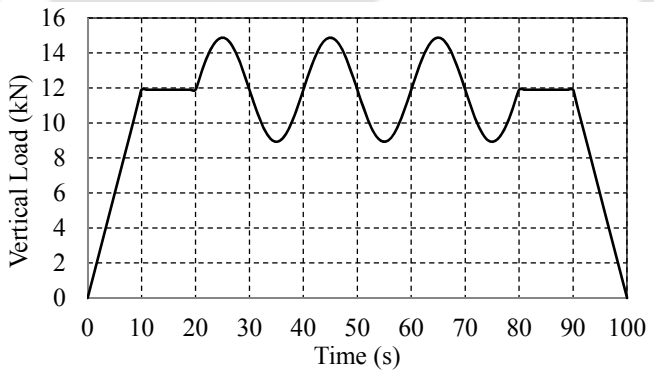

Fig. 4.2 Vertical load history for square and circular isolator

The load is distributed equally at all the nodes of the top surface. The vertical load of 12.0kN ± 3.0kN is maintained on both square and circular isolators. Vertical stiffness and compression modulus are evaluated from the result of vertical load analysis.

4.2.4. Loading History for Horizontal Load

The analysis is carried out by subjecting the isolator under cyclic displacement, while maintaining a constant vertical load of 12.0 kN on the isolator. Three cycles of specific displacement amplitude consisting of push and pull segments with maximum displacement up to 60 mm is applied on the top of isolator. The applied horizontal displacement is increased by ±10mm at the end of every three cycles. The cyclic horizontal displacement history used in the analysis is shown in Fig. 4.3.

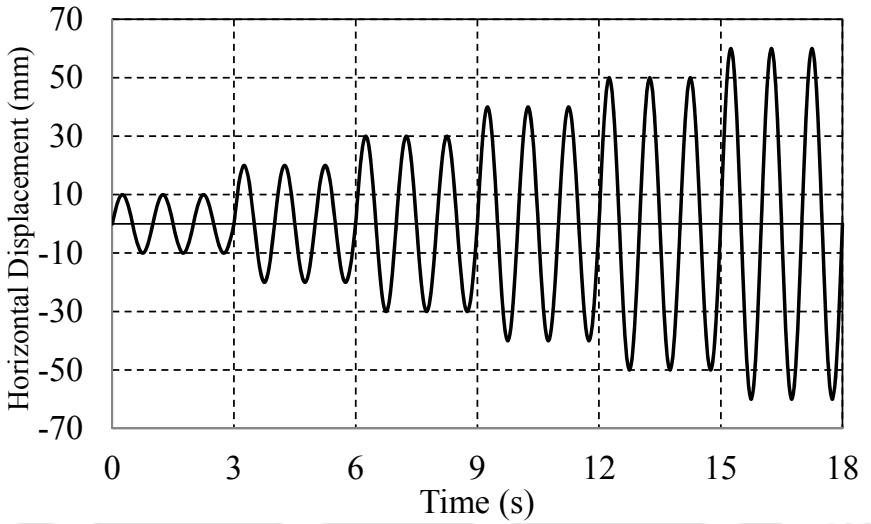

Fig. 4.3 Imposed horizontal displacement history vs time

4.2.5. Solution Method

The full transient dynamic analysis is carried out to determining the time-varying responses of the isolator. The full method uses the full system matrices to calculate the transient responses. It is the most general of method of analysis used in ANSYS. This method allows calculation of all types of non-linearities, loads, displacements and stresses in a single pass and there is no mass matrix approximations involved. Full method is used in analysing the bearings because of the material non-linearity, non-linearity of the contact element and also the varying time steps. Displacement based convergence criterion is used for analysis under combined vertical and horizontal load.

4.3. Finite Element Analysis of Square Isolator

The FREI is meshed using the elements described in previous section and the meshed isolator along with the selected axes are shown in Fig. 4.4. It may be noted that the X axis matches with fibres oriented along 0°, while Y axis matches with fibres along 90°. The orientation of horizontal loading 0^0 and 45^0 are along X-axis and 45^0 to X-axis respectively. Both the bonded and un-bonded isolators are analysed using the same meshed isolator. However, the end connections with the top and bottom surfaces of isolators are appropriately addressed for the simulation of bonded and un-bonded cases. The detailed results from the analyses are presented for proper understanding of the behaviour of these isolators.

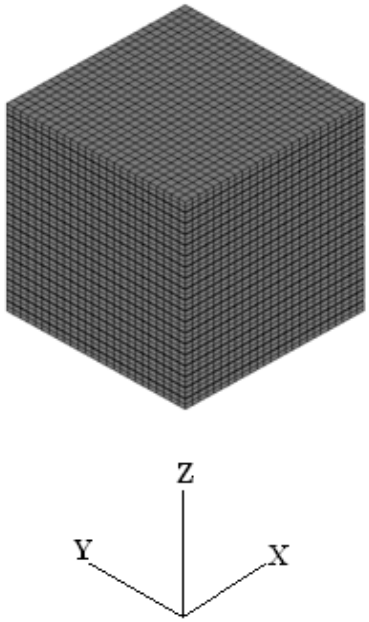

Fig. 4.4 Meshed square isolator

4.3.1. Analysis for Horizontal Stiffness

The free body diagram of bonded and un-bonded isolators (Nezhad, 2011) is shown in Fig 4.5. In case of bonded FREI, the top and bottom surfaces of isolator always remain in contact with the support and load application point does not change with the increase

of lateral displacement. Equilibrium of isolator is established by the balancing moment generated at top and bottom surfaces of isolator.

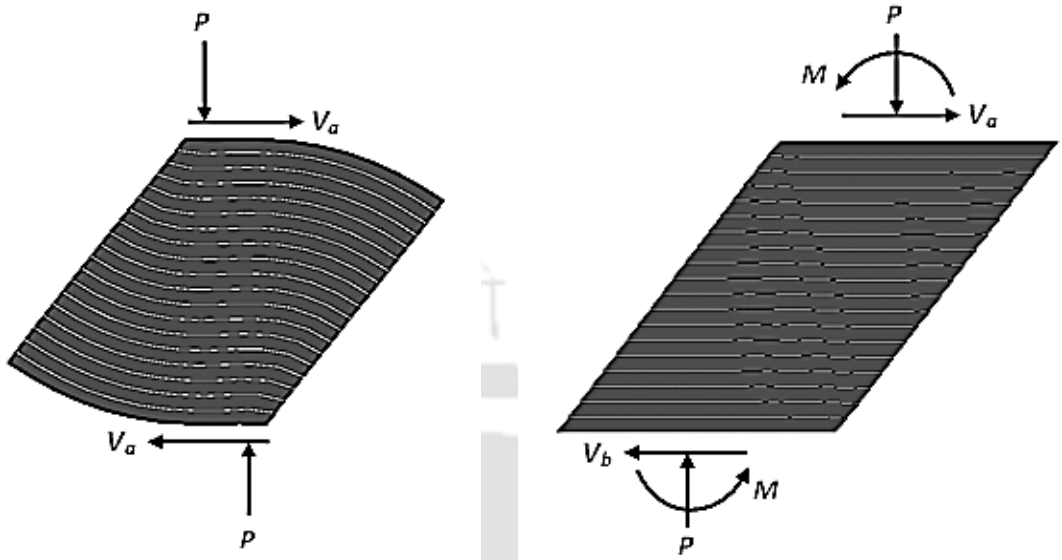

(a) U-FREI (b) Bonded FREI

Fig. 4.5 Free body diagram in laterally deformed FREI with different boundary condition

As a result of this moment, tensile stresses normal to the surface are generated in region outside the central compression core. On the contrary, the point of application of vertical load resultant at external top and bottom surfaces of deformed U-FREI shift towards the pressed end. The offset of the resultant compressive loads produces a couple which balances the overturning moment caused by the shear developed in the top and bottom surfaces of isolator as shown in Fig. 4.5(b). Due to this, no tensile stresses are transferred at the contact support of un-bonded isolators.

FE analysis of un-bonded and bonded FREIs are carried out by applying a constant vertical load of 12 kN on the top surface of the isolator along with horizontal displacement up to 60 mm applied in incremental order to ascertain the horizontal stiffness. In the analysis of un-bonded isolator, contact and target elements are introduced between isolator and load application plane. However, for the analysis of bonded isolator, the same model as un-bonded one is considered by replacing the

contact as well as target elements and connecting top and bottom surfaces of isolator directly to the rigid end plates, which is the load application plane. The horizontal stiffness of bonded FREI which is calculated using Eqn. 3.1 and FE analysis is shown in Table 4.1. A simple formula $K_h = G_e A/t_r$ generally used for SREI is also used to calculate the horizontal stiffness of bonded FREI. However, this simple formula is likely to give higher horizontal stiffness of bonded FREI because flexibility of fibre reinforcement is not considered in this equation.

A nearly linear lateral load displacement relation is obtained in the range of small displacement from FE analysis for both the bonded and un-bonded square FREI as shown in Fig. 4.6. Slope of this line is the horizontal stiffness of isolator. As shown in Fig. 4.6, the lateral response of bonded FREI is almost linear, while the response of U-FREI is nonlinear, which is due to the roll over deformation under horizontal load.

Table 4.1 Horizontal stiffness (N/mm) of bonded square FREI

Analytical $(K_h = \frac{GA}{t_r})$	**From Eq. (3.1)**	**FE Analysis**
73.68	73.65	70.7

The horizontal stiffness of U-FREI decreases with the increase in horizontal displacement. Fundamental time period of un-bonded isolator thus increases with the decrease in stiffness, which results in increasing seismic mitigation capacity of the isolator. Thus, laterally stable U-FREI has superior seismic isolation capacity as compared to bonded FREI. A stable un-bonded isolator maintains positive incremental tangent stiffness over the range of lateral displacement [Nezhad 2011]. The result as obtained from FE model (Fig. 4.6) is also observed to maintain positive tangent stiffness for the displacement range employed in the analysis.

The lateral shear load resisted by the isolator is transmitted to the super structure. It is observed from Fig. 4.6 that up to 12mm displacement, the force that would be

transmitted by bonded and U-FREI is almost same. However, beyond 12mm, the force transmitted by U-FREI is significantly lower as compared to bonded FREI. At maximum displacement of 60mm, the lateral force transmitted by bonded FREI is 70% higher than U-FREI. Hence, it can be concluded that with same size of isolator, performances of U-FREI is far superior to bonded FREI. Similar observations were made by Nezhad et al. [2011], Kelly and Calabrese [2013].

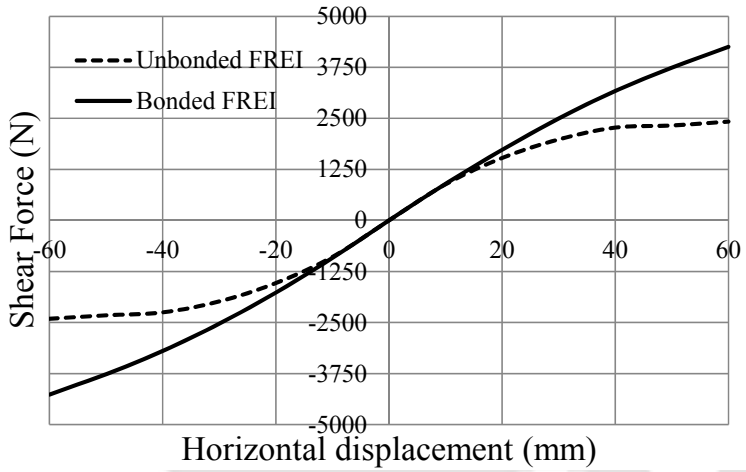

Fig. 4.6 Lateral load *vs* displacement of the bonded and un-bonded square isolator

4.3.2. Stress and Strain of Square Isolator

A constant vertical load of 12 kN is applied on the isolator while cyclic horizontal displacement as shown in Fig. 4.3 is applied at the top of isolator. Isolator are analysed under the action of cyclic displacement applied along two different horizontal directions, i.e. along X axis and 45° to the X axis. Further, for denoting stresses, the local axes are designated as axis 1 and axis 3, which are parallel to X and Z axis respectively.

4.3.2.1. Square isolator with 0^0 loading direction

Contour of normal stress S_{33} corresponding to maximum applied displacement of 60mm

is shown in Fig. 4.7 for both bonded and un-bonded isolators. The normal stress S_{33} acts along Z axis.

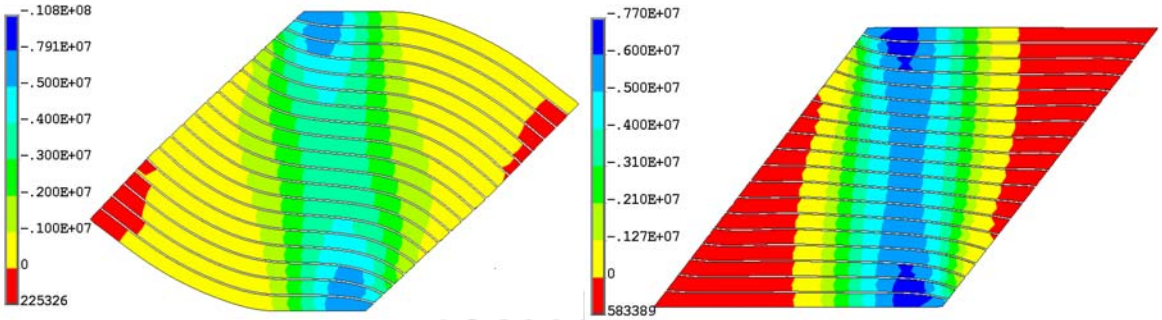

(a) Un-bonded (b) Bonded

Fig. 4.7 Contour of normal stress S_{33} (N/m^2) in rubber layer of isolator at horizontal displacement 60mm and 0^0 loading direction (Positive value indicate tension)

The compression load of bonded FREI is carried by central compression core within the overlapping region between the top and bottom faces of isolator. As the lateral deformation increases, area of compression region decreases and peak compression increases in the bonded FREI. The compression in the central core is almost constant throughout the height of the isolator as can be seen from Fig. 4.7(b). Thus, while the compression is carried through the overlapping region between top and bottom surfaces, the unbalanced moment is carried by tension stresses in the regions outside the overlap. Vertical load of U-FREI is carried by the central compression core, similar to bonded FREI (Fig. 4.7a). However, the maximum compressive stresses in U-FREIs are developed only in the pressed corner at top and bottom surfaces and the magnitude of peak compression that develop in both isolators are comparable. Further, when an un-bonded isolator is deformed laterally under the action of horizontal loading, the near end bottom surfaces of isolator leaves contact and moves upward causing tension in fibre reinforcement. Similarly, the opposite end of the top surface of isolator moves downward and loses contact with the support. Tension is developed in the region outside the central overlapping region while central regions remain under compression.

However, due to un-bonded application, no tensile stress is transferred to the isolator's contact support. The unbalanced moments are resisted by the vertical load through offset of the force resultants on the top and bottom surfaces. It may also be noted that the tensile stress S_{33} developed in U-FREI is lesser than those of bonded FREI. Hence, peeling stress demand on the bond between the rubber and fibre reinforcement in case of U-FREI is lesser than that of bonded FREI.

Figs. 4.8(a)-(c) show the distribution of the normalized stress S_{33}/P_n along the horizontal plane of 10th rubber layer located at mid-height of the isolator at lateral displacement of 60mm, 40mm and 20mm. Vertical pressure P_n is the pressure due to vertical load of 12kN applied to the top of isolator.

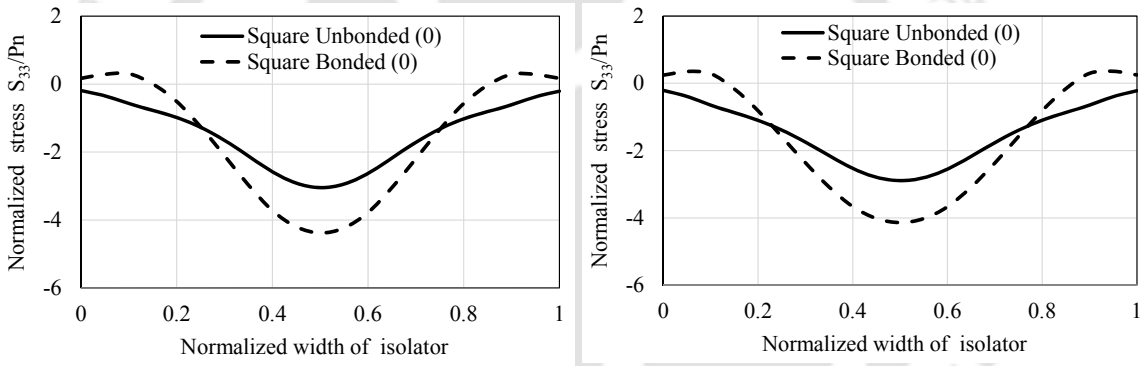

(a) 60mm horizontal displacement (b) 40mm horizontal displacement

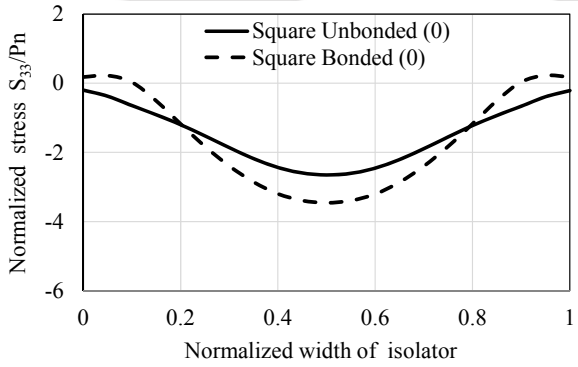

(c) 20 mm horizontal displacement

Fig. 4.8 Distribution of normalized stress S_{33}/P_n in the mid rubber layer at mid-height of isolator at different horizontal displacement (0^0 loading direction)

It is observed for bonded isolator that normal compressive stress increases with the

increase in the horizontal displacement while the length of compression region decreases. Development of considerable tensile stress is observed in bonded FREI along with the presence of warping effect. However, for un-bonded application, the compressive stress does not vary much with the increase in horizontal displacement and there is no development of tensile stress as well. Further, peak pressure at the middle of bonded isolator is 44% higher than that of un-bonded isolator corresponding to 60mm horizontal displacement and hence, U-FREIs are less susceptible to Euler buckling as compared to bonded FREI.

Contour of normal stress S_{33} for square un-bonded and bonded isolator are shown in Fig. 4.9 along middle of 10^{th} rubber layer (mid-height of the isolator) corresponding to the maximum 60 mm horizontal displacement. The entire mid-rubber layer at mid-height of the un-bonded isolator is under compression as shown in Fig. 4.9(a). Central core of this layer is highly compressed and high stress is shared by larger area along Y direction as compared to X direction of the isolator.

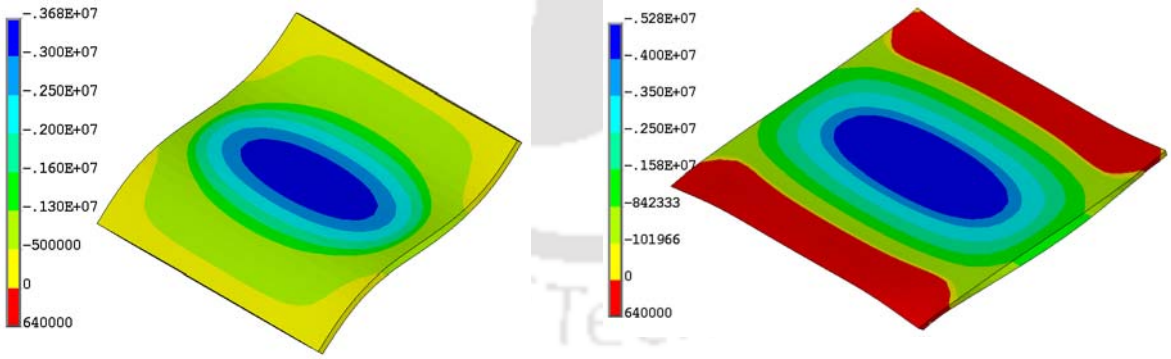

(a) Un-bonded isolator at 60mm displacement

(b) Bonded isolator at 60mm displacement

Fig. 4.9 Contour of normal stress S_{33} (kN/m^2) in mid rubber layer at mid-height of isolator at horizontal displacement 60mm (0^0 loading direction) (Positive value indicates tension)

However, the mid-rubber layer at mid-height of bonded isolator outside overlapping

region is under tension as shown in Fig. 4.9(b). Like un-bonded isolator, the spread of compression along Y direction of isolator is more as compared to X direction.

Fig. 4.10 shows the contour of normal stress S_{11} in the isolator acting along X direction corresponding to 60mm lateral displacement.

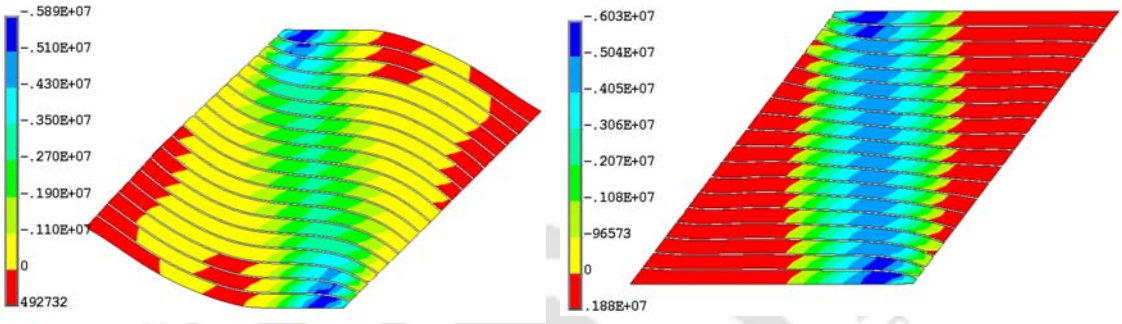

(a) Un-bonded (b) Bonded

Fig. 4.10 Contour of normal stress S_{11} (N/m^2) in rubber layer of isolator at horizontal displacement 60mm and 0^0 loading direction (Positive value indicates tension)

Fig. 4.10(b) indicates that the overlapping region of bonded FREI between the top and bottom faces are under biaxial compression. However, region outside the overlapping zone are under biaxial tension. Similar to the bonded FREI, the central column region of U-FREI also resists the biaxial compression as is evident from Fig. 4.7(a) and 4.10(a). It may be seen from Fig. 4.10(a) and (b) that the peak values of compressive stress in both the isolators are similar; but the compressive stress in central core of U-FREI is much lesser than that of bonded FREI. Similarly, the peak tensile stress in bonded FREI is significantly lower than for bonded FREI.

Fig. 4.11(a)-(c) shows the distribution of the normalized stress S_{11}/P_n along the length of 10th rubber layer for 60mm, 40mm and 20mm displacement. It is observed that the normal compression stress increases with the increase in the horizontal displacement for bonded FREI, while the same does not vary much for un-bonded application. Development of significant tensile stress in bonded FREI along with the existence of warping effect is observed, while no tensile stress is developed in the un-bonded

isolator for the considered range of lateral displacement. Peak pressure in the bonded isolator is 55% higher than that of un-bonded isolator corresponding to 60mm horizontal displacement.

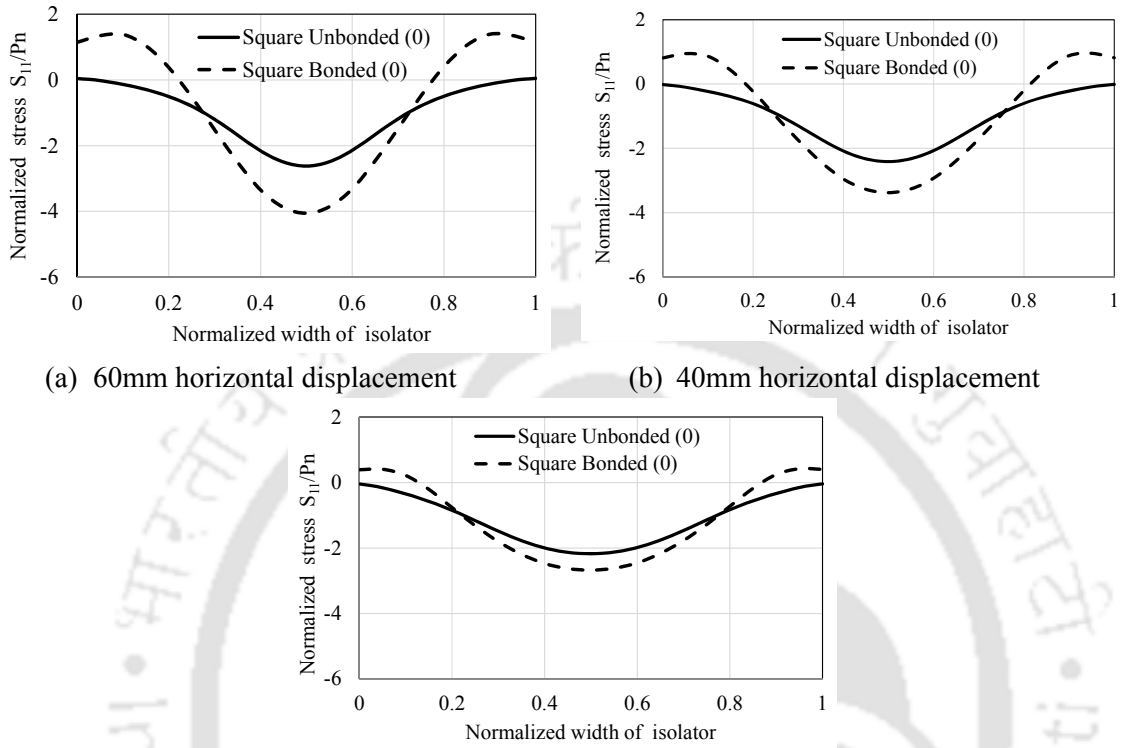

(a) 60mm horizontal displacement (b) 40mm horizontal displacement

(c) 20 mm horizontal displacement

Fig. 4.11 Distribution of normalized stress S_{11}/P_n in the mid rubber layer at mid-height of isolator at different horizontal displacement (0^0 loading direction)

Contour of normal stress S_{11} for square un-bonded and bonded isolator are shown in Fig. 4.12 along middle of 10^{th} rubber layer (mid-height of the isolator) corresponding to the maximum 60 mm horizontal displacement.

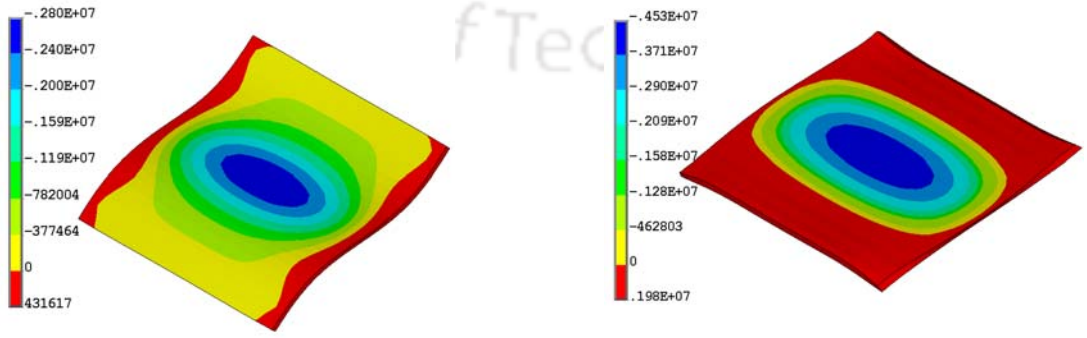

(a) Un-bonded isolator at 60mm displacement (b) Bonded isolator at 60mm displacement

Fig. 4.12 Contour of normal stress S_{11} (kN/m^2) in mid rubber layer at mid-height of isolator at horizontal displacement 60mm (0^0 loading direction) (Positive value indicate tension)

The entire middle rubber layer at mid-height of un-bonded isolator is under compression except the extreme edges along Y direction, which is under tension. However, for bonded isolator around 50% area of middle rubber layer at mid-height is under tension. The observed peak tensile stresses on the edges of bonded isolator are about five times more than peak tensile stresses of un-bonded isolator.

Shear strain in the rubber material must be very large for efficient functioning of an elastomeric isolator. Fig. 4.13 shows the contour plot of shear strain of un-bonded and bonded isolator corresponding to 60mm horizontal displacement.

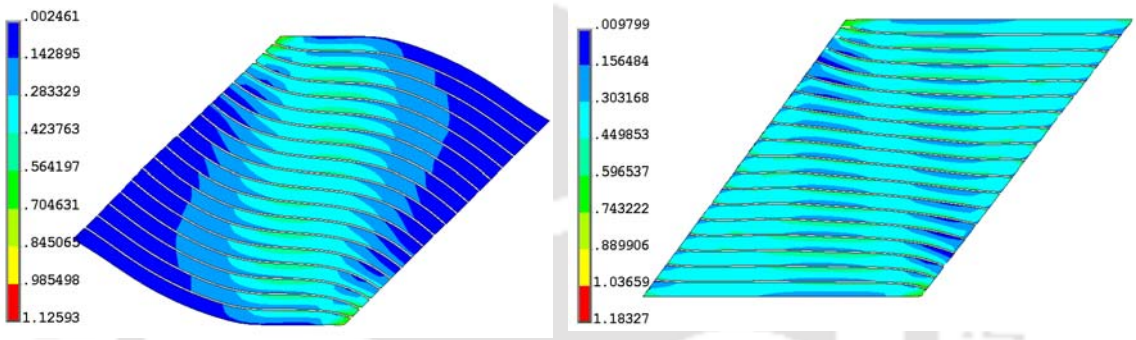

(a) Un-bonded (b) Bonded

Fig. 4.13 Contour of shear strain in the rubber layer of isolator at horizontal displacement 60mm (0^0 loading direction)

Fig. 4.14(a)-(c) illustrates the distribution of shear strain along the rubber plane at mid height of the isolator at different lateral displacements. It may be seen from Fig. 4.14 that the peak shear strain values at the mid-section of middle layer of elastomer of both bonded and un-bonded isolators are quite comparable.

It is observed that U-FREI shows uniform shear strain only in the region in contact with top and bottom support, while almost constant shear strain is observed across the width of the bonded isolator. Shear strain in U-FREI is found to decrease from peak to almost zero where the isolator is not in contact with the support. Further, for 60 mm displacement, the shear strain in the isolator can be approximated as (60mm/104.9mm) ≈0.57. This value is in reasonable agreement with the result shown in Fig. 4.13 and Fig. 4.14.

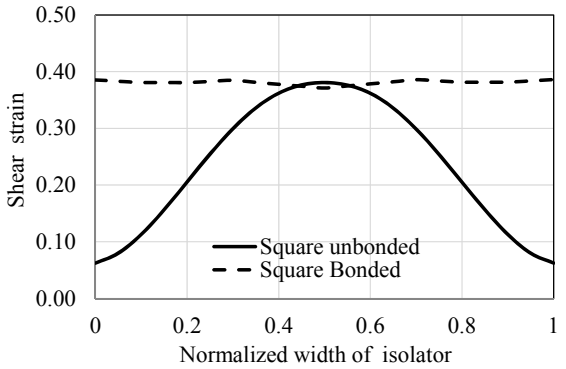

(a) 60mm horizontal displacement

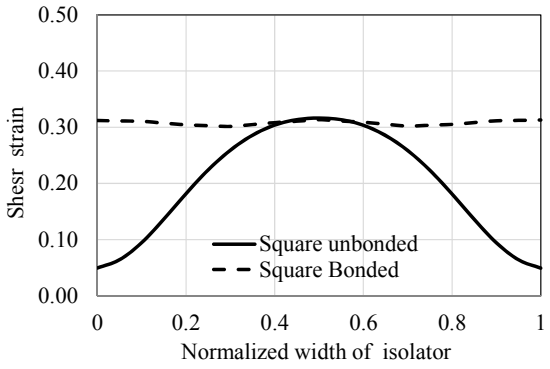

(b) 40mm horizontal displacement

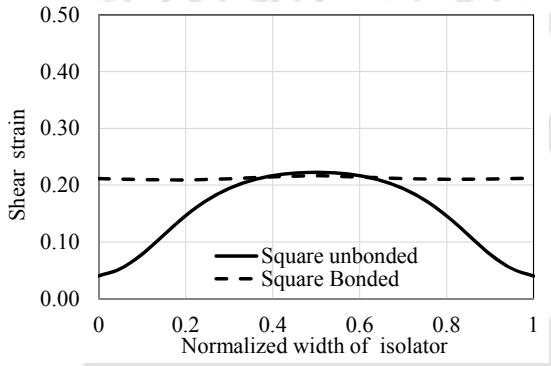

(c) 20 mm horizontal displacement

Fig. 4.14 Shear strain in the mid rubber layer at mid-height of isolator at different horizontal displacement (0^0 loading direction)

Fig. 4.15 shows the contour of shear strain along middle of 10^{th} rubber layer (mid-height of the isolator) corresponding to the maximum 60 mm horizontal displacement.

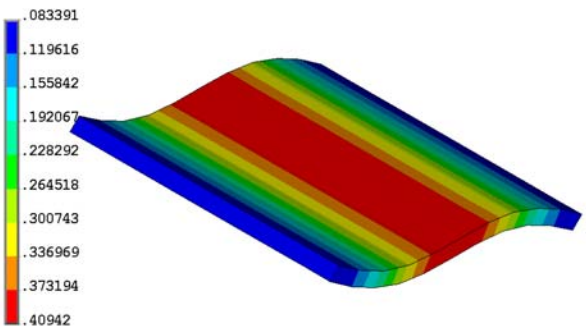

(a) Un-bonded isolator at 60mm displacement

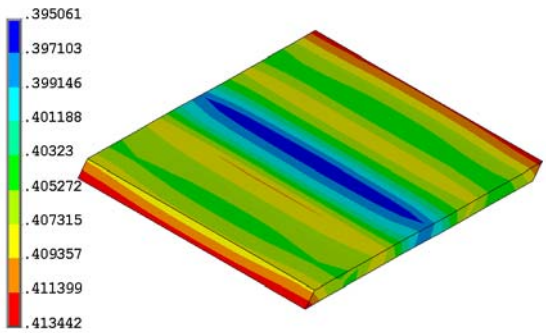

(b) Bonded isolator at 60mm displacement

Fig. 4.15 Shear strain in the mid rubber layer at mid-height of square isolator at 60mm displacement (0^0 loading direction)

While the shear strain is uniform at the mid rubber layer along both X and Y-directions of bonded isolator, the un-bonded isolator shows that the shear strain is highest in the mid-zone of the layer and the same is almost insignificant near the edges. Similar trend may be seen in Fig. 4.14 corresponding to different magnitude of horizontal displacement.

4.3.2.2. Square isolator with 45^0 loading direction

As the earthquake excitations are random in nature, studies are also conducted by applying the cyclic displacement along 45°to the X axis. The effects of direction of excitation on the performance of isolators are evaluated.

Normal stress S_{33} in the isolators corresponding to 60mm displacement for both bonded and un-bonded isolators are shown in Fig. 4.16.

The compression load of bonded FREI is carried by central compression core in the overlapping region between the top and bottom surfaces of isolator. The compressive stress is nearly constant throughout the height of the isolator as shown in Fig. 4.16(b). Vertical load of U-FREI is also carried by the central compression core, similar to bonded FREI (Fig. 4.16(a). The maximum pressure within the U-FREI is less than the maximum pressure of bonded FREI excluding the local pressed corner at top and bottom surfaces. Stable roll off surfaces at top and bottom from the contact surfaces are observed.

Fig. 4.17(a)-(c) shows the distribution of the normalized stress S_{33}/P_n in the 10^{th} rubber layer for 60mm, 40mm and 20mm displacement. It is observed that for bonded isolator, normal compressive stress increases with the increase in the horizontal displacement and length of compression region decreases. However, for un-bonded application, rate of change of normal compressive stress is not significant with the increase in horizontal

displacement. Peak pressure in the bonded isolator is 45% higher than that of un-bonded isolator for 60mm horizontal displacement.

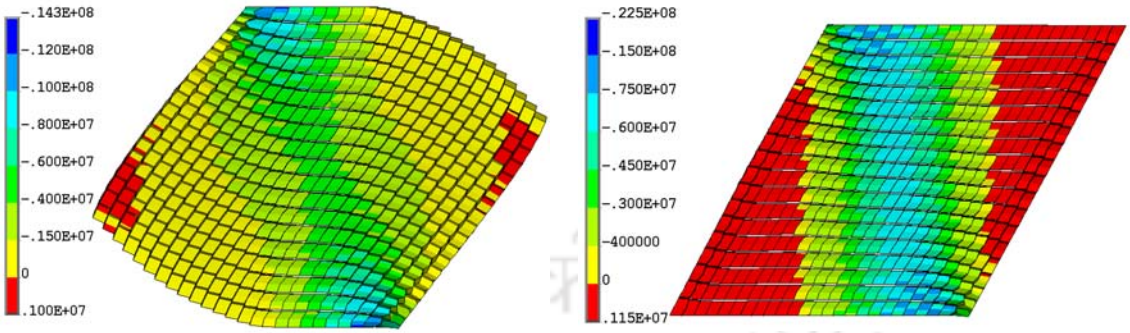

(a) Un-bonded (b) Bonded

Fig. 4.16 Contour of normal stress S_{33} (N/m^2) in rubber layer of isolator at horizontal displacement 60mm and 45^0 loading direction (Positive value indicate tension)

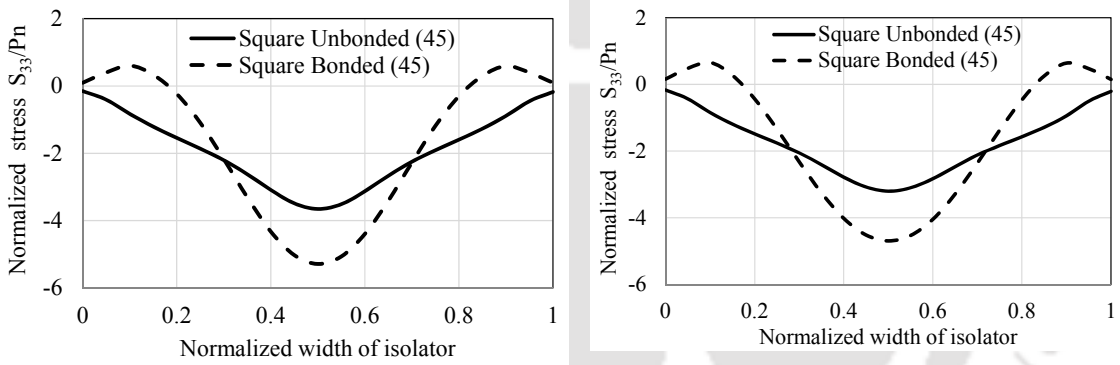

(a) 60mm horizontal displacement (b) 40mm horizontal displacement

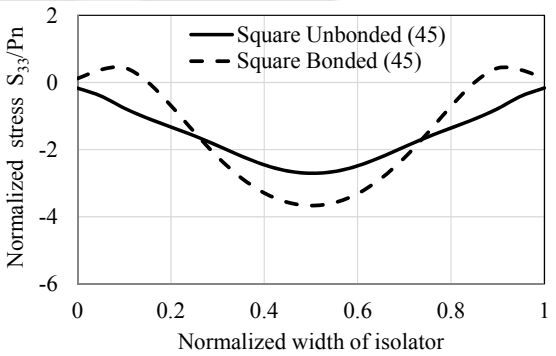

(c) 20 mm horizontal displacement

Fig. 4.17 Distribution of normalized S_{33}/P_n in the mid rubber layer at mid-height of isolator at different horizontal displacement (45^0 loading direction)

Similar to 0° loading case, development of significant tensile stress along with the

presence of warping effect is observed in bonded FREI, while no tensile stress is developed along the mid-height of the un-bonded isolator.

Fig. 4.18 shows the contour of normal stress S_{11} in the isolator for 60mm lateral displacement with 45^0 loading direction. Fig. 4.16 (b) and 4.18(b) of bonded FREI indicate that the overlapping region between the top and bottom support surfaces is under biaxial compression, while region outside the overlapping zone are under biaxial tension.

Similar to the bonded FREI, the central column region of U-FREI resists the biaxial compression as observed from in Fig. 4.16(a) and 4.18(a) with biaxial tensile stresses outside the contact zone.

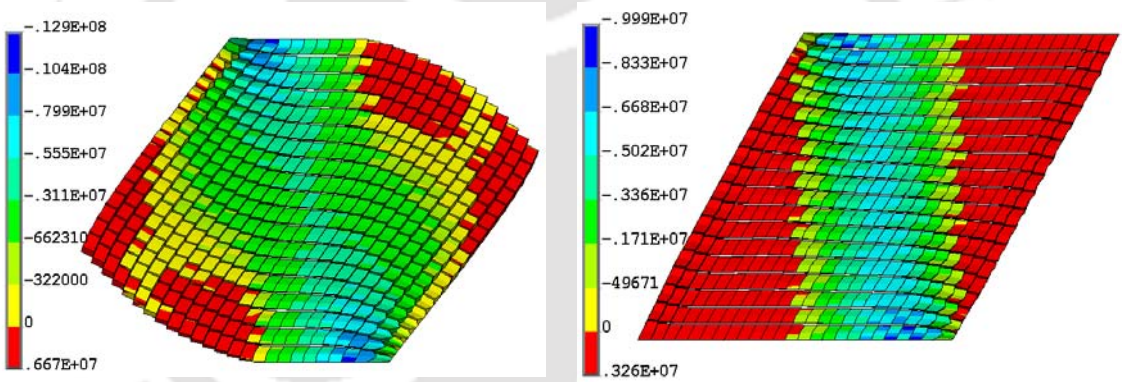

(a) Un-bonded (b) Bonded

Fig. 4.18 Contour of normal stress S_{11} (N/m^2) in rubber layer of isolator at horizontal displacement 60mm and 45^0 loading direction (Positive value indicate tension)

Fig. 4.19(a)-(c) shows the distribution of the normalized stress S_{11}/P_n along the length of 10^{th} rubber layer for 60mm, 40mm and 20mm displacement. Peak pressure in the bonded isolator is 68% higher than that of un-bonded isolator for 60mm horizontal displacement.

Fig. 4.20 shows the contour plot of shear strain of un-bonded and bonded isolator for 60mm horizontal displacement.

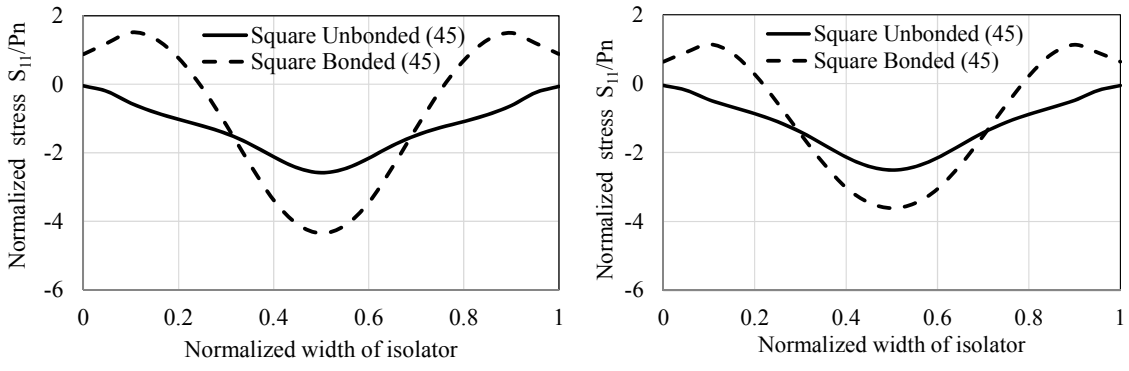

(a) 60mm horizontal displacement (b) 40mm horizontal displacement

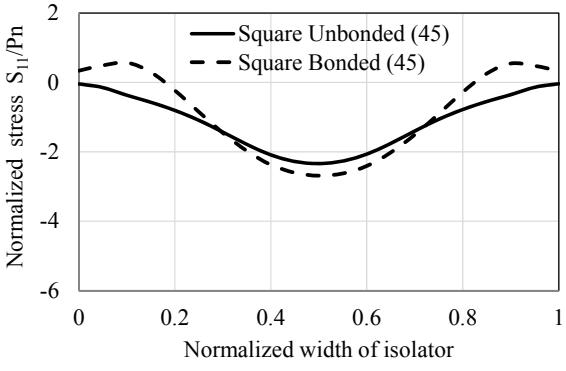

(c) 20 mm horizontal displacement

Fig. 4.19 Distribution of normalized S_{11}/P_n in the mid rubber layer at mid-height of isolator at different horizontal displacement (45^0 loading direction)

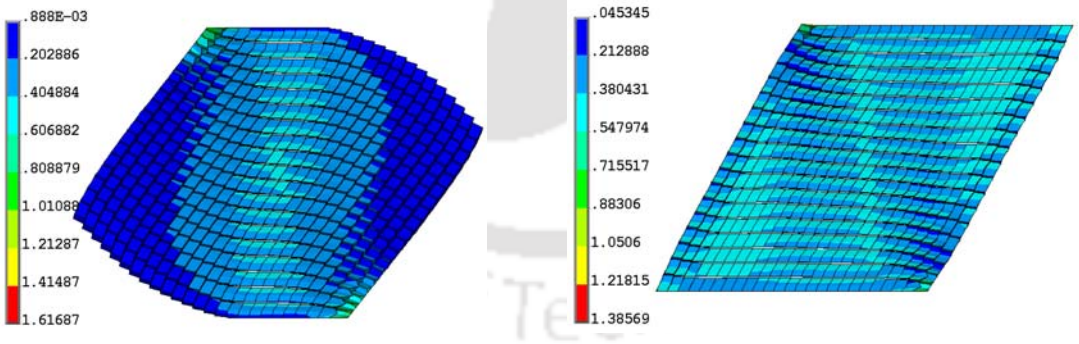

(a) Un-bonded (b) Bonded

Fig. 4.20 Contour of shear strain in the rubber layer of isolator at horizontal displacement 60mm (45^0 loading direction)

Fig. 4.21(a)-(c) illustrates the graphical representation of distribution shear strain along the direction of loading at mid height of the isolator rubber layer.

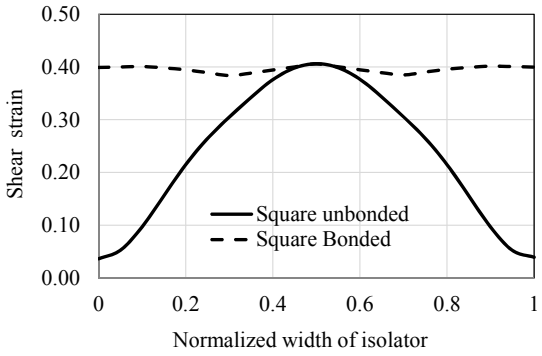

(a) 60mm horizontal displacement

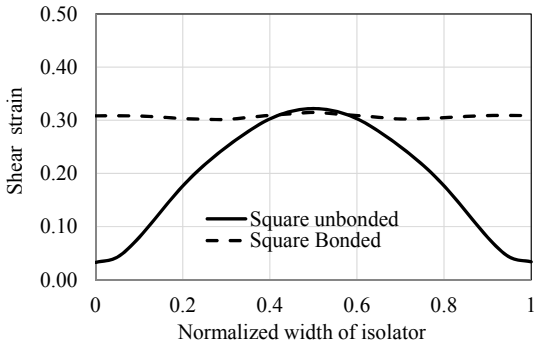

(b) 40mm horizontal displacement

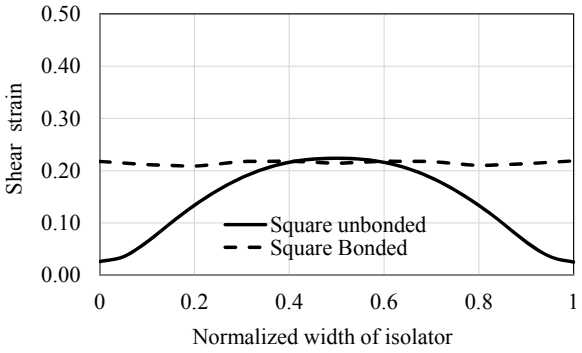

(c) 20 mm horizontal displacement

Fig. 4.21 Shear strain in the mid rubber layer rubber layer at mid-height of isolator at different horizontal displacement (45^0 loading direction)

Shear strain at the edge of un-bonded isolator is almost zero and increases at the middle of isolator. However for bonded isolator shear strain is almost constant at middle rubber layer along the direction of applied horizontal displacement direction of isolator.

4.3.3. Force Displacement Hysteresis Behaviour of Square Isolator

The total force in the loading direction on all the nodes of the top surface are summed to get the total shear force. Shear force is then plotted against horizontal applied displacement to get the hysteresis loop. Important parameter like effective horizontal stiffness and damping are obtained from the hysteresis loops. It may be observed from hysteresis loop that the U-FREI undergoes large amount of change in stiffness from

small to large strain. The effective stiffness is defined by Kelly and Takhirov [2001] as

$$K^h_{eff} = (F_{max} - F_{min})/(d_{max} - d_{min}) \quad (4.1)$$

where, F_{max} is maximum value of shear force

F_{min} is minimum value of shear force

d_{max} is maximum value of displacement

d_{min} is minimum value of displacement

The equivalent viscous damping ratios (β) of the isolators for different loading cases are obtained from hysteresis loop. The area contained in the hysteresis loop in force v/s displacement curve gives the energy dissipated. The damping ratio is calculated as

$$\beta = W_d/(4\pi W_s) \quad (4.2)$$

where, W_d is dissipated energy = hysteresis loop area

W_s is elastic energy

$$W_s = (K^h_{eff}(\Delta_{max})^2)/2 \quad (4.3)$$

Δ_{max} is average of positive and negative maximum displacement

$$\Delta_{max} = (d_{max} + |d_{min}|)/2 \quad (4.4)$$

4.3.3.1. Force-displacement hysteresis behaviour of square isolator with 0^0 loading direction

The hysteresis loop of un-bonded isolator and deformed shape corresponding to 60mm displacement are shown is Fig. 4.22 and Fig. 4.23 respectively. Similarly, the hysteresis loop of bonded isolator and deformed shape for 60mm displacement are shown in Fig. 4.24 and Fig. 4.25 respectively. Effective horizontal stiffness (K^h_{eff}) and damping of square un-bonded and bonded FREI for various displacements (0° Loading) are shown in Table 4.2.

Table 4.2 Properties of un-bonded and bonded isolator for loading under 0° direction

	un-bonded		bonded	
Displacement (mm)	**Effective Horizontal Stiffness (K_{eff}^{h}) (kN/m)**	**Damping (β) (%)**	**Effective Horizontal Stiffness (K_{eff}^{h}) (kN/m)**	**Damping (β) (%)**
10	88.3	12.3	89.7	12.1
20	76.5	12.8	86.4	12.3
30	66.2	13.1	83.2	12.3
40	56.9	13.9	79.3	12.5
50	46.2	15.2	74.7	12.8
60	39.3	16.1	70.7	13.1

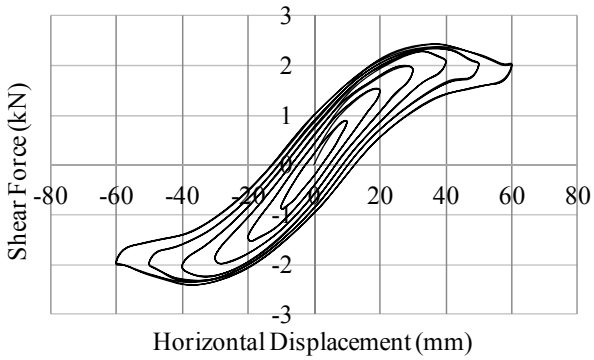

Fig. 4.22 Shear force *vs* horizontal displacement for un-bonded isolator at 0° loading

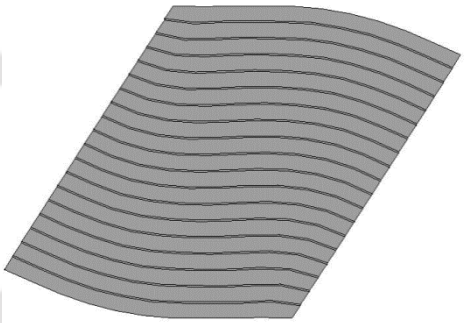

Fig. 4.23 Un-bonded isolator at 60mm displacement (0° Loading)

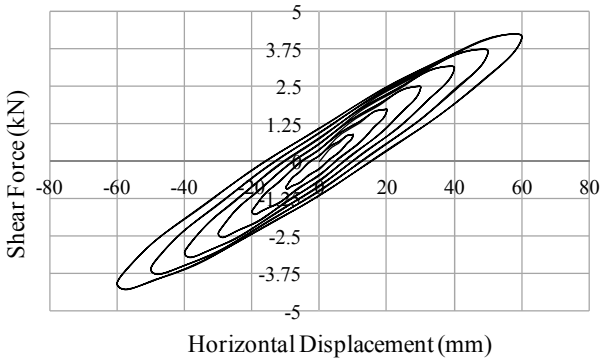

Fig. 4.24 Shear force *vs* horizontal displacement for bonded isolator at 0°

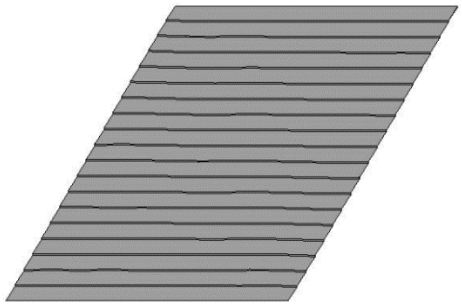

Fig. 4.25 Bonded isolator at 60mm displacement (0° Loading)

4.3.3.2. Force-displacement hysteresis behaviour of square isolator with 45^0 loading direction

The hysteresis loop of un-bonded isolator with loading in 45^0 direction of isolator and displaced shape of isolator for 60mm displacement is shown is Fig. 4.26 and Fig. 4.27

respectively. Similarly, the hysteresis of square bonded isolator and displaced shape of isolator for 60mm displacement is shown in Fig. 4.28 and Fig. 4.29 respectively.

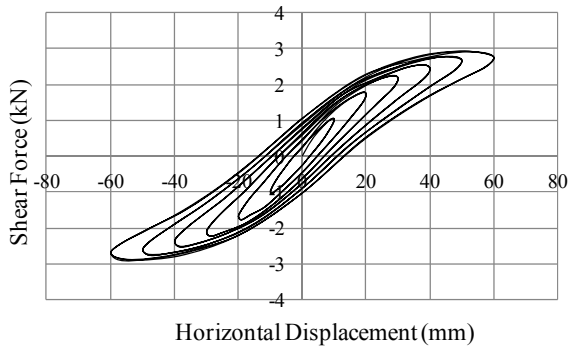

Fig. 4.26 Shear force *vs* horizontal displacement for un-bonded isolator at 45° loading

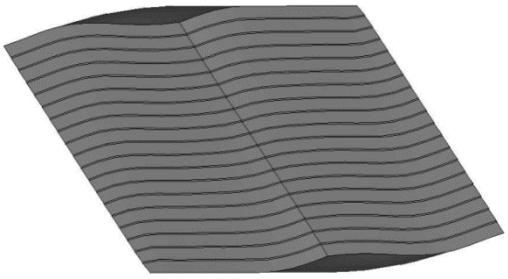

Fig. 4.27 Un-bonded isolator at 60mm displacement (45° Loading)

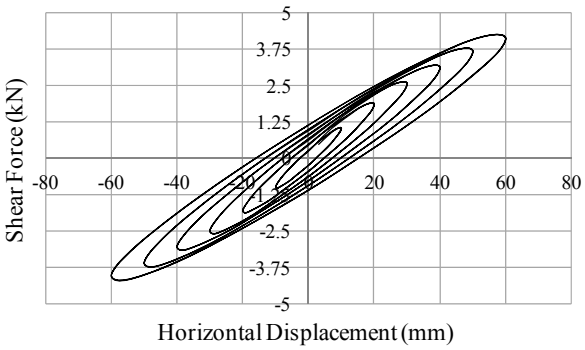

Fig. 4.28 Shear force *vs* horizontal displacement for bonded isolator at 45° loading

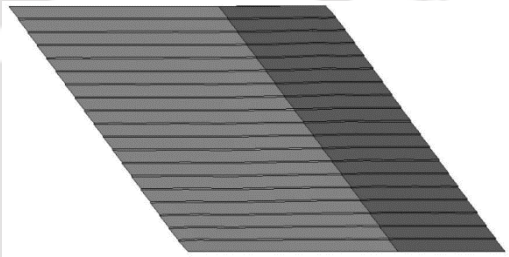

Fig. 4.29 Bonded isolator at 60mm displacement (45° Loading)

Effective horizontal stiffness (K_{eff}^{h}) and damping of square un-bonded and bonded FREI for various displacements (45° Loading) are shown in Table 4.3.

4.3.4. Discussion on FE result of Square Isolators

It is observed that the effective horizontal stiffness (K_{eff}^{h}) of square bonded and U-FREI as calculated from Eqn. 4.1 are nearly same at low applied displacement (up to 10 mm). This is due to the fact that the contacts between upper and lower surfaces of un-

bonded isolator are not lost at small horizontal displacement and hence the behaviour of un-bonded isolator is similar to bonded isolator. As the imposed horizontal displacement increases for un-bonded isolator, the separations of top and bottom surfaces become significant. Thus, as the magnitude of horizontal displacement increases, the stiffness of un-bonded isolator reduces quite sharply, while the reduction in stiffness for bonded one is comparatively much lesser. This phenomena is observed for horizontal loading along both the directions of isolator. The magnitude of effective horizontal stiffness of bonded isolator at the end of applied maximum displacement of 60 mm is about 30-40 % lesser than that of the bonded isolator. Effective stiffness of isolator corresponding to applied horizontal displacement along 45^0 is generally observed to be a bit higher than that for 0^0 loading.

Damping values of isolators are calculated using Eqn. 4.2 and it is observed that for un-bonded isolator, the value increases with the increase in displacement, while for bonded isolator, changes in damping values are insignificant with displacement for both the loading cases.

Table 4.3 Properties of un-bonded and bonded square isolator for loading under 45° direction

	un-bonded		**bonded**	
Displacement (mm)	**Effective Horizontal Stiffness (K_{eff}^h) (kN/m)**	**Damping (β) (%)**	**Effective Horizontal Stiffness (K_{eff}^h) (kN/m)**	**Damping (β) (%)**
10	104.8	12.1	104.0	12.2
20	89.1	12.4	94.3	12.2
30	74.7	13.0	87.2	12.3
40	63.7	13.3	79.6	12.4
50	55.4	13.8	75.4	12.6
60	48.2	14.3	70.6	13.0

4.4. Finite Element Analysis of Circular Isolator

The circular isolator is meshed using the elements described in the previous section and the meshed geometry is shown in Fig. 4.30. End boundary condition considered for analysis of circular bonded and un-bonded isolator is same as the square isolator. Horizontal stiffness of circular isolator shall be same irrespective of the orientation of applied displacement. Hence results of horizontal displacement along X-axis are presented in this study.

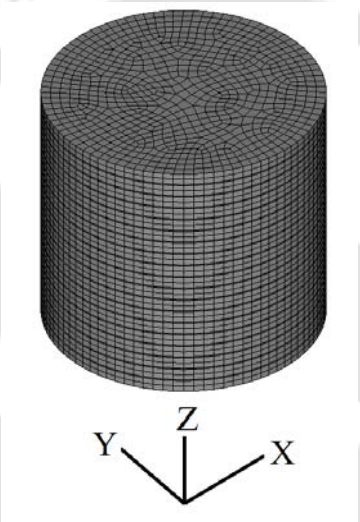

Fig. 4.30 Meshed circular isolator

4.4.1. Analysis for Horizontal Stiffness

FE analysis of circular isolator is carried out similar to square isolator. A constant vertical load of 12 kN is applied on top surface of the isolator and horizontal displacement is applied to evaluate the horizontal stiffness of both bonded and un-bonded isolator at various displacement magnitudes. The horizontal displacement upto 60mm is applied by increasing ±10mm at the end of every three cycles. The horizontal stiffness of bonded circular FREI which is calculated using Eqn. 3.1 and FE analysis are shown in Table 4.4. The general formula $K_h = G_e A/t_r$ used to calculate the horizontal stiffness of steel isolator is used to calculate the horizontal stiffness of bonded circular

FREI. This formula overestimate the horizontal stiffness for a bonded circular FREI due to the presence of flexible fibre reinforcement.

A linear lateral load displacement relation is obtained in the range of small displacement from FE analysis for both the bonded and un-bonded circular FREI as shown in Fig. 4.31. Slope of this line is the horizontal stiffness of circular isolator. As shown in Fig. 4.31, the lateral response of bonded FREI is almost linear, while the response of U-FREI is nonlinear, which is due to the roll over deformation under large applied horizontal displacement.

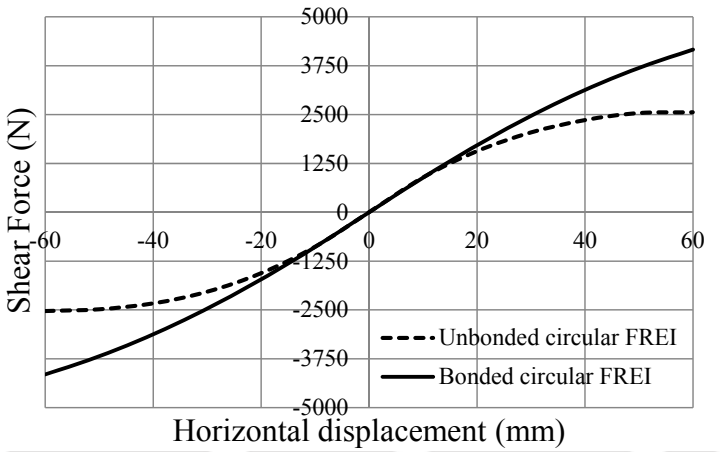

Fig. 4.31 Lateral load *vs* displacement of the bonded and un-bonded circular FREI

The horizontal stiffness of U-FREI decreases with the increase in horizontal displacement. Fundamental time period of un-bonded isolator thus increases with the decrease in stiffness, which results in increasing the performance of isolator during high intensity earthquake. Thus, laterally stable U-FREI has superior seismic isolation capacity as compared to bonded FREI. A stable un-bonded isolator maintains positive tangent stiffness over the range of lateral displacement. The result as obtained from FE model (Fig. 4.31) is also observed to maintain positive tangent stiffness for the displacement range employed in the analysis.

It is observed from Fig. 4.31 that up to 16 mm lateral displacement, the force that would

be transmitted by bonded and U-FREI is almost same. However, beyond 16mm, the force transmitted by U-FREI is significantly lower as compared to bonded FREI. The lateral force transmitted by bonded FREI is 60% higher than that of U-FREI during the maximum 60 mm horizontal displacement. Hence, it can be concluded that with the same size of isolator, performances of U-FREI is far superior to bonded FREI.

Table 4.4 Horizontal stiffness (N/mm) of bonded circular FREI

Analytical $(K_h = \frac{GA}{t_r})$	**From Eq. (3.1)**	**FE Analysis**
72.59	68.79	69.3

4.4.2. Stress and Strain of Circular Isolator

Contour of normal stress S_{33} corresponding to maximum applied displacement of 60 mm is shown in Fig. 4.32 for both bonded and un-bonded circular isolators. The normal stress S_{33} acts along Z axis.

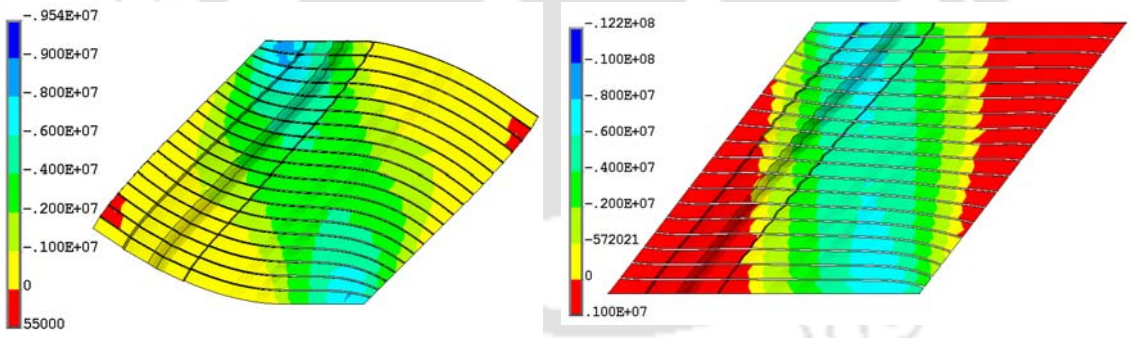

(a)Un-bonded circular (b) Bonded circular

Fig. 4.32 Contour of normal stress S_{33} (kN/m^2) in rubber layer of circular isolator at horizontal displacement 60mm (Positive value indicate tension)

The compression load of bonded FREI is carried by central compression core within the overlapping region between the top and bottom faces of isolator. As the lateral deformation increases, area of compression region decreases and peak compression increases in the bonded FREI. The compression in the central core is almost constant

throughout the height of the isolator as can be seen from Fig. 4.32(b). Thus, while the compression is carried through the overlapping region between top and bottom surfaces, the unbalanced moment is carried by tension stresses in the regions outside the overlap.

Vertical load of U-FREI is carried by the central compression core, similar to bonded FREI (Fig. 4.32a). However, the maximum compressive stresses in U-FREIs are developed only in the pressed corner at top and bottom surfaces and the magnitude of peak compression that develop in both isolators are comparable. Further, when an un-bonded isolator is deformed laterally, near end of the loading direction leaves the contact and moves upward causing tension in fibre reinforcement. Similarly, the opposite end of the isolator moves downward and loses contact with the support. Tension is developed in the region of no contact while other regions remain under compression. However, due to un-bonded application, no tensile stress is transferred to the isolator's contact support. The unbalanced moments are resisted by the vertical load through offset of the force resultants on the top and bottom surfaces. It may also be noted that the tensile stress S_{33} developed in U-FREI is lesser than those of bonded FREI. Hence, peeling stress demand on the bond between the rubber and fibre reinforcement in case of U-FREI is lesser than that of bonded FREI.

Figs. 4.33(a)-(c) show the distribution of the normalized stress S_{33}/P_n along the horizontal plane of 10^{th} rubber layer located at mid-height of the isolator at lateral displacement of 60mm, 40mm and 20mm. It is observed for bonded isolator that normal compressive stress increases with the increase in the horizontal displacement while the length of compression region decreases. Development of considerable tensile stress is observed in bonded FREI along with the presence of warping effect. However, for un-bonded application, the compressive stress does not vary much with the increase in horizontal displacement and there is no development of tensile stress as well. Further,

peak pressure at the middle of bonded isolator is 52% higher than that of un-bonded isolator corresponding to 60mm horizontal displacement and hence, U-FREIs are less susceptible to Euler buckling as compared to bonded FREI.

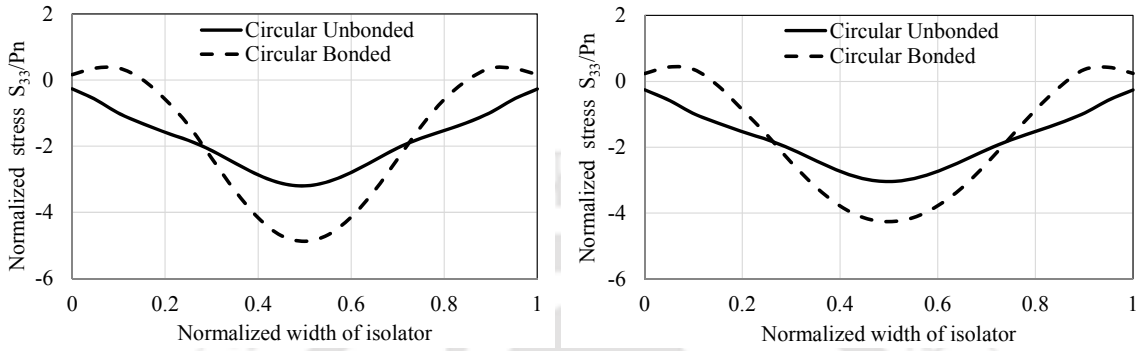

(a) 60mm horizontal displacement (b) 40mm horizontal displacement

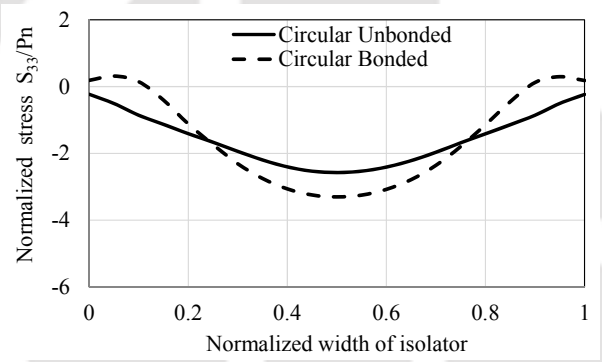

(c) 20 mm horizontal displacement

Fig. 4.33 Distribution of normalized S_{33}/P_n in the mid rubber layer rubber layer of circular isolator at 60 mm horizontal displacement

Fig. 4.34 shows the contour of normal stress S_{11} in the circular isolator corresponding to 60mm lateral displacement. Fig. 4.34(b) indicates that the overlapping region of bonded circular FREI between the top and bottom faces are under biaxial compression. However, region outside the overlapping zone are under biaxial tension. Similar to the bonded FREI, the central column region of U-FREI also resists the biaxial compression as is evident from Fig. 4.32(a) and 4.34(a). It may be seen from Fig. 4.34(a) and (b) that the peak values of compressive stress in both the isolators are similar; but the compressive stress in central core of U-FREI is much lesser than that of bonded FREI.

Similarly, the peak tensile stress in bonded FREI is significantly lower than for bonded FREI.

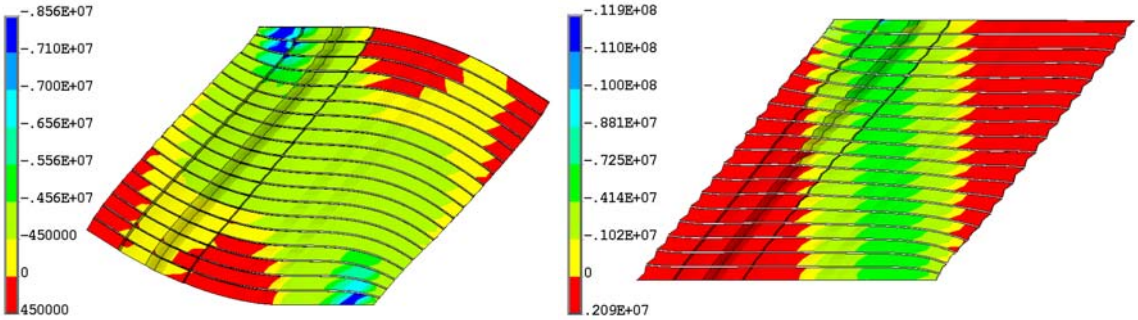

(a)Un-bonded circular isolator (b) Bonded circular isolator

Fig. 4.34 Contour of normal stress S_{11} (kN/m^2) in rubber layer of isolator at horizontal displacement 60mm (Positive value indicate tension)

Fig. 4.35(a)-(c) shows the distribution of the normalized stress S_{11}/P_n along the length of 10th rubber layer for 60mm, 40mm and 20mm displacement.

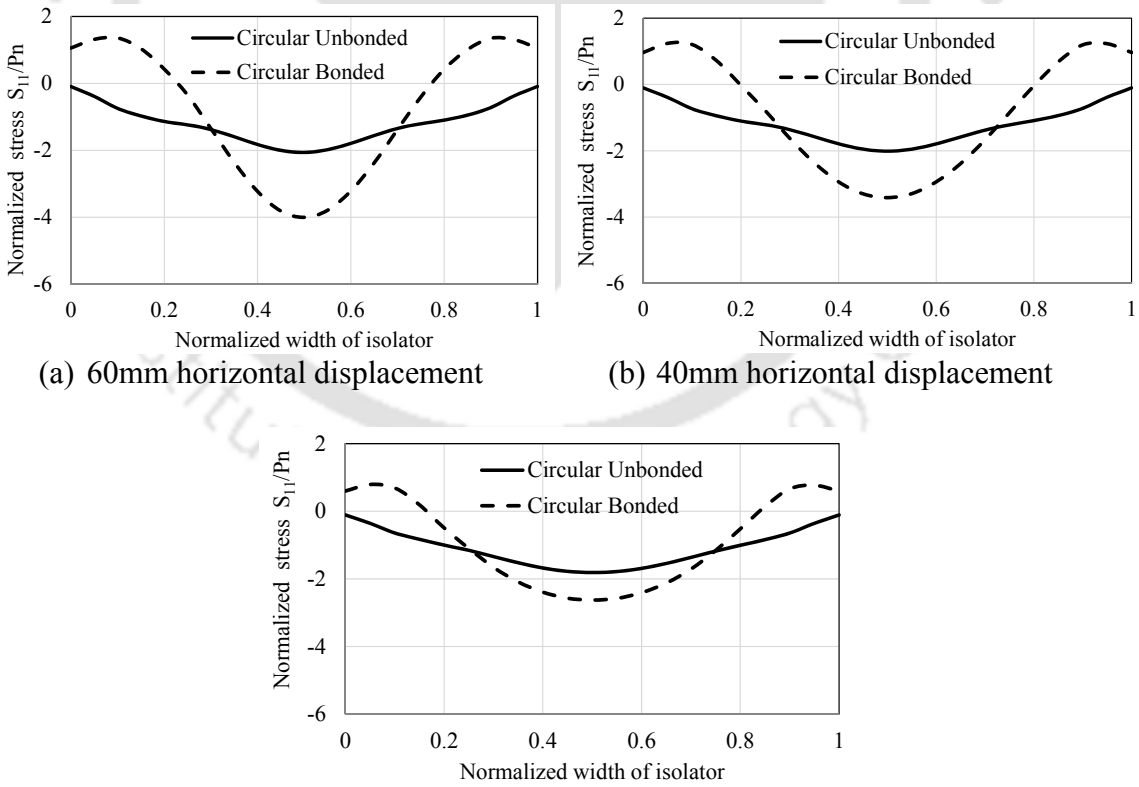

(a) 60mm horizontal displacement (b) 40mm horizontal displacement

(c) 20 mm horizontal displacement

Fig. 4.35 Distribution of normalized S_{11}/P_n in the mid rubber layer rubber layer of circular isolator at 60 mm horizontal displacement

It is observed that the normal compression stress increases with the increase in the horizontal displacement for bonded FREI, while the same does not vary much for un-bonded application. Development of significant tensile stress in bonded FREI along with the existence of warping effect is observed, while no tensile stress is developed in the un-bonded isolator for the considered range of lateral displacement. Peak pressure in the bonded isolator is 94% higher than that of un-bonded isolator corresponding to 60mm horizontal displacement.

Fig. 4.36 shows the contour plot of shear strain of un-bonded and bonded circular isolator corresponding to 60mm horizontal displacement. Fig. 4.37(a)-(c) illustrates the distribution of shear strain along the rubber plane at mid height of the isolator at different lateral displacements.

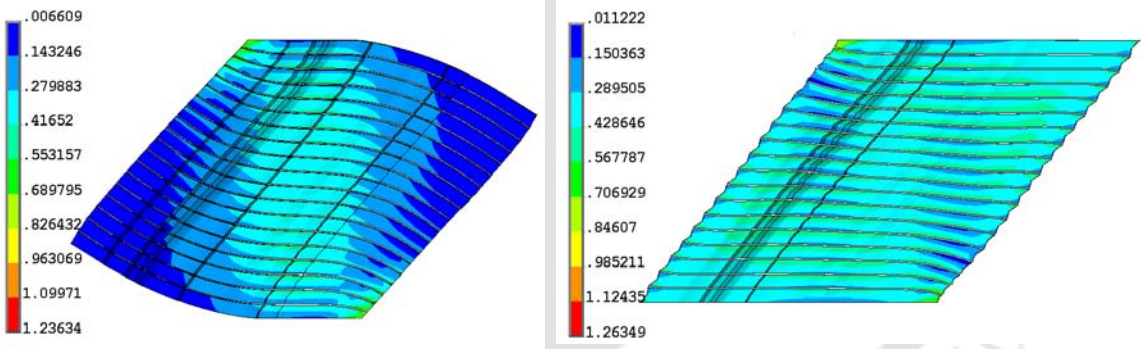

(a) Un-bonded circular isolator (b) Bonded circular isolator

Fig. 4.36 Contour of shear strain in the rubber layer of circular isolator at horizontal displacement 60mm

It may be seen from Fig. 4.36 that the peak shear strain values at the mid-section of middle layer of elastomer of both bonded and un-bonded isolators are fairly comparable. It is observed that U-FREI shows uniform shear strain only in the region in contact with top and bottom support, while almost constant shear strain is observed across the width of the bonded isolator. Shear strain in U-FREI is found to decrease from peak to almost zero where the isolator is not in contact with the support. Further, for 60 mm displacement, the shear strain in the isolator can be approximated as

(60mm/104.9mm) ≈0.57. This value is in reasonable agreement with the result shown in Fig. 4.36 and Fig. 4.37.

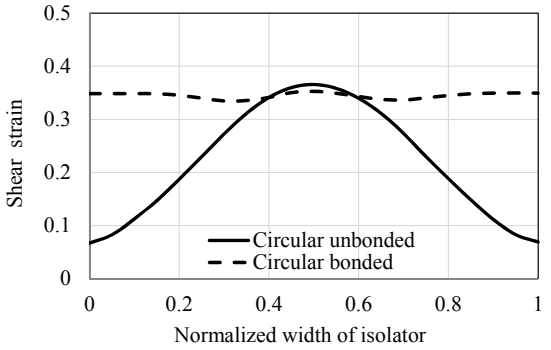

(a) 60mm horizontal displacement

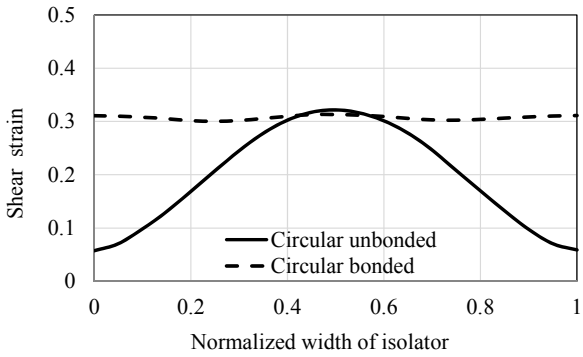

(b) 40mm horizontal displacement

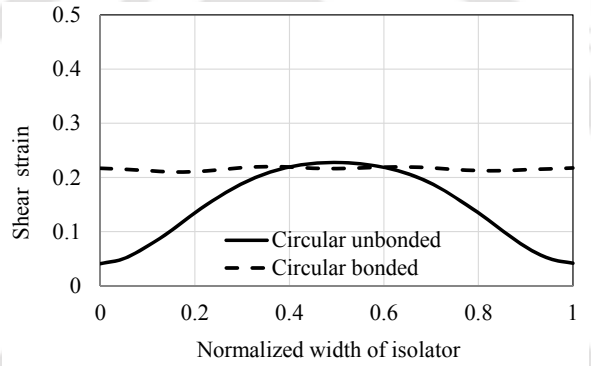

(c) 20 mm horizontal displacement

Fig. 4.37 Shear strain in the mid rubber layer rubber layer of circular isolator at 60 mm horizontal displacement

4.4.3. Force Displacement Hysteresis Behaviour of Circular Isolator

The hysteresis loop of circular un-bonded isolator and displaced shape of isolator for 60 mm displacement are shown is Fig. 4.38 and Fig. 4.39 respectively.

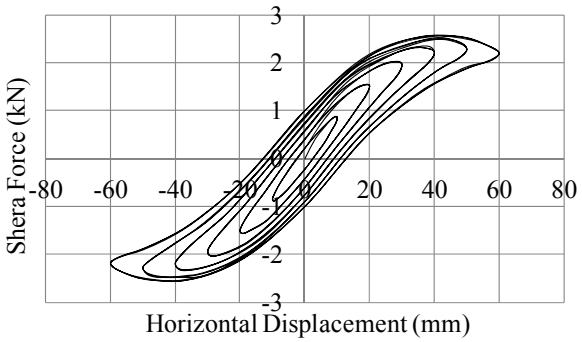

Fig. 4.38 Shear force v/s horizontal displacement for circular un-bonded isolator

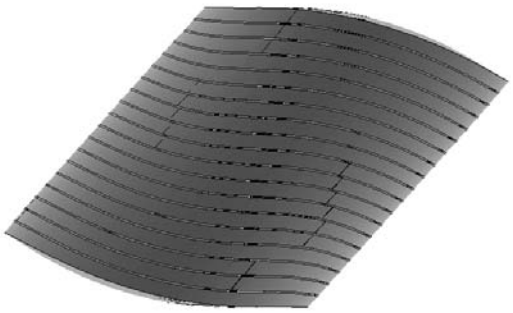

Fig. 4.39 Circular un-bonded isolator at 60 mm displacement

The hysteresis of circular bonded isolator and displaced shape of isolator for 60 mm displacement is shown in Fig. 4.40 and Fig. 4.41 respectively.

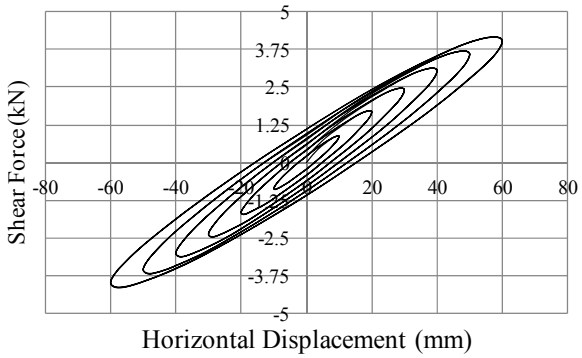

Fig. 4.40 Shear force v/s horizontal displacement for circular bonded isolator

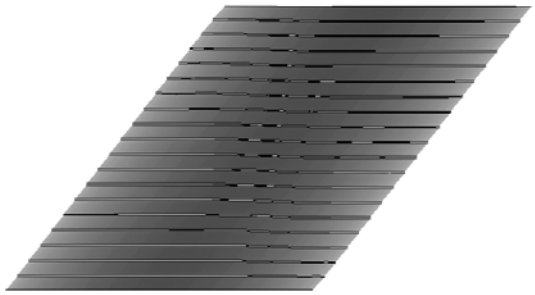

Fig. 4.41 Circular bonded isolator at 60 mm displacement

The effective stiffness and damping are calculated by using the Eqn. 4.1 and 4.2 as described in section 4.3.3. Effective horizontal stiffness (K_{eff}^{h}) and damping of circular un-bonded and bonded FREI for various displacements (0° Loading) are shown in Table 4.5.

Table 4.5 Horizontal response of un-bonded and bonded circular isolator

	un-bonded		bonded	
Displacement (mm)	**Effective Horizontal Stiffness (K_{eff}^{h}) (kN/m)**	**Damping (β) (%)**	**Effective Horizontal Stiffness (K_{eff}^{h}) (kN/m)**	**Damping (β) (%)**
10	88.8	12.2	88.8	12.2
20	77.8	12.7	85.7	12.2
30	68.0	13.1	82.1	12.4
40	57.8	13.8	78.1	12.4
50	50.3	14.3	73.9	12.7
60	42.6	14.9	69.3	13.0

4.4.4. Discussion on FE Result of Circular Isolator

The effective horizontal stiffness (K_{eff}^{h}) of circular bonded and U-FREI as calculated from Eqn. 4.1 are found to be nearly same at low applied displacement. The differences in stiffness increases as the magnitude of horizontal displacement increases. It is seen that the horizontal stiffness is higher for the bonded isolator as compared to the un-

bonded isolator for any given magnitude of applied displacement. The magnitude of effective horizontal stiffness of bonded isolator at the end of applied maximum displacement of 60 mm is about 38.5 % lesser than that of the bonded isolator. The percentage reduction of effective horizontal stiffness of un-bonded circular isolator with increase in horizontal displacement is in similar range of un-bonded square isolator. Hence the seismic performances of both square and circular un-bonded isolators are fairly comparable to each other.

Damping values of isolators are calculated using Eqn. 4.2 and it is observed that for un-bonded isolator, the value increases with the increase in displacement, while for bonded isolator, changes in damping values are insignificant with displacement. Comparison of mechanical properties of square and circular isolators are may be outlined as below.

1. Horizontal stiffness of both bonded and un-bonded circular FREIs are quite comparable to those of square FREI.
2. Maximum compression stresses developed at the central overlapping portion of circular un-bonded isolator and tensile stress at the edges are also comparable to the compressive and tensile stress developed in square un-bonded isolator for applied displacement along X-axis.

4.5. Effect of Mesh Size on Analysis Result

As discussed in the previous section, non-linear analysis of FE model of FREI with fine mesh takes huge time for getting converged solution. Sample analyses are carried out for studying the influence of such mesh sizes on the result of isolators. Fig.4.42 shows three FE models of FREI with different discretization named as coarse, fine and very fine mesh size. Fig. 4.42(a) shows the isolator discretize by considering coarse mesh size and this takes minimum computational time for solution convergence. Fig. 4.42(b)

shows the isolator discretize by considering fine mesh size to check the sensitivity of FE mesh sizing. Fine mesh of Fig. 4.42(b) is further refined to check the variation of result and the discretized model of FREI with very fine mesh is shown in Fig. 4.42(c).

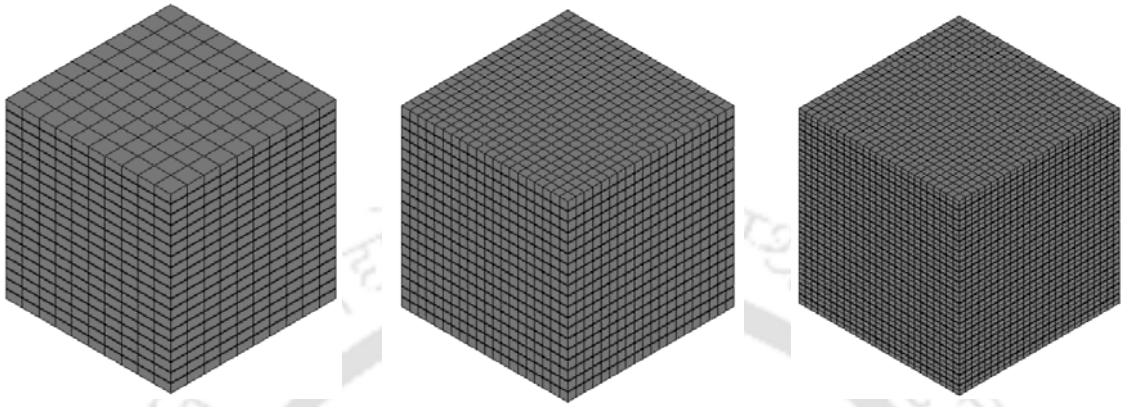

(a) Coarse mesh (b) Fine mesh (c) Very fine mesh

Fig. 4.42 FE model of FREI with different discretization

Fig. 4.43 shows the results of distribution of normalized stress S_{33}/P_n in the mid rubber layer of un-bonded isolator at different horizontal displacement (0^0 loading direction) with coarse and fine mesh size.

The stress distribution pattern, peak values corresponding to the coarse mesh (Fig. 4.42(a)) for 60mm, 40mm and 20mm horizontal displacements are very close to the corresponding results of fine mesh (Fig. 4.42(b)) as shown in Fig. 4.43(a-c).

Analysis has been carried out with further refined mesh (Fig. 4.42(c)) and the distribution of normalized stress S_{33}/P_n in the mid rubber layer of un-bonded isolator at different horizontal displacement (0^0 loading direction) with coarse mesh and very fine mesh is shown in Fig.4.44. It may be seen from Fig.4.44 that the stress distribution is much smoother, though the peak values are almost in the same range. In view of this, all the results are generated based on the very fine mesh for square and circular isolators.

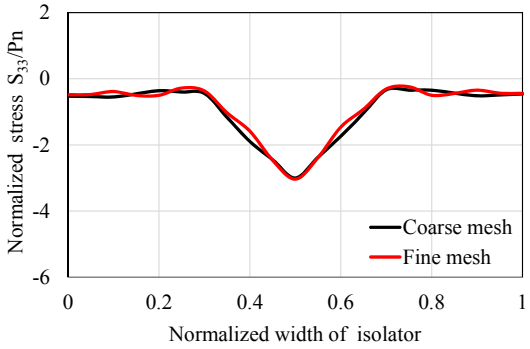

(a) 60mm horizontal displacement

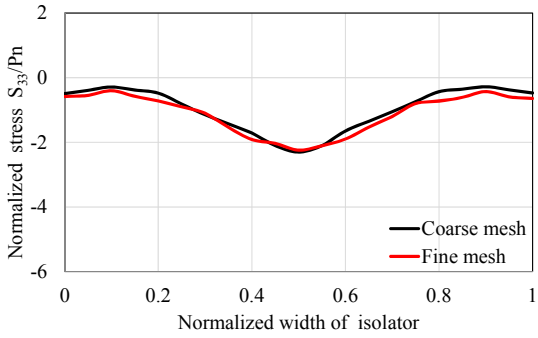

(b) 40mm horizontal displacement

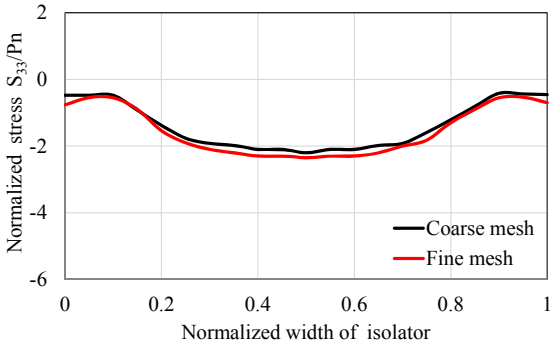

(c) 20 mm horizontal displacement

Fig. 4.43 Distribution of normalized stress S_{33}/P_n in the mid rubber layer of un-bonded isolator at different horizontal displacement (0^0 loading direction) with coarse and fine mesh.

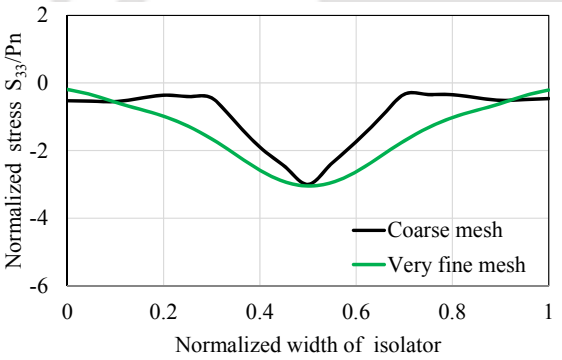

(a) 60mm horizontal displacement

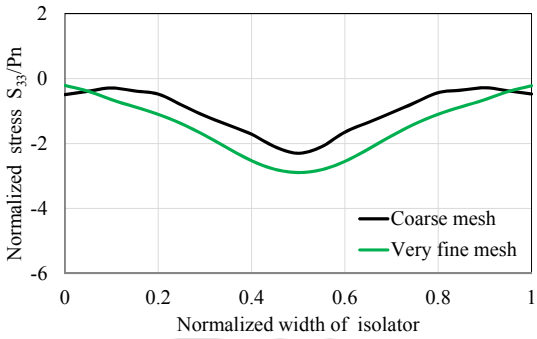

(b) 40mm horizontal displacement

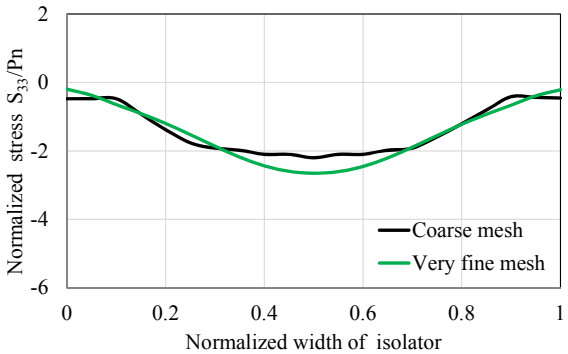

(c) 20 mm horizontal displacement

Fig. 4.44 Distribution of normalized stress S_{33}/P_n in the mid rubber layer of un-bonded isolator at different horizontal displacement (0^0 loading direction) with coarse and very fine mesh

4.6. Effect of Vertical Loading on Shear Capacity of FREI

The vertical load acting on the bearing may change at the time of application of horizontal load during experimental investigation or during an earthquake. The effect of such load variation has been studied by considering ±25% variation in vertical load. Analyses are carried out by applying 75% and 125% of vertical load and results are presented below. Fig. 4.45 and Fig. 4.46 show the results for cases with variation in vertical loads. Table 4.6 shows the values of maximum and minimum shear, which the un-bonded square FREI can take for cases with different vertical loads. Thus, it is observed that no significant differences in the numerical analysis results have occurred.

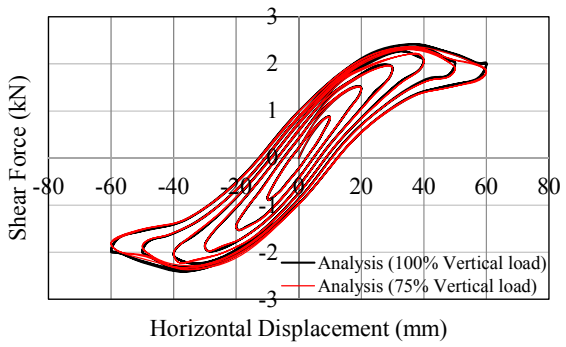

Fig. 4.45 Shear force *vs* horizontal displacement comparison for un-bonded square isolator at 0° loading with 100% and 75% of total vertical load

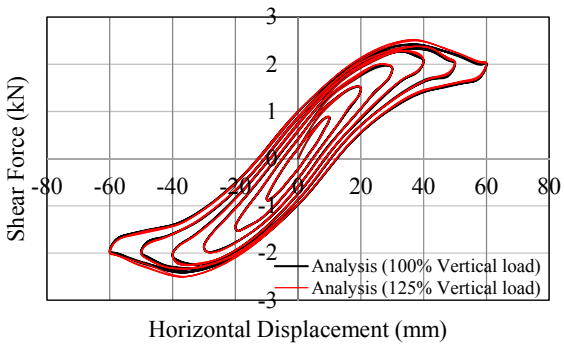

Fig. 4.46 Shear force *vs* horizontal displacement comparison for un-bonded square isolator at 0° loading with 100% and 125% of total vertical load

Table 4.6 Maximum and minimum values of shear for cases with different vertical load

Vertical Load (%)	Maximum shear force (kN)	Minimum shear force (kN)
75	2.37	-2.37
100	2.42	-2.41
125	2.52	-2.50

4.7. Concluding Remarks

In this chapter FE analyses of square and circular FREIs are carried out to evaluate the stress and strain in elastomer. The effective horizontal stiffness of isolators are

evaluated from the analysis. Comparison of FE analysis result and experimental results are carried out in the subsequent chapter. The design parameters of base isolators are required to meet specific target stiffness and time period for effective seismic isolation. Three dimensional FE analyses are carried out on two identical square and a circular FREIs. While one is a conventional bonded type, the other one is considered as un-bonded and appropriate boundary conditions are simulated for the analyses. Cyclic horizontal displacement up to 60 mm is applied along with the constant vertical load. Two different directions are considered for the application of lateral displacement of square isolator for ascertaining the effect of loading direction on the behaviour of layered FREI. The horizontal stiffness of bonded FREI has been found to agree well with the existing closed form solution. However, in the absence of closed form solutions for U-FREI, the observed magnitude of stiffness from FE analysis forms a basis for design. It is observed from analysis, that the top and bottom surfaces of U-FREI exhibit stable roll off the contact surfaces without effecting solution convergence. The following conclusions are made based on the present study:

- Horizontal stiffness of U-FREI is significantly lesser than bonded FREI at higher displacement and hence efficiency for seismic isolation is higher. This behaviour of FREI is observed by various researchers in the past also.
- Initial stiffness of un-bonded isolator corresponding to 45^0 loading is higher than that for 0^0 loading.
- As observed from FE analysis, significantly lower tensile stresses are developed in the rubber and reinforcement layers and hence lower peeling stress demand on the bond between layers in U-FREI, which is also confirmed from the findings of existing research literature on FREI.
- The cross section area of square and circular FREI considered as same. Though

shapes are different, the total rubber layer thickness is same, i.e 95 mm. Hence their performance and mechanical properties are comparable.

- The effective horizontal stiffness and vertical stiffness of both the isolator is very close. This shows that circular isolators can be replaced by square isolator of same area without significant reduction in performance. Wastage of material is less and fabrication is also easier for square or rectangular shape isolator.
- The U-FREI can be used for seismic isolation of low cost housing in remote areas as they are light weight, less expensive. The weight and cost of isolator is reduced by eliminating thick end plates, using fibre reinforcement and less stringent bonding requirement further reduces cost of manufacturing.

Chapter 5

Experimental Study on Force-Displacement Behaviour of U-FREI

5.1. Introduction

Experimental studies are carried out to verify the FE analysis result of square U-FREI. The square U-FREIs having the same material and geometrical properties as mentioned in chapter 3 is used for testing. An experimental set-up is made to apply the cyclic vertical load for the evaluation of vertical stiffness. Similarly, an experimental set-up is made for the evaluation of horizontal stiffness, where the isolator is subjected to constant vertical load and cyclic horizontal displacement. This chapter describes the results of experimental investigation and their comparison with those obtained from FE analysis.

5.2. Test for Evaluation of Vertical Stiffness

This section present the experimental investigations of FREI subjected to vertical loading in order to evaluate the vertical stiffness of the isolator. The isolators are tested for un-bonded end conditions i.e. external top and bottom surfaces of isolator are not bonded to top and bottom plates. This test is conducted in the structural engineering laboratory of Indian Institute of Technology, Guwahati, Assam, India.

5.2.1. Test Set-up and Instrumentation

A servo-control hydraulic actuator (Make: MTS, USA) is used for applying vertical load on the top surface of the isolator. This actuator provides an integrated high-

performance solution to dynamic force generation requirement. Force transducers produce an electrical signal proportional to the force exerted by the actuator. They achieve at least 99% accuracy throughout the actuator range. A linear variable differential transformer (LVDT) provides a piston rod displacement feedback signal to the system control electronics. The LVDT is coaxially mounted within the actuator piston rod and produces an analog signal with excellent linearity. For structural test applications, hydraulic actuator equipped with a swivel rod end and a swivel base allows the actuator to pivot freely at both ends. This configuration reduces moment loads on the test specimen and load cell. The vertical actuator is hanged from rigid steel frame and the actuator has a maximum displacement range of ± 125 mm and maximum loading capacity of 100kN.

Test set-up for the evaluation of vertical stiffness of FREI is shown in Fig. 5.1. The test specimen is placed on a hard surface just below the head of the actuator. Four bolts from the rigid bottom surface are connected to the loading head of the actuator to maintain alignment of actuator during loading. This test is conducted under load control of actuator and vertical displacement of the isolator is recorded by data acquisition system.

Fig. 5.1 Set-up for test under vertical load

5.2.2. Test Results and Discussion

Test under vertical loading is performed to determine the stiffness of the bearing in vertical direction. The specimen is first monotonically loaded up to 12.0kN and three cycles of sinusoidal loading with amplitudes ±3.0kN are applied. During the final stage, the specimen is monotonically unloaded. The vertical loading history for vertical load test is shown in Fig. 4.2. The vertical loading is applied at the top surface of the bearing and displacement of isolator in vertical direction is recorded.

The result of the vertical test is presented in Fig 5.2. The vertical axis represents the vertical load applied on the specimen and horizontal axis represents the displacement at the top surface of bearing. As seen from Fig 5.2, the vertical stiffness of bearing increases under higher pressure. This may be due to the increase in in-plane fibre sheet tension at higher pressure, which is due to enhancement in effective fibre modulus for straightening of fibre [Kelly and Takhirov, 2002].

The average stiffness of the square U-FREI is computed as the slope of straight line interpolating the hysteresis loop, obtained during the cyclic vertical load test. Similar strategy was adopted by [Kelly and Takhirov, 2001] and the straight line is shown by dotted line in Fig 5.2.

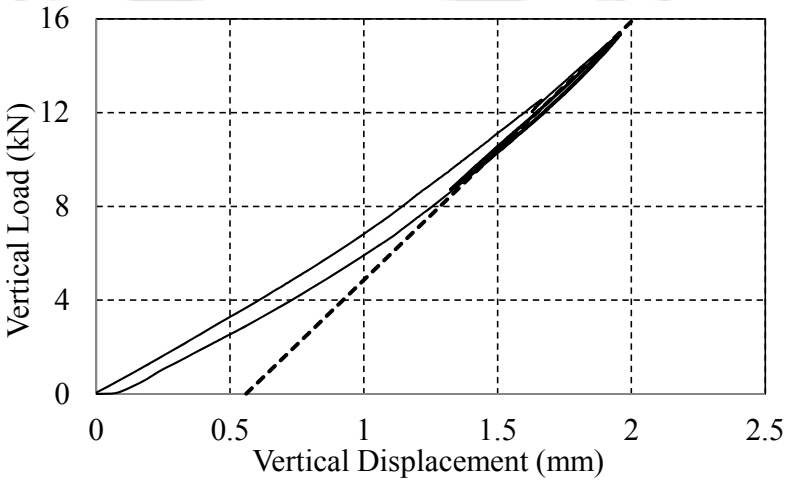

Fig. 5.2 Vertical load vs vertical displacement (test result)

The summary of vertical stiffness as obtained from the test is shown in Table 5.1. The test result of vertical stiffness shows a close agreement with the value calculated from the simple formula given by Eqn. 3.19. In order to provide effective seismic isolation, an isolator must have very high vertical stiffness and low horizontal stiffness. These criteria are satisfied by the tested square U-FREI. As seen from the test result, the vertical stiffness of U-FREI is around 125 times higher than the maximum horizontal stiffness as obtained from FE analysis of U-FREI for 0° loading direction. This higher vertical stiffness of elastomeric bearings ensures that the rocking vibration modes do not participate in the response of base isolated structures (Nezhad *et at*, 2009)

Table 5.1 Vertical test result of square isolator.

Monotonically increasing vertical load (kN)	Cyclic amplitude load magnitude (kN)	Vertical stiffness from Eqn. (3.19) (kN/m)	Average vertical stiffness during cyclic test (kN/m)
12.0	3.0	10653.96	11035

5.3. Test for evaluation of Horizontal Stiffness

The FE analysis results of the un-bonded square FREI presented in previous chapter are validated with experimental findings. The isolators used for the test are having the same material and geometrical properties as used in FE analysis. The detailed experimental setup for test under horizontal displacement and comparison of experimental findings with results from obtained from FE analysis are presented.

5.3.1. Test under Horizontal Load: Arrangement and Instrumentation

The experimental setup for the lateral cyclic loading test of the FREIs comprises of (a) weights for application of vertical load on the isolator, (b) servo-control hydraulic actuator for the application of horizontal cyclic displacement and (c) data acquisition

system for acquiring response data. A schematic of the bearing test setup plan and elevation is shown in the Fig. 5.3 and Fig. 5.4. Four isolators are placed at the corners of a steel plate and loading of 48kN is placed on the steel plate. Isolators and loads are placed symmetrically so that each isolator carries equal load of 12kN, which is the design load of the isolator.

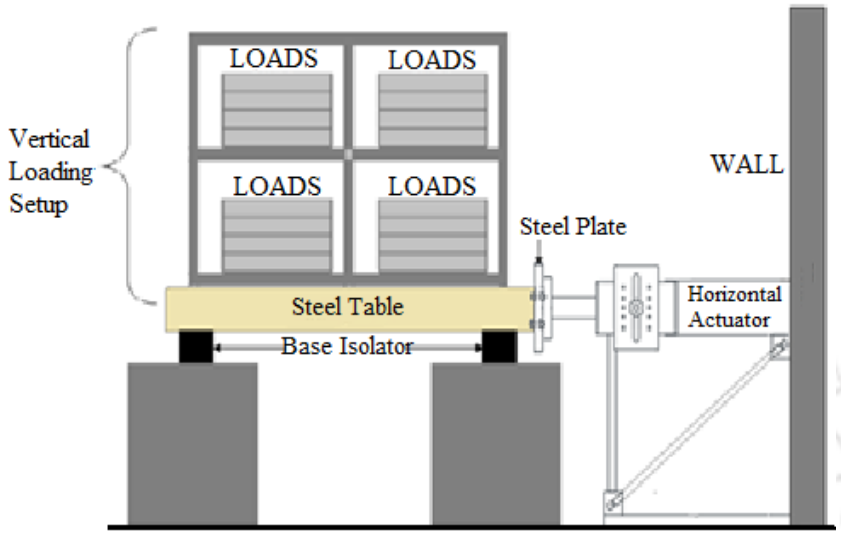

Fig. 5.3 Front view of the experimental set up for lateral loading test

Actual experimental set up is shown in Fig. 5.5. For the known applied displacements, forces are recorded in the data acquisition system.

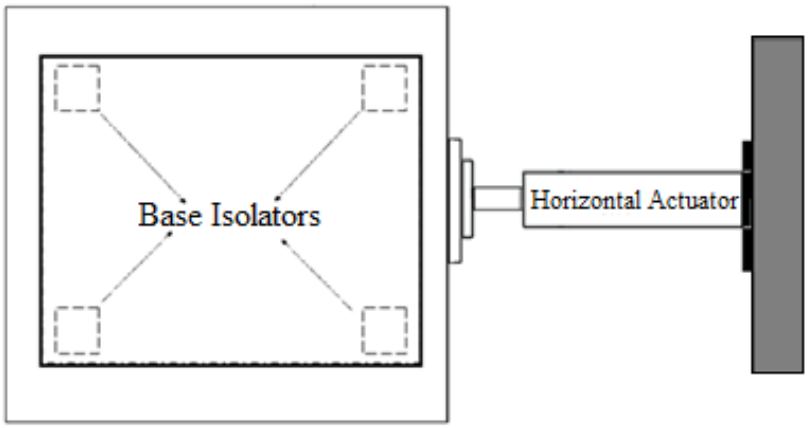

Fig. 5.4 Top cross sectional view of the experimental set up

Fig. 5.5 Actual experimental set up

5.3.2. Lateral Cyclic Loading

The lateral loading history used for the experimental study is as shown in Fig. 4.3. Three cycles of sinusoidal displacement with ±10mm amplitude is applied at the top of isolator. Amplitudes of displacement is increased by 10mm at the end every three cycles upto the maximum amplitudes of displacement is 60mm. The experiment has been repeated for horizontal displacements applied along X-axis and 45° to X-axis of isolator. In the first test run, horizontal displacement is applied along X-axis of the isolator. Second test run is conducted by rotating the isolator at 45° so as to apply the horizontal displacement at 45° to X-axis. The resulting hysteresis data as obtained from the test are utilized for the evaluation of dynamic properties of the isolators.

5.4. Comparison of Numerical and Experimental Results

The results of detailed FE analysis as well as experimental studies on the square U-FREIs are presented in the form of force displacement hysteresis plot.

5.4.1. Result of Loading along 0^0 Orientation

The force-displacement hysteresis loops of the square U-FREI subjected to 0^0 loading as obtained from FE analysis and experiment are shown in Fig. 5.6. The lateral force-displacement hysteresis loops are plotted for all the six amplitudes of applied displacement.

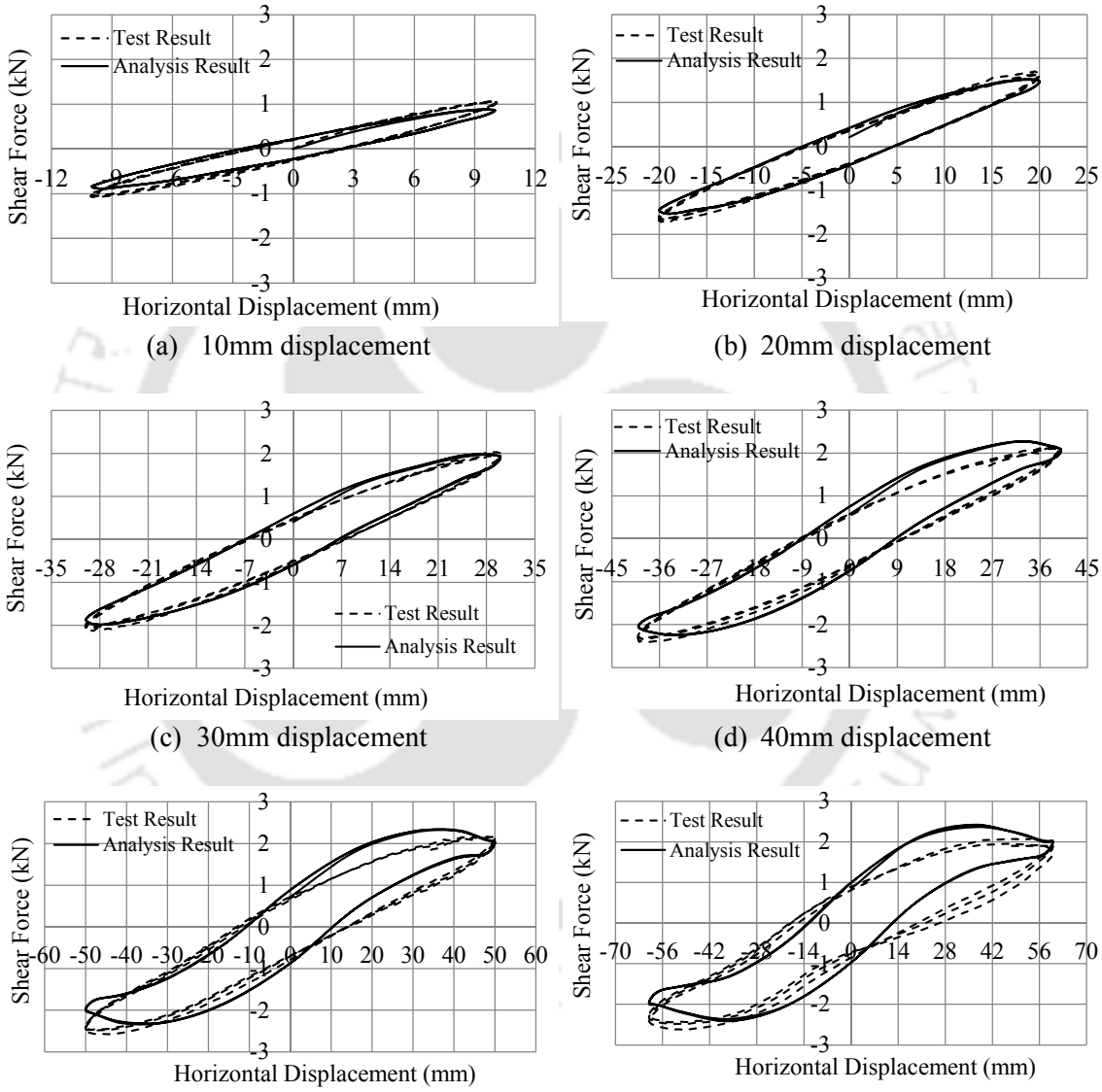

Fig. 5.6 Shear force *vs* horizontal displacement at various displacement (0^0 loading direction)

Comparison of FE analysis result and experimental result of effective horizontal stiffness (K_{eff}^{h}) and damping of square U-FREI subjected to loading along 0^0 for various

displacement amplitudes are shown in Table 5.2. The values of lateral stiffness as obtained from the experiment are quite comparable to those from the FE based results, whereas some discrepancies are observed in the damping values. The load-displacement curves (Fig.5.6) show some difference between experimental and analytical results at relatively higher displacement. It was observed by Sanchez et. al [2013] that the vertical load acting on the bearing is subject to change depending on the rocking motion of the setup and the overturning moments that result from it. The effect of such load variation has also been studied in the present work by considering ±25% variation in vertical load. However, it is observed that no significant differences in the analytical results have occurred. Thus, the reasons for such discrepancy of results between experimental and analytical may be attributed to minor imperfection in the manufactured model of FREI.

Table 5.2 FE and experimental evaluation for un-bonded isolator (for 0^0 loading direction)

	FE analysis result		**Experimental result**	
Displacement (mm)	**Effective Horizontal Stiffness (K_{eff}^h) (kN/m)**	**Damping (β) (%)**	**Effective Horizontal Stiffness (K_{eff}^h) (kN/m)**	**Damping (β) (%)**
10	88.3	12.3	98.2	10.1
20	76.5	12.8	84.3	10.5
30	66.2	13.1	68.4	11.2
40	56.9	13.9	56.9	11.6
50	46.2	15.2	47.5	12.1
60	39.3	16.1	39.4	12.5

5.4.2. Result of Loading along 45^0 Orientation

The test set up for the evaluation of horizontal stiffness for loading along 45^0 to X-axis is same as loading along X-axis, except that the bearings are rotated by 45^0. Similar to the previous section, the force-displacement hysteresis loops of the square U-FREI subjected to loading along 45^0 are shown in Fig. 5.7.

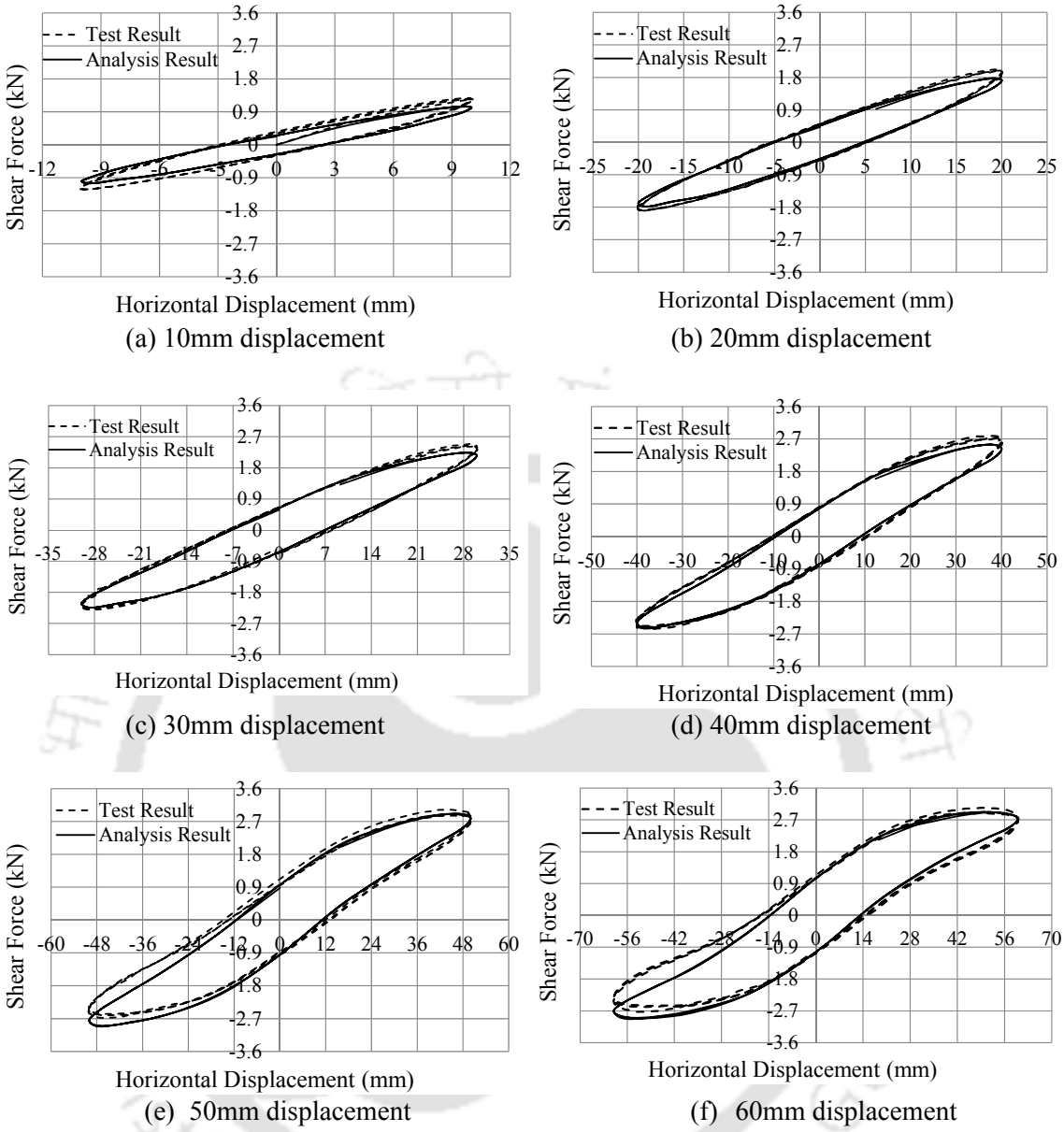

(a) 10mm displacement (b) 20mm displacement

(c) 30mm displacement (d) 40mm displacement

(e) 50mm displacement (f) 60mm displacement

Fig. 5.7 Shear force *vs* horizontal displacement at various displacement (45^0 loading direction)

Comparison of FE based result and experimental result of effective horizontal stiffness (K_{eff}^{h}) and damping of square U-FREI subjected to loading along 45^0 are shown in Table 5.3. Similar to the 0^0 loading case, the values of lateral stiffness as obtained from the experiment are comparable to those obtained from the FE based results with some disparities in damping values.

Table 5.3 FE and experimental evaluation for un-bonded isolator (for 45^0 loading direction)

	FE analysis result		Experimental result	
Displacement (mm)	**Effective Horizontal Stiffness (K_{eff}^h) (kN/m)**	**Damping (β) (%)**	**Effective Horizontal Stiffness (K_{eff}^h) (kN/m)**	**Damping (β) (%)**
10	104.8	12.1	102.6	10.8
20	89.1	12.4	96.7	11.0
30	74.7	13.0	78.5	11.9
40	63.7	13.3	65.8	12.5
50	55.4	13.8	55.2	12.8
60	48.2	14.3	45.9	13.1

The comparison of shear force-displacement hysteresis loops obtained from experiments and FE analysis for loading along 45^0 to X-axis (Fig.5.7) shows the discrepancy is relatively lesser as compared to those corresponding to loading along X-axis. The value of lateral stiffness for displacement along 45^0 to X-axis is slightly higher than those corresponding to displacement along X-axis.

5.5. Displaced Shape of Isolator

Isolators are tested for various displacements ranging from 10 mm to 60 mm. The deformed shapes of isolator as obtained from experimental study corresponding to loading directions of 0^0 and 45^0 are shown in Fig. 5.8 and Fig. 5.9 respectively. The top and bottom surfaces of U-FREI exhibit stable roll off the contact surfaces without damage and resulting in development of very low tensile stresses in that zone. It may be noted that no visual distresses are observed in these isolators even after subjecting them up to 60 mm displacement along both 0^0 and 45^0 directions. Further, deformed shapes of isolator obtained from experimental investigation (Fig. 5.8 and Fig. 5.9) are observed to be in very good agreement with those obtained from FE analysis (Fig. 4.27 and Fig. 4.31).

(a) at 10mm maximum displacement (0^0 loading direction)

(b) at 20mm maximum displacement (0^0 loading direction)

(c) at 30mm maximum displacement (0^0 loading direction)

(d) at 40mm maximum displacement (0^0 loading direction)

(e) at 50mm maximum displacement (0^0 loading direction)

(f) at 60mm maximum displacement (0^0 loading direction)

Fig. 5.8 Deformations of square U-FREI at 60mm horizontal displacement (0^0 loading direction)

(a) at 10mm maximum displacement (45^0 loading direction)

(b) at 20mm maximum displacement (45^0 loading direction)

(c) at 30mm maximum displacement (45^0 loading direction)

(d) at 40mm maximum displacement (45^0 loading direction)

(e) at 50mm maximum displacement (45^0 loading direction)

(f) at 60mm maximum displacement (45^0 loading direction)

Fig. 5.9 Deformations of square U-FREI at 60mm horizontal displacement (45^0 loading direction)

5.6. Concluding Remarks

In this chapter, comparison of magnitudes of vertical stiffness, horizontal stiffness and damping of un-bonded square isolators are examined utilizing both the numerical and experiment method. Influence of direction of horizontal loading on the square isolator is studied and accuracy of results from FE analysis is verified for different load cases. On the basis of detailed analysis of experimental and numerical results presented in previous sections following conclusions are drawn.

- Vertical stiffness of square FREI as obtained from experiments shows good agreement with the vertical stiffness calculated from simple closed form formula. The vertical stiffness is also very high so as to sustain the vertical load

of the structure and prevent rocking vibration modes of base isolated structure. Hence FREI can be used as an effective base isolation device alternative to SREI.

- Horizontal stiffness as obtained from analytical solution shows close agreement with those from experimental study, though some discrepancies are observed in the load-displacement curves for relatively higher displacements.
- Horizontal stiffness of un-bonded isolator corresponding to 45^0 loading is observed to be slightly higher than that for 0^0 loading.
- About 55% reduction in stiffness is observed when the displacement is increased from 10 mm to 60 mm for both the direction of loadings. Thus effectiveness of un-bonded isolator with constant vertical load increases with increase in amplitudes of horizontal displacements.
- Damping percentages increases with the increase in horizontal displacement, which varies in the range of 10- 16% for both the directions of loadings.
- Experimentally observed displaced shapes of the isolators corresponding to both the directions of loadings are observed to agree very well with those from numerical analysis.

भारतीय प्रौद्योगिकी संस्थान गुवाहाटी
Indian Institute of Technology Guwahati

Chapter 6

Shake Table Testing of 1/5th Scaled Base Isolated Masonry Building

6.1. Introduction

The poor resistance of old masonry buildings to horizontal seismic actions, demonstrated by catastrophic collapses after strong earthquakes and the geometric constraints suggested by technical codes discouraged their usage during last decades. On the other hand, masonry, especially brick masonry has a greater durability as compared to that of other materials as established by many such constructions of the past still in existence. Furthermore, brick masonry can also ensure optimal energy efficient performance.

Base isolation is an efficient and viable method to reduce the vulnerability of un-reinforced masonry structure in high seismic risk zone. Earthquake energy transmitted to the structure can be reduced by shifting the fundamental horizontal period of structure from the dominant range of earthquake periods. Base isolators are installed in the interface of substructure and superstructure to achieve the desired horizontal period of structure.

In this chapter the feasibility study of U-FREI as an alternative to SREI for seismic isolation of un-reinforced masonry buildings is presented. Previous study revealed that light weight U-FREI has potential of providing superior performance in seismic isolation of low-rise buildings utilizing stable roll over displacement. Installation of U-FREI in the interface of superstructure and substructure of an un-reinforced masonry building would be simple and hassle free. Therefore, there is a need to study the effectiveness of U-FREI in seismic isolation of un-reinforced masonry buildings for

reduction of their inherent vulnerability. Shake table testing of a two storey model masonry building supported on U-FREI is carried out to ascertain its effectiveness in controlling seismic response. To compare the performance of U-FREI, same building is placed directly on the shake table without isolator and fixed base (FB) condition is simulated by restraining the base of the building with the shake table. Dynamic response characteristic of base isolated (BI) masonry building subjected to different intensities of input earthquakes are compared with the response of the same building without base isolation system. Acceleration response amplification, peak response values of test model with and without base isolation system are compared for different intensities of table acceleration.

The objective of the present study is to investigate the dynamic response of un-reinforced brick masonry building model supported on U-FREI. Influence of orientation of U-FREI with respect to direction of seismic excitation is also evaluated. Vertical stiffness, horizontal stiffness and damping values of the U-FREIs have been estimated analytically and experimental validation is also presented in the previous chapters. This investigation is undertaken considering seismic vulnerability of low-rise residential, school and hospital buildings made of un-reinforced masonry in the North-Eastern part of India. The North-Eastern part is located in the most severe seismic Zone-V in the seismology map of India. Moreover this zone has abundant natural resources like stone, lime stone etc. but has limited resources for the construction of reinforced concrete buildings. Due to difficult mountainous terrain, accessibility to different location having sizable population is limited. The un-bonded light weight, low cost FREI, which are easy to install shall serve the purpose of constructing low cost seismic resistant building housing important dwelling as well as the building of general public importance.

6.2. Test Model and Isolation System

A two-storey un-reinforced masonry building model of one-fifth scale is considered for the experimental study. Brick masonry is commonly used building material in urban and rural India and hence bricks are used for construction of the test model. Size of the test model has been finalized considering capacity and size of the available shake table. Scaled model of FREI is designed to carry estimated gravity load and horizontal displacement simultaneously. Details of testing of the model FREI under cyclic load have been presented in Chapter 5. Details of the test model and model FREIs are presented in the following sub-section.

6.2.1. Scaling and Similitude

A scale factor of 1:5 is considered for the present study considering the size of shake table (2.5m X 2.5m) and its payload capacity. The *laws of similitude* [Harris and Sabnis, 1999] are followed to arrive at appropriate input motion, dimensions of test model as well as for finalization of additional mass requirement for gravity load simulation. The similitude requirements are derived from dimensional analysis which depends on physical characteristics like length, force, time, temperature etc. Table 6.1 shows the derived scaling relationship of the parameters relevant to the present study.

Table 6.1 Similitude scaling relationship

Parameters	Scale	Prototype / 1/5-scale model
Length	S	5
Mass	S^2	25
Displacement	S	5
Time	$\sqrt{S}$	2.236
Acceleration	S	5

The mass of the prototype building is 121.4 x10^3 Kg, whereas the total mass of the test model is 970 kg. Hence the additional mass of 3,885 kg required for fulfilling similitude requirement is uniformly distributed over different floors of the model.

6.2.2. Test Model and its Construction Details

A storey masonry building is constructed for shake table testing subjected to different input earthquake accelerations. The geometrical details of the building are given in Table 6.2. In the model building, beams are provided at the base level, which rest on four U-FREIs placed at four corners of the building. The plan and elevation of the building mounted on U-FREIs are shown in Fig. 6.1.

Table 6.2 Building Parameter

Parameter	Model Building
Length (m)	1.5
Width (m)	1.1
Height of storey (m)	0.6
Thickness of slab (m)	0.08
Dimension of base beam (m x m)	0.125x0.150
Total weight of building (kg)	971

Material used for construction of test model are M25 grade of concrete, Fe415 steel reinforcement and fly ash brick. The dimensions of building elements of test model are obtained by scaling of corresponding element of the prototype as per similitude requirement. This elements are design as per load prescribed in various Indian Standard and Seismic Zone-V as per seismic zoning map of India. Lifting hook are provided at the base ring beams for handling and placing of test model during different stages of experiments. Base beam and lift hooks are designed to take care the loads of entire test structure and these are shown in Fig. 6.2a.

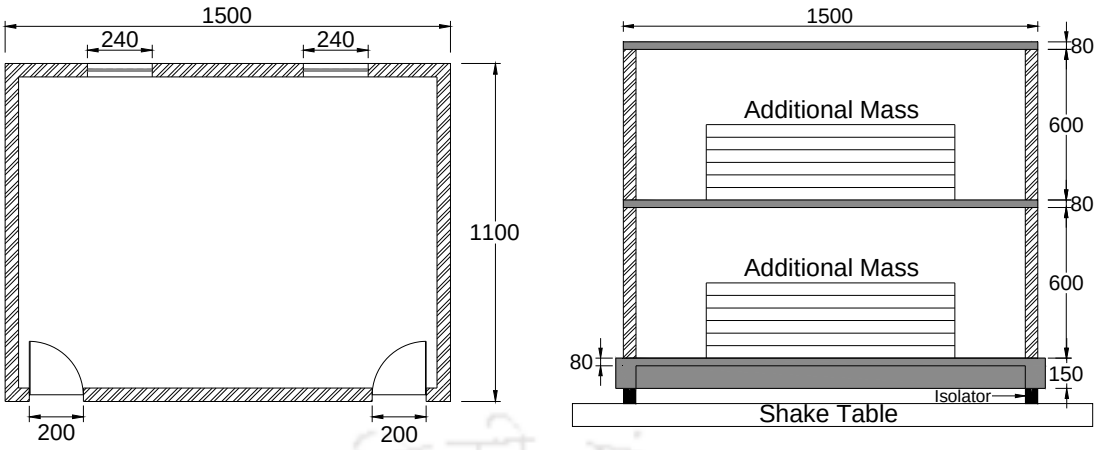

Fig. 6.1 Plan and elevation of model building

Brick masonry wall are constructed directly above the base level slab. On the top of brick wall first floor and roof level slabs are placed directly without any joint. The storey height of the model is 0.60m. The total height of the test model is 1.51m including the base ring beam and two level slabs. The base level as well as first floor and roof level slab has plan area of 1.50m x 1.10m. There are 8 nos. of hooks of 20mm diameter provided as at corner of base beam as shown in Fig. 6.2a for handling of the model. Details of reinforcement provided in base level ring beam and all three slabs are shown in Fig. 6.2b.

6.2.3. Properties of U-FREI

U-FREIs are designed for low horizontal stiffness so as to achieve the desired horizontal frequency and high vertical stiffness so that no undesirable vertical or rocking mode is excited. Stability of bearings under combined gravity load and imposed lateral displacement is ensured. A BI building is generally designed for a natural frequency of 0.5 Hz for deflecting energy associated with higher modes of vibration, while keeping the base displacement within acceptable limit. FREIs for the isolated scaled test model of un-reinforced masonry building has been designed and extensively tested for the evaluation of mechanical properties. U-FREIs have shown excellent potential in reduction of dynamic response of structures mounted on such isolators.

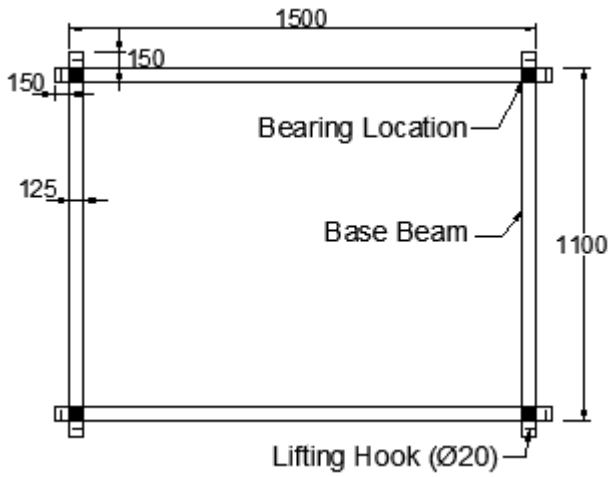

(a) Base ring beam and lifting hook

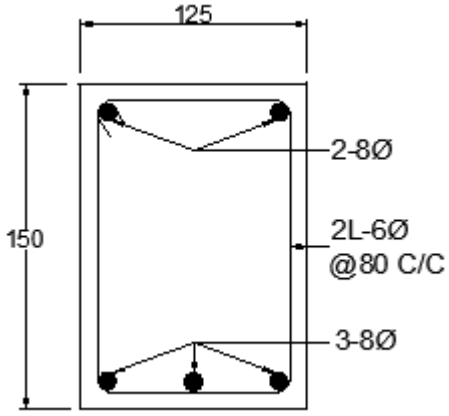

(b) Base ring beam reinforcement

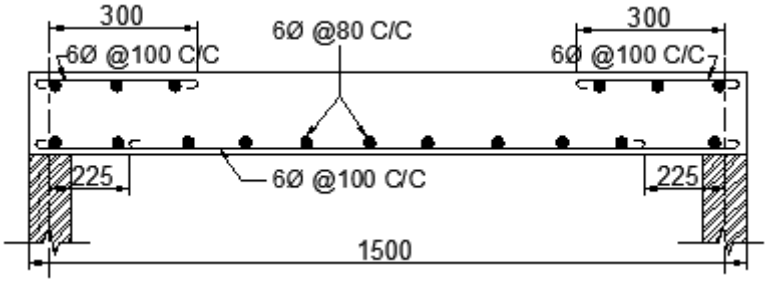

(c) Slab reinforcement details

Fig. 6.2 Base ring beam plan, reinforcement detail of beam and slab

Geometrical and material properties of isolators designed to achieve effective isolation are listed in Chapter 3. Each layer of elastomer is interleaved with bi-directional ($0^0/90^0$) carbon fibre reinforcement layer. Details of FREI bearing used for seismic isolation of the test model is shown in Chapter 3.

Experimental investigation on behaviour of U-FREI under horizontal cyclic displacement (along X-axis and 45^0 to X-axis) are already carried out and presented in Chapter 5. Lateral force vs displacement hysteresis behaviour of U-FREIs are also shown in Chapter 5. It may be observed that the stiffness of U-FREI reduces with increase in the amplitude of horizontal displacement. The reduction in stiffness is about 50% of initial stiffness at maximum horizontal displacement.

6.3. Shake Table Testing Setup and Instrumentation Details

The test model is excited by prescribed earthquake excitation using shake. Shake table reproduces prescribed earthquake acceleration histories through servo-control hydraulic actuator system. Floor responses measured by the accelerometers and LVDT's are recorded using data acquisition system.

A schematic diagram showing arrangement of instrumentation for acquiring responses of test model and details of experimental arrangements for shake table testing of the test model is shown in Fig. 6.3.

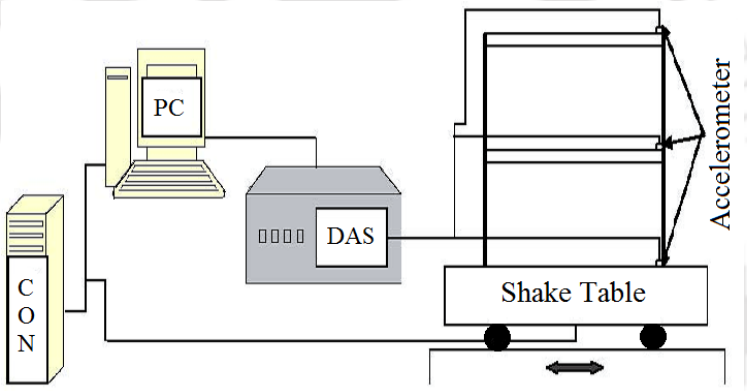

Fig. 6.3 Schematic diagram of instrumentation for laboratory test model

A uni-axial shake table of 2500 x 2500 mm size with a pay load capacity of 50 kN and equipped with a servo-control hydraulic actuator to excite test model in a linear displacement range up to ± 500 mm is used. The shake table is capable of producing maximum acceleration up to ±2g. Uni-axial force balance accelerometers (Model: ES-U2, Make: Kinemetrics Inc., USA) have been used for measuring acceleration responses of test models during shake table test. This force balance accelerometer can measure acceleration amplitudes from ambient noise level to a maximum of ±2g. These accelerometers has the capability to amplify and conditioning measured digital data. The amplified and conditioned digital signals can directly be transferred to a compatible data acquisition system. A forty eight channels dynamic data acquisition system

manufactured by HBM GmBH, Germany (Model: MGC plus) is used to record digital data measured by accelerometers. Two LVDT's are also used to measure the displacement of the model building during shake table testing.

The BI test model supported on four isolators placed at the four corner of the base floor is shown in Fig. 6.4(a). The same model as used as FB test model is shown in Fig. 6.4(b). Concrete blocks as shown in Fig. 6.4 are placed on each floor to account for the compensating mass. Uni-axial force balanced accelerometers have been fixed at each floor level of the test model as shown in Fig. 6.4. The accelerometer recording data from the shake table level is marked as sensor 1. While the accelerometers recoding data at base beam level, first floor level and roof level are marked as sensor 2, sensor 3 and sensor 4 respectively. These accelerometers are connected to data acquisition system for recording structural responses from different floor levels. Location of LVDT's to measure the displacement at base beam level and first floor level of model during earthquake excitations are also shown in Fig. 6.4. The LVDT's recoding data at base beam level and first floor levels are marked as LVDT1 and LVDT2 respectively.

(a) Base isolated building (b) Fixed based building

Fig. 6.4 Building models on shake table

6.4. Sample Ground Motions for Shake Table Test

Four different earthquake ground motions are considered for exciting the test model using shake table. Earthquake records with different peak accelerations, frequency contents and durations have been selected as input motion for the shake table testing. These earthquakes component were recorded during Koyna (1967): Comp - Longitudinal, Parkfield (1966): Comp - C02065, El Centro (1940): Comp - 180, Victoria (1980): Comp - CPE045 transverse earthquakes. These input earthquake are referred as Koyna, Parfield, El Centro and Victoria respectively in the subsequent sections. The descriptions of relevant characteristics of the earthquake records are presented in Table 6.3.

Table 6.3 Characteristics of selected earthquake records

Earthquake Components	Peak Ground Acceleration (g)	Frequency Range (rad/sec)
Koyna (1967): Comp - Longitudinal	0.63	0-12
Parkfield (1966): Comp - C02065	0.48	0-40
El Centro (1940): Comp - 180	0.32	0-65
Victoria (1980): Comp - CPE045	0.62	0-160

Acceleration time histories of the four selected input earthquakes are shown in Fig. 6.5. Time interval and hence the duration of earthquake records used for shake table excitation are scaled as per similitude requirement. Table 6.4 shows the original and scaled time interval of earthquakes record used for the study. Time scaled representation of the four selected earthquakes acceleration histories are shown in Fig.6.6.

Table 6.4 Time interval of earthquake records selected for shake table excitations

Earthquake Motions	Original Time Interval (sec)	Scaled Time Interval (sec)
Koyna (1967): Comp - Longitudinal	0.01	0.004472
Parkfield (1966): Comp - C02065	0.01	0.004472
El Centro (1940): Comp - 180	0.02	0.008944
Victoria (1980): Comp - CPE045	0.01	0.004472

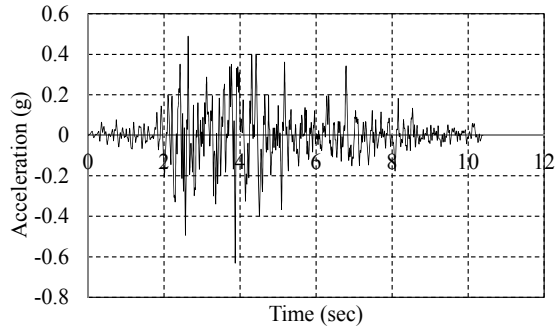

(a) Koyna (1967): Comp - Longitudinal

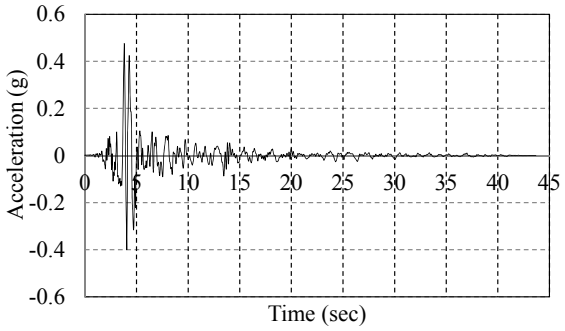

(b) Parkfield (1966): Comp - C02065

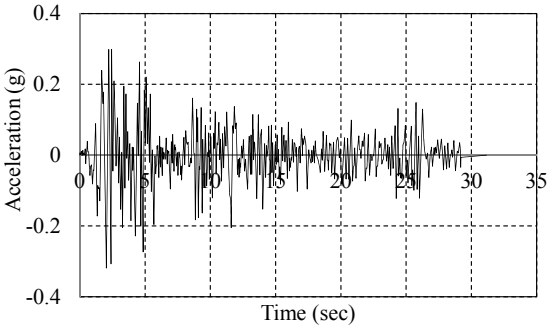

(c) El Centro (1940): Comp - 180

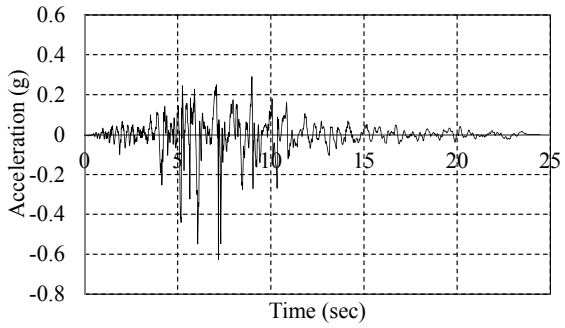

(d) Victoria (1980): Comp - CPE045

Fig. 6.5 Accelerations histories of four selected earthquake components

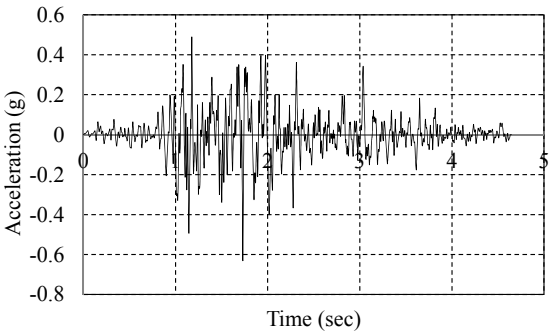

(a) Koyna (1967): Comp - Transverse

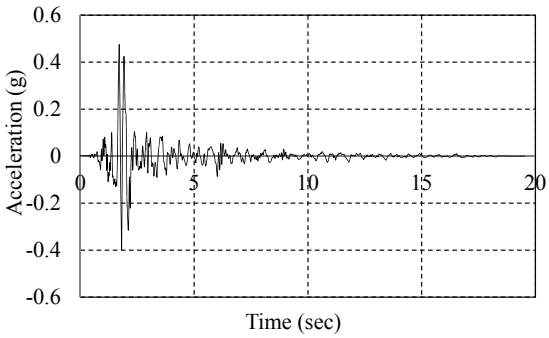

(b) Parkfield (1966): Comp - C02065

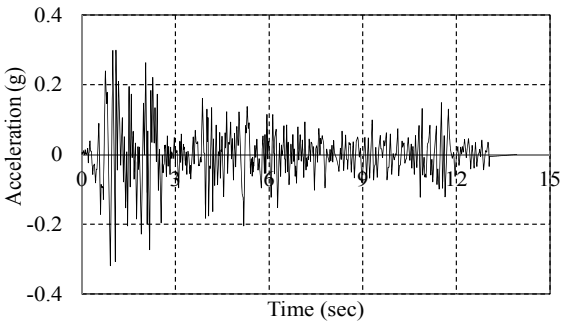

(c) El Centro (1940): Comp - 180

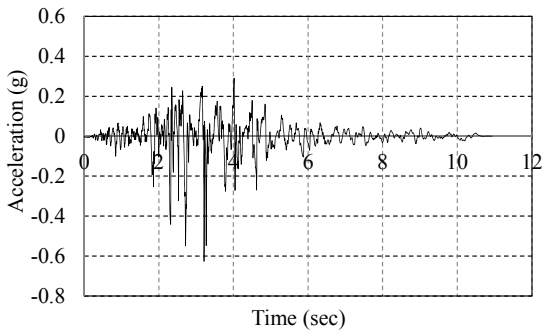

(d) Victoria (1980): Comp - CPE045

Fig. 6.6 Time scaled accelerations histories of four selected earthquake components

6.5. Shake Table Test Result

Shake table testing of scaled un-reinforced masonry test model under different earthquake excitations are presented. The un-reinforced masonry structure have low lateral resistance when excited by seismic motion. However, the magnitude of acceleration amplitude, which the structure will sustain without any damage is not known at the beginning of the shake table test. Hence, the shake table testing of the BI model is first started with an intensity level of 10% of the peak ground acceleration (PGA) of all the four scaled earthquake excitations. Subsequently it has been increased to 20%, 30%, 50%, 70% and 100% of the PGA of those prescribed accelerations. The shake table testing of model supported on U-FREI is carried out first and the test is repeated by placing the model directly on the shake table and restraining the base of the model to the shake table.

The result of the experimental studies using intensity levels of 30% and 100% of PGA for shake table acceleration along X-axis of FREIs are presented. Similarly the result of shake table acceleration along 45^0 to X-axis of FREIs are presented for intensity levels 30% and 70% of PGA.

6.5.1. Test Results for Excitation along X-axis of FREI

The time histories of acceleration at shake table level (sensor 1) and at the base beam level (sensor 2) of the model for all the four earthquake excitations corresponding to intensity level 30% of PGA of all four earthquakes are shown in Fig. 6.7. It is observed that the peak acceleration amplitude recorded at the base beam level of the structure for Koyna earthquake is only 12.5% of input acceleration intensity. It is also seen that significant reduction in magnitude of peak acceleration at base beam level have taken place for all the cases of earthquake excitation. This will reduce the induced lateral

force at different levels in the super structure under earthquake excitations.

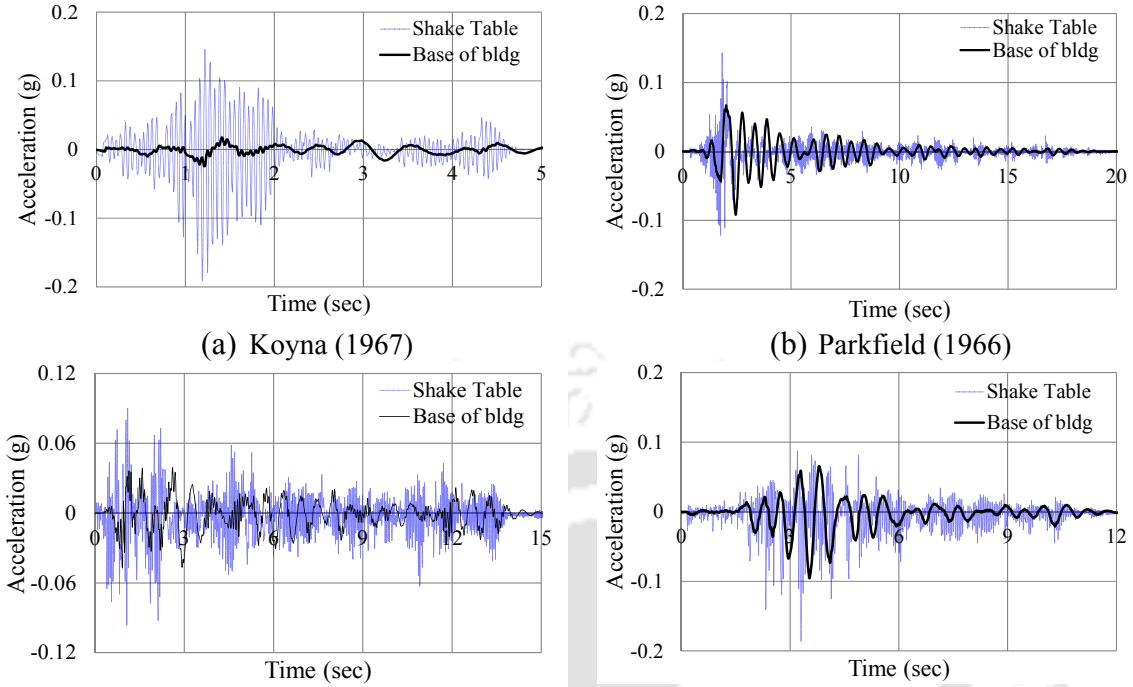

Fig. 6.7 Acceleration response at shake table level and base beam level subjected to 30% intensity level of four earthquakes applied along X-axis

Further, acceleration time histories recorded at first floor level (sensor 3) and roof level (sensor 4) are plotted along with the base beam level acceleration history (sensor 2) in Fig. 6.8. The values of accelerations at different time instances have been found to be almost same at different floors along the height of the building. This indicates that the BI building has not experienced any noticeable acceleration amplification along the height of the building unlike conventional buildings.

Displacement amplitudes are also measured at base beam level (LVDT 1) and first floor level (LVDT 2). Displacement time histories at these two levels are compared in Fig. 6.9. It is observed that magnitude of peak displacement at base beam level and first floor level are almost same, which indicates that there is negligible inter-storey drift in the structure, indicating a rigid body motion of the structure above isolation level. Thus, no significant seismic forces are generated in the building elements and hence the un-reinforced masonry building has withstood the seismic excitations of specified intensity

without any damage.

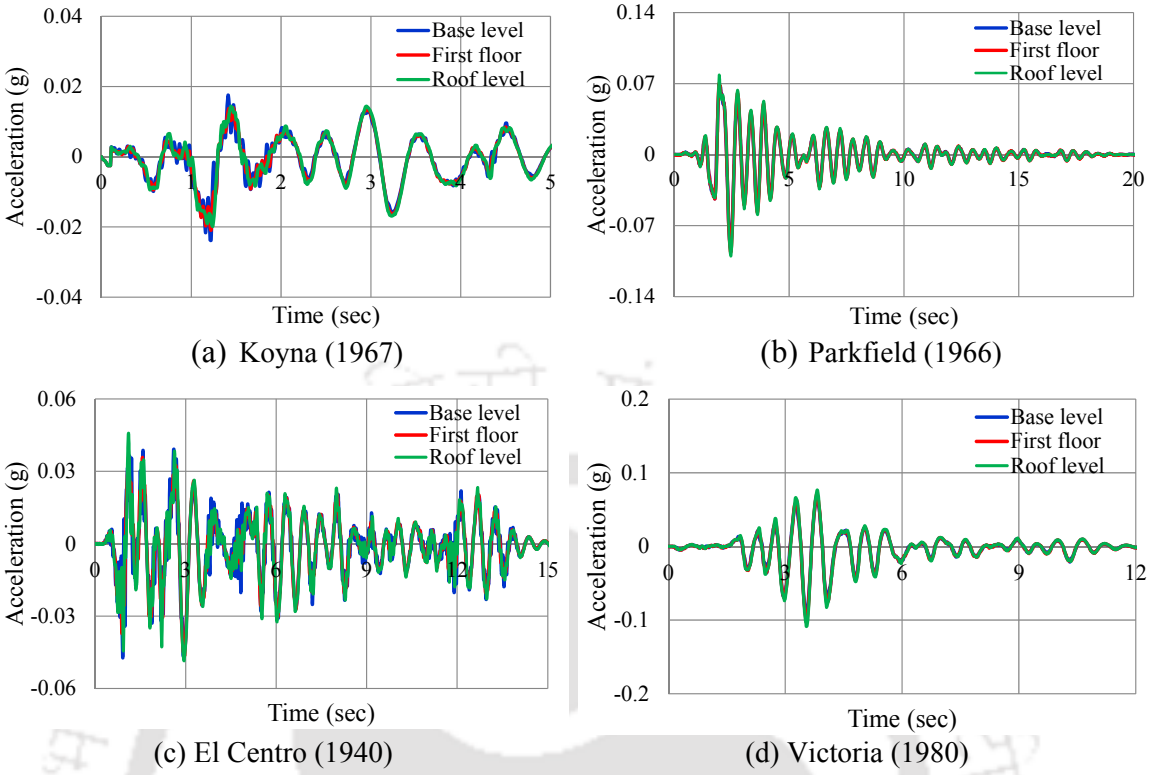

(a) Koyna (1967) (b) Parkfield (1966)

(c) El Centro (1940) (d) Victoria (1980)

Fig. 6.8 Comparison of acceleration responses at base, first floor and roof level subjected to 30% intensity level of four earthquakes applied along X-axis

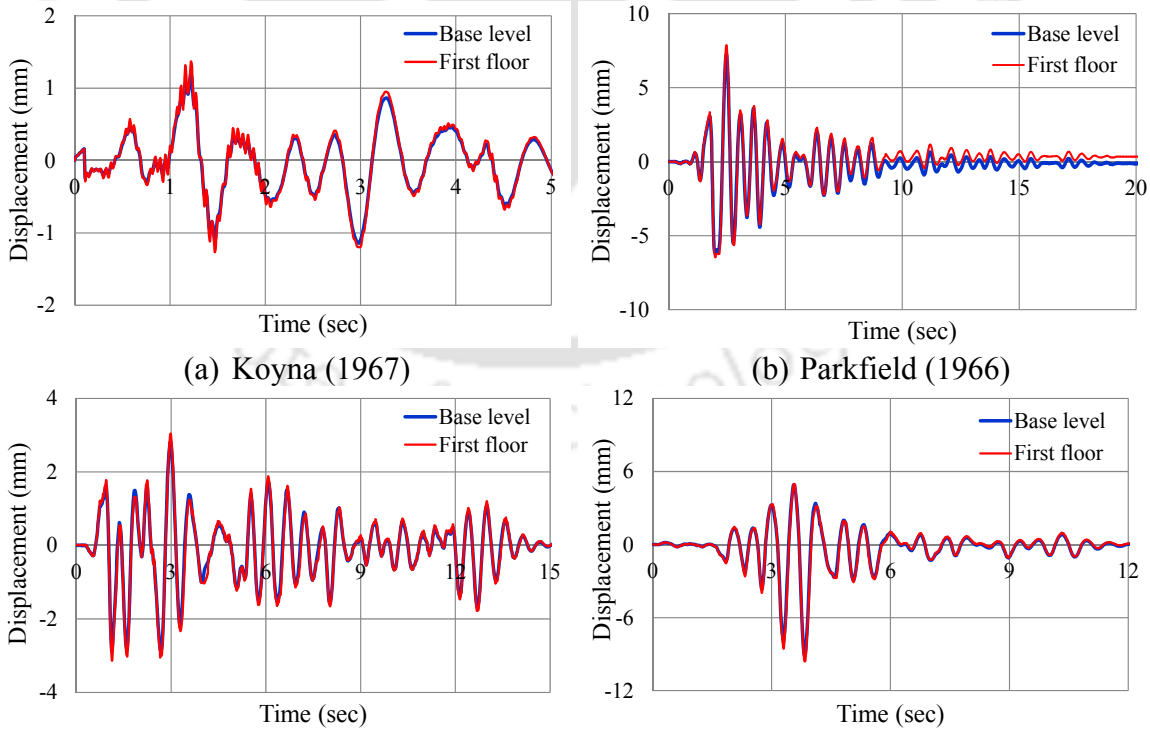

(a) Koyna (1967) (b) Parkfield (1966)

(c) El Centro (1940) (d) Victoria (1980)

Fig. 6.9 Displacement at base level and first floor level subjected to 30% intensity level of four earthquakes applied along X-axis

Peak acceleration and displacement at different floor levels of the model subjected to 30% intensity of all four input earthquakes are shown in Table 6.5. The largest lateral displacement experienced by the isolator is 9.098mm when the model is excited by Victoria earthquake. Analytical and experimental result shows that U-FREIs are able to maintain stability up to 60mm of horizontal displacement. It may be noted that under the Victoria earthquake, the first floor level displacement is recorded as 9.597mm, which is almost equal to the base beam level displacement, indicating the rigid body motion of superstructure of the BI model building. Further, maximum displacement of 1.204mm is recorded corresponding to Koyna earthquake, where the maximum reduction in acceleration at the base level beam is recorded. It is also observed that after the completion of each test run, the bearings and hence the isolated structure return to its original vertical position and bearings remain stable during the test.

Table 6.5 Peak acceleration and displacement at different levels of model subjected to 30% intensity level of four earthquakes along X-axis.

Earthquake	Peak Accelerations (g)				Peak Displacement (mm)	
	At Shake Table	At Base	At First Floor	At Roof Level	At Base level	At First Floor
Koyna	0.189	0.0238	0.0209	0.0198	1.204	1.369
Parkfield	0.143	0.0920	0.0960	0.1002	7.253	7.872
El Centro	0.096	0.0471	0.0463	0.0485	2.876	3.136
Victoria	0.186	0.0954	0.1024	0.1086	9.098	9.597

Similar studies are repeated for higher intensity excitation and the time histories of acceleration at shake table level (sensor 1) and at the base beam level (sensor 2) of the model corresponding to full intensity (100%) of time scaled prescribed accelerations histories of all four selected earthquakes are shown in Fig. 6.10. It is observed that the peak acceleration at base beam level is reduced by 86%, 55%, 52% and 80% for Koyna, Parkfield, El Centro and Victoria earthquakes respectively. The reduction in amplitudes

of transmitted acceleration is increased for all four input earthquake excitations with increase in intensity of excitations is evident from Fig. 6.10. The efficiency of U-FREIs improve with higher degree of displacements at the isolator level because of reduction in acceleration transmissibility.

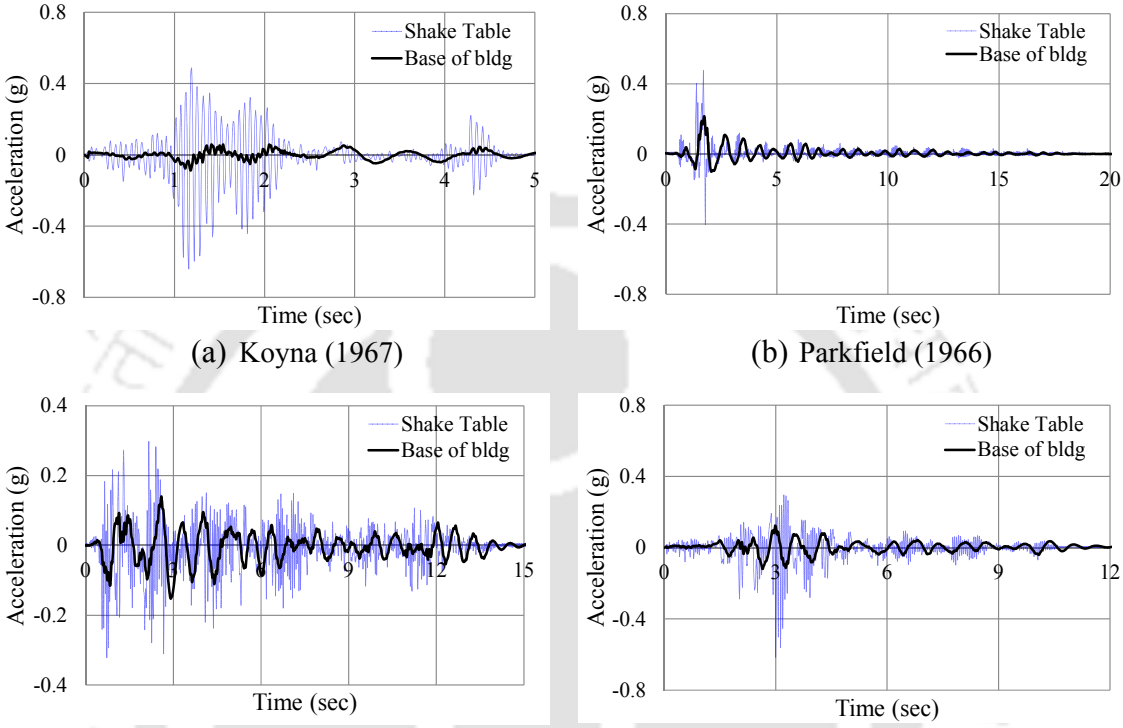

(a) Koyna (1967) (b) Parkfield (1966)

(c) El Centro (1940) (d) Victoria (1980)

Fig. 6.10 Acceleration response at shake table level and base level subjected to four earthquakes (full intensity) applied along X-axis

Further, acceleration time histories recorded at first floor level (sensor 3) and roof level (sensor 4) are plotted along with the base beam level acceleration history (sensor 2) are shown in Fig. 6.11. There is no amplification of accelerations even at higher intensity of input earthquake and significant reduction of acceleration at different floor level indicates the effectiveness of U-FREI.

Displacement histories at base beam level (LVDT 1) and first floor level (LVDT 2) are compared in Fig. 6.12. It is also observed that displacement at different time instances at base beam level and first floor level are almost same. Thus, superstructure of test model has undergone a rigid body motion as expected.

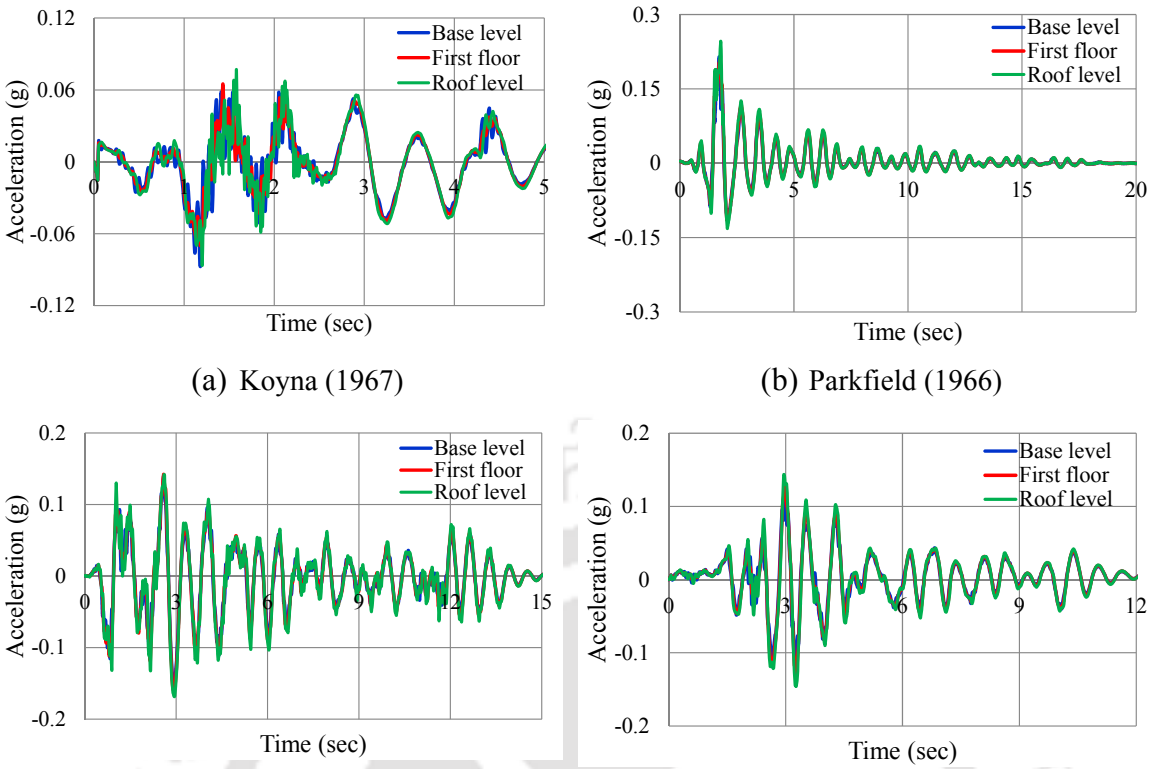

(a) Koyna (1967)

(b) Parkfield (1966)

(c) El Centro (1940)

(d) Victoria (1980)

Fig. 6.11 Comparison of acceleration responses at base level, first floor and roof level subjected to four earthquakes (full intensity) applied along X-axis

Peak acceleration and displacement recorded at different floor levels for 100% intensity level of all the four input earthquakes are shown in Table 6.6. The largest lateral displacement of isolator is recorded as 36.199 mm, when the model is excited using Parkfield earthquake. No instability of model is observed during the testing. Further, for the same input earthquake excitation, the first floor level displacement is recorded as 39.920mm only, which is 3.721mm more than the base beam level displacement. Hence, the drift amount is only 0.62% for floor height of 600mm. The test model has consistently shown very low inter-storey drift and insignificant acceleration amplification along the height of the structure. The U-FREIs have not shown any distress and the un-reinforced brick masonry building has performed commendably well as no damage is observed in any part of the building model.

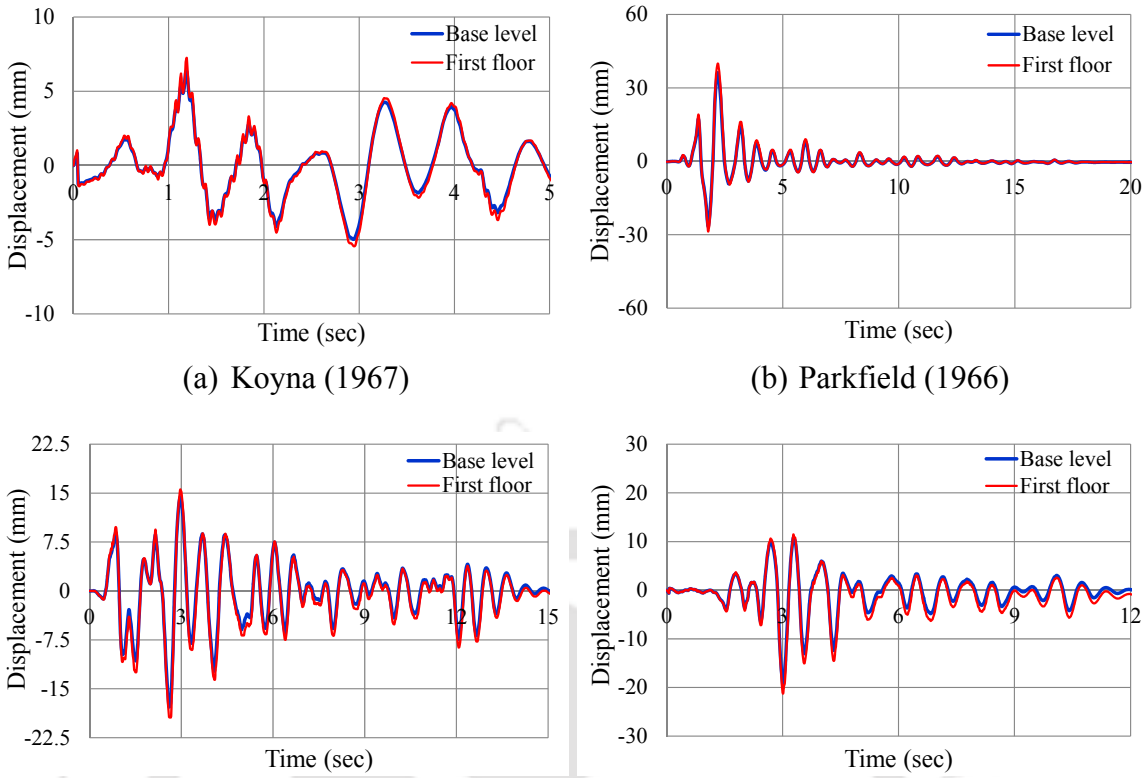

(a) Koyna (1967) (b) Parkfield (1966)

(c) El Centro (1940) (d) Victoria (1980)

Fig. 6.12 Displacement at base level and first floor level subjected to four earthquakes (full intensity) applied along X-axis

Table 6.6 Peak acceleration and displacement at different levels of model subjected to four earthquakes (full intensity) along X-axis

Earthquake	Peak Accelerations (g)				Peak Displacement (mm)	
	At Shake Table	At Base	At First Floor	At Roof Level	At Base level	At First Floor
Koyna	0.632	0.0873	0.0700	0.0867	6.326	7.240
Parkfield	0.476	0.2145	0.2081	0.2463	36.199	39.920
El Centro	0.319	0.1524	0.1601	0.1686	17.789	19.409
Victoria	0.615	0.1230	0.1310	0.1459	19.452	21.251

The peak amplitude of acceleration and displacement at different floor levels (Table 6.6) for this intensity level are significantly larger as compared to those (Table 6.5) for 30% intensity level of input table acceleration. However, the percentage reduction of responses is also comparatively higher indicating the improved efficiency of U-FREI with increased displacement.

6.5.2. Test Results for Excitation along 45^0 to X-axis of FREI

The effectiveness of isolator is also tested by applying the same excitation in diagonal direction (i.e. 45^0 to X-axis) with different intensities of acceleration of all the four earthquakes. The time histories of acceleration at shake table level (sensor 1) and at the base beam level (sensor 2) of the model for all the four earthquake excitations corresponding to 30% intensity of input earthquake acceleration along 45^0 to X-axis of FREIs are shown in Fig. 6.13. The reduction in peak floor acceleration varies with the input earthquake excitation characteristics.

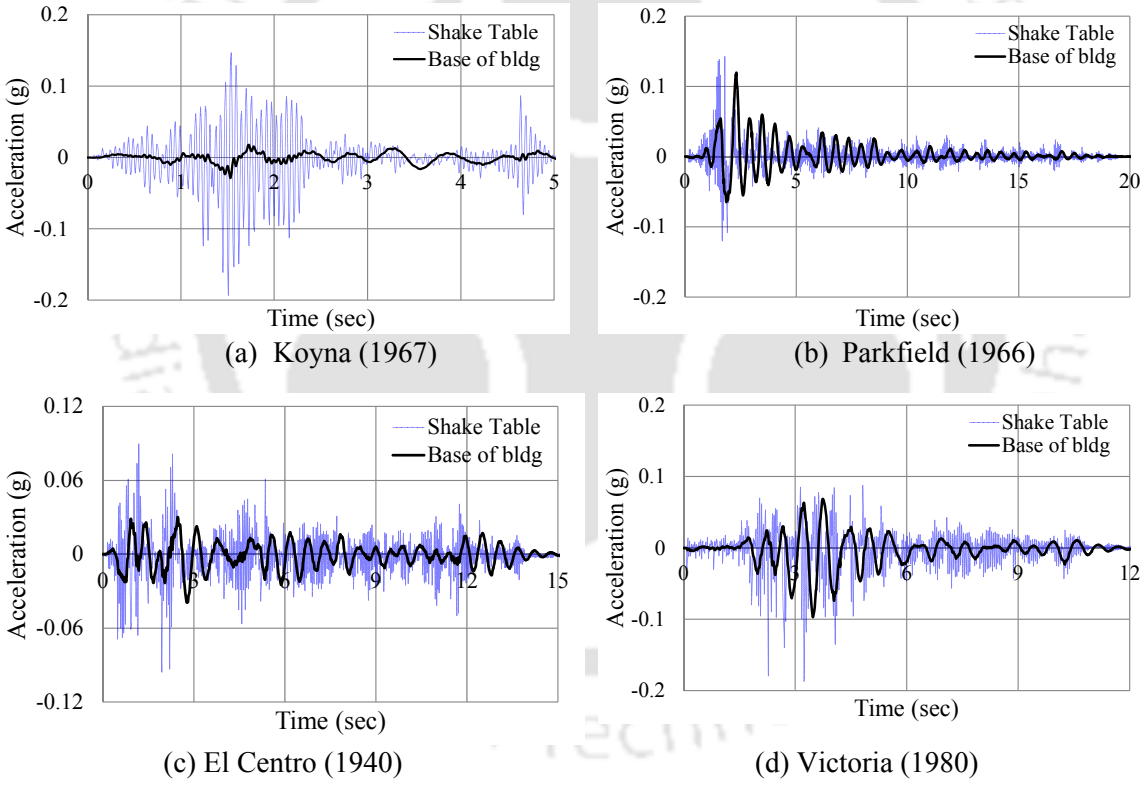

Fig. 6.13 Acceleration response at shake table level and base level subjected to 30% intensity level of four earthquakes applied along 45^0 to X-axis

Acceleration time histories recorded at different floors are plotted in Fig. 6.14. The peak values of accelerations recorded at different floor levels are very close. Similar trend is also observed in earlier case for loading along X axis of FREI.

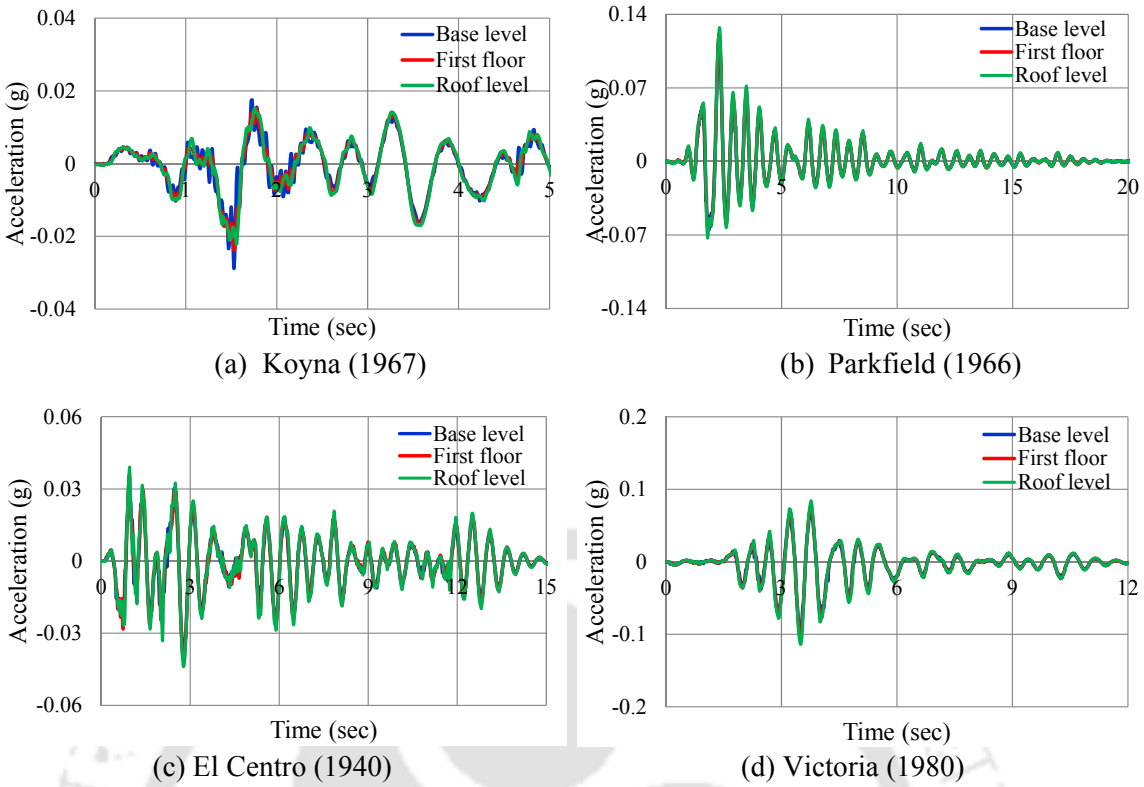

Fig. 6.14 Comparison of acceleration responses at base level, first floor and roof level subjected to 30% intensity level of four earthquakes applied along 45^0 to X-axis

Displacement amplitude recorded at base beam level (LVDT 1) and first floor level (LVDT 2) are compared and shown in Figure 15. It is observed that displacement at different time instants at base beam level and first floor level are very close, indicating negligible existence of inter-storey drift in the structure.

Peak acceleration and displacement at different floor levels for 30% intensity of input earthquake excitation of all the four earthquakes along 45^0 to X-axis are shown in Table 6.7. The values are comparable to those corresponding to loading along X direction as seen from Table 6.5. It may again be observed that significant reduction in magnitude of peak acceleration at base beam level have taken place for all the cases of excitations. Further, the magnitudes of peak acceleration of different floors are almost same, which indicates the absence of any noticeable acceleration amplification along the height of the building. Similarly, magnitude of peak displacement at base beam level and first

floor level are almost same, which indicates that there is negligible inter-storey drift in the structure. The largest lateral displacement experienced by the isolator at base beam level is 9.533mm during the Victoria input earthquake excitation. For same input earthquake, the first floor level displacement is recorded as 10.032mm only, which is 0.50 mm more than that of base level displacement. Hence, the drift amount is only 0.08% for floor height of 600mm.

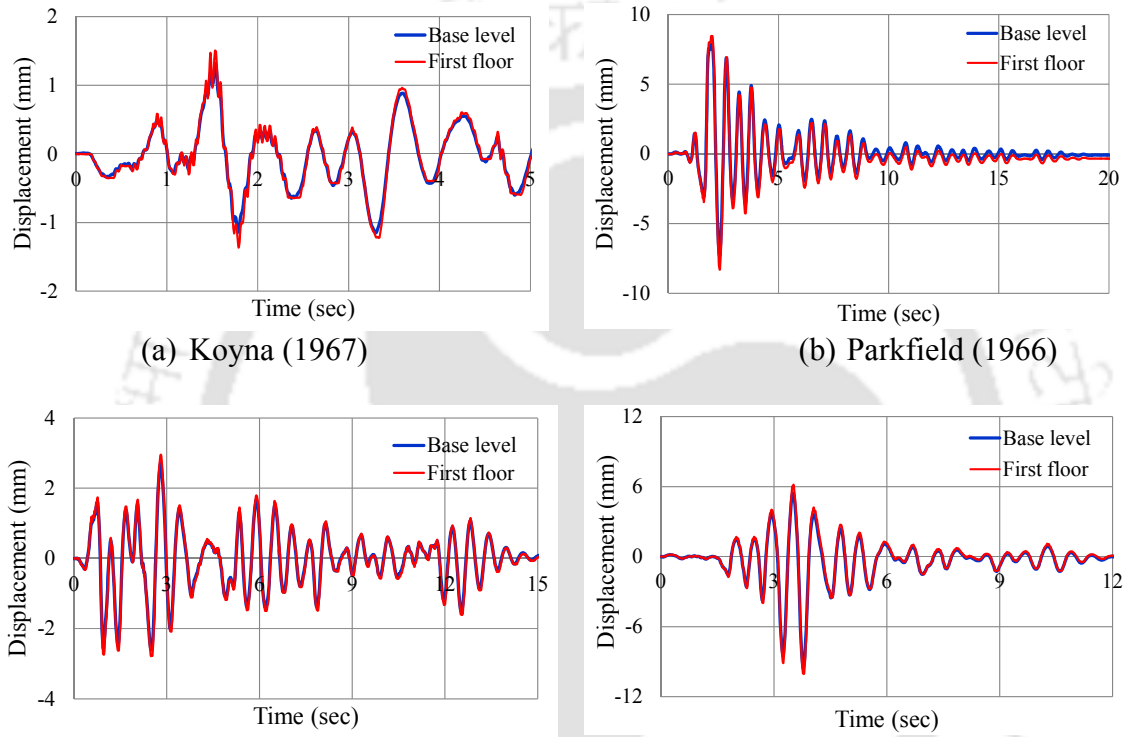

Fig. 6.15 Displacement at base level and first floor level subjected to 30% intensity level of four earthquakes applied along 45^0 to X-axis

Table 6.7 Peak acceleration and displacement at different levels of model subjected to 30% intensity level of four earthquakes along 45^0 to X-axis

Earthquake	Peak Accelerations (g)				Peak Displacement (mm)	
	At Shake Table	At Base	At First Floor	At Roof Level	At Base level	At First Floor
Koyna	0.189	0.0288	0.0238	0.0221	1.316	1.504
Parkfield	0.143	0.1194	0.1217	0.1274	7.867	8.464
El Centro	0.096	0.0391	0.0408	0.0439	2.706	2.954
Victoria	0.187	0.0970	0.1060	0.1140	9.533	10.032

The study is repeated by considering 70% intensity of scaled accelerations for all four input earthquakes along 45^0 to X-axis and the acceleration time histories are shown in Fig. 6.16. Acceleration time histories recorded at different floor levels are plotted in Fig. 6.17. The peak values of accelerations recorded at different floor levels are found to be comparable. This indicates the seismic forces distribution is uniform along the height of the test model.

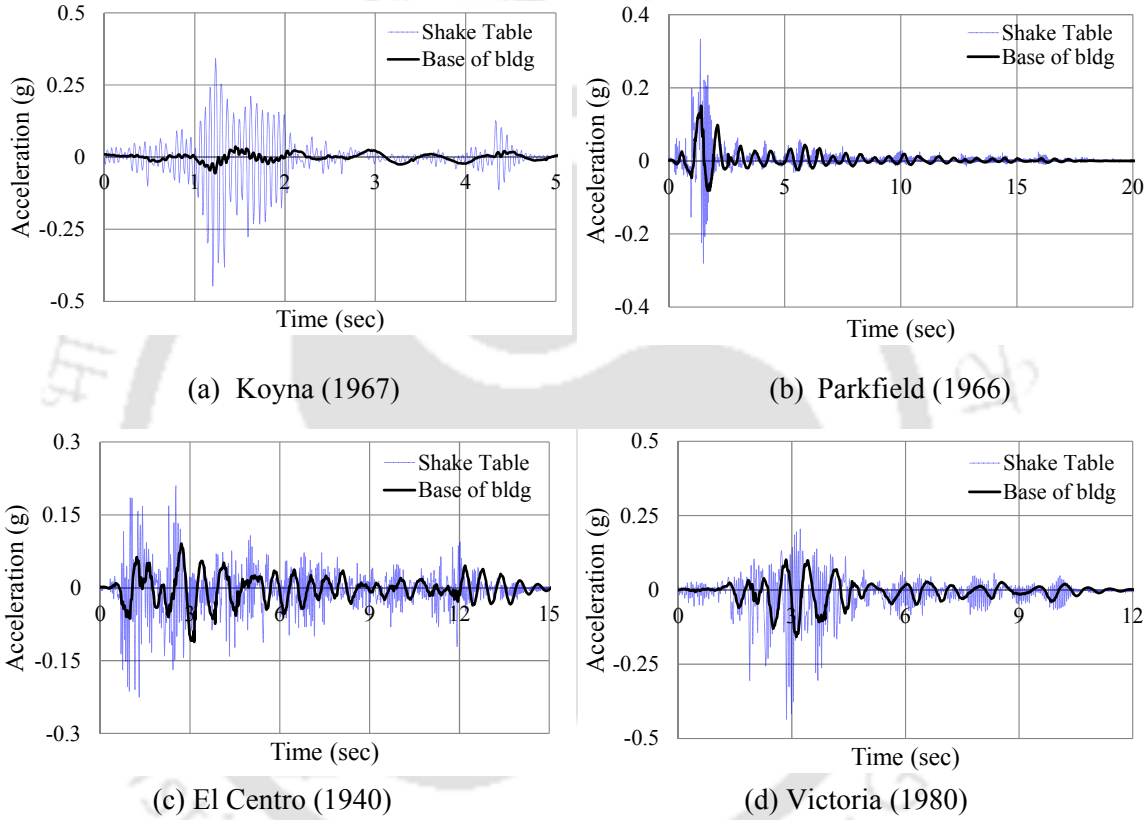

(a) Koyna (1967) (b) Parkfield (1966)

(c) El Centro (1940) (d) Victoria (1980)

Fig. 6.16 Acceleration response at shake table level and base level subjected to 70% intensity level of four earthquakes applied along 45^0 to X-axis

Displacement amplitude recorded at base beam level and first floor level are compared in Fig. 6.18. It is observed that displacement time histories at base beam level and first floor level are nearly overlapping each other, indicating very small inter-storey drift in the structure.

Peak acceleration and displacement at different floor levels for 70% intensity of all the four input earthquakes along 45^0 to X-axis are shown in Table 6.8.

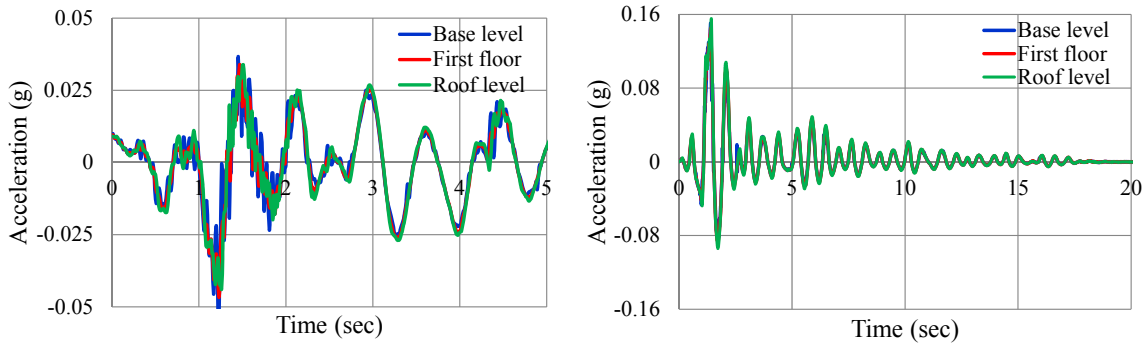

(a) Koyna (1967) (b) Parkfield (1966)

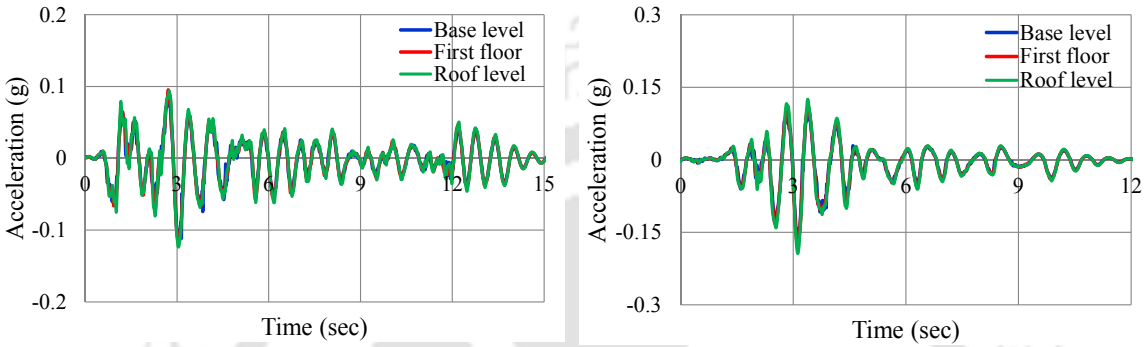

(c) El Centro (1940) (d) Victoria (1980)

Fig. 6.17 Comparison of acceleration responses at base level, first floor and roof level subjected to 70% intensity level of four earthquakes applied along 45^0 to X-axis

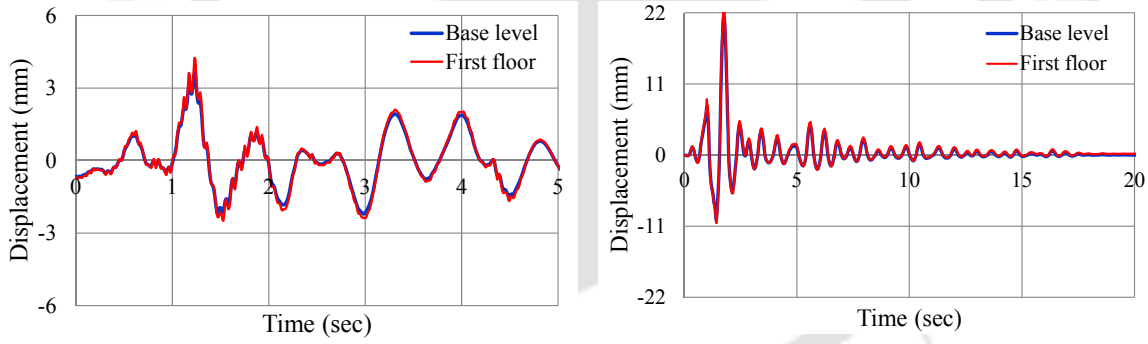

(a) Koyna (1967) (b) Parkfield (1966)

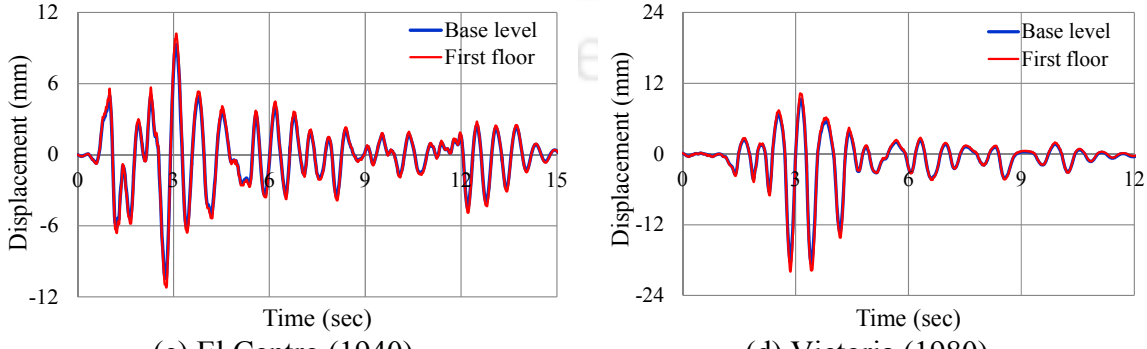

(c) El Centro (1940) (d) Victoria (1980)

Fig. 6.18 Displacement at base level and first floor level subjected to 70% intensity level of four earthquakes applied along 45^0 to X-axis

The largest lateral displacement recorded at base beam level is 18.611mm corresponding to Victoria earthquake, while the first floor level displacement is recorded as 19.939mm. Thus, the inter-storey drift is only 0.22% for floor height of 600mm. Comparison of different floor accelerations corresponding to 30% and 70% intensities of corresponding input earthquakes reveal that the performance of isolator in terms of reduction in acceleration transmissibility increases with the increase in intensity of input earthquake acceleration.

Table 6.8 Peak acceleration and displacement at different levels of model subjected to 70% intensity level of four earthquakes along 45^0 to X-axis

Earthquake	Peak Accelerations (g)				Peak Displacement (mm)	
	At Shake Table	At Base	At First Floor	At Roof Level	At Base level	At First Floor
Koyna	0.442	0.0549	0.0467	0.0439	3.619	4.240
Parkfield	0.333	0.1505	0.1449	0.1554	21.211	23.056
El Centro	0.223	0.1114	0.1158	0.1234	10.439	11.211
Victoria	0.435	0.1579	0.1790	0.1938	18.611	19.939

Fig. 6.19(a) and (b) show the displaced shape of isolator during peak horizontal displacement, when masonry building model is subjected to 100% intensity of Parkfield input earthquake along X-axis and 70% intensity of same input earthquake along 45^0 to X-axis. The maximum horizontal displacement recorded during the 100% intensity of Parkfield input earthquake is 36.2mm, which is 38% of total rubber thickness (95mm). The cyclic lateral displacement test result shows that the model U-FREIs are capable of safely withstanding horizontal displacement up to 60mm. These bearings can significantly reduce the shear force transmitted to the superstructure with the increase in bearing displacement.

(a) 100% of PGA applied along X-axis of FREI

(b) 70% of PGA applied along 45^0 to X-axis of FREI

Fig. 6.19 Displaced shape of isolator during shake table test for Parkfield input earthquake

Rollover deformation properties of U-FREI up to some extent can be seen in Fig. 6.19(a). Part of top and bottom surfaces of the isolator initially in contact with the bottom of model building and shake table respectively loose contact during the testing. After the completion of tests, the bearings have returned to its original position, signifying the stable behaviour of bearing. The bearings have also not shown any damage even after repeated testing.

6.6. Comparison of Responses of BI and FB Test Model

Shake table testing of BI and FB models are carried out for different intensities earthquake excitations. Comparisons of performance of BI and FB model are shown for 30% and 100% intensities of input earthquake excitations along X-axis of FREI.

Maximum acceleration recorded at roof level of the BI model corresponding to full intensity level of Parkfield earthquake acceleration is 0.246g. No damage is observed in the model un-reinforced masonry building for this level of input earthquake acceleration. Peak acceleration at roof level of FB model is recorded as 0.228g for 30% intensity of PGA of Koyna input earthquake excitation. This magnitude of roof

acceleration is close to maximum acceleration recorded during the shake table testing of BI model with 100% intensity of PGA of Parkfield earthquake excitation. Hence, shake table testing of FB model building is restricted to 30% intensity of PGA of corresponding input earthquake excitation of all the four selected earthquakes. Comparison of various dynamic parameter of both BI and FB model subjected to different intensity level of PGA of all the four input earthquakes are presented.

Fig. 6.20 presents the peak acceleration at different floor levels of BI and FB model excited with different intensities of PGA of input earthquake excitations along X-axis of FREI.

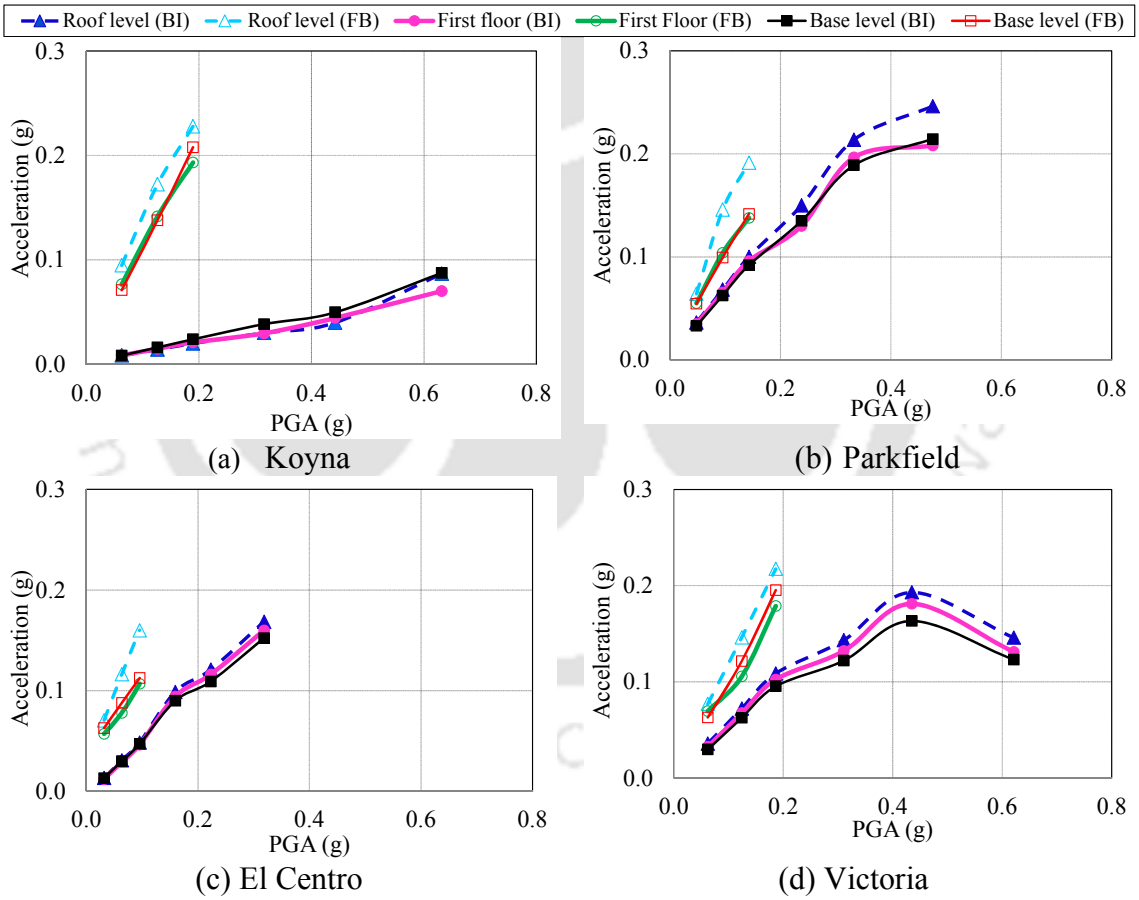

(a) Koyna (b) Parkfield

(c) El Centro (d) Victoria

Fig. 6.20 Comparison of peak acceleration values of BI and FB model subjected to different intensity levels of input earthquakes

It is observed that at 30% intensity of input Koyna earthquake, the roof level acceleration of FB model is 11 times more than that of the BI model. The lowest level

of amplification of acceleration at roof level in FB model is observed corresponding to the input excitation of Parkfield earthquake, which is twice the acceleration recorded at the roof of BI model.

From the Fig. 6.20(b) and (d), it observed that the rate of increase in accelerations at different floor levels of BI building model reduce substantially with increase in intensity of input earthquake acceleration. However, this trend is not observed in Fig. 6.20(a), where the accelerations at different floor levels of BI model are very low as compared to that of FB model. Thus, the efficiency of the isolation system is generally observed to improve with higher intensities of earthquake excitations.

Fig. 6.21 shows plot for peak base shear of FB and BI model for different intensities of input earthquakes along X-axis.

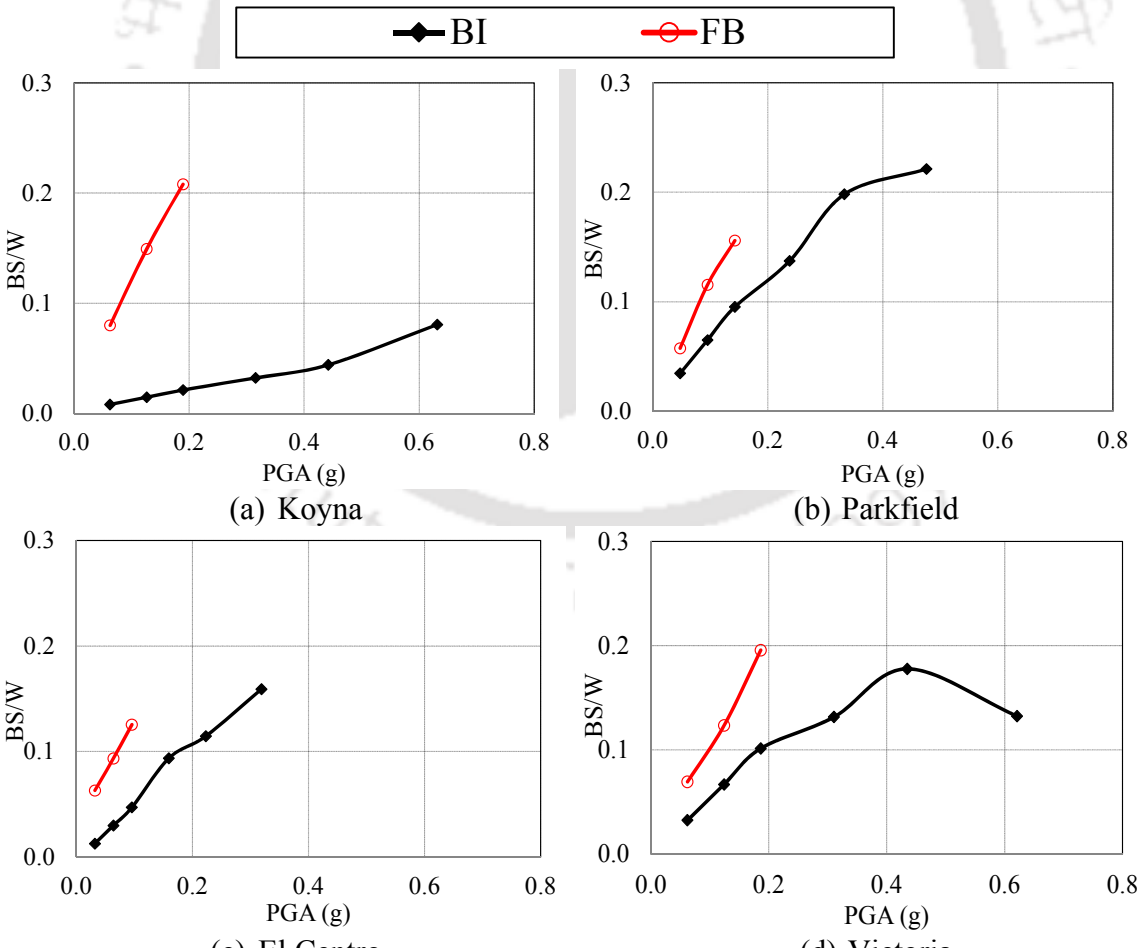

(a) Koyna (b) Parkfield

(c) El Centro (d) Victoria

Fig. 6.21 Comparison of peak base shear of BI and FB model subjected different intensity levels of input earthquakes

The peak base shear in FB model is much higher than that of BI model for any corresponding level of input earthquake intensity. Further, it may also be noted that while the peak base shear increases with increase in earthquake intensity, the rate of increase is generally reduced in BI model at higher intensity of earthquake, indicating the efficiency of un-bonded isolator in seismic response mitigation with the increasing acceleration amplitude of the earthquakes.

Fig. 6.22 contains the amplification profile of peak acceleration at all three floor levels of BI and FB model with respect to different acceleration amplitude for all four considered earthquake motions. It is observed that accelerations are amplified for FB model and rate of increase is generally more along the height of the model. However, in case of BI model, accelerations are not amplified along the height of model building. Peak acceleration along different floor level is almost half of the input earthquake intensities. Further, it is also seen from Fig. 6.22 that the amplifications of acceleration at three floors level of BI model are comparable.

Fig. 6.23 to Fig. 6.26 show the comparison of peak inertia force, shear force and base moment of BI and FB model for intensity level of 30% of PGA of all the four input earthquake excitations. For BI model, the base is taken as reference to plot all the profiles. Inertia force, shear force and base moments are significantly higher for FB model as compared to those of the BI model for all the four considered input earthquakes. These results establish the effectiveness of base isolation system developed in this study. Time histories of base shear corresponding to intensity of 30% of PGA of all the four input earthquakes are plotted in Fig. 6.27. Reasonable reduction is observed in base shear in case of BI model as compared to FB model even for such low acceleration amplitudes. The performance improves further with higher level of induced displacement at the U-FREIs.

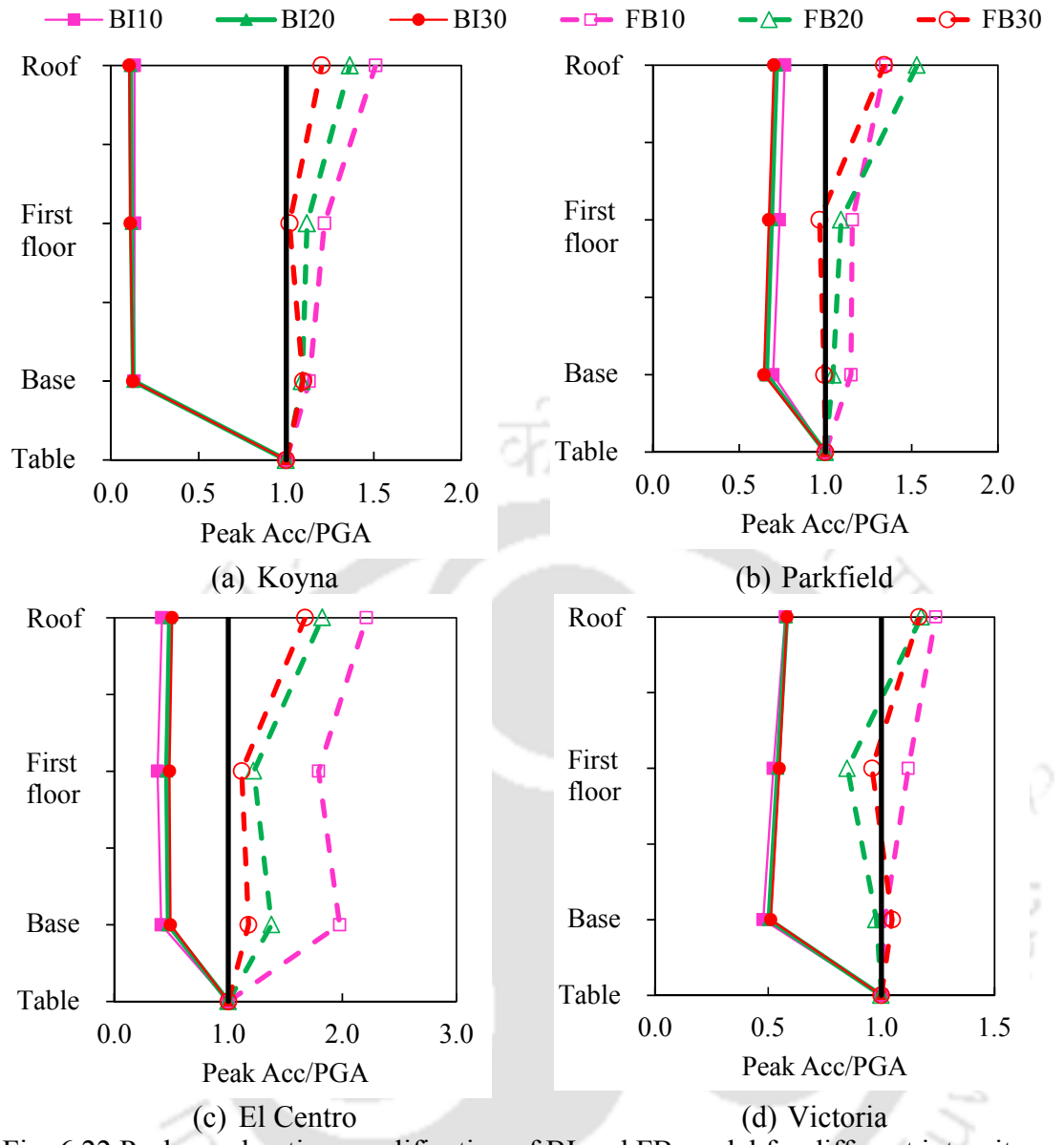

Fig. 6.22 Peak acceleration amplification of BI and FB model for different intensity levels of input earthquakes

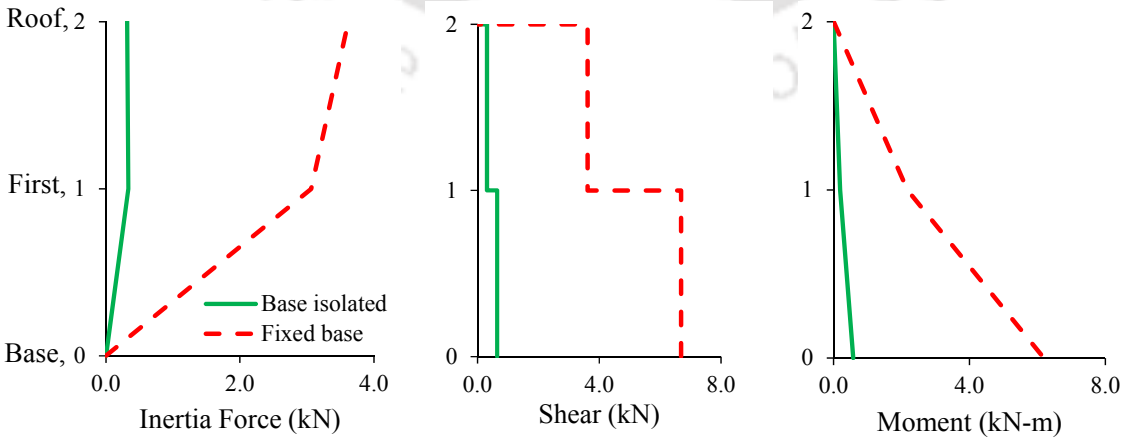

Fig. 6.23 Comparison of peak responses of BI and FB model corresponding to 30 % intensity level of Koyna earthquake

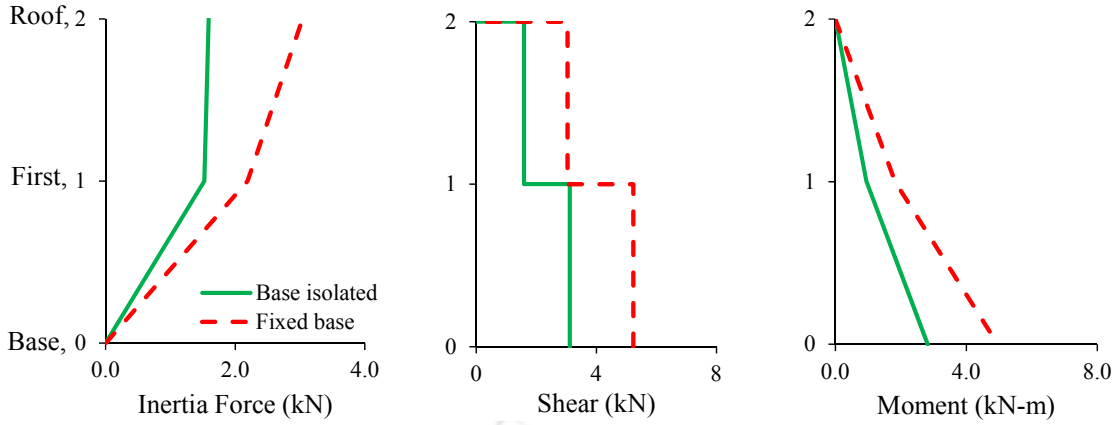

Fig. 6.24 Comparison of peak responses of BI and FB model corresponding to 30% intensity level of Parkfield earthquake

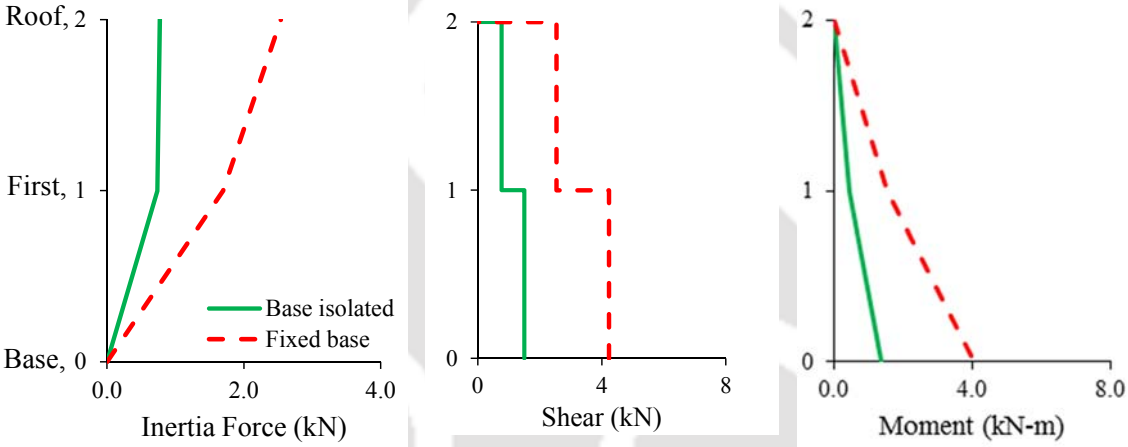

Fig. 6.25 Comparison of peak responses of BI and FB model corresponding to 30% intensity level of El Centro earthquake

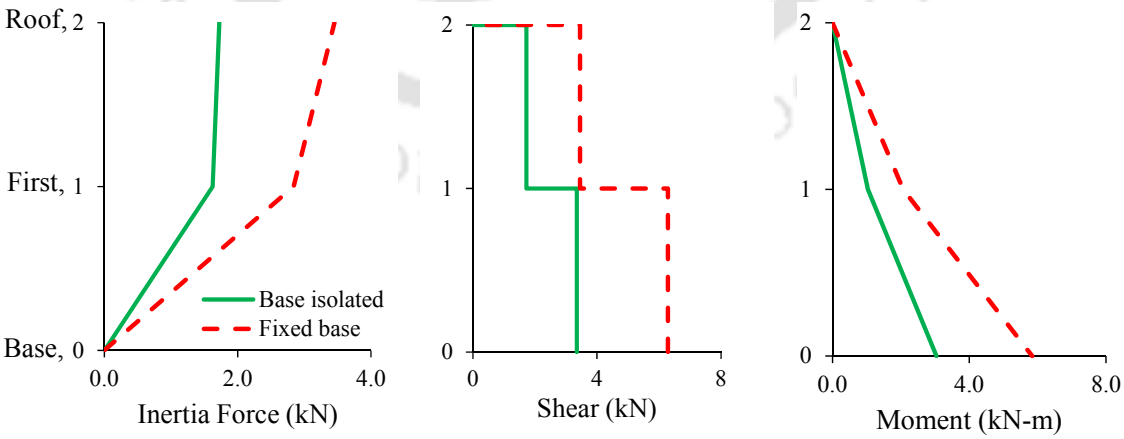

Fig. 6.26 Comparison of peak responses of BI and FB model corresponding to 30% intensity level of Victoria earthquake

Fundamental frequency of the BI model building is determined by carrying out fast Fourier transform (FFT) of the lateral roof acceleration recorded during the shake table test and these frequencies for different intensity levels of PGA of input earthquakes accelerations are shown in Table 6.9. Fig. 6.28 shows the FFT of roof lateral acceleration corresponding to intensity of 100 % of PGA of all the four input earthquake accelerations.

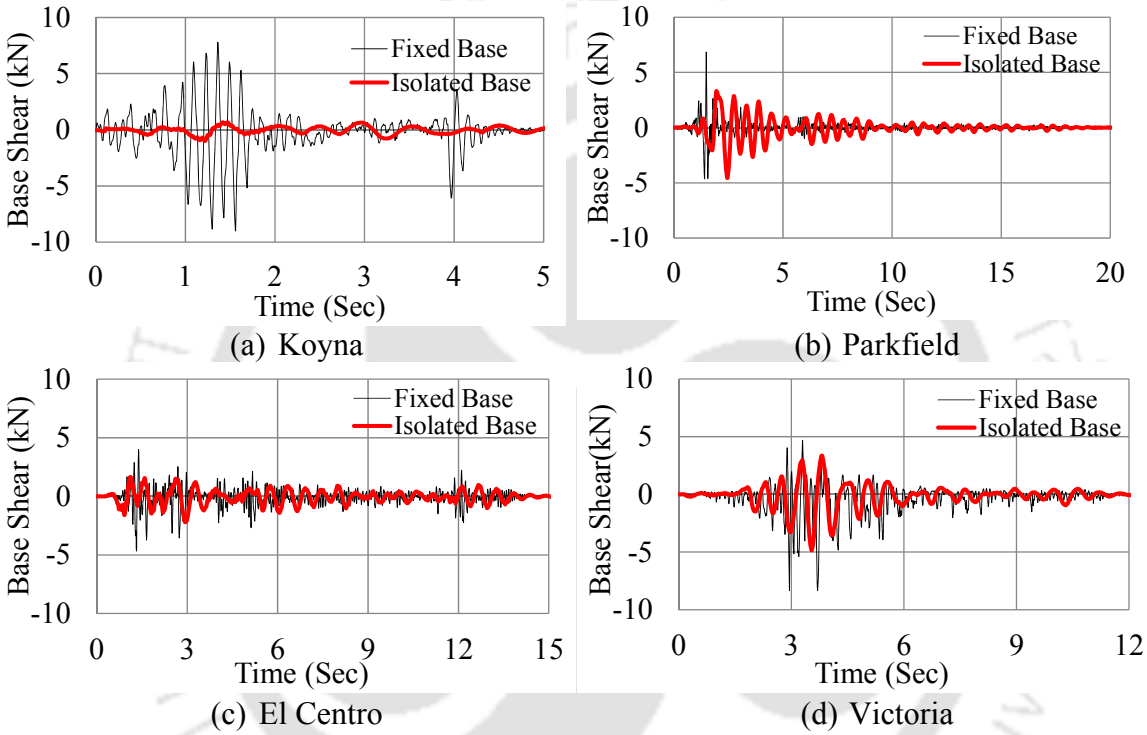

Fig. 6.27 Time history at base level of BI and FB model corresponding to 30% intensity level of four input earthquake motions

Horizontal load-displacement hysteresis behaviour of U-FREI is highly nonlinear. Due to this non linearity, vibration frequency of the BI building varies in accordance with different intensities of PGA of earthquake excitations. As may be seen from Table 6.9 and Fig. 6.28, fundamental frequency of the model building varies with the variation in input earthquakes characteristics. Fundamental frequencies are also observed to vary for a particular input earthquake with intensities of input earthquake excitations. It is observed that fundamental frequency of BI structure decreases with the increase in

intensity of input earthquake acceleration, which indicates the increase in seismic isolation efficiency of isolator.

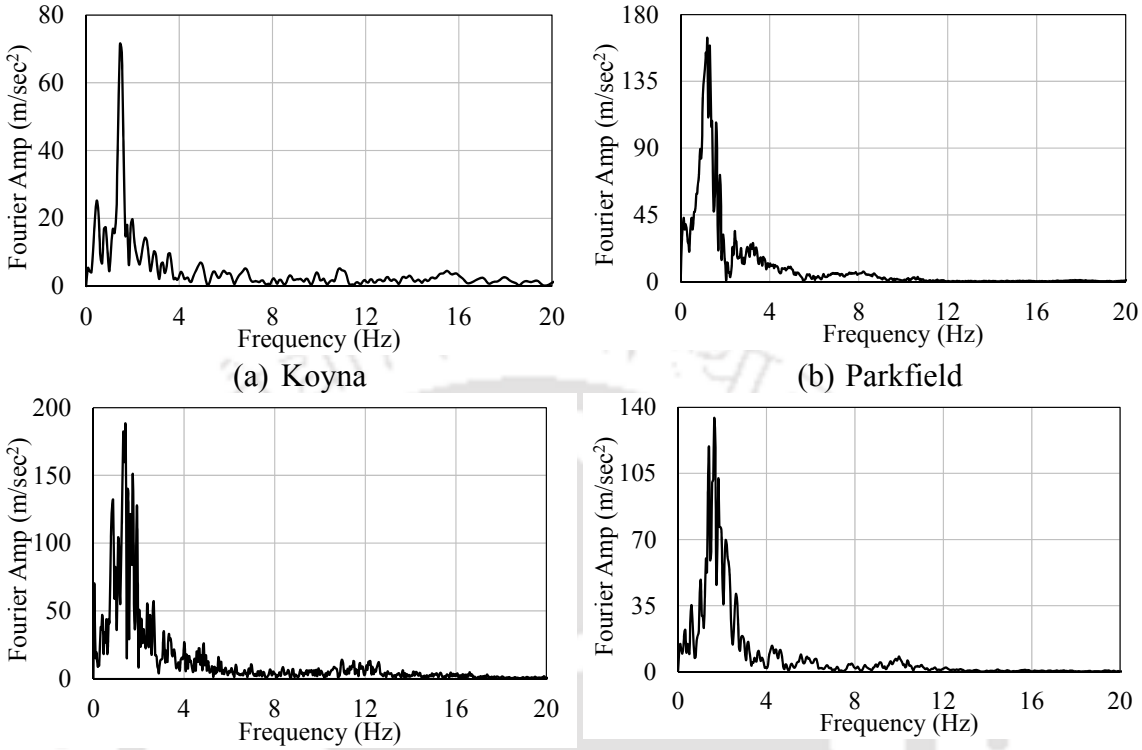

Fig. 6.28 Fourier amplitude spectra of roof acceleration of base isolated model corresponding to four input earthquakes (full intensity)

Table 6.9 Fundamental frequency of base isolated model corresponding to different input earthquakes of varying intensities

Earthquake	Fundamental frequency (Hz)		
	at 10% of PGA	at 50% of PGA	at 100% of PGA
Koyna	1.969	1.488	1.457
Parkfield	1.791	1.607	1.199
El Centro	1.939	1.734	1.411
Victoria	1.821	1.692	1.635

6.7. Concluding Remarks

A two storey 1/5th scale un-reinforced masonry building supported on four un-bonded square isolators is tested on a shake table subjected to four different input earthquakes. It is observed that the bearings have regained their original un-deformed configuration

after the completion of test. Further, no damages of bearing and cracks on the masonry structure are observed by visual inspection after completion of each test run.

The same masonry building is also tested by placing it directly on the shake table to ascertain the seismic response as FB structure. Scope of this study is limited to the elastic behaviour of masonry building during shake table test. The maximum intensity of excitation is restricted as a fraction of PGA of input earthquakes such that no damage occurs in the FB structure. It is observed that at 30% intensity of PGA of excitation the FB structure attained the maximum acceleration at roof level, which is same as that of BI building model with full intensity of PGA of input motions. There is no damage in any part of BI building model at full intensity of PGA of input motions. Hence, the comparison of seismic responses of BI and FB models are limited up to an intensity of 30% of PGA of input earthquakes. Substantial reduction in floor accelerations, base shear and base moments are observed in BI model as compared to FB model.

The following conclusions are drawn:

1. U-FREIs are observed to be very effective in reducing seismic responses of structures.
2. The effectiveness in seismic isolation increases with increased in horizontal displacement of isolators, which also maintains a stable rollover configuration at large displacement.
3. The U-FREIs are observed to be effective irrespective of loading directions.
4. There is an immense potential of introducing U-FREI in un-reinforced masonry buildings to reduce the seismic vulnerability of those structures.

Chapter 7

Numerical Study on Un-reinforced Masonry Test Model Supported on FREI

7.1. Introduction

This chapter describes the numerical study of un-reinforced masonry test model supported on FREI for evaluation of dynamic response under four different prescribed earthquake motions. The feasibility of FREI as an alternate of SREI for seismic isolation of un-reinforced masonry building is already presented in previous chapters. Experimental study as carried out on a $1/5^{th}$ scaled two storey un-reinforced masonry building supported on four square U-FREI is presented in Chapter 6. Stiffness and damping values of square U-FREIs are estimated through FE analysis and these results are also verified comparing the same obtained from experimental investigation. However, shake table testing of base isolated model building is not always feasible due to high cost and time required for the preparation of model and test setup. Thus, as an alternative, numerical simulation of the model building is carried out using SAP2000 Version 14 in order to know the dynamic response of the base isolated building. Results of shake table testing of model building supported on U-FREIs are compared with the numerical result to validate the adopted numerical modelling approach. Acceleration and displacement at various floor levels are evaluated while the analysis is carried out for different prescribed ground motion as input. Different response parameters as obtained from shake table testing are compared with those obtained from the numerical analysis.

7.2. Modelling of Test Structure

SAP2000 Version 14 developed by Computers and Structures, Inc, Berkeley, USA is used for modelling and analysis of the base isolated test structure. Modelling and analysis of un-reinforced masonry test model building and FREIs are described briefly as below.

Base level beams of the test model building are modelled as beam element. The test model building supported on isolator undergoes nearly rigid body motion as observed during shake table test. Inter-storey drift at different levels of the test model building is found to be insignificant. Thus, in order to simplify the modelling, the brick walls are modelled using plate element. Floor slabs are also modelled using plate elements. Extruded view of the model building is shown in Fig. 7.1.

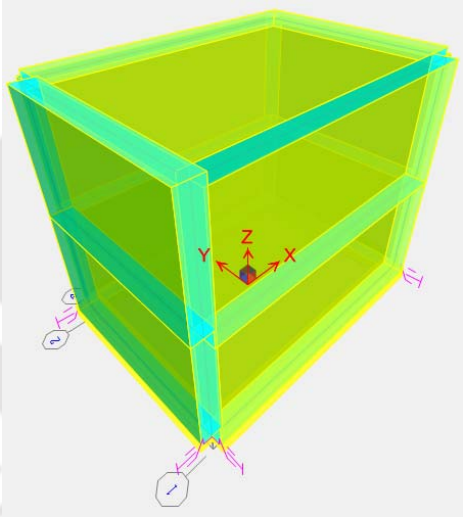

Fig. 7.1 SAP2000 model of test building

7.3. Modelling of FREI

Isolators are modelled as equivalent multi-linear spring. Back bone curve obtained from force displacement hysteresis loops recorded during testing of isolator is used to represent the properties of multi-linear spring. Multi-linear pivot hysteretic plasticity model is used to define the property of spring.

The experimentally obtained force displacement hysteresis loops of U-FREI under horizontal cyclic loading along X-axis (Fig. 7.2a) and along 45^0 to X-axis (Fig. 7.2b) are used to define the link/support properties as adopted for modelling of isolator.

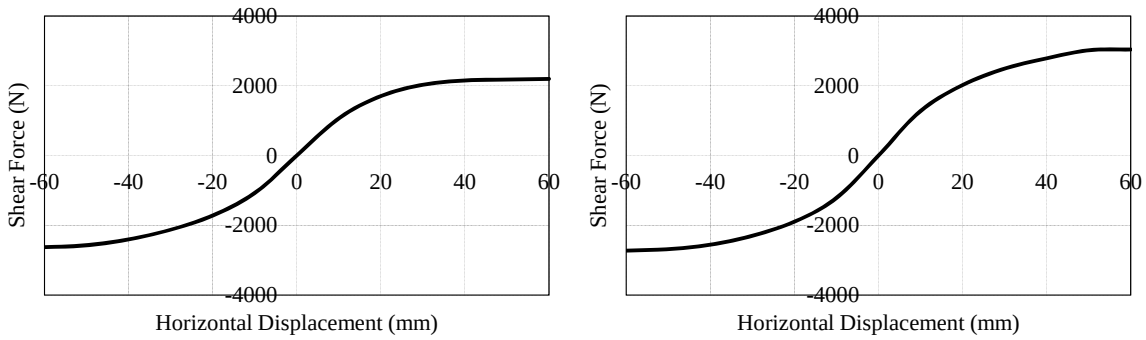

(a) along X-axis (b) 45^0 to X-axis

Fig. 7.2 Lateral load *vs* displacement of U-FREI during cyclic loading test

7.4. Comparison of Numerical and Shake Table Test Results

Numerical analyses of isolated system is carried out using scaled earthquake motions, which are presented in Chapter 6. The analysis is repeated for different acceleration intensity level of four earthquakes. Comparison of time histories of acceleration obtained from shake table test and numerical analysis at different level of the test model building corresponding to Koyna earthquake (full intensity) applied along X-axis are shown in Fig. 7.3. It may be observed that the pattern of acceleration time histories at a floor level from experimental and numerical exercises are quite similar. It is further observed that the peak acceleration obtained from analysis at base beam level and roof level are 6.1% and 3.4% lesser than those of the experimental results for the same earthquake. Similarly, at first floor level, the peak acceleration recorded from the numerical analysis is 14.5% higher than the experimental result. Comparisons of RMS values of acceleration recorded at different levels are also shown in Fig. 7.3. RMS

values of acceleration obtained from the experimental investigations are observed to be 5.0-10.4% lower than those obtained from the numerically simulated model. Therefore, the numerical model of the base isolated building may be considered as acceptable for evaluation of dynamic response characteristics of such building.

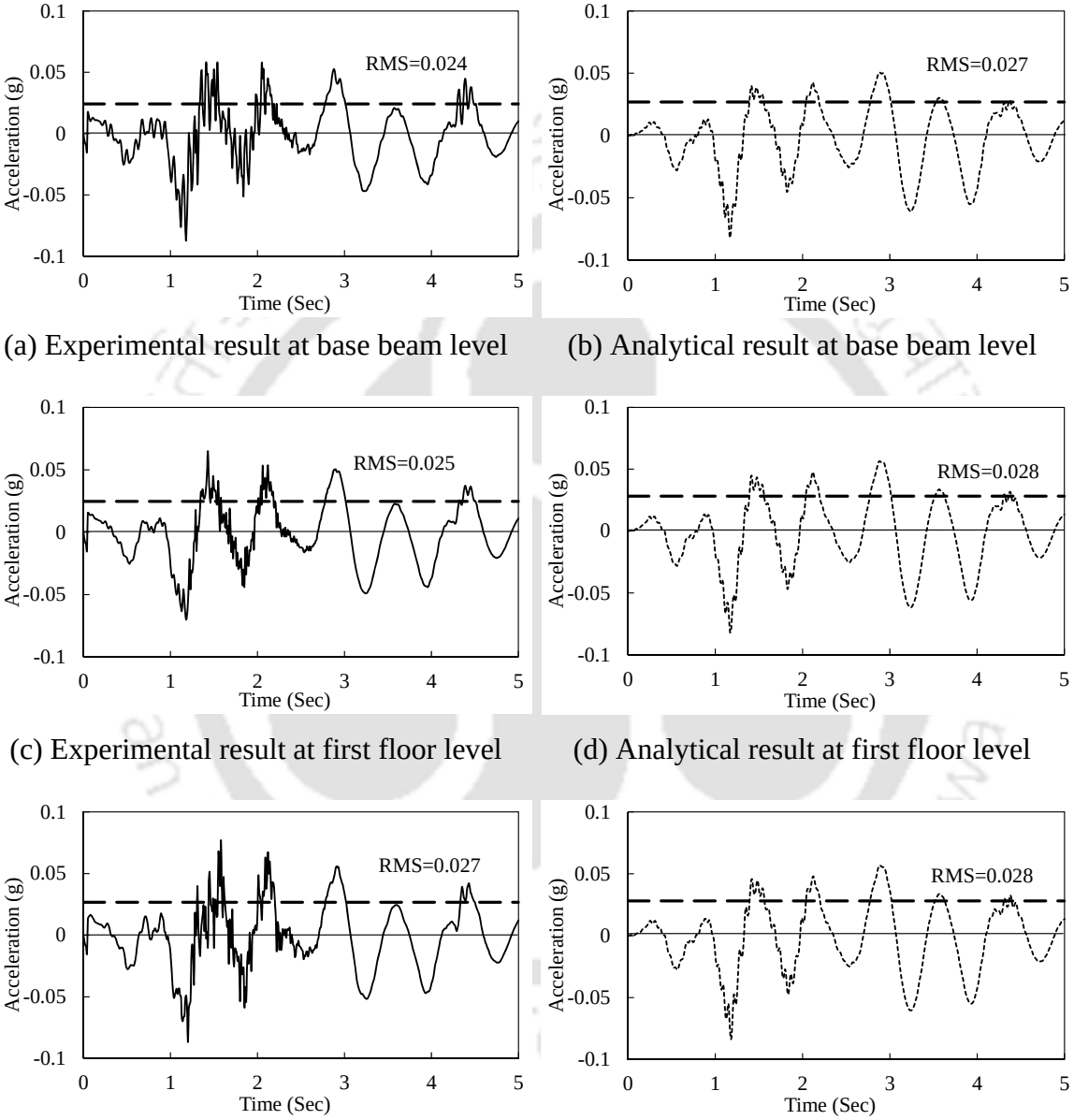

(a) Experimental result at base beam level (b) Analytical result at base beam level

(c) Experimental result at first floor level (d) Analytical result at first floor level

(e) Experimental result at roof level (f) Analytical result at roof level

Fig. 7.3 Comparison of experimental and analytical acceleration responses at different levels of model subjected to Koyna earthquake (full intensity) applied along X-axis

Similar exercises are repeated by considering other earthquake motion with different characteristics. Comparison of time histories of acceleration obtained from shake table

test and numerical analysis at different level of the test model corresponding to full intensity of scaled acceleration history of Parkfield earthquake applied along X-axis are shown in Fig. 7.4.

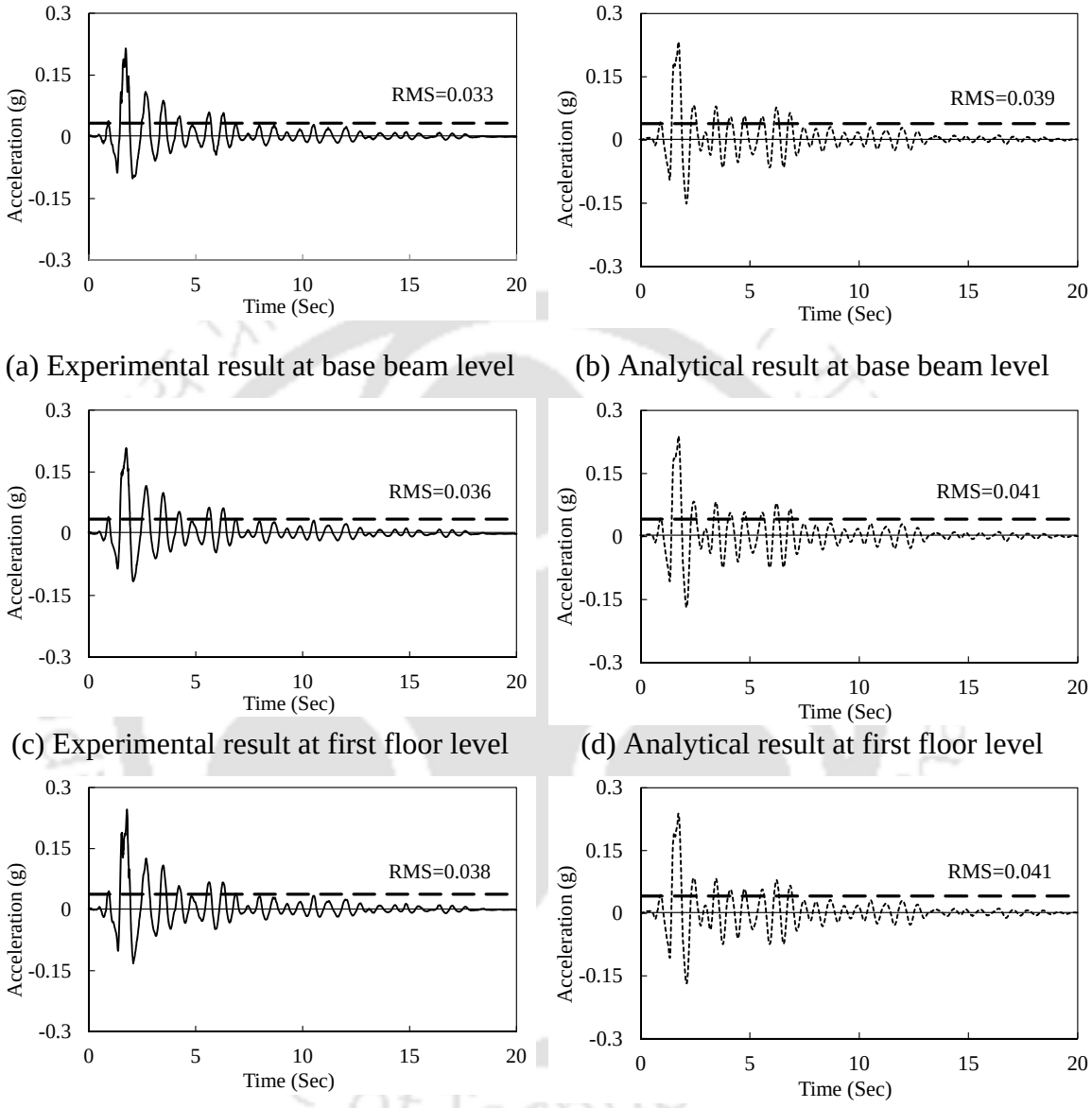

(a) Experimental result at base beam level (b) Analytical result at base beam level

(c) Experimental result at first floor level (d) Analytical result at first floor level

(e) Experimental result at roof level (f) Analytical result at roof level

Fig. 7.4 Comparison of experimental and analytical acceleration responses at different levels of model subjected to Parkfield earthquake (full intensity) applied along X-axis

Peak accelerations as obtained from the numerical analysis are 7.8% and 13.1% higher than those obtained from the experiment at base level and first floor level respectively, whereas the roof acceleration obtained from experiment is 3.1% lesser than the numerical analysis. RMS values of acceleration obtained from the experimental

investigations are observed to be 7.6-14.9 % lower than those obtained from numerically simulated model.

Comparison of time histories of acceleration obtained from shake table test and numerical analysis at different level of the test model building corresponding to full intensity of scaled acceleration history of El Centro earthquake applied along X-axis are shown in Fig. 7.5.

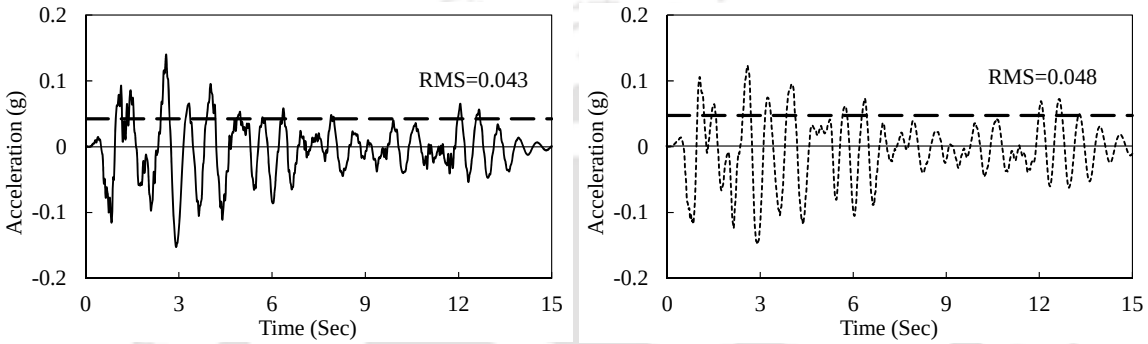

(a) Experimental result at base beam level

(b) Analytical result at base beam level

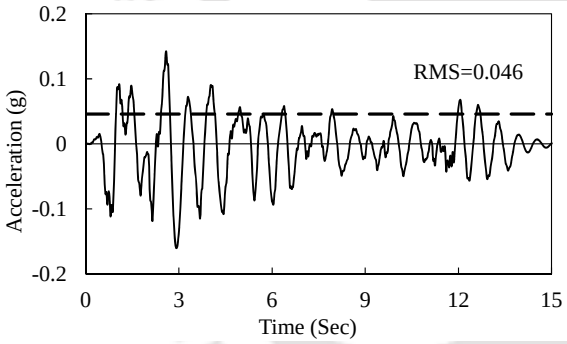

(c) Experimental result at first floor level

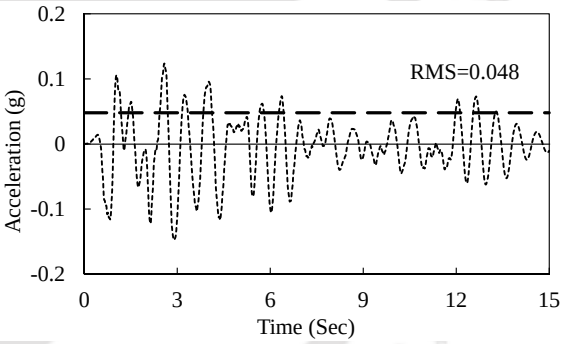

(d) Analytical result at first floor level

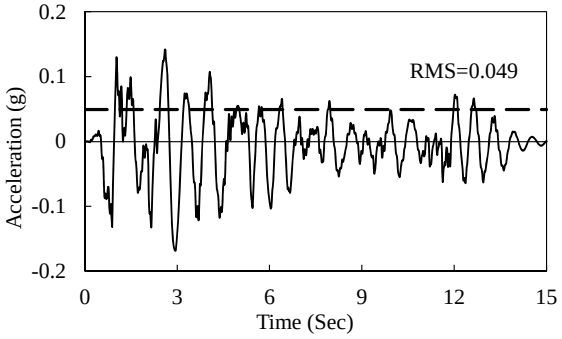

(e) Experimental result at roof level

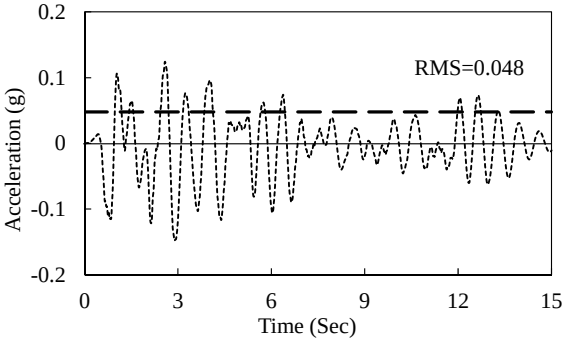

(f) Analytical result at roof level

Fig. 7.5 Comparison of experimental and analytical acceleration responses at different levels of model subjected to El Centro earthquake (full intensity) applied along X-axis

Peak acceleration as obtained from the numerical analysis are 2.8%, 8.5% and 13.9% lesser than those obtained from the experimental result at base, first floor and roof level

respectively. RMS values of acceleration obtained from the experimental investigations are observed to be 3.8% and 10.7% lower than those obtained from numerical analysis at base beam level and first floor level respectively. However, RMS value of acceleration at roof level obtained from numerical analysis is 2.9% lesser than the experimentally evaluated result.

Comparison of time histories of acceleration obtained from shake table test and numerical analysis at different level of the test model building corresponding to full intensity of scaled acceleration history of Victoria earthquake applied along X-axis are shown in Fig. 7.6. Peak acceleration as obtained from the numerical analysis are 13.5%, 11.0% and 0.5% higher than those from the experimental result at base, first floor and roof level respectively. RMS values of acceleration obtained from the experimental investigations are observed to be 3.9-13.4% lower than the result obtained from the numerical analysis. It is observed that there is very good agreement in the pattern of response acceleration time histories between experimental and numerical analysis for all four sample earthquake motions. However, small differences between peak values of responses are observed.

Similar to acceleration time histories, displacement time histories are also compared to check the accuracy of numerical modelling. Comparison of displacement response histories obtained from shake table test and numerical analysis at different level of the test model building subjected to full intensity of scaled acceleration history of Koyna earthquake applied along X-axis are shown in Fig. 7.7. Peak displacement at base beam level obtained from the experiment is 8.3% lesser than those obtained from the numerical analysis. Similarly, at first floor level peak displacement as obtained from experiment is 4.5% higher than those obtained from numerical analysis. RMS values of displacement obtained from experiments are 14.3% and 9.7% lesser than those obtained

from the numerical analysis at base and first floor level respectively.

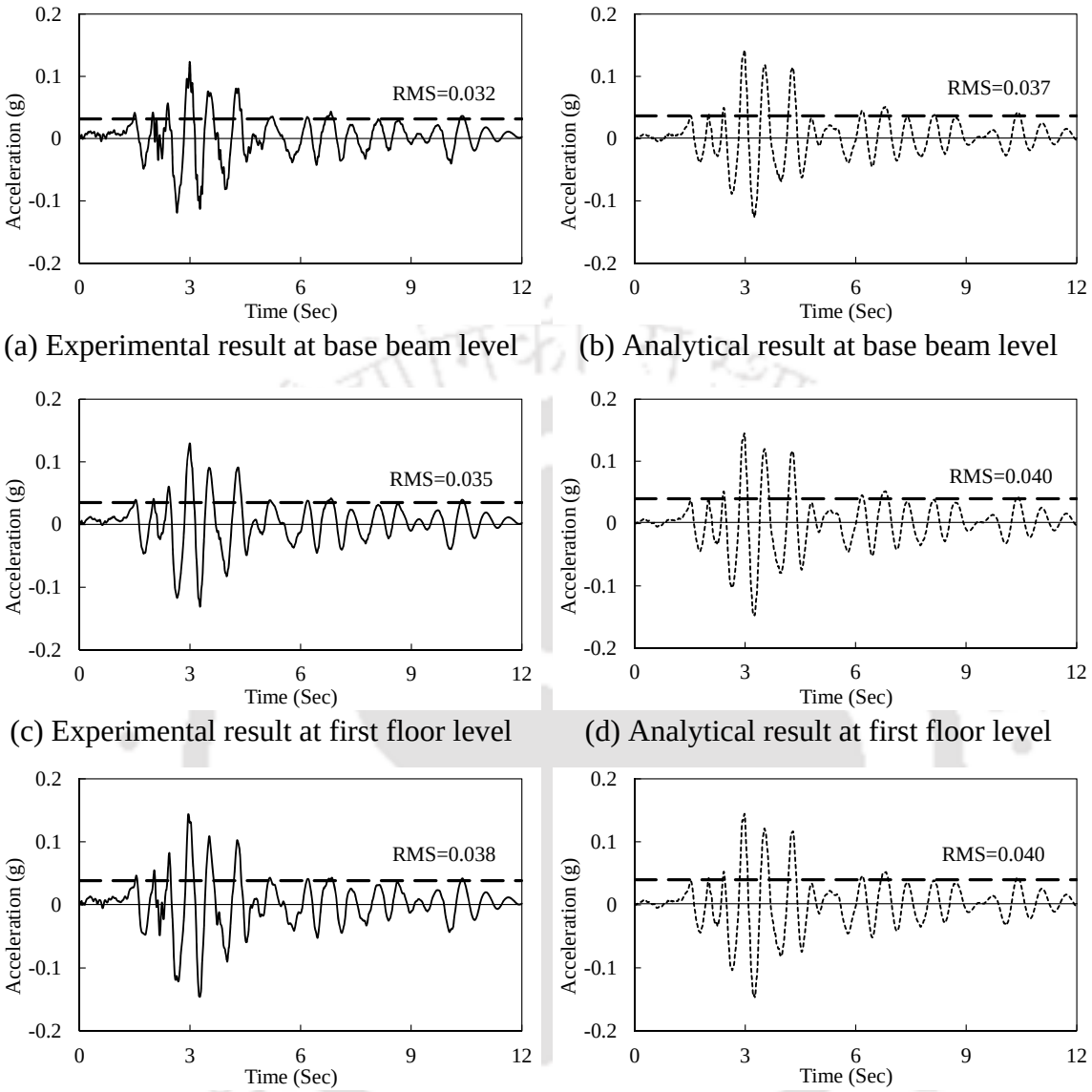

(a) Experimental result at base beam level (b) Analytical result at base beam level

(c) Experimental result at first floor level (d) Analytical result at first floor level

(e) Experimental result at roof level (f) Analytical result at roof level

Fig. 7.6 Comparison of experimental and analytical acceleration responses at different levels of model subjected to Victoria earthquake (full intensity) applied along X-axis

Comparison of displacement response histories obtained from shake table test and numerical analysis at different level of the test model building subjected to full intensity of scaled acceleration history of Parkfield earthquake applied along X-axis are shown in Fig. 7.8.

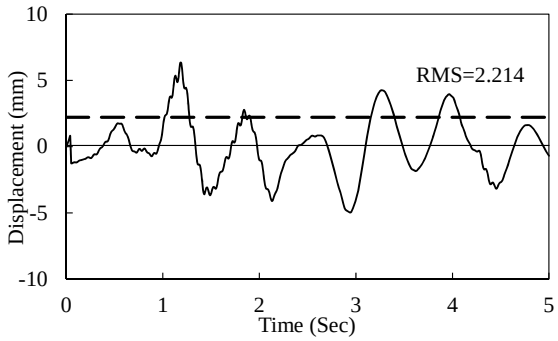

(a) Experimental result at base beam level

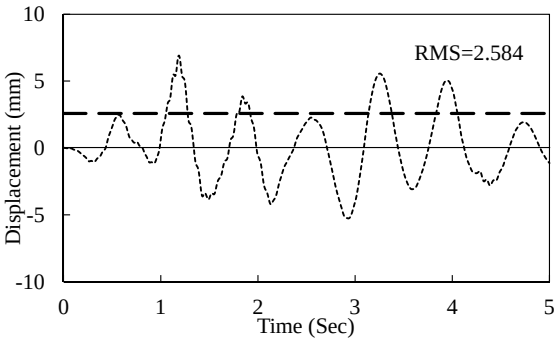

(b) Analytical result at base beam level

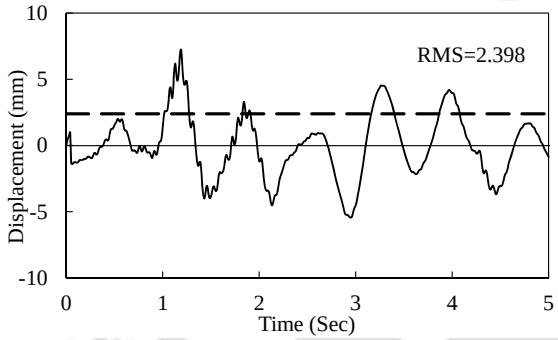

(c) Experimental result at first floor level

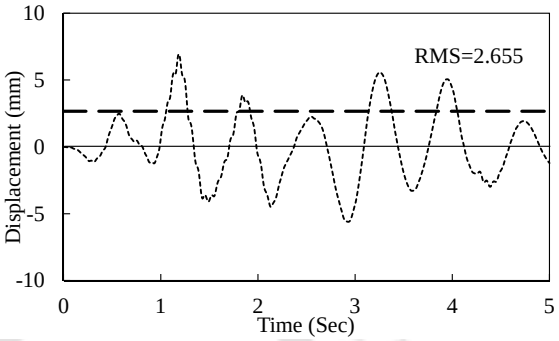

(d) Analytical result at first floor level

Fig. 7.7 Comparison of experimental and analytical displacement at base level and first floor level subjected to Koyna earthquake (full intensity) applied along X-axis

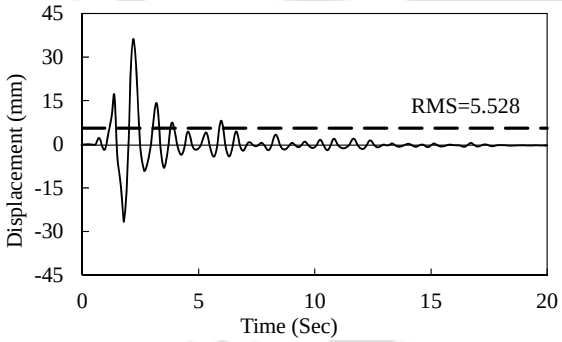

(a) Experimental result at base beam level

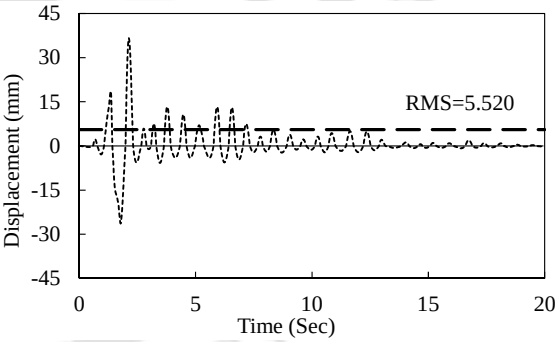

(b) Analytical result at base beam level

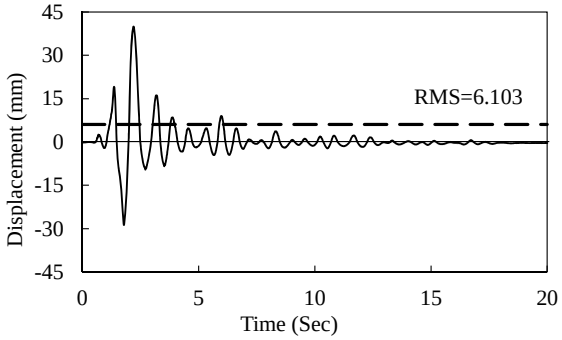

(c) Experimental result at first floor level

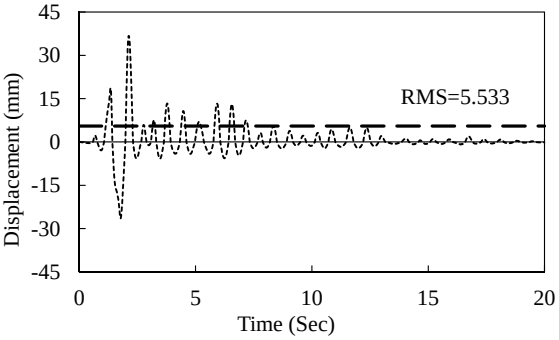

(d) Analytical result at first floor level

Fig. 7.8 Comparison of experimental and analytical displacement at base level and first floor level subjected to Parkfield earthquake (full intensity) applied along X-axis

Peak displacement as obtained from the experiment is 1.2% lesser than that obtained from the numerical analysis at base level, while the same is 8.7% higher at first floor level. RMS values of displacement obtained from experiment are 0.1% and 10.3% higher than those obtained from the numerical analysis at base and first floor level respectively.

Comparison of displacement response histories obtained from shake table test and numerical analysis at base beam level and first floor level of the test model building subjected to full intensity of scaled acceleration history of El Centro earthquake applied along X-axis are shown in Fig. 7.9. Peak displacements as obtained from the experiment are 3.7% and 13.0% higher than those obtained from the numerical analysis at base and first floor level respectively. RMS values of displacements obtained from experiment are 14.2% and 4.9% lesser than that obtained from numerical analysis at base level and at first floor level respectively.

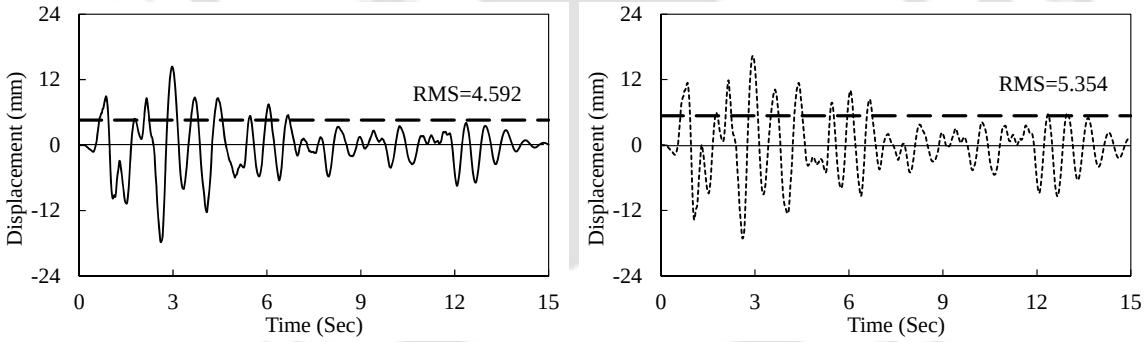

(a) Experimental result at base beam level

(b) Analytical result at base beam level

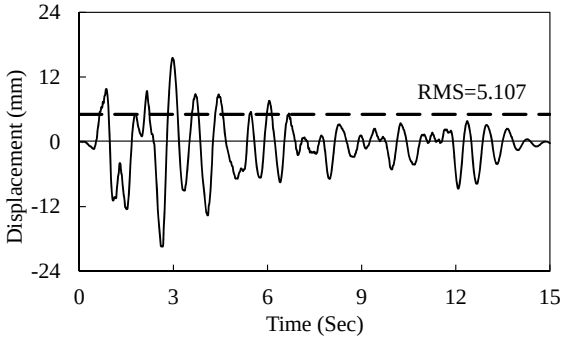

(c) Experimental result at first floor level

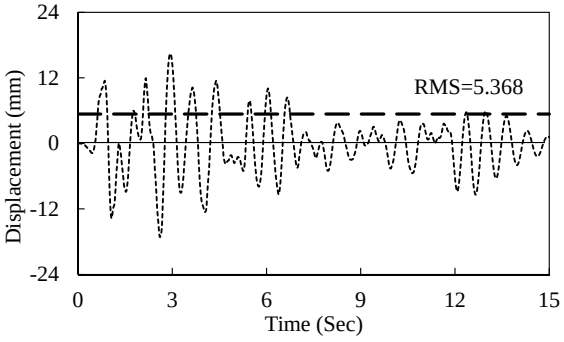

(d) Analytical result at first floor level

Fig. 7.9 Comparison of experimental and analytical displacement at base level and first floor level subjected to El Centro earthquake (full intensity) applied along X-axis

Comparison of displacement response histories obtained from shake table test and numerical analysis at base beam level and first floor level of the test model building subjected to full intensity of scaled acceleration history of Victoria earthquake applied along X-axis are shown in Fig. 7.10.

Peak displacement as obtained from the experiment are 6.6% and 15.0% higher than those obtained from numerical analysis at base level and first floor level respectively. RMS values of displacements as obtained from experiment are 14.6% and 4.0% lesser than those obtained from the analysis at base level and first floor level respectively.

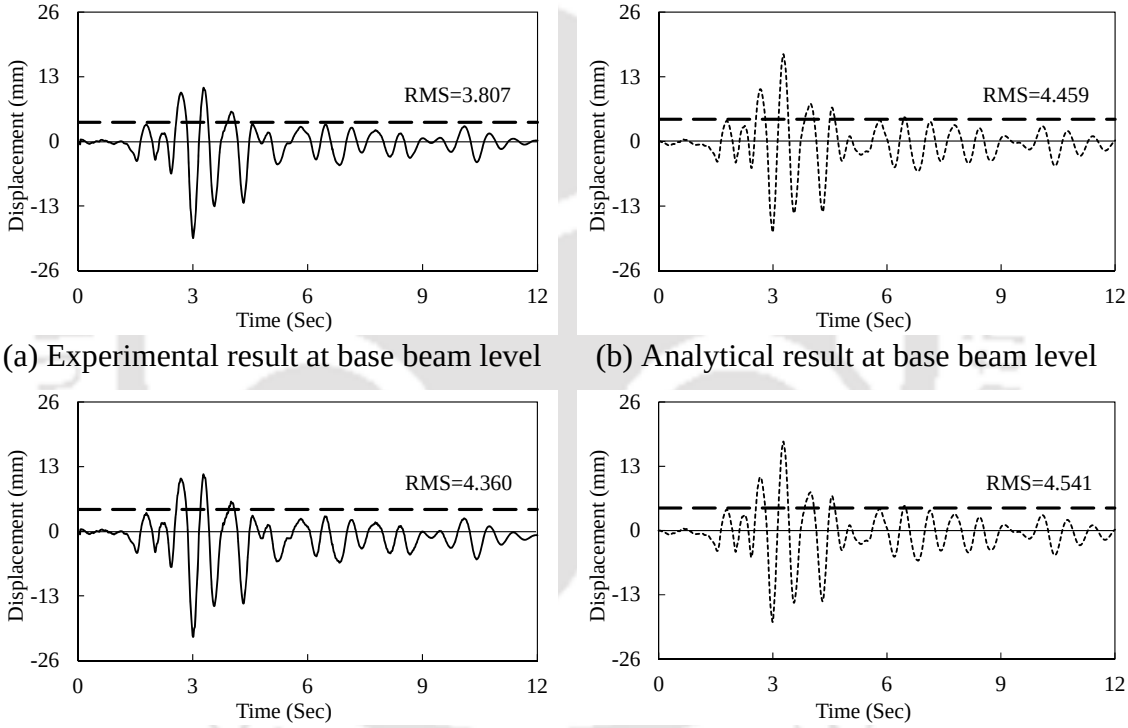

(a) Experimental result at base beam level (b) Analytical result at base beam level

(c) Experimental result at first floor level (d) Analytical result at first floor level

Fig. 7.10 Comparison of experimental and analytical displacement at base level and first floor level subjected to Victoria earthquake (full intensity) applied along X-axis

It is also observed that the displacement at different time instances at base beam level and first floor level are almost same under a particular earthquake excitation. It may be concluded that there is insignificant inter-storey drift in the structure as observed from numerical analysis as well, indicating a rigid body motion of the structure above isolation level. Thus, no significant seismic forces are generated in the building

elements and the building remain undamaged under all the sample earthquake motions. Peak acceleration and displacement obtained from numerical analysis at different floor levels subjected to all the four input earthquakes (full intensity) applied along X-axis are shown in Table 7.1.

Table 7.1 Numerical analysis results of peak acceleration and displacement at different levels of model subjected to four earthquakes (full intensity) along X-axis

Earthquake	Peak Accelerations (g)				Peak Displacement (mm)	
	Input	At Base	At First Floor	At Roof Level	At Base level	At First Floor
Koyna	0.632	0.0823	0.0819	0.0838	6.900	6.928
Parkfield	0.476	0.2327	0.2393	0.2388	36.632	36.726
El Centro	0.319	0.1482	0.1475	0.1480	17.147	17.181
Victoria	0.615	0.1423	0.1473	0.1467	18.251	18.472

The largest lateral displacement experienced by the isolator is 36.632 mm when excited by Parkfield input earthquake. Testing under horizontal cyclic displacement on the same isolator has shown that U-FREI is able to maintain stability up to 60 mm. It may be observed that during the Parkfield earthquake excitation, the first floor level displacement is recorded as 36.726mm, which is almost equal to the base beam level displacement, indicating the rigid body motion of superstructure of the base isolated model building. The observed maximum displacement from numerical analysis is only 1.2% lesser than the results obtained from shake table test for the same input earthquake excitation.

The accuracy of numerical analysis of the isolated model building is further studied by considering a different angle of applied earthquake excitation, e.g. considering the excitation to act along 45^0 to X-axis.

Comparison of time histories of acceleration obtained from shake table test and numerical analysis at different levels of the test model building subjected to 70%

intensity of scaled acceleration for Koyna earthquake applied along 45^0 to X-axis are shown in Fig. 7.11.

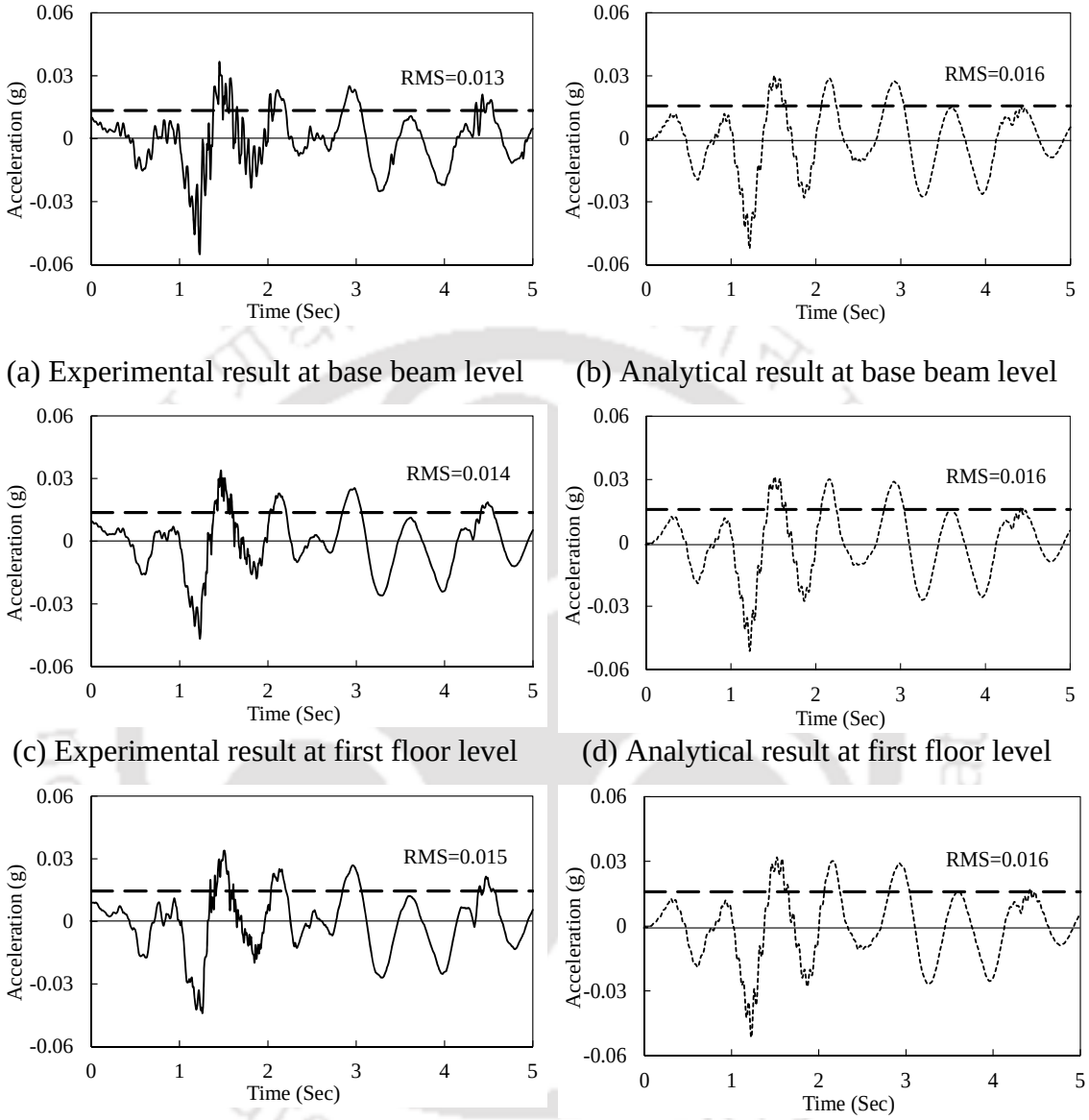

(a) Experimental result at base beam level (b) Analytical result at base beam level

(c) Experimental result at first floor level (d) Analytical result at first floor level

(e) Experimental result at roof level (f) Analytical result at roof level

Fig. 7.11 Comparison of experimental and analytical acceleration responses at different levels of model subjected to 70% intensity level of Koyna earthquake applied along 45^0 to X-axis

It is observed that the peak acceleration obtained from experiment is 5.4% higher than that obtained from numerical analysis at base beam level. However, at first floor level and roof level, the peak acceleration obtained from experiment are 8.8% and 14.6% lesser respectively than those obtained from the numerical analysis. RMS values of

acceleration from test are around 8.3-14.2% lower than those obtained from the numerical analysis.

Similarly, comparison of time histories of acceleration obtained from shake table test and numerical analysis at different levels of the test model building subjected to 70% intensity of scaled acceleration for Parkfield earthquake applied along 45^0 to X-axis are shown in Fig. 7.12.

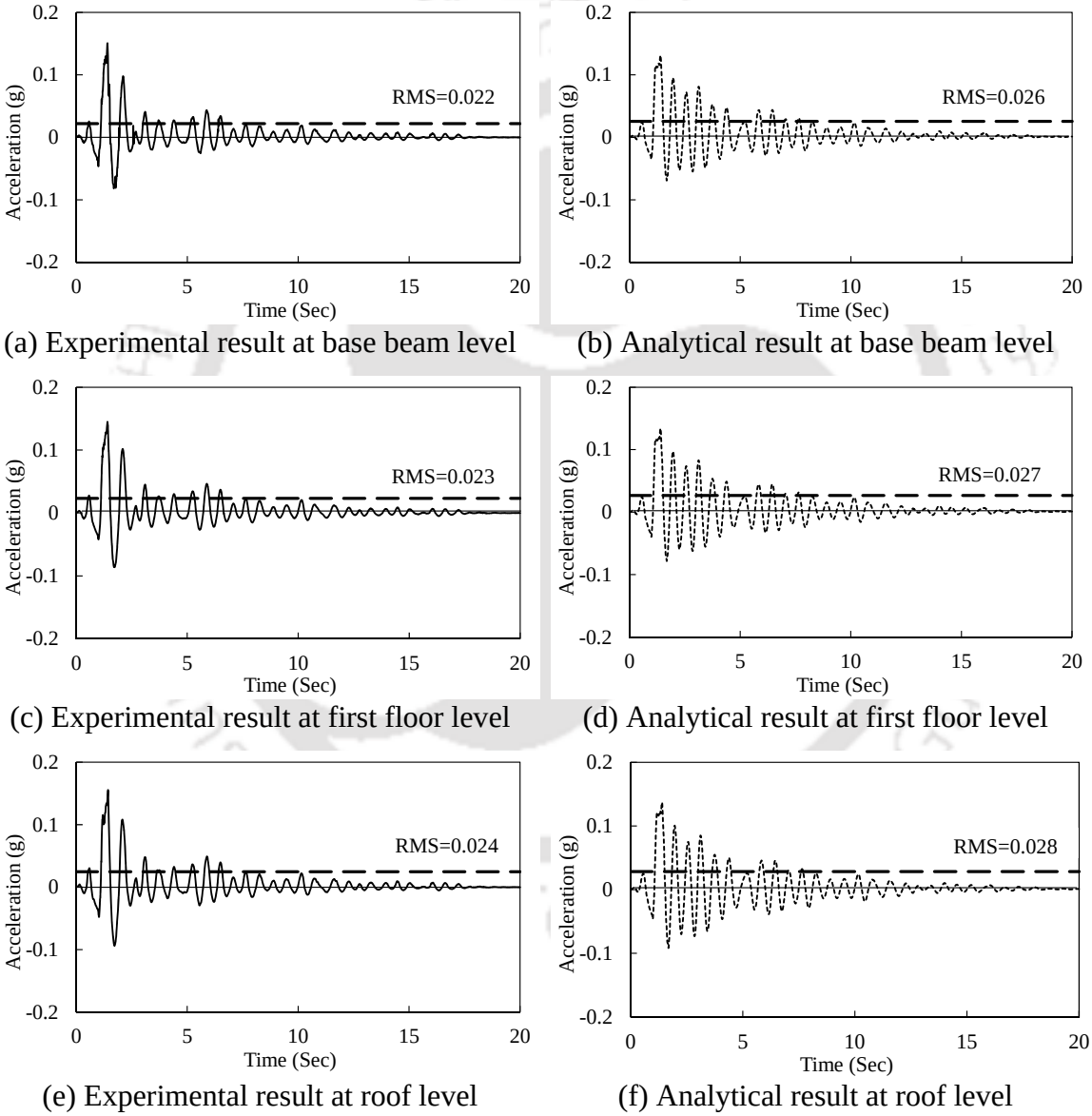

(a) Experimental result at base beam level (b) Analytical result at base beam level

(c) Experimental result at first floor level (d) Analytical result at first floor level

(e) Experimental result at roof level (f) Analytical result at roof level

Fig. 7.12 Comparison of experimental and analytical acceleration responses at different levels of model subjected to 70% intensity level of Parkfield earthquake applied along 45^0 to X-axis

Peak acceleration from experiment are 14.7%, 8.2% and 13.4% higher than those obtained from the numerical analysis at base, first floor and roof level respectively.

RMS values of acceleration from experiment are 15.0%, 13.7% and 14.2% lesser than those obtained from the numerical analysis at base, first floor and roof level respectively.

Comparison of time histories of acceleration obtained from shake table test and numerical analysis at different levels of the test model building subjected to 70% intensity of scaled acceleration for El Centro earthquake applied along 45^0 to X-axis are shown in Fig. 7.13.

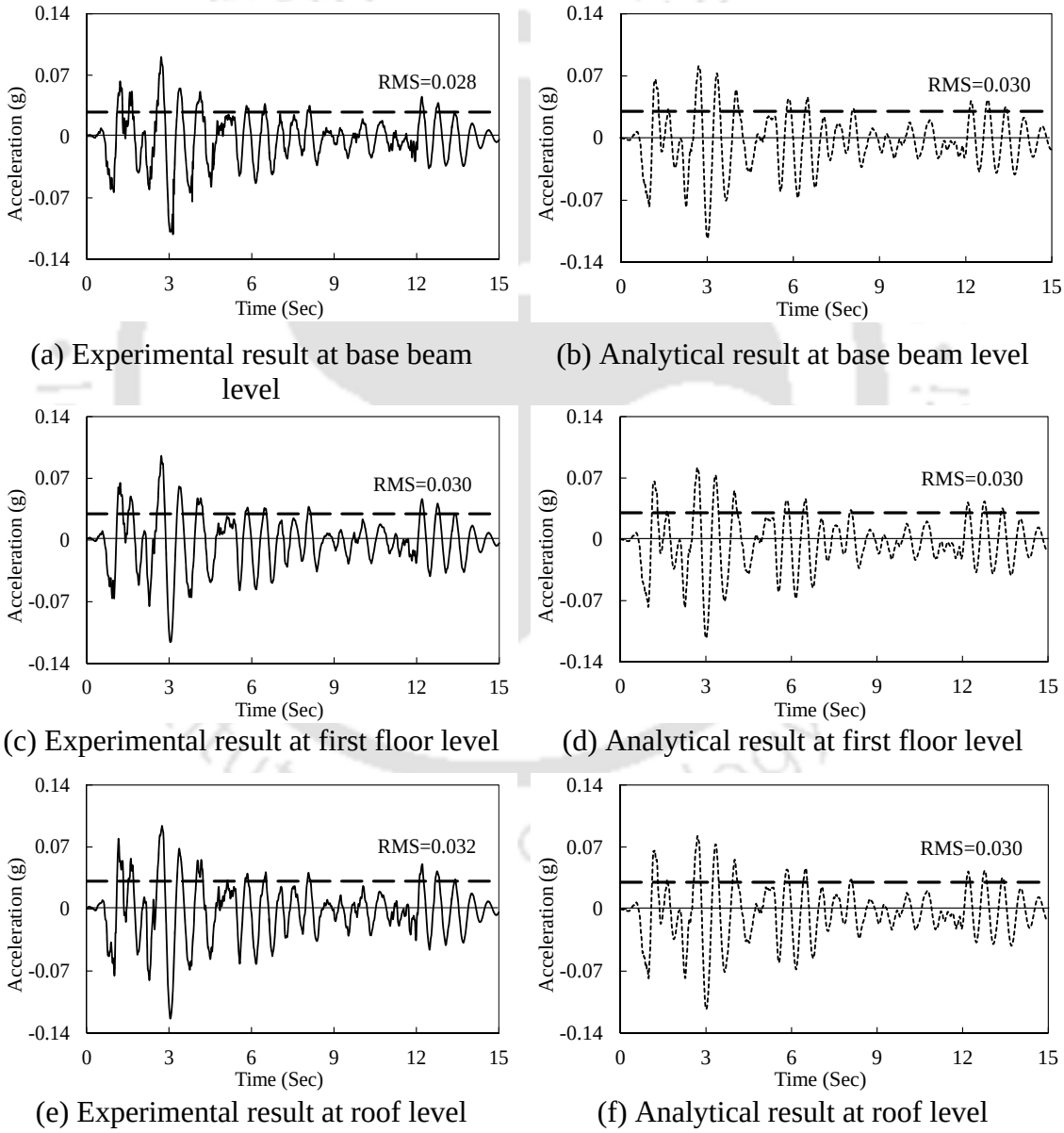

(a) Experimental result at base beam level

(b) Analytical result at base beam level

(c) Experimental result at first floor level

(d) Analytical result at first floor level

(e) Experimental result at roof level

(f) Analytical result at roof level

Fig. 7.13 Comparison of experimental and analytical acceleration responses at different levels of model subjected to 70% intensity level of El Centro earthquake applied along 45^0 to X-axis

Peak acceleration at base level from experiment is 1.6% lesser and at first floor and roof level are 2.7% and 9.5% higher respectively than those obtained from the numerical analysis. RMS value of acceleration from experiment is 7.6% lesser than that obtained from the numerical analysis at base level, while the same is 4.0% higher at roof level. The RMS values of acceleration at first floor level from experiment as well as numerical analysis are exactly matching.

Comparison of time histories of acceleration obtained from shake table test and numerical analysis result at different levels of the test model building subjected to 70% intensity of scaled acceleration for Victoria earthquake applied along 45^0 to X-axis are shown in Fig. 7.14.

Peak accelerations at base beam level is obtained from experiment is 11.5% lesser than that obtained from numerical analysis. However, at roof level the peak acceleration obtained from the experiment is 7.6% higher than that obtained from numerical analysis. At first floor level the peak acceleration obtained from experiment and numerical analysis are exactly matching with each other. RMS values of acceleration as obtained from experiment are 14.7%, 8.3% and 1.7% lesser than those obtained from the numerical analysis at base, first floor and roof level respectively.

Comparison of displacement response histories obtained from shake table test and numerical analysis at base beam level and first floor level of the test model building subjected to 70% intensity of scaled acceleration history of Koyna earthquake applied along 45^0 to X-axis are shown in Fig. 7.15. Peak displacements as obtained from the experiment is 5.8% lesser at base beam level and 10.2% higher at first floor as compared to the numerical analysis result. RMS values of displacement as obtained from experiment are 14.4% and 6.7% lesser than those obtained from the numerical analysis at base level and first floor level respectively.

Comparison of displacement response histories obtained from shake table test and numerical analysis at base beam level and first floor level of the test model building subjected to 70% intensity of scaled acceleration history of Parkfield earthquake applied along 45^0 to X-axis are shown in Fig. 7.16. Peak displacements as obtained from the experiment are 14.3% and 20.1% higher than those obtained from the numerical analysis at base and first floor level respectively. RMS value of displacement at base beam level and first floor level obtained from the experiment are 20.5% and 15.6% lesser respectively than those obtained from numerical analysis at the same level.

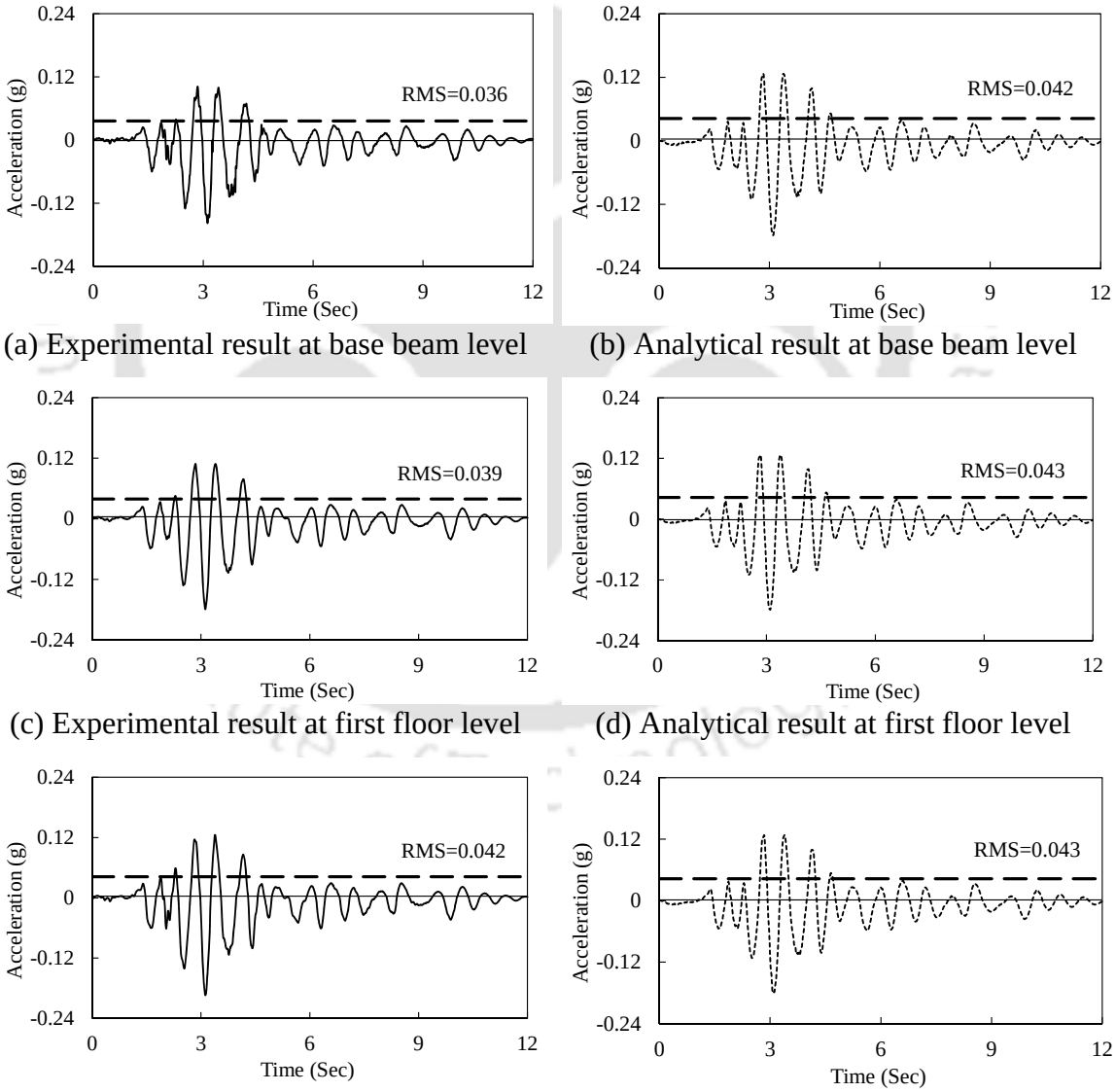

(a) Experimental result at base beam level (b) Analytical result at base beam level

(c) Experimental result at first floor level (d) Analytical result at first floor level

(e) Experimental result at roof level (f) Analytical result at roof level

Fig. 7.14 Comparison of experimental and analytical acceleration responses at different levels of model subjected to 70% intensity level of Victoria earthquake applied along 45^0 to X-axis

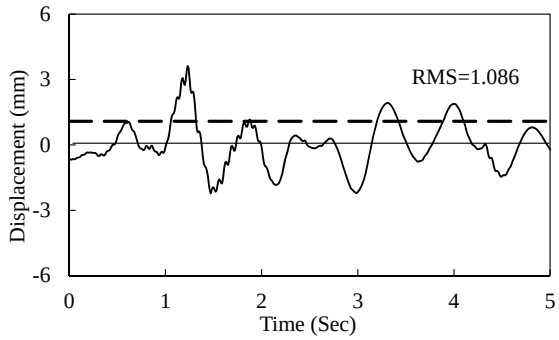

(a) Experimental result at base beam level

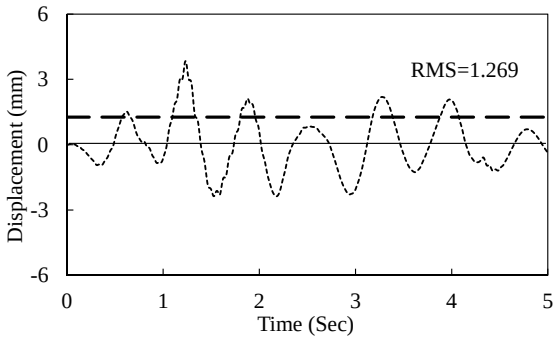

(b) Analytical result at base beam level

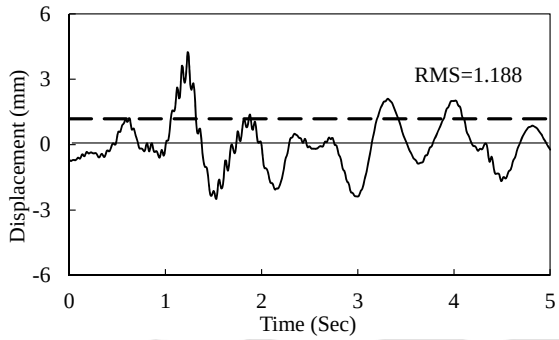

(c) Experimental result at first floor level

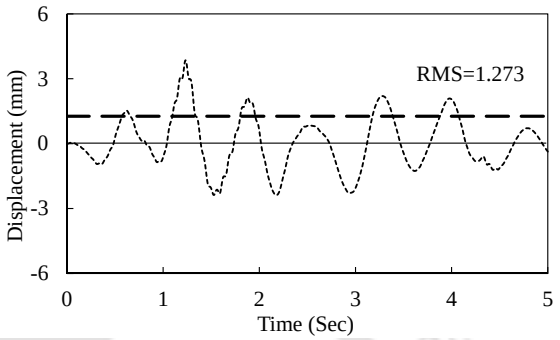

(d) Analytical result at first floor level

Fig. 7.15 Comparison of experimental and analytical displacement at base level and first floor level subjected to 70% intensity level of Koyna earthquake applied along 45^0 to X-axis

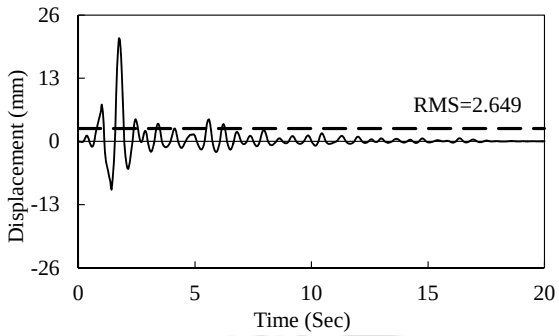

(a) Experimental result at base beam level

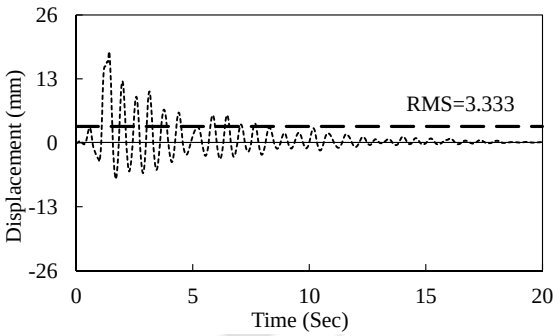

(b) Analytical result at base beam level

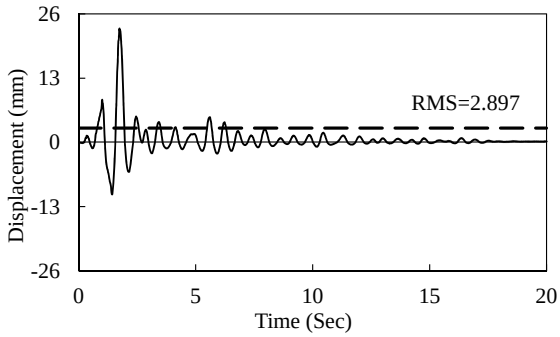

(c) Experimental result at first floor level

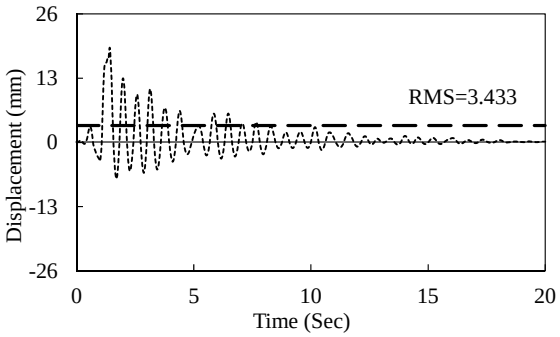

(d) Analytical result at first floor level

Fig. 7.16 Comparison of experimental and analytical displacement at base level and first floor level subjected to 70% intensity level of Parkfield earthquake applied along 45^0 to X-axis

Comparison of displacement response histories obtained from shake table test and numerical analysis at base beam level and first floor level of the test model building subjected to 70% intensity of scaled acceleration history of El Centro earthquake applied along 45^0 to X-axis are shown in Fig. 7.17. Peak displacement at base level obtained from the experiment is 3.3% lesser and at first floor level is 3.5% higher than that obtained from numerical analysis. RMS values of displacement as obtained from experiment are 10.3% and 3.3% lesser than those obtained from the numerical analysis at base and first floor level respectively.

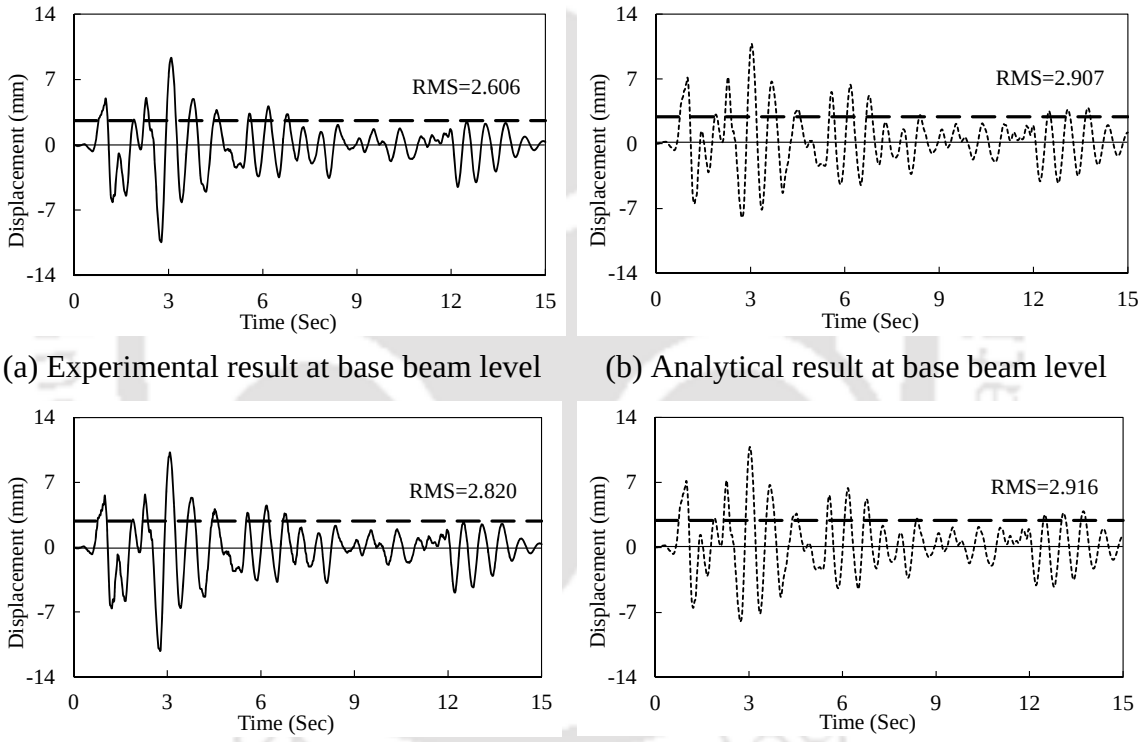

(a) Experimental result at base beam level (b) Analytical result at base beam level

(c) Experimental result at first floor level (d) Analytical result at first floor level

Fig. 7.17 Comparison of experimental and analytical displacement at base level and first floor level subjected to 70% intensity level of El Centro earthquake applied along 45^0 to X-axis

Comparison of displacement response histories obtained from shake table test and numerical analysis at base beam level and first floor level of the test model building subjected to 70% intensity of scaled acceleration history of Victoria earthquake applied along 45^0 to X-axis are shown in Fig. 7.18.

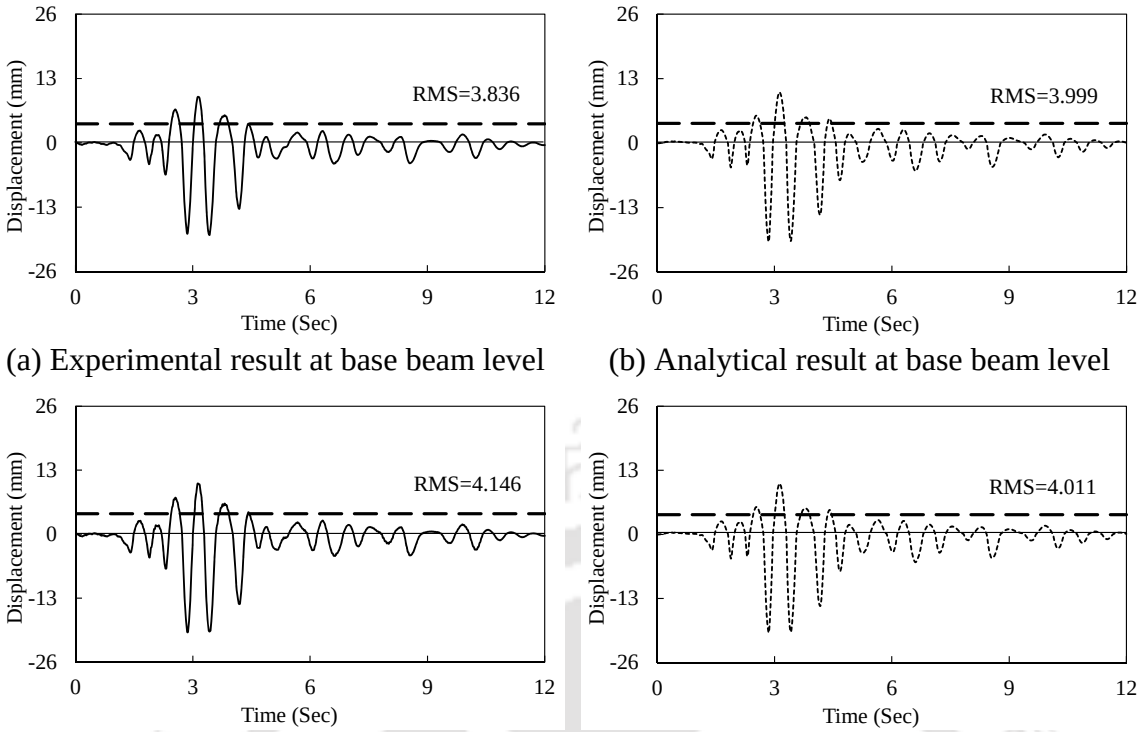

(a) Experimental result at base beam level (b) Analytical result at base beam level

(c) Experimental result at first floor level (d) Analytical result at first floor level

Fig. 7.18 Comparison of experimental and analytical displacement at base level and first floor level subjected to 70% intensity level of Victoria earthquake applied along 45^0 to X-axis

Peak displacement at base level as obtained from the experiment is 6.5% lesser than that obtained from numerical analysis, while at first floor level peak displacement is exactly matching with each other. RMS value of displacement at base level as obtained from experiment is 4.1% lesser than that obtained from the numerical analysis, while the same is 3.4% higher at first floor level.

Peak acceleration and displacement obtained from numerical analysis at different floor levels of test model building subjected to 70% intensity level of all the four input earthquakes applied along 45^0 to X-axis are shown in Table 7.2.

The largest lateral displacement as experienced by the isolator is 19.895mm, when excited by Victoria input earthquake excitation. Testing under horizontal cyclic displacement on the same isolator has shown that U-FREIs are able to maintain stability up to 60mm along 45^0 to X-axis. The peak displacement at first floor level is 19.939 during the input Victoria earthquake excitation, which is almost equal to the base beam

level displacement, indicating the rigid body motion of superstructure of the base isolated model building.

Table 7.2 Numerical analysis results of peak acceleration and displacement at different levels of model subjected to 70% intensity level of four earthquakes along 45^0 to X-axis

Earthquake	Peak Accelerations (g)				Peak Displacement (mm)	
	At Shake Table	At Base	At First Floor	At Roof Level	At Base level	At First Floor
Koyna	0.442	0.0521	0.0512	0.0514	3.840	3.848
Parkfield	0.333	0.1312	0.1340	0.1371	18.555	19.192
El Centro	0.223	0.1131	0.1127	0.1127	10.790	10.830
Victoria	0.435	0.1785	0.1790	0.1801	19.895	19.939

Thus, even under changed line of action of excitation, it is seen that the pattern of acceleration time history as observed from laboratory test and numerical simulation are in very good agreement. Similar observations are true for displacement time history also. However, some differences are observed in peak and RMS values of experimental and numerical analysis result. Therefore, the simple analysis technique presented in this chapter may be used for prediction of seismic response of low rise building supported on U-FREI.

7.5. Concluding Remarks

In this chapter, 3D FE model of the two storey base isolated test model building is carried out for the evaluation of dynamic response characteristics. Four different earthquake motion, namely, Koyna, Parkfield, El Centro and Victoria are used as input excitation. The entire exercise is repeated for loading direction along X-axis and 45^0 to X-axis. The floor acceleration time histories and floor displacement time histories from numerically simulated model are observed to agree quite well with those obtained from the experimental observations. On the basis of the detailed analysis of observed

dynamic response corresponding to various input earthquakes, the following conclusions are drawn.

1. The multi-linear hysteresis model, which is used for the simulation of FREI is able to predict the pattern of floor acceleration and displacement quite well for all the input earthquakes.
2. Acceleration and displacement response from numerically simulated model differs up to the extent of 1-15% range compared to experimental result. For seismic analysis of base isolated building supported on U-FREI, the responses from numerically simulated model can be very effectively used as basis for design.

Chapter 8

Summary and Conclusions

8.1. Summary

The present work is an effort towards the development of FREI to be used for reducing seismic vulnerability of low rise un-reinforced masonry buildings. The study is a combination of numerical and experimental exercises. The main components of this study are (i) development of lightweight, low cost FREI for seismic response control of a $1/5^{th}$ scaled low rise un-reinforced masonry building, (ii) numerical simulation of the behaviour of FREI using FE method and detailed transient dynamic analysis for the evaluation of stiffness, damping and stress-strain profile, (iii) experimental investigation on FREI for characterisation of mechanical properties, (iv) validation of results from FE analysis using experimentally observed data, (v) shake table testing of base isolated un-reinforced masonry model building supported on FREI, (vi) numerical simulation of base isolated un-reinforced masonry building and validation of seismic response results with that obtained from shake table testing.

In the course of study, various important factors which influence the dynamic characteristics of un-reinforced masonry building supported on U-FREI such as hysteretic behaviour of FREI under cyclic loading, deformed configuration of FREIs at large displacement, influence of input earthquakes along different axis of isolators etc. have been examined.

Expression for the evaluation of vertical and horizontal stiffness of bonded FREIs are proposed by previous researchers considering the influence of flexibility of fibre reinforcement. These formulae are used to determine the stiffness of bonded FREI in the present study. Similarly, critical buckling load carrying capacity of bonded FREI is

evaluated using three different formulae proposed in the past literature. However, due to complex behaviour of U-FREI under lateral loading, formulation of bonded FREI for vertical and horizontal stiffness are not applicable and no such works for U-FREIs are also available in literature. The approximate sizes of U-FREIs in the present study are considered based on geometry arrived at for bonded isolator.

Thus, in order to understand the behaviour of considered size of FREI and effects of different directions of horizontal loading on it, three dimensional FE modelling and nonlinear analysis are carried out. The square and circular isolators with both bonded and un-bonded end conditions are analysed to determine horizontal stiffness, damping, stress and strain at different level. The un-bonded boundary condition is appropriately modelled to simulate the contact behaviour of U-FREI. Comparison of stress and strain of bonded and un-bonded isolators along the height and across the middle rubber layer are presented for loading along X-axis and 45^0 to X-axis of isolator. Force-displacement hysteresis loops and damping of isolators are obtained from the analysis result. In FE analysis, mesh size plays an important role for efficient analysis and solution convergence. Influence of mesh size on the analysis result of bonded and un-bonded isolators are studied. Effect of variation of vertical load on the shear capacity of isolator is also studied.

Testing of square U-FREI is carried out to determine the vertical stiffness, horizontal stiffness and damping properties under different loading conditions. Necessary setup for experimental studies are prepared for applying vertical load and horizontal cyclic displacement on the isolator. Force-displacement hysteresis loops are plotted to determine the effective horizontal stiffness and damping of the isolator. These force-displacement hysteresis loops obtained from testing are compared with that obtained from the FE analysis result. The displaced shapes of isolator under different amplitudes

of horizontal displacement are monitored and compared with those obtained from FE analysis.

Shake table testing of a two storey 1/5th scaled model un-reinforced masonry building supported on U-FREI is carried out to ascertain its effectiveness in controlling seismic response. Four different input earthquakes excitation are applied with different intensities along X-axis and along 45^0 to X-axis of isolator. To compare the performance of U-FREI, same building is placed directly on the shake table without isolator and fixed base condition is simulated by restraining the base of the building with the shake table. Dynamic response characteristic of base isolated masonry building subjected to different intensities of input earthquakes are compared with the response of the same building without base isolation system. Acceleration response amplification, peak response values of test model with and without base isolation system are compared for different intensities of table acceleration.

The dynamic response characteristics of the un-reinforced masonry building supported on U-FREI and subjected to different intensities of seismic excitation are evaluated analytically by considering a multi-linear pivot hysteretic plasticity model for the simulation of FREI. The analytical results such as acceleration and displacement along the height of the building are compared with the corresponding results obtained from the shake table test. Very good agreements are observed between experimental and analytically evaluated responses along the height of the masonry building model.

8.2. Major Findings

Major findings from the present study may be summarised as below:

1) The study based on available research literatures reveals that vertical stiffness of FREIs are around three times higher than the same size of SREI. This is

primarily due to the fact that the number of elastomer layer can be increased in FREI as compared to SREI due to insignificant thickness of fibre reinforcement. Shape factor of FREI is increased due to higher number of elastomeric layer and hence the compression modulus of isolators. Thus, FREI has higher vertical load carrying capacity as compared to that of SREI.

2) As no classical solution is available for the evaluation of stiffness of U-FREIs, the selection of preliminary geometry of U- FREI can be considered based on the available formulae for bonded FREIs.
3) FE solution of U-FREI has shown that the effective horizontal stiffness of U-FREIs are significantly lesser than bonded FREIs at higher displacement. At maximum observed displacement level, the lateral force transmitted by bonded FREI is about 70% higher than that of U- FREI and hence efficacy for seismic isolation is higher. It is also observed from the FE analysis that the lower tensile stresses are developed in the rubber and reinforcement in U-FREI, resulting in lower peeling stress demand on bond between layers in U-FREI.
4) FE solution has shown that circular FREI can easily be replaced with square FREI, which is easy to manufacture with lesser wastage of material.
5) Variation of vertical load upto ±25% has insignificant effect on the shear capacity of the un-bonded isolator.
6) Horizontal stiffness as obtained from FE analysis result shows close agreement with that obtained from experimental study except some discrepancies at higher displacement. Effectiveness of un-bonded isolator increases with increase in amplitudes of horizontal displacements. U-FREI can be used as an effective base isolation device for low rise building alternative to SREI.
7) The displaced shapes of the isolators obtained from the test corresponding to

different direction of loadings are very similar to the displaced shape of isolator obtained from the FE analysis. The fairly close agreement of analysis results with that of experimental findings indicate that the FE analysis can be used as very effective analysis tool for design of FREI with both bonded and un-bonded end conditions.

8) Shake table studies of masonry building supported on U-FREI confirmed the effectiveness of U-FREI in reducing seismic responses of test model. U-FREIs are effective irrespective of loading directions and seismic isolation efficiency increases with increased displacement. The highest reduction of peak acceleration response is observed as 88% at the base beam level when the base isolated masonry building is subjected to full intensity of Koyna earthquake excitations.
9) Comparison of acceleration response obtained from shake table test shows that roof acceleration of fixed base test masonry building is 11 times higher than that at roof of base isolated test masonry building for full intensity of Koyna earthquake excitation. This result shows the effectiveness of U-FREI in reducing the dynamic response of masonry structure.
10) The analytical result of base isolated masonry building carried out using SAP2000 shows good agreement with the result obtained from shake table test.
11) FREI can be confidently used for seismic isolation of low cost building replacing conventional SREI.

8.3. Suggestions for Future Work

The application seismic base isolation to mitigate the seismic demand of structure has gained popularity across the world except the developing countries. In developing

countries these techniques are not so popular due to their higher cost of production. The low cost alternative is a viable option to minimize the seismic vulnerability of building situated in most severe seismic zones. The strategy of seismic isolation using U-FREI will be very useful for earthquakes protection of low rise buildings. Therefore, further research in the field of seismic base isolations are necessary for safety against earthquake disaster. The following additional works in this field will further strengthen the earthquake resistant design strategy of buildings:

- The seismic response of base isolated structure supported on U-FREI or other base isolated system is dependent on the characteristics of earthquake motions. Hence probabilistic methods for computation of responses of base isolated structures need to be examined.
- A prototype structure located in the most vulnerable seismic Zone-V of India may be seismically isolated using the U-FREI. The dynamic response characteristic of the building should be recorded for performance evaluation and system identification.
- Application of FREI may be explored for other vibration control problems.

References

Aiken I. D., Kelly J. M. and Tajirian F. F., (1989), "Mechanics of Low Shape Factor Elastomeric Seismic Isolation Bearings", *Report No. UCB/EERC-89/13*, Earthquake Engineering Research Center, University of California, Berkeley.

Aiken I. D., Kelly J. M., Clark P. W., Tamura K., Kikuchi M. and Itoh T., (1992), "Experimental Studies of the Mechanical Characteristics of Three Types of Seismic Isolation Bearings", *Proceedings, Tenth World Conference on Earthquake Engineering*, Madrid, Spain, July.

Aiken I. D., Kelly J. M., Clark P. W., Tamura K., Kikuchi M., and Itoh T., (1992), "Experimental Studies of Mechanical Characteristics of Three Types of Seismic Isolation Bearings", *Proceedings, Tenth World Conference on Earthquake Engineering*, Madrid, Spain, July.

Amin A. F. M. S., Wiraguna S. I., Bhuiyan A. R. and Okui Y., (2006), "Hyperelastic Model for Finite Element Analysis of Natural and High Damping Rubbers in Compression and Shear", *Journal of Engineering Mechanics, ASCE*, Vol. 132(1), pp. 54-64.

ANSYS®, Release 14.0, Help System, Analysis Guide, ANSYS, Inc, USA.

Arya A. S., (1994), "Concepts and Techniques for Seismic Base-Isolation of Structures", *Earthquake Engineering, 10th World Conference*, Balkema, Rotterdam, pp-6639-6648.

Ashkezari G. D., Aghakouchak A. A. and Kokabi M., (2008), "Design, Manufacture and Evaluation of the Perofrmance of Steel Like Fibre Reinforced Elastomeric Seismic Isolators", *Journal of Material Processing Technology, ELSEVIER*, Vol. 197, pp. 140-150.

Braga F. and Laterza M., (2004), "Field Testing of Low-rise Base Isolated Building", *Engineering Structures, ELSEVIER*, Vol. 26, pp. 1599-1610.

Buckle I.G., (1985), “New Zealand Seismic Base Isolation Concepts and their

Application to Nuclear Engineering", *Nuclear Engineering and Design*, Vol. 84, pp. 313-326.

Chalhoub M. S. and Kelly J. M., (1991), "Analysis of Infinite-Strip-Shaped Base Isolator with Elastomer Bulk Compression", *Journal of Engineering Mechanics, ASCE*, Vol. 117(8), pp. 1791-1805.

Computers and Structures Inc., (2009), "CSI Analysis Reference Manual for SAP2000®, ETABS® and SAFE®, Reference Manual", *Computers and Structures Inc.*, Version 14, Berkeley, California, USA.

Constantinou M. C., (2004), "Friction Pendulum Double Concave Bearing", *Technical Report*, State University of New York, Buffalo.

Chang C. H., (2002), "Modeling of Laminated Rubber Bearings using an Analytical Stiffness Matrix", *International Journal of Solids and Structures, ELSEVIER*, Vol. 39, pp. 6055-6078.

Chang H., (1988), "Nonlinear Elastomer Analysis - Survey of Computer Codes and Case Study for Caliper Seal", *Computers & Structures, ELSEVIER*, Vol. 30(5), pp. 1165-1173.

Choudhury A. M., (2010), "Study on Size Effect of RC Beam-column Joints with and without Retrofitting under Cyclic Loading", *PhD Thesis*, Civil Engineering Department, Indian Institute of Technology, Guwahati.

Clough R. W. and Penzien J., (1975), "Dynamics of Structures", *McGraw-Hill*, New York.

Datta T. K., (2003), "A State-of-the-art Review on Active Control of Structures", *ISET Journal of Earthquake Technology*, 40(1), pp. 1-17.

Deb S. K., (1993), "Earthquake Protection of Medium-rise Reinforced Concrete Buildings by Base Isolation", *PhD Thesis, Department of Earthquake Engineering*, University of Roorkee, India.

Derham C. J., Kelly J. M. and Thomas A. G., (1985), "Nonlinear Natural Rubber

Bearings for Seismic Isolation", *Nuclear Engneering and Design, ELSEVIER*, Vol. 84, pp. 417-428.

Dezfuli F. H. and Alam M. S., (2013), "Multi-criteria Optimization and Sesimic Performance Assessment of Carbon FRP-based Elastomeric Isolator", *Engineering Structures, ELSEVIER*, Vol. 49, pp. 525-540.

Giuliani G. C., (1991), "Design Experience on Seismically Isolated Buildings", *Nuclear Engineering and Design, ELSEVIER*, Vol. 127, pp. 349-366.

Herrmann L. R., Ramaswamy A. and Hamidi R., (1989), "Analytical Parameter Study for Class of Elastomeric Bearings", *Journal of Structural Engineering, ASCE*, Vol. 115(10), pp. 2415-2434.

Holzapfel G. A., (1996), "On Large Strain Viscoelasticity: Continuum Formulation and Finite Element applications to Elastomeric Structures", *International Journal for Numerical methods in Engineering*, Vol. 39, pp. 3903-3926.

Imbimbo M. and Kelly J. M., (1998), "Influence of Material Stiffening on Stability of Elastomeric Bearings at large Displacements", *Journal of Engineering Mechanics, ASCE*, Vol. 124(9), pp. 1045-1049.

IS: 3400 Part 1 (2004), "Methods of Test for Vulcanized Rubbers, Part 1 Tensile Stress-Strain Properties", *Bureau of Indian Standard*, New Delhi.

IS: 3400 Part 2 (2003), "Methods of Test for Vulcanized Rubbers, Part 2 Rubber, Vulcanized or Thermoplastic – Determination of Hardness (Hardness between 10 IRHD and 100 IRHD", *Bureau of Indian Standard*, New Delhi.

IS: 3400 Part 4 (2003), "Methods of Test for Vulcanized Rubbers, Part 4 Accelerated Ageing", *Bureau of Indian Standard*, New Delhi.

IS: 3400 Part 10 (2003), "Methods of Test for Vulcanized Rubbers, Part 10 Compression Set at Constant Strain", *Bureau of Indian Standard*, New Delhi.

Jankovich E., Leblanc F. and Durand M., (1981), "A Finite Element Method for the Analysis of Rubber Parts, *Experimental and Analytical Assessment", Computers &*

Structures, ELSEVIER, Vol. 14(5-6), pp. 385-391.

Jerrams S., Sanders K. and Goo K. B., (2001), "Realistic Modelling of Earthquake-Isolation Bearings", *Journal of Material Processing Technology, ELSEVIER*, Vol. 118, pp. 158-164.

Kang B. S., Kang G. J. and Moon B. Y., (2003), "Hole and Lead Plug Effect on Fibre Reinforcement Elastomeric Isolator for Seismic Isolation", *Journal of Material Processing Technology, ELSEVIER*, Vol. 140, pp. 592-597.

Kelly J. M., (1986), "Aseismic Base Isolation: Review and Bibliography", Computational Mechanics Publications, *Soil Dynamics and earthquake Engineering*, Vol. 5(3), pp. 202-216.

Kelly J. M. and Takhirov S. M., (2001), "Analytical and Experimental Study of Fibre-Reinforced Elastomeric Isolator", *PEER Report, 2001/11*, Pacific Earthquake Engineering Research Center, University of California, Berkeley.

Kelly J. M. and Takhirov S. M., (2002), "Analytical and Experimental Study of Fibre-Reinforced Strip Isolators", *PEER Report, 2002/11*, Pacific Earthquake Engineering Research Center, University of California, Berkeley.

Kelly J. M., (2003), "Tension Buckling in Multilayer Elastomeric Bearings", *Journal of Engineering Mechanics, ASCE*, Vol. 129(12), pp. 1363-1368.

Kelly J. M., (2009), "Base Isolation: Origins and Development", *National Information Service for Earthquake Engineering*, University of California, Barkeley, pp. 1-6.

Kelly J. M. and Calabrese A., (2012), "Mechanics of Fibre Reinforced Bearings", *PEER Report*, 2012/101, Pacific Earthquake Engineering Research Center, University of California, Berkeley.

Kikuchi M. and Aiken I. D., (1997), "An Analytical Hysteresis Model for Elastomeric Seismic Isolation Bearings", *Earthquake Engineering and Structural Dynamics*, Vol. 26(2).

Koh C. G. and Kelly J. M., (1989), "Viscoelastic Stability Model for Elastomeric Isolation Bearings", *Journal of Structural Engineering, ASCE*, Vol. 115(2), pp. 285-302.

Koh C. G. and Lim H. L., (2001), "Analytical Solution for Compression Stiffness of Bonded Rectangular Layers", *International Journal of Solids and Structures, ELSEVIER*, Vol. 38, pp. 445-455.

Kulak R. F. and Wang C. Y., (1991), "Design and Analysis of Seismically Isolated Structures", *Nuclear Engineering and Design, ELSEVIER*, Vol. 127, pp. 419-432.

Lakshmanan H., Kumar K. S., Sreekala R., Muthumani K., Guru J. and Gopalakrishnan N., (2008), "Experimental Investigations on the Seismic Response of a Base-Isolated Reinforced Concrete Frame Model", *Journal of Performance of Constructed Facilities, ASCE*, Vol. 22(5), pp. 289-296.

Lee L., (1985), "Large Shake Table Test of a Base Isolated Masonry Model using a Sand-slide Measure", *University of California*, Berkeley, USA.

Lee S. J. and Oh J. W., (1999), "Stability of Rubber Bearings for Seismic Isolation", *Transactions of 15th International Conference on structural Mechanics in Reactor Technology*, Seoul, Korea, August 15-20.

Lim C. K and Herrmann L. R., (1987), "Equivalent Homogeneous FE Model for Elastomeric Bearings", *Journal of Engineering Mechanics, ASCE*, Vol. 113(1), pp. 106-125.

Lin S., Ahmadi G. and Tadjbakhsh I. G., (1989), "Comparative Study of Base Isolation Systems", *Journal of Engineering Mechanics, ASCE*, Vol. 115(9), pp. 1976-1992.

Matsuda A. (2004), “Evaluation for Mechanical Properties of Laminated Rubber Bearings Using Finite Element Analysis”, *Journal of Pressure Vessel Technology, ASME*, Vol. 126, pp. 134-140.

Michael G. P., Tait M. J. and Nezhad H. T., (2011), “Stability of Fibre-reinforced Bearings in an Un-bonded Application”, *Journal of Composite Materials, SAGE*, Vol.

45(10), pp. 1873-1884.

Moon B. Y., Kang G. J., Kang B. S. and Kelly J. M., (2002), "Design and Manufacturing of Fibre Reinforced Elastomeric Isolator for Seismic Isolation", *Journal of Material Processing Technology, ELSEVIER*, Vol. 130-131, pp. 145-150.

Moon B. Y, Kang G. J., Kang B. S. and Cho D. S., (2004), "Design of Elastomeric Bearing System and Analysis of its Mechanical Properties." *KSME International Journal*, Vol. 18(1), pp. 20-29.

Mordini A. and Strauss A., (2008), "An Innovative Earthquake Isolation System using Fibre Reinforced Rubber Bearings", *Engineering Structures, ELSEVIER*, Vol. 30, pp. 2739-2751.

Naeim F. and Kelly J. M., (1999), "Design of Seismic Isolated Structures: From Theory to Practice", *John Wiley & Sons*, INC.

Nagarajaiah S., Reinhorn A. M. and Constantinou M. C., (1991), "Nonlinear Dynamic Analysis of 3D Base-Isolated Structures", *Journal of Structural Engineering, ASCE*, Vol. 117(7), pp. 2035-2054.

Nagarajaiah S. and Xiaohong S., (2000), "Response of Base-Isolated USC Hospital Building in Northridge Earthquake", *Journal of Structural Engineering, ASCE*, Vol. 126(10), pp. 1177-1186

Naghshineh A. K., Akyuz U. and Caner A., (2014), "Comparison of Fundamental Properties of New Types of Fibre-mesh-reinforced Seismic Isolators with Conventional Isolators", *Earthquake Engineering and Structural Dynamics*, Vol. 43, pp. 301-316.

Nath R. J., Deb S. K. and Dutta A., (2013), "Base Isolated RC Building – Performance Evaluation and Numerical Model Updating using Recorded Earthquake Response", *Earthquakes and Structures*, Vol. 4(5), pp. 1-17.

Nezhad H. T., Tait J. M. and Drysdale R. G., (2008), "Lateral Response Evaluation of Fibre-Reinforced Neoprene Seismic Isolator Utilized in an Unbonded Application", *Journal of Structural Engineering, ASCE*, Vol. 134(10), pp. 1627-1637.

Nezhad H. T., Tait J. M. and Drysdale R. G., (2008), “Testing and Modeling of Square Carbon Fibre-reinforced Elastomeric Seismic Isolators”, *Structural Control and Health Monitoring, Wiley InterScience*, Vol. 15, pp. 876-900.

Nezhad H. T., Tait M. and Drysdale R. G., (2009), "Parametric Study on the Response of Stable Unbonded-Fibre Reinforced Elastomeric Isolator (SU-FREIs)", *Journal of Composite Materials*, Vol. 43(15), pp. 1569-1587.

Nezhad H. T., Tait M. and Drysdale R. G., (2009), "Shake Table Study on an Ordinary Low-Rise Building Seismically Isolated with SU-FREIs (Stable Unbonded-Fibre Reinforced Elastomeric Isolators)", *Earthquake Engineering and Structural Dynamics*, Wiley InterScience, Vol. 38, pp. 1335-1357.

Nezhad H. T., Tait M. J. and Drysdale R. G., (2009), “Simplified Analysis of a Low-rise Building Seismically Isolated with Stable Un-bonded Fibre Reinforced Elastomeric Isolators”, *Canadian Journal of Civil Engineering*, Vol. 36(7), pp. 1182-1194.

Nezhad H. T., Tait M. and Drysdale R. G., (2011), "Bonded versus Unbonded Strip Fibre Reinforced Elastomeric Isolators: Finite Element Analysis", *Composite structures, ELSEVIER*, Vol. 93, pp. 850-859.

Nezhad H. T., (2014), "Horizontal stiffness solutions for unbonded fibre reinforced elastomeric bearings", *Structural Engineering and Mechanics*, Vol. 49 (3), pp. 395-410.

Osgooei P. M., Tait M. J. and Konstantinidis D., (2014), “Three-dimensional Finite Element Analysis of Circular Fiber-reinforced Elastomeric Bearings under Compression”, *Composite structures, ELSEVIER*, Vol. 108, pp. 191-204.

Osgooei P. M., Tait M. J. and Konstantinidis D., (2014), “Finite Element Analysis of Unbonded Square Fiber-reinforced Elastomeric Isolators (FREIs) under Loading in Different Directions”, *Composite structures, ELSEVIER*, Vol. 113, pp. 164-173.

Park K. S., Jung H. J. and Lee I. W., (2002), "A Comparative Study on Aseismic Performances of Base Isolation Systems for Multi-span Continuous Bridge", *Engineering Structures, ELSEVIER*, Vol. 24, pp. 1001-1013.

Paulson T. J., Abrams D. P. and Mayes R. L., (1991), "Shaking-Table Study of Base

Isolation for Masonry Buildings", *Journal of Structural Engineering, ASCE*, Vol. 117(11), pp. 3315-3336.

Roeder C. W and Stanton J. F., (1983), "Elastomeric Bearings: State-of-the-Art", *Journal of Structural Engineering, ASCE*, Vol. 109(12), pp. 2853-2871.

Russo G. and Pauletta M., (2013), "Sliding Instability of Fibre-reinforced Elastomeric Isolators in Un-bonded Applications", *Engineering Structures, ELSEVIER*, Vol. 48, pp. 70-80.

Russo G., Pauletta M. and Cortesia A., (2013), "A Study on Experimental Shear Behavior of Fibre-reinforced Elastomeric Isolators with Various Fibre Layouts, Elastomers and Aging Conditions", *Engineering Structures, ELSEVIER,* Vol. 52, pp. 422-433.

Sanchez J., Masroor A., Mosqueda G., and Ryan K., (2013), "Static and Dynamic Stability of Elastomeric Bearings for Seismic Protection of Structures", *J. Struct. Engng, ASCE* Vol. 139, pp. 1149-1159.

Sasso M., Palmieri G., Chiappini G. and Amodio D., (2008), "Characterization of Hyperelastic Rubber-Like Materials by Biaxial and Uniaxial Stretching Tests Based on Optical Methods", *Polimer Testing, ELSEVIER*, Vol. 27, pp. 995-1004.

Spizzuoco M., Calabrese A. and Serino G., (2014), "Innovative Low-cost Recycled Rubber-Fiber Reinforced Isolator: Experimental Tests and Finite Element Analyses", *Engineering Structures, ELSEVIER*, Vol. 76, pp. 99-111.

Stanton J. F., Scroggins G., Taylor A. W. and Roeder C. W., (1990), "Stability of Laminated Elastomeric Bearings", *Journal of Engineering Mechanics, ASCE*, Vol. 116(6), pp. 1351-1371.

Sussman T. and Bathe K. J., (1987), "A Finite Element Formulation for Nonlinear Incompressible Elastic and Inelastic Analysis", *Computers & Structures, ELSEVIER*, Vol. 26(1/2), pp. 357-409.

Tabaddor F., (1987), "Rubber Elasticity Models for Finite Element Analysis", *Computers & Structures, ELSEVIER*, Vol. 26(1/2), pp. 33-40.

Timoshenko S. P. and Goodier J. N., (1970), “Theory of Elasticity”, *McGraw-Hill*, New York.

Tsai H. C. and Lee C. C., (1998), "Compression Stiffness of Elastic Layers Bonded Between Rigid Plates", *International Journal of Solids Structures, ELSEVIER*, Vol. 35(23), pp. 3053-3069.

Tsai H. C. and Hsueh S. J., (2001), "Mechanical Properties of Isolation Bearings Identified by a Viscoelastic Model", *International Journal of Solids and Structures, ELSEVIER*, Vol. 38, pp. 53-74.

Tsai H. C. and Kelly J. M., (2001), “Stiffness Analysis of Fibre-Reinforced Elastomeric Isolator”, *PEER Report, 2001/05*, Pacific Earthquake Engineering Research Center, University of California, Berkeley.

Tsai H. C. and Kelly J. M., (2002), “Stiffness Analysis of Fibre-Reinforced Rectangular Seismic Isolator”, *Journal of Engineering Mechanics, ASCE*, Vol. 128(4), pp. 462-470.

Tsai H. C. and Kelly J. M., (2002), “Bending Stiffness of Fibre-Reinforced Circular Seismic Isolator”, *Journal of Engineering Mechanics, ASCE*, Vol. 128(11), pp. 1150-1157.

Tsai H. C., (2003), "Flexure Analysis of Circular Elastic Layers Bonded Between Rigid Plates", *International Journal of Solids and Structures, ELSEVIER*, Vol. 40, pp. 2975-2987.

Tsai H. C., (2004), “Compression Stiffness of Infinite-strip Bearings of Laminated Elastic Material Interleaving with Flexible Reinforcements”, *Journal of Material Processing Technology, ELSEVIER*, Vol. 41, pp. 6647-6660.

Tsai H. C. and Kelly J. M., (2005), “Buckling Load of Seismic Isolator Affected by Flexibility of Reinforcement”, *International Journal of Solids and Structures, ELSEVIER*, Vol. 42, pp. 255-269.

Tsai H. C. and Kelly J. M., (2005), "Buckling of Short Beams with Warping Effect Included", *International Journal of Solids and Structures, ELSEVIER*, Vol. 42, pp. 239-253.

Tsai H. C., (2005), "Compression Analysis of Rectangular Elastic Layers Bonded Between Rigid Plates", *International Journal of Solids and Structures, ELSEVIER*, Vol. 42, pp. 3395-3410.

Tsai H. C., (2006), "Compression Stiffness of Circular Bearings of Laminated Elastic Materials Interleaving with Flexible Reinforcements", *International Journal of Solids and Structures, ELSEVIER*, Vol. 43, pp. 3484-3497.

Tsai H. C., (2008), "Deformation Analysis of Infinite-Strip Bearings of Laminated Elastic Materials Interleaving with Tension-Only Reinforcements", *International Journal of Solids and Structures, ELSEVIER*, Vol. 45, pp. 2836-2849.

Van Engelen N. C., Konstantinidis D. and Tait M. J., (2012), "Investigation of Base Isolated Structures Utilizing Stable Unbonded Fibre Reinforced Elastomeric Isolators", *15 World Conference on Earthquake Engineering*, Lisbon, Portugal, Sept 24-28, 2012.

Vemuru V. S. M., Nagarajaiah S., Masroor A. and Mosqueda G., (2014), "Dynamic Lateral Stability of Elastomeric Seismic Bearings", *Journal of Structural Engineering, ASCE,* (DOI: 10.1061/(ASCE)ST.1943-541X.0000955).

Wang Y. P., (2002), "Fundamentals of Seismic Base Isolation", International Training Programs for Seismic Design of Building structures, *National Center for Research on Earthquake Engineering,* Taiwan.

Wipplinger L. A., (2004), "Dynamic Testing of a Masonry Structure on a Passive Isolation System", *Journal of Architectural Engineering, ASCE*, Vol. 10(1), pp. 15-21.

Wu Y. M. and Samali B., (2002), "Shake Table Testing of a Base Isolated Model", *Engineering Structures, ELSEVIER*, Vol. 24, pp. 1203-1215.

Zayas V. A., Low S. S., and Mahin S. A., (1989), "A Simple Pendulum Technique for Achieving Seismic Isolation", Earthquake Spectra, Vol. 6(2), pp. 317-334.

Publications from this thesis work

(A) Journals:

1. Das Animesh, Dutta Anjan and Deb S.K, "Performance of Fibre-Reinforced Elastomeric Base Isolators under Cyclic Excitation", Structural Control and Health Monitoring, (http://onlinelibrary.wiley.com/21 May 2014, DOI: 10.1002/stc.1668).

2. Das Animesh, Dutta Anjan and Deb S.K, "Shake Table Studies of Ordinary Brick Masonry Building Supported on Fibre Reinforced Elastomeric Isolator", *Earthquake Engineering and Structural Dynamics*, Wiley InterScience, Communicated.

(B) Conferences:

1. Das Animesh, Dutta Anjan and Deb S.K, "Modeling of fibre reinforced elastomeric base isolator", *15 World conference of on earthquake engineering*. Lisbon, Portugal, Sept 24-28, 2012.